Hydrodynamic and Dispersion Studies in an Estuary Physical Model incorporated with an Idealized Groundwater

Teddy Tedjakusuma

0833769

Cardiff School of Engineering

PhD Thesis

2018

ACKNOWLEDGEMENT

ABSTRACT

A study on hydrodynamic and dispersion has been undertaken in an estuary physical model. The model represented the Severn Estuary in the UK which has the second largest tidal range in the world. The scale of the model was 1:125 vertically and 1:25,000 horizontally. Experiments in nine sample points showed that water level was different in those points. Velocity measurements showed that the velocity in the physical model coild be analysed using the wave resonance theory. The velocity profile measurements showed that the balance between ebb and flood tide, and this balance were different in different sampling points. The experiments were then compared to the computer modelling results. The water level model showed accordance with the experimental results. The velocity model results were then calibrated using several parameters, namely n-Manning, COED, and momentum correctioncoefficient (β). The calibration was then continued by the refinement of boundary condition and bathymetry. Studies on dispersion in the estuary physical model revealed that longitudinal dispersion coefficient affected the dispersion significantly, while the lateral turbulent diffusion affected the dispersion less significantly.Constant dispersion coefficient was compared with the variable dispersion coefficient, and the results showed that the constant dispersion coefficient gave a better representation of the dispersion process. Studies were also undertaken in an idealized groundwater which was linked to the estuary physical model. The static and dynamic conditions of the groundwater were studied. For static condition which was also undertaken to calibrate the water level probes, the change of water level in the groundwater clearly followed the changes in the estuary water levels, with a delay of water level according to the distance between the borehole and the estuary boundary. Dynamic condition of the groundwater as a results of tide in the estuary clearly shows the phase difference and the tide range at each borehole according to their distance to the estuary boundary. The effect between pump and tide was studied, and this showed clearly the effects of each component on groundwater level. Through Darcy's analysis it was proved that the groundwater hydrodynamics follow the Darcy's principle. Finally the dispersion in the groundwater were studied using two scenarios, namely open-open boundary and close-open boundary. Analysis results showed that open-open boundary gave lower dispersion coefficient than the close-open boundary.

TABLE OF CONTENTS

LIST OF FIGURES

LIST OF TABLES

LIST OF APPENDIXES

CHAPTER 1

INTRODUCTION

1.1 General

Water is one of the most essential substances needed by human beings to support their life, such as drinking, washing, sanitatizing, etc. Water is available in various places on the earth, such as in seas and oceans (96.5%), groundwater (1.7%), glaciers and the ice caps of Antarctica and Greendlance (1.7%), and in the air as vapor, clouds and precipitation (0.001%) (Gleick, 1993). Among these bodies, estuaries have a strategic position and many functions, and therefore they are among the most populated places in the world. Due to rapid population growth, estuaries have been suffered from pollution, mainly by domestic and industrial activities.

To deal with the water pollution problems it is important to establish the understanding of pollutant transport, especially in regards with the pollutant mixing and dispersion in water. In addition, instead of studying dispersion in one water body, it will be more beneficial if such work is carried out by considering the interaction between connecting water bodies, such as surface water and groundwater, so that the work can include the processes affected by such interactions. In the present study, dispersion processes areexplored in an estuary as the main subject and in groundwater as the supporting subject. The aim of this study is to establish the dispersion coefficients in the two water bodies, and in particular to investigate the effect of using constant and variable dispersion coefficientson dispersion modelling in estuaries. An estuary physical model is available in the Hydraulics Laboratory, at Cardiff University, which represents the Severn Estuary and is used to carry out hydrodynamicstudies. The experimental results consisting of water level and velocity data are then used to calibratecomputer models, such as DIVAST (Depth Integrated Velocity and Solute Transport), which has beenset up for the Severn Estuary physical

model. The dispersion experiment and modelling are then carried out to establish the dispersion coefficient.

Furthermore, an idealized groundwater basin has been incorporated within the estuary physical model and is used herein to explore the hydrodynamic and dispersion processes in groundwater flows. The experiments also include measurements of water levels and dye tracer concentrations. Both water level and dye tracer data are needed to simulate the dispersion in advection-diffusion model. An analysis based on Darcy's equation is applied to the water level data in the groundwater basin to estimatethe groundwater permeability coefficient. A simple mathematical model based on the advection diffusion equation is then used to analyze the experimental results andestimate the dispersion coefficient for groundwater flows.

1.2 Estuaries, Opportunities and Challenges

Generally speaking, an estuary is the meeting zone between a river and the sea. However there are technically many different definitions of an estuary.According to Pritchard,D.W. (1967), an estuary is defined as a semi-enclosed coastal body of water, which has a free connection with the open sea, and within which sea water is measurably diluted with freshwater derived from land drainage.

An estuary is a water body which is one of the most productive natural habitats in the world because the inflow of both seawater and freshwater provide high levels of nutrients, in both the water column and sediments. Estuaries are generally open dynamic ecosystems, with a connection to the open sea through which seawater enters according to the repetition of the tides. The seawater entering an estuary is diluted by the freshwater flowing in from rivers and streams.

Estuaries have various aspects of importance, including (US-EPA, 2012):
- Biologically: Thousands of species of birds, mammals, fish, and other wildlife depend on estuarine habitats as places to live, feed, and reproduce. Because they are biologically productive, estuaries provide ideal areas for migratory birds to rest and re-fuel during their long journeys.

- Environmentally: Water draining from uplands carries sediments, nutrients, and other pollutants to estuaries. As the water flows through wetlands, such as swamps and salt marshes, much of the sediments and pollutants are filtered out. This means that outflowing river and groundwater pass trough estuaries on way to ocean. Plants, animal, and sediments take up nutrients and toxicants. For example, trace metals which is associated with fluvial suspended solids accumulate mainly in areas with low hydrodynamic energy. These marshes are characterized by vegetation, sediments rich inlitter and low flow velocities during flooding which promotessedimentation of the fine grained fraction of suspended solids (Teuchies et. al, 2013)
- Socially: Estuaries provide places for recreational activities, scientific studies, and aesthetic enjoyment. This may increase the interaction among the society and therefore enhance the social quality of the community living around.
- Economically: Estuaries have important commercial value and these resources provide economic benefits for tourism, fisheries, and recreational activities. This will of course help imporove the economy of the society around the estuary. Estuaries have also economic potentials as the sources of energy, by building barrages etc. to generate power.

The important roles of estuaries, as mentioned above, have encouraged many studies on estuarine problems, including: ecosystemservices, estuarine management (including habitat protection and recreation, monitor of estuary change, development control, policy review, etc), estuarine pollution, economic aspects of estuaries, and energy potential of estuaries.Such studies aim at helping maintain and improvethe quality of an estuary, so that they can serve the need of humanbeings and other living organisms.

Due to their strategic position for various economic and social activities, estuaries have grown to encompass large cities, including *mega cities* (cities with more than 10 million people).Beside their economic benefits, however, the growth of mega-cities in estuarine areas has also posed major environmental problems. Pollution caused by various activities has made many estuaries unclean and unsafe.

Many chemical substances are known to maintain a relatively high concentration in water, accumulate in estuarine sediments (McCain et al., 1988) or biologically accumulate in sediment-dwelling organisms (Meador et al., 1995). Pollutants enter estuaries through storm drains, industrial discharges, runoff from grass yards, streets, and farmlands, discharges from sewage treatment plants, and atmospheric deposition. Pollutants commonly found in estuaries are heavy metals (such as copper, zinc, mercury), toxins (such as pesticides, herbicides, paint, oil and gasoline), nutrients (such as nitrogen and phosphorus) which can cause eutrophication, and pathogens or disease-causing organisms (including bacteria, viruses, and other parasites).

Estuarine pollution occurs in many places world-wide, especially in areas of rapid population growth. For example, in China the estuaries of its two greatest rivers, the Yangtze and the Yellow rivers, have been declared dead zones by the United Nations due to the high amounts of pollutants (Agence France-Press, 2006). Another example of a heavy polluted estuary is a semi-close estuary of the Persian Gulf. The Gulf's marine ecosystem is under considerable stress from the impacts of coastal reclamations, oil exploration and tanker movement, industrial developmentand desalination projects – to mention but a few. More than one million barrels of oil are spilled into the Persian Gulf annually; up to 30% of the sewage discharged into the sea is untreated; and low levels of pollutants, including pesticides, polychlorinated biphenyls (PCBs) and organic phosphorous compounds, have been found in marine organisms and biota (Sheppard, 2010).

In addition to the pollution sources mentioned above, desalination technology has also contributed to estuarine environmental problems. Desalination refers to any of several processes that remove some amount of salt and other minerals from saline water, in order to produce fresh water suitable for human consumption or irrigation. Along with recycled wastewater, this is one of the few rainfall-independent water sources. However, the process of desalination is not by itself environmentally friendly and seawater desalination plants also contribute to the wastewater discharges that affect coastal water quality. This is mostly due to the highly saline brine that is discharged into the sea, which may be increased in temperature, contain residual chemicals from

pre-treatment processes, heavy metals from corrosion or intermittently used cleaning agents etc. The effluent from desalination plants is a multi-component waste, with multiple effects on water, sediment and marine organisms. Improvements in the knowledge on how desalination technology has increased the pollution should be encouraged, especially on how heat and brine aretransported and how to deal with these pollutants.

The health and environmental impact of the pollution problems in estuaries have raised concerns on how estuaries are treated. Efforts such as wastewater treatment plant developments, contamination reduction, prevention of contaminant spills, and cleaning up of contaminants have been undertaken in many places around estuarine areas. Another effort to maintain the quality of life around estuaries has been to develop the waterfront, that is, an area or city specifically designed along estuarine banks with the water environment as the developmental focal point. Waterfronts generally include any property that is adjacent to a water body, be it an ocean, lake, river or stream. Waterfront developments and redevelopments have been a topical issue since the 1970s, when Baltimore, Maryland, began its redevelopment project, converting old, underused waterfront properties into economically viable space. Numerous other large and small scale developments have been undertaken since then, in such glamorous cities as Sydney, Australia, and London, and in small towns, such as Portland, Michigan and Grand Haven (Ryckbost, 2005) and Cardiff.Wood and Handley (1999) stated that water quality improvements are a necessary precursor to waterfront revitalizations worldwide. Water quality parameters which are key in revitalizing waterfronts include (Connor, 2006): aesthetic aspects (i.e. turbidity and colour), dissolved oxygen, pathogens, regionally significant species(species that are considered to be an important component of the natural communities in the region, for example salmons, herrings, ducks etc.) and ecosystem services. Development and redevelopment of waterfronts have therefore encouraged the improvement of water quality in estuaries. In this regard studies on the hydrodynamic and water quality characteristics in waterfronts are important to evaluate the effect of waterfront developments on water quality and to maintain the quality of water in the region. In

particular, the study on the transport of pollutant is important in waterfront developments to ensure that waterfront developmentslead to improvementsin the quality of the water.

1.3 Estuary and Its Interaction with Groundwater

Among the important aspects of estuarine studies is the interaction between the estuary and the surrounding groundwater. For many decades, the influence of groundwater on the coastal water environment, and *vice versa,* has drawn considerable attention of researchers and environmental engineers. The coastal groundwater table fluctuates with the tide in coastal areas. Firstly, the groundwater table fluctuation can directly affect beach stability. During flood tides, the peak seawater level is higher than the beach groundwater and flow intrudes into the unconfined aquifer. During the ebb tide, the groundwater hydraulic gradient will expel water from the coastal unconfined aquifer. The seepage and inflow fluctuations can significantly influence the stability of sediment transport along the beach. When the groundwater table is higher than the average sea water level, the beach is eroded easier. Contrarily, if the groundwater table is lower than the average sea level, then sediment generally deposits on the beach. Secondly, the groundwater fluctuation can directly affect water exchange and substance movement between the seawater and groundwater.

In this study the interaction of groundwater and surface water is explored in relation with how dispersion occurs in the system. This is important for practical purposes. For example, if waste is generated from a cattle farm, it may infiltrate into the ground and then to the groundwater. From the groundwater it can enter the estuary and then finally to the sea. Therefore any pollution in the groundwater may affect the quality of riveror estuary water connected to it. It is understandable that the rate of dispersion is different between the groundwater and surface water, since there are solid particles in the groundwaterwhich make dispersion lower than it is in surface waters. A study which involves dispersion in both groundwater and surface water will therefore help understand dispersion processes in the whole system, including groundwater and

surface water. This will in turn help the management of pollution in more effective way.

Rivers generally interact with groundwater in four basic ways (Winter et al., 1998):

(1) Rivers can gain water from inflow of groundwater through the streambed (gaining from the stream);

(2) They can lose water to groundwater resources by outflow through the streambed (losing from the stream);

(3) They can experience both, gaining in some reaches and losing in other reaches, or both gain and lose in the same reach at different river flow levels etc.;

(4) Groundwater extraction can cause the hydraulic gradients to fluctuate during the irrigation season by lowering the water table and reversing flow directions, such that a flow gaining stream becomes a flow losing stream.

Each type of groundwater-surface water interaction affects the transport of pollutants in both systems. For example, for a gaining stream, the pollutant coming from the groundwater will be transported in the river and finally the estuary, while in the losing stream the pollutant coming from the river will be transported to the groundwater. The knowledge of the interaction nature is therefore important to study pollutant transport and dispersion between these two water bodies.

Limited studies have been carried out on how pollutants are transported in the surface-groundwater system, while this is an important topic without which pollutant transport can only be studied separately and hence not be explained according to its true nature. In this regard a part of this study is allocated to the nature of surface water and groundwater interaction and how it affects the pollutant transport and dispersion as a whole.

Severn Estuary as The Case Study

The Severn estuary is the estuary of the river Severn, which is the longest river in Great Britain. The estuary also forms the mouth of four major rivers, including the Severn, Wye, Usk and Avon and a number of other smaller rivers. The border of the estuary stretches from the estuary up beyond Aust upstream, which corresponds to the site of the old Severn Bridge. The estuary is about 2 miles (3.2 km) wide at Aust, and about 9 miles (14 km) wide between Cardiff and Weston-super-Mare (see Fig 1.1).

Fig. 1.1 Map of Severn Estuary

(Source: Severn Estuary Partnership)

With a length of 354 km and flowing past major cities, such as Avonmouth (near Bristol), Cardiff, and Gloucester, the catchment of the river (which is 11,420 km^2) is mainly (about 80%) managed for agriculture and forestry. TheSevern basin districtcontains important habitats and wildlife areas, including 28 Special Sites of Conservation and five special protection areas. A special protection area (SPA) is a designation under the European Union Directive on the Conservation of Wild Birdswith features that depend on the water and its quality. Besides, the Severn River Basin District is home to over 5.3 million people and covers an area of

21,590 km^2.The area surrounding the estuary is also designated as a wetland of national and international importance. Quality wise, in 2009 the river Severn was judged to have about 29% of its water body of at least good ecological status/potential, and 37% of its water body was at least of good biological status.

The main causes of not achieving the expected quality are, among others: diffuse source inputs from agriculture, point source inputs from industry sewage works etc.; physical modification barriers to fish migration; physical modification in the form of urbanization; physical modifications due to land drainage; and physical modifications due to flood protection barriersetc.

In order to improve the conditions in the river/estuary, management actions have been planned by the government, including involvement from the following communities and stakeholders: agricultural and rural land managers; angling, fisheries and conservation groups; central government; the environmental agency; industry, manufacturing and other businesses; local and regional government; mining and quarrying industries; navigation communities (including ports); urban and transport; water industry; and individuals and communities.

This study takes the Severn Estuary as its case study; that is, it used a physical model of the estuary as its representation. A study of the hydrodynamic and dispersion processes in this physical model, along with the computer model predictions, was used to give a description on how the two processes happen in the estuary and therefore expected to give a contribution on how to manage the estuary.

1.4 Mixing and Dispersion in Estuaries

1.4.1 Mixing

The transport of pollutants in an estuary is related to the mixing process. There are many factors affecting mixing in estuaries, including small scale diffusion and larger scale variations across the basin in the advective mean velocities (Fischer et. al., 1979). Turbulent diffusion serves to transfer mass between stream lines, while

longitudinal dispersion comes about mainly because of the flow along different stream linesgoing at different speeds. The difference between the turbulence and advection is as follows: If the current meter is held at a fixed point in an estuary and a long record is examined, spectral analysis can disclose fluctuations with a wide range of period. Fluctuations with a period of less than a few minutes can be identified as turbulence, and the transport resulting therefrom can be termed diffusive transport. The term "advection" can then be assigned to the remaining motion. The advective velocity is not constant, neither in time, space, or direction. The velocity record obtained at a single point will contain semidiurnal and diurnal tidal variations, wind-induced variations of almost any period, aninertial frequency caused by the earth's rotation, and tributary inflows. The direction of the velocity vectors will often not be parallel to the channel axis, even if one can be defined. Often the flow is going in different directions at different depths; often the flow is one way near the shore and the opposite way in the centre of the channel. Obviously, the analysis of mixing in terms of the interaction of advection and diffusion is much more complicated in estuaries than in rivers, due to tidal action and large scale gravitational circulation associated with salinity intrusion in estuaries (Jabbari, 2006).

Most of mixing process in estuarycan be related to one of three sources, namely the wind, the tide, and the river. Most of the analysis to be found in the engineering technical literature discusses the effect of only one or at most two sources, for example the current driven by the wind in a tideless bay or the circulation driven by the river inflow in a tideless estuary.

1.4.2   Dispersion

Dispersion is the movement of particles by the mean velocity distribution or velocity shear. Dispersion is of fundamental importance to life in the sea, as this is the way by which essential substances are widespread in the sea and how the pollutants are diluted in the sea. For example, ammonia excreted by fish would be toxic to aquatic life if it was not mixed and diluted with the surrounding waters (Lewis, 1997).

On occasions, the dispersive processes are not sufficient to ensure adequate dilution and, in the case of nutrients, a build-up may lead to excessive growth of planktonic algae, producing a 'bloom'. Some algal blooms are toxic to fish and when the algae die off, they form blankets on the seabed which can suffocate benthic animal communities.

Fluid mechanics related to the effects of stratification is a sound basis for understanding the mechanisms observed in the sea, including dispersion. It is important to have a background in the way in which turbulence is related to the spreading of a substance. Dispersion is the mechanism in which the combined influence of turbulence and spatial variations in the mean velocity enhances the process of dilution (Lewis, 1997).

Dispersion accounts for the effects of spatial differences in velocities (either primary or secondary) over the channel cross-section and is countered by the effects of diffusion, usually dominated by turbulent diffusion. In most open channel flows, longitudinal dispersion is the dominant process by several orders of magnitude (Boxall, 2007). The rate of spreading of a substance under given conditions of velocity shear and vertical mixing can be quantified in terms of a dispersion coefficient.

The selection of the dispersion coefficient value is very important in water quality modelling. Inaccuracies in determining the dispersion coefficient value can result in underestimating or overestimating the pollutant concentration, and hence can affect many engineering designs, such as:
- inappropriate design of wastewater treatment plant;
- improper design of water supply plants, which are based on an assumed certain quality of raw water in the stream;
- inaccurate evaluation of water quality in relation to water resource management.

Various previous studies have proposed variable dispersion coffecicient, which is the function of water depth and shear velocity. Theoretically, the dispersion coefficient is

a variable, as will be described in the next chapter. However, for practical reasons several commercial models have generally treated the dispersion coefficient as a constant.The effect of predicting this coefficient inaccurately may, nevertheless, result in problems as mentioned above (e.g. the inappropriate design of wastewater treatment plants etc.)

The present study will focus on the development of the dispersion coefficient selection, especially comparing constant and variable dispersion representations. It is expected from this study that the selection of a dispersion coefficient is carefully undertaken.

1.5 Computer and Physical Modelling

In pollution studies, including estuarine pollution, computational techniques have helped improve our understanding of pollutant transport (through modelling studies of various processes)and have led to improved predictive accuracy in the degree and extent of pollution. The technique involves developing numerical schemes for solving the governing equations for the hydrodynamic and water quality processes in estuarine basins.

In particular, water quality modelling involves the prediction of water pollution using mathematical simulation techniques. A typical water quality model consists of a collection of formulations representing physical mechanisms that determine the mass and momentum conservation of a fluid package and any pollutants in a water body.

On the other hand, physical hydraulic models have been used historically to investigate the design and operation issues in hydraulic engineering, and to study water problems in the aquatic environment, including estuaries. The advantage of physical models is that can represent fine grid scale processes which are not easy to be described by mathematical models, due to the complexity of the processes and the lack of knowledge of these processes(Sassaman et al., 2009). Physical models can therefore describe the processes more accurately for controlled conditions, with numerous data provided through experiments which involve a range of parameters

thatcan be studied in some detail. For example, the diverse situation of local scour of alluvial bed sediments around piers, submerged pipelines, and other hydraulic structures comprising a set of situations for which physical models have been the main means to obtain substantial insight and engineering design recommendations. Physical modelling of water intake performance comprises another set of situations in which great reliance is placed on hydraulic modelling (ASCE, 2000).

However, there are shortcomings with physical models, which are usually termed *scale effects* and *laboratory effects.* The former term describes the incomplete satisfaction of a full set of similitude criteria associated with a particular situation. Scale effects increase in severity as the ratio of the prototype to model size increases or the number of physical processes to be replicated simultaneously increases. Laboratory effects arise because of limitations in space, model constructability, or instrumentation impeding the acquisition of precise measurements. They may also arise from incorrect replication of boundary conditions (ASCE, 2000). Large physical models can also be expensive to maintain and operate. They occupy extensive laboratory space, may have to be retained for many years as a project evolves, and many deteriorate with frequent wetting and drying.

Considering the advantages and disadvantages of each type of model (i.e. computer and physical models), integrated modelling may be most effectively undertaken using a physical model in combination with a numerical model, utilizing the strengths of both modelling methods as discussed earlier. The combined use of the two modelling methods may have the following potential advantages:

- Component processes of a complex flow situation can be investigated using the best-suited method; and
- Costs of maintenance and operation of a large physical model may be reduced.

The physical model may be better suited for investigating complex local flow and transport processes, whereas the numerical model may be more suited to investigating processes occurring over longer distances and over long time periods.

This combination can minimize modelling costs from retaining a physical model for a long period or by using it for numerous repetitive tests. A physical model can also be used to develop and calibrate a numerical model, which is then used to carry out the majority of tests in a study, with the hydraulic model being used only for limited studies. In most cases, the numerical model then remains available for further subsequent tests (ASCE, 2000).

In considering the advantages of such a combination, the present study has involved both physical and computer models, where the experimental results from the physical model were used to calibrate the computer model with particular emphasis on replicating the hydrodynamic and dispersion processes.

1.6 Importance of Bathymetric Data and Boundary Conditions

The efficacy of modelling work depends on how accurate the model can replicate the corresponding processes in nature. In order to improve the level of model accuracy, it is common to adjust the model with such parameters as the Manning's bed roughness coefficient, the eddy viscosity coefficient, and the momentum correction coefficient by testing severalvalues of these parameters until the model approaches the corresponding experimental data.

However, a key input data set which is often overlooked but also governs the accuracy of any modelling work are the bathymetric data. The bathymetric data are often accepted without question when modelling work is to be carried out. Using bathymetric data without checking its accuracy and then calibrating the computer model with the experimental data can be misleading and can result in false conclusions about the modelling results. This may also arise through the use of bathymetric gridgeneration algorithms, where the data is smoothed to provide depths at the relevant grid nodes. However, such smoothing algorithms can often effectively move significant sub-grid scale bathymetric variations etc. In combined physical-computer model studies, it is particularly important to have the correct bathymetric data and to ensure that the bathymetry of the physical and computer models are the

same or at least close. The design of the physical model is based on the bathymetric data taken from bathymetric survey, and the same data are used in the computer model for the same location. However, limitations in the construction of the physical model may have caused some deviations from the raw data, while the representation of the bathymetric data in the computer model depends upon the grid size etc. As a result the bathymetry between the computer and physical models may be different and therefore the measurement and the modelling results may also not always be expected to match. It is therefore important to make sure that the bathymetric data of the physical and computer models are as close as possible. After the construction of the physical model, the bathymetry should be re-measured and the actual bathymetry of the physical model should be used in the computer model.

In this study a part of the work is intended to show the importance of using the correct bathymetric data in both modelling tools for good comparisons between the respective results.

Other input data are the boundary conditions which affect the model performance. These data can be of various kinds, including:

- Water level data
- Discharge data
- Velocity data

This study will show how the boundary condition accuracy can affect the accuracy of the model predictions. This is done by comparing the performance of the model using simulated boundary conditions, which includeswater levels obtained from a sinusoidal function, and using water level data measured in the seaward boundary of the physical model.

1.7 Aims of The Thesis

From the above description about the opportunities and challenges in estuaries the understanding of dispersion process is an important consideration for helping maintain and improve water quality in estuarine basins. This understanding can give correct

information about water pollution and in turn help make strategies for water quality protection. For example, correct information of dispersion process will be useful in planning of wastewater treatment plant, and will give information of how pollutant spread and to what extent. The key of predicting dispersion processes is the correct determination of the dispersion coefficient, which indicates how fast dispersion occurs. This will be determined by the following steps:

1. Carrying out experiments in order to obtain the hydrodynamic and dispersion data. For this case the hydrodynamic data obtained includes: water levels and velocities, and the data for dispersion studies is based primarily on dye tracing.

2. Setting up the computer model and fitting the computer model to the physical model.

3. Modelling of hydrodynamic and dispersion processes before bathymetry data refinement. This is done by comparing the water level and velocity data between the computer model and the physical model. In this step the calibration of the model was also done in order to fit the computer model to the physical model.

4. Refining the bathymetry data. This is done in the middle of the study, which enables a comparison to be undertaken of the model performance before and after the bathymetry refinement.

5. Modelling hydrodynamic and dispersion after refining the bathymetry data. This is simply repeating the work of item 4 with the new bathymetry data.

6. Carrying out experiments and model analysis for the groundwater basin. This is done to collect data related to the hydrodynamic and dispersion in groundwater and use it to model the dispersion process in such flow fields. The aim of this experiment is to show the dispersion process in groundwater as a linked system with the surface water, in this case the estuary.

1.8 Structure of The Thesis

The present study has been written up with the following structure:

Chapter 2 consists of a literature study, which provides the theoretical basis of this study, including hydrodynamics in surface water and groundwater, dispersion in surface water and groundwater, estuary-groundwater interactions, and bathymetry refinement using the PIV method.

Chapter 3 describes the computer model, including: the governing equations of motion, the depth integrated hydrodynamic and solute transport equations and the numerical solution procedure.

Chapter 4 describes the experimentation methods, including the Severn estuary physical model, the groundwater physical model, the water level and velocity measurements, and the dispersion experiments.

Chapter 5 elaborates on the study results for the hydrodynamics in the estuarine physical model, including the experimental and modelling results.

Chapter 6 details the study results for dispersion in the estuarine physical model, including the experimental and modelling results.

Chapter 7 presents the study results for the hydrodynamic and dispersion processes in the groundwater and the corresponding process interactions with the estuary.

Chapter 8 offers conclusion and recommendations for further studies.

CHAPTER 2
LITERATURE STUDY

2.1 General

Studies on dispersion have been long carried out, with Taylor's (1953) being regarded one of their pioneers. These studies were mainly concerned with the determination of the dispersion coefficient which is the main measure of the process. Results of those studies indicated that dispersion coefficient depended on several factors, including velocity profiles, bed roughness, cross-sectional shape of the channel, bends, and width-to depth ratio.

Those studies were carried out by laboratorial works, field survey, analytical methods, or model development. Very limited amount of those studies were delivered in physical model, while physical model is considered useful, understandable, schematic representation of a piece of reality (Han, 2013). The advantages of using physical model have been described in Chapter 1. The present study is therefore attempting to establish other approach in determining the dispersion coefficient, which is by using physical model combined with computer model.

This approach compares the computer model with the physical model while treating the physical model as the ground truth. This means that unlike previous studies which focused on certain parameter/parameters which affect dispersion, the present study is attempting to find the dispersion coefficient by calibrating the computer model against the physical model.

Specific work is aimed to compare variable dispersion coefficient with constant dispersion coefficient. The reason for that is that field, the use of constant dispersion coefficient is common due to practical reason i.e. does not need to account for many parameters. However, this may be misleading because the results may be very

different with the results using variable dispersion coefficient. It has been described in the previous chapter, the difference may be significant and it can affect both technically and economically.

2.2 Mixing

Mixing in estuaries results, as it does in rivers, from a combination of small scale turbulent diffusion and a larger scale variation of the field of advective mean velocitities. In rivers the combination is fairly simple; the advective velocity field defines a set of approximately steady stream lines. The main role of turbulent diffusion is to transfer mass between stream lines, and longitudinal dispersion comes about mainly because the flow along different stream lines is going at different speeds. In estuaries mixing can be also described in terms of advection by a mean flow along stream lines and turbulent diffusion between stream lines, but matters are nowhere near as simple as in rivers. The first problem is to differentiate diffusion from advection. If a current meter is held at a fixed point in an estuary and a long record is examined, spectral analysis can disclose fluctuationds with a wide range of period. Fluctuations with a period of less than a few minutes can be identified as turbulence, and the transport resulting therefrom can be termed diffusive transport, just as we have done in rivers. The term "advection" can be assigned to the remaining motion. The advective velocity is not constant, however, either in time, space, or direction. The velocity record obtained at a single point will contain semidiurnal and diurnal tidal variations, wind-induced variations of almost any period, an inertial frequency caused by the earth's rotation, and fluctuations of longer periods caused by the monthly and longer term variation of the tidal cycle and by seasonal variations of meteorological influences and tributary inflows. The direction of the velocity vector will often not be parallel to the channel axis, even if one can be defined. Often the flow is going in different directions at different depths; often the flow is one way near the shore and the opposite way in the center of the channel. Obviously, the analysis of mixing in terms of the interaction of advection and diffusion is much more complicated in estuaries than in rivers.

The proper way to begin seems to be make things as simple as possible by considering different mechanisms in turn. Most of what is seen in an estuary can be related to one of three sources, the wind, the tide, and the river. Most of the analysis to be found in the engineering technical literature discuss the effect of only one or at most two sources, for example the current driven by the wind in a tideless bay or the circulation driven by the river inflow in a tideless estuary.

Mixing in estuaries is affected by 3 factors:

1) Wind:wind is usually the dominant source of energy in large lakes, the open ocean, and some coastal areas. But in estuaries it may or may not play a major role.

2) Tide: the tide generates mixing in two ways. Friction of the tidal flow running over the channel bottom generates turbulence and leads to turbulent mixing, and the interaction of the tidal wave with the bathymetry generates larger scale with currents.

3) River flow: The river, or rivers if more than one enters the same estuary, delivers a discharge of fresh water. Analytical and laboratory studies usually assume that all the fresh water passing a given section comes from a single upstream source. The complications that arise when a number of rivers supply fresh water around the periphery do not change the qualitative description of how fresh water affects mixing and it is usually preferred to to concentrate on what is known of the effect of a single source.

2.3 Dispersion and Diffusion in Surface Water

2.3.1 Early research

Taylor's work (1953) on diffusion is regarded the first significant research on dispersion. He introduced a concept of the longitudinal dispersion coefficient for longitudinal mixing in a straight circular tube in a turbulent flow. He derived his equation theoretically to give:

$$k = \frac{a^2 u_o}{192\,D}\,(2.1)$$

where k = diffusion coefficient, u_o = maximum velocity at the axis, a = pipe radius, and D = molecular diffusion coefficient.

For turbulent flow in a pipe, the equation can be written as:

$$k = 10.1\,a.\,u_*(2.2)$$

where u_* = shear velocity = $(\frac{\tau_o}{\rho})^{1/2}$ and τ_o = friction stress exerted by the turbulent fluid of density ρ on the pipe wall.

In 1959, Elder extended Taylor's analysis to describe the diffusion of marked fluids in the turbulent flows in open channels. He derived a dispersion equation assuming a logarithmic velocity profile and that the mixing coefficients for momentum transfer and mass transfer in the vertical direction were the same.

The equation derived by Elder is given as:

$$K_x = 5.93\,hu_*(2.3)$$

in which K_x = longitudinal dispersion coefficient, h = the depth of flow, and u_* = shear velocity.

2.3.2   Dispersion in natural streams and rivers

Applications of Taylor's method for determining the dispersion coefficient in the laboratory and natural rivers were carried out by Fischer (1966). He concluded from both laboratory and flume experiments that in a three-dimensional flow the dominant mechanism for dispersion was the lateral velocity variation.

Using the lateral velocity profile instead of the vertical velocity profile, Fischer then obtained an integral relationship for the dispersion coefficient in natural streams having large width-to-depth ratios. The result was given as:

21

$$K_x = -\frac{1}{A}\int_0^B hu' \int_0^y \frac{1}{\varepsilon_t h}\int_0^y hu' dy\, dy\, dy \quad (2.4)$$

in which $h = h(y)$ depth, $u' =$ deviation of the velocity from the cross-sectional mean velocity, $W =$ channel width, $A =$ cross sectional area, $y =$ Cartesian coordinate in the lateral direction, and $\varepsilon_t=$ transverse turbulent diffusion coefficient.

Eq. (2.4) is rather difficult to use because detailed transverse profiles of both velocity and cross-sectional geometry are required. As a result, Fischer (1975) developed a simpler equation by introducing an approximation of the triple integration, velocity deviation, and transverse turbulent diffusion coefficients. The result equation gives:

$$K_x = 0.011\,\frac{U^2 B^2}{h u_*} \quad (2.5)$$

where $U =$ mean longitudinal velocity, and $B =$ channel width.

Eq (2.5) has the advantage of simplicity in that it can predict the dispersion coefficient by using only the data of cross-sectional mean parameters, which are easily obtained for a stream.

A simple equation of the dispersion coefficient was developed by McQuivey and Keefer (1974) using the similarity between the 1D solute dispersion equation and the 1D flow equation. They initially derived an equation which related the longitudinal dispersion coefficient and the flow dispersion coefficient. Then, by applying a linear least-squares regression of the field data, they derived an empirical equation for the longitudinal dispersion coefficient as follows:

$$K_x = 0.58\left(\frac{h}{u_*}\right)^2 UB \quad (2.6)$$

An equation for the dispersion coefficient was also derived by Koussis and Rodriguez-Mirasol (1998) using the original theory and the equation proposed by Fischer (1967), and applying von Karman's defect law. The equation derived is given as:

$$K_x = \Phi \frac{u_* B^2}{h} \quad (2.7)$$

They proposed a value of 0.6 for Φ and obtained this value by applying a regression analysis of 16 field data sets. They compared their model with Fischer's model (i.e. Eq. (2.5)) and postulated that the results obtained from their equation were closer to the measured data.

Using dimensional analysis and regression analysis, Seo and Cheong (1998) derived an equation for the longitudinal dispersion coefficient. They used the one-step Huber method in analysing 59 data sets, measured in 26 rivers in the USA. They used 35 of these measured data sets to establish their equation and then verified it against other data sets. Their equation can be written as:

$$K_x = 5.92 \left(\frac{U}{u_*}\right)^{1.43} \left(\frac{B}{h}\right)^{0.62} h u_* \quad (2.8)$$

Hunt (1999) used a similarity technique to find an analytical solution to the one-dimensional equation in which the dispersion coefficient was linearly proportional to the distance downstream of an instantaneous point source. He compared his solution with the results obtained using the constant coefficient model,and the dead-zone model of Hays (1966) against the field data of Day and Wood (1976) and Day (1977). Hunt's comparisons considered the attenuation of the peak concentration, the variance of the concentration distribution, and a dimensionless concentration distribution obtained by Day and Wood (1977a, b). Hunt concluded that in all cases the variable dispersion coefficient model provided a much more accurate description of the experimental results.

Deng et al (2001) also developed an analytical method to determine the longitudinal dispersion coefficient in Fischer's triple integral expression for natural rivers. The method was based on the hydraulic geometry relationship for stable rivers and on the assumption that the uniform-flow formula is valid for local depth-averaged variables. For straight alluvial rivers, they derived a new transverse profile equation for channel

shape and a local flow depth and then determined the lateral distribution of the deviation of the local velocity from the cross-sectionally averaged value.

The transverse profile equation is given as:

$$u' = \left[\alpha (1 - \xi^\beta)^{2/3} \left(\frac{\beta+1}{\beta} \right)^{2/3} - 1 \right] U \quad (2.9)$$

where α = revision coefficient accounting for the difference between the flow depth and hydraulic radius satisfying the following constant:

$$\int_0^B h'_u dy = 0 \quad (2.10)$$

in which ξ = dimensionless lateral coordinate = y/b, β = channel shape parameter, and u' = deviation of local depth mean velocity from the cross-sectional mean velocity

This equation describes the lateral distribution of the deviation of the velocity u(y) from the cross-sectional mean velocity.

The study of Deng will be used in this study in terms of: transverse profile equation, dispersion equation, etc.

The suggested expression for the transverse mixing coefficient equation and the direct integration of Fischer's triple integral were employed to determine a new theoretical equation for the longitudinal dispersion coefficient. By comparing 73 sets of field data and the equations proposed by the other investigators, Deng et al. postulated that the derived equation containing the improved transverse mixing coefficient predicted the longitudinal dispersion coefficient for natural rivers more accurately.

The equation obtained is as follows:

$$\frac{K_x}{H u_*} = \frac{0.15}{8 \varepsilon_{t0}} \left(\frac{B}{H} \right)^{\frac{5}{3}} \left(\frac{U}{u_*} \right)^2 \quad (2.11)$$

where: ε_{t0} = transverse mixing coefficient.

The study of Fischer will be used in this study, in regards with: dispersion coefficient used and method of determining the dispersion coefficient.

Kashefipour and Falconer (2002) also developed an equation for predicting the longitudinal dispersion in riverine flows, based on 81 sets of measured data, and obtained from 30 rivers in the USA. This equation relates the dispersion coefficient to the hydraulic and geometric parameters of the flow and was derived using dimensional and regression analysis. The equation obtained is given as:

$$K_x = 10.612 \left(\frac{U}{u_*}\right) hU \quad (2.12)$$

They then compared their model with the other models, including the models of Seo and Cheong (1998), Mc Quivey and Keefer (1974), and Koussis and Mirasol (1998), and found that accuracy of their model compared favorably with the other models.

Estimation of the longitudinal dispersion coefficient was also carried out by Ahsan (2008) in small segments of natural streams. He compared four different models for dispersion, and then applied those equations to several data in the literature and selected the most appropriate model.The expression suggested byDeng et al (2001) was then found to perform better than other models. It has a distinguishingfeature that it involves the effect of transverse mixing andtherefore it clarifies its dispersion mechanism.

2.3.3 Estimation of dispersion coefficient using hydraulic parameters

The effects of cross-sectional shape and velocity distribution on the dispersion coefficient were studied by Sooky (1969). Assuming a logarithmic velocity profile and power-function velocity profile, he developed a dimensionless dispersion equation as the function of the width-to-depth ratio for a uniform flow in straight open channels for which the cross sections were triangular and circular.

Through the analysis of the field data of Godfrey and Frederick (1970), Sooky showed that the dimensionless dispersion coefficient increased as the width-to-hydraulic

radius ratio increased. However, this work did not describe the natural dispersion in real streams adequately because the equation was derived assuming a uniform channel cross section.

Bansal (1971), using dispersion data obtained from the U.S. Geological Survey, also demonstrated that the dimensionless dispersion coefficient increased as the width-to-hydraulic radius ratio increased.

A study on the longitudinal dispersion of a buoyant contaminant in a shallow channel was carried out by Smith (1976). He derived a nonlinear diffusion equation for a longitudinal dispersion of a buoyant pollutant in a slowly varying current. The essential simplifying feature was that the water depth was assumed to be much smaller than the channel width. It was found that for small concentration gradients there was a transverse circulation which led to a marked reduction of the longitudinal dispersion. For large concentration gradients the longitudinal circulation predominated and the longitudinal dispersion increased.

The effect of the width-to-depth ratios on the dispersion coefficient in rectangular channels was carried out by Chatwin and Sullivan (1982). They determined analytically the dispersion coefficient for a laminar flow, and expanded it for turbulent flows in a flat-bottomed channel of large width-to-depth ratio. However, in practice, it is difficult to use their method for predicting the dispersion coefficient, because detailed information on the velocity profile and cross sectional geometry were required to calculate the dispersion coefficient.

The dependence of the longitudinal dispersion on the width-to-depth ratio was also examined by Asai and Fujisaki (1991) using the k-ε model. They showed that the dispersion coefficient increased as the width-to-depth ratio increased up to 20; as the width-to-depth ratio increased further, the dispersion coefficient tended to decrease.

Iwasa and Aya (1991) also derived an equation to predict the dispersion coefficient in natural streams and canals by analyzing their laboratory data and previous field data collected by Nordin and Sabol (1974) and others. The resulting equation is given as:

$$K_x = 2.0 \left(\frac{B}{h}\right)^{1.5} hu_* \quad (2.13)$$

Because natural streams are sinuous and have sudden contractions, expansions and dead zones of water, the dispersion coefficient of the natural streams tends to increase compared with that of the simple and straight open channels. Thus, the effects of canal and flume data in the derivation of Eq. (2.14) cause the equation to underestimate the natural stream dispersion coefficient.

A series of laboratory experiments to obtain the magnitude of the longitudinal dispersion coefficient was carried out by Guymer (1998). The experiments were conducted on a large scale channel with a sinuous plan-form geometry to obtain the magnitude of the longitudinal dispersion coefficient. He studied a constant trapezoidal cross-section and a variable cross-sectional "natural" shape under different discharges. Temporal concentration distributions recorded for the trapezoidal section tended towards a Gaussian form and provided values of a longitudinal dispersion coefficient comparable with those obtained for previous similar studies. The more "natural" cross-sectional geometry channel exhibited strongly skewed distributions and increased the value of the longitudinal dispersion parameter by over 150%. Guymer observed a variation of the longitudinal dispersion coefficient with discharge and explained that it was the effects of the longitudinally varying cross-sectional shape.

Swamee et al. (2000) presented investigations on the longitudinal dispersion of a solute injected from an outfall source into a channel. By assuming logarithmic and exponential equations for mass-time curve, they derived an equation for calculating solute concentrations at any point of a river in the downstream reach of an originating source. They defined several dispersion parameters and related those parameters to the flow properties and channel geometry using dimensional analysis.

Using a new channel shape equation for straight channels and a more versatile channel shape equation for natural streams, Deng et al. (2002) developed a method for predicting the longitudinal dispersion coefficient in single-channel natural streams.

Those streams included straight and meandering geometries. The method involved derivation of a new triple integral expression for the longitudinal dispersion coefficient and development of an analytical method for the prediction of this coefficient for natural streams. They verified the proposed method using 70 sets of field data collected from 30 streams in the United States, ranging from straight manmade canals to sinuous natural rivers. The new method predicts the longitudinal dispersion coefficient, where more than 90% of the calculated values range from 0.5 to 2 times the observed values.

A series of experiments in three self-formed channels with known discharges was carried out by Boxall and Guymer (2007) in order to investigate longitudinal mixing. The channels were operated at various flow rates within each of the channels by monitoring the development of tracer plumes during transit through the channels. Using an optimization procedure, they found that coefficients required for the solution of the one-dimensional advection dispersion equation (1D-ADE) were in the range of 0.02-0.2 m^2/s. They found that the coefficients varied as functions of the longitudinal meander location, channel form and discharge. They made predictions of these longitudinal mixing coefficients using a mathematical technique requiring only channel form properties and flow rate as inputs. Predicted values were typically within 20% of the measured values, although deviation of up to 50% was found for the lowest discharges in each channel. They assumed that this large error was likely to have been caused by increased dead zone effects, associated with channel bathymetry at low discharges that were not captured by the method.

Sooky (1969) studied the effect of cross-sectional shape on velocity distribution on the dispersion coefficient, Godfrey and Frederick (1970) studied the effect of width-to-hydraulic ration on the dimensionless dispersion coefficient, Bansal (1971) also studied the effect of the width-to-hydraulic radius ratio on the dimensionless dispersion coefficient, Smith (1976) studied the longitudinal dispersion of a buoyant contaminant in a shallow channel, Chatwin and Sullivan (1982) studied the effect of width-to-depth ratios on the dispersion coefficient in rectangular channels. Smith (1983) also obtained a general expression for the longitudinal dispersion coefficient

for a passive contaminant in varying channels. Asai and Fujisaki (1991) examined the dependence of the longitudinal dispersion in the width-to-depth ratio using the k-ε model. Iwasa and Aya (1991) also derived an equation to predict the dispersion coefficient in natural streams and canals. Guymer (1998) carried out a series of laboratory experiments to obtain the magnitude of the longitudinal dispersion coefficient. Swamee et al. (2000) investigated the longitudinal dispersion of a solute injected from an outfall source into a channel. Deng et al. (2002) developed a method for predicting the longitudinal dispersion coefficient in single-channel natural streams. Boxall and Guymer (2007) carried out a series of experiments in three self-formed channels with known discharges in order to investigate longitudinal mixing.

2.3.4 *Effects of velocity distribution on dispersion*

Liu (1977) derived a dispersion coefficient equation using Fischer's equation (Eq. 2.5), taking into account the role of lateral velocity gradients in the dispersion in natural streams giving:

$$K_x = \beta \frac{U^2 B^2}{h u_*} \quad (2.14)$$

in which β is a parameter that represents a function of the channel cross section shape and the velocity distribution across the streams.

He suggested that the parameter β could be determined by considering sinuosity, sudden contractions and expansions, and dead zones in the natural stream. By least-square fitting to the field data obtained by Godfrey and Frederick (1970) and others, he deduced the following expression:

$$\beta = 0.18 \left(\frac{u_*}{U}\right)^{1.5} \quad (2.15)$$

He postulated that the maximum deviation of the field data from the prediction values by using his equation was less than six fold.

Seo and Baek (2004) developed a theoretical method for predicting the longitudinal dispersion coefficient based on the transverse velocity distribution in natural streams. Among the velocity profile equations tested in this study, the beta distribution equation, which was a probability density function, was considered to be the most appropriate model for explaining the complex behaviour of the transverse velocity structure of irregular natural streams. They developed a new equation for the longitudinal dispersion coefficient that was based on the beta function for the transverse velocity profile. The equation is:

$$K_x = \gamma_1 \frac{U^2 B^2}{h u_*} \quad (2.16)$$

where γ_1 is a variable which depends on cross stream geometry and transverse mixing.

2.3.5 Effect of transverse mixing coefficient on dispersion

Deng et al. (2001) suggested an expression for the transverse mixing coefficient and used it to derive an expression for a longitudinal dispersion coefficient through direct integration of Fischer's triple integral. They derived the following expression:

$$K_x = \frac{0.15}{8 \, \varepsilon_t} \left(\frac{U}{u_*}\right)^2 \left(\frac{B}{h}\right)^{1.67} h u_* \quad (2.17)$$

where

$$\varepsilon_t = 0.145 + \frac{1}{3520} \left(\frac{U}{u_*}\right) \left(\frac{B}{h}\right)^{1.38} \quad (2.18)$$

Eq. (2.18) has a distinguishing feature in that it includes the effects of transverse mixing and therefore it clarifies the dispersion mechanism.

2.3.6 Effect of bed surface and side roughness on dispersion

Abd El-Hadi and Daver (1976) related the longitudinal dispersion coefficient to parameters such as bed roughness and other hydrodynamic characteristics of channel flows. They performed experiments in a recirculating flume with different bed

roughness simulations, and reported that the dimensionless dispersion coefficient was a function of both relative roughness height and the relative roughness spacing. They also showed that the relation between K and hu_* was clearly nonlinear beyond values of about 0.009 m^2/s for hu_*.

The effect of a large-scale bed and side roughness on dispersion was studied experimentally by Magazine et al. (1988). They derived an empirical predictive equation for the estimation of the dimensionless dispersion coefficient using roughness parameters of the channel, such as the Reynolds number, details of boundary size, and spacing of roughness elements to account for blockage effects. Based on the experimental results of their study and an analysis of the available existing dispersion data, they developed the following equation:

$$K_x = 75.86\, P^{-1.632} RU \quad (2.19)$$

in which P = a generalized roughness parameter incorporating the influence of the resistance and blockage effects, which are the result of the roughness elements. For the prediction of the dispersion coefficient in natural streams, they proposed the following equation:

$$P = 0.4\, \frac{U}{U_*} \quad (2.20)$$

Schulz and Priegnitz (2011) investigated the influence of surface roughness on longitudinal dispersion under controlled conditions. They performed tracer experiments with variations in channel bed materials. By the use of measured tracer breakthrough curves, they calculated the average flow velocity, mean longitudinal dispersion, and mean longitudinal dispersivity. Longitudinal dispersion coefficients ranged from 0.018 m^{2}s^{-1} in channels with a smooth bed surface up to 0.209 m^{2}s^{-1} in channels with coarse gravel as the bed material. The longitudinal dispersion was found to be linearly related to the mean flow velocity. Accordingly, the longitudinal dispersivities ranged between 0.152 ± 0.017 m in channels with a smooth bed surface and 0.584 ± 0.015 m in identical channels with a coarse gravel substrate. Grain size

31

and surface roughness of the channel bed were found to correlate positively to the longitudinal dispersion. This finding contradicts several existing relationships between surface roughness and dispersion.

2.4 Summary

From all of the description of the dispersion processes analysed to-date it is clear that the dispersion coefficient (in this case the longitudinal dispersion coefficient) is a variable that depends on many factors as described in the literature review above (such as hydraulic parameters, velocity distribution, mixing coefficient, bed surface and side roughness, etc). However, since the commercial models commonly use constant dispersion coefficient, it will be useful to compare the modelling results using both kinds of dispersion coefficients, in order to evaluate whether or not the use of the constant dispersion coefficient is acceptable.

Various approaches about dispersion coefficient have been described in this chapter. Different approaches have been carried out by previous researchers, including developing models or equations (for example Elder, Koussi and Rodriguez-Mirasol, Seo and Cheong), carrying out analytical approach (Taylor, Deng, Catwin & Sullivan, Seo & Baek), delivering laboratory experiments (Fischer, Boxall & Guymer, Guymer, Abd El-Hadi & Daver, Magazine), doing field investigation (Godfrey & Frederick, Swamee), or using other's data to develop models (Kashefipour and Falconer, Iwasa and Aya).

The previous studies also focused on specific parameter(s) of dispersion, for example turbulent flow in circular tube (Taylor), turbulent flows in open channels (Elder), dispersion coefficient in the laboratory and natural rivers (Fischer), effect of cross-sectional shape and velocity distribution (Sooky), width-to-hydraulic radius ratio (Godfrey and Frederick), width-to-depth ratio (Chatwin and Sullivan, Asai and Fujisaki), and role of velocity gradient (Liu).

The present study will propose different approach, which is to utilize the combination between computer and physical models, in order to find the best dispersion coefficient

value for a case study estuary. This study does not focus on special aspects of the dispersion process, it involves various aspects which have been studied in the previous studies. The bed roughness will be included in the calibration of the model using Manning's n coefficient, the geometric of the estuary enable ones to study the effect of width-to-depth ratio or width-to-hydraulic radius to the dispersion coefficient, and the velocity variation is also searched in order to relate velocity gradient with dispersion coefficient.

CHAPTER 3

MATHEMATICAL MODELS OF HYDRODYNAMICS AND DISPERSION

3.1 Estuary modelling

The computer model used in this study is based on DIVAST (Depth-Integrated Velocity and Solute Transport) model, which was developed by Falconer (1993) and subsequently refined by Falconer and Lin (1997).The model is based on the continuity and momentum equations, and a depth-integrated time variant-model, which has been developed for estuarine and coastal modelling. It is suitable for water bodies that are dominated by horizontal, unsteady flow and do not show significant vertical stratification.The model simulates two-dimensional distribution of currents, water surface elevation and various water quality parameters with the modelling domain as function of time. The model takes into account the hydraulic characteristics governed by the bed topography and boundary conditions (Falconer, 2001).

In general, models can be classified as 1D, 2D and 3D models. In the case of modeling water bodies, 1D model means that the flow is only considered in one direction, that is the main stream direction (or longitudinal direction). 2D model is applied when there are two directions of flow considered, which are longitudinal (X) and transversal (Y) directions. In 2D vertical direction (Z direction) is not considered, meaning that the magnitude of vertical flow is negligible compared to X and Y flows. 3D model takes account the three directions, which are longitudinal (X), transversal (Y), and vertical (Z) directions.

Considering that the Severn estuary physical model is relatively shallow and because the main purpose of hydrodynamic study is to calibrate the computer model, using only X and Y directions is considered sufficient. Therefore this study will use only 2D model instead of 3D.

3.1.1 Hydrodynamic modelling

For many hydraulic flow problems the vertical velocity component w is small in comparison to the horizontal velocity components u and v, and the continuity and Navier-Stokes equations can be integrated over the depth and solved numerically to give the depth averaged velocity (or flow) field. Such flow fields often occur in wide estuaries, harbours, bays etc.

Using following notation illustrated in Fig. 3.1, where h = depth of bed below datum, and η = water surface level above, or below, datum (usually Still Water Level or Lowest Astronomical Tide), then depth integration of the continuity equations gives (Falconer, 1994):

$$\frac{\partial \eta}{\partial t} + \frac{\partial UH}{\partial x} + \frac{\partial VH}{\partial y} = 0 \quad (3.1)$$
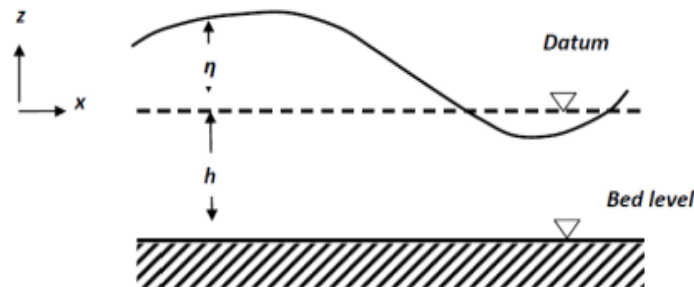
Fig. 3.1 Coordinate system and notation for depth integrated equations

(after Falconer, 1994)

where U and V are depth average velocity components and H is the total depth $(\eta+h)$.

Likewise, depth integration of the 3D Navier-Stokes equation for turbulent, incompressible flow in the x-direction gives:

$$\underbrace{\frac{\partial UH}{\partial t}}_{1} + \underbrace{\beta \left[\frac{\partial U^2 H}{\partial x} + \frac{\partial UVH}{\partial y}\right]}_{2} = \underbrace{fVH}_{3} - \underbrace{gH\frac{\partial \eta}{\partial x}}_{4} - \underbrace{\frac{H}{\rho}\frac{\partial Pa}{\partial x}}_{5} + \underbrace{\frac{\tau_{xw}}{\rho}}_{6}$$

$$- \underbrace{\frac{\tau_{xb}}{\rho}}_{7} + \underbrace{2\frac{\partial}{\partial x}\left[\bar{\varepsilon}\frac{\partial UH}{\partial x}\right] - \frac{\partial}{\partial y}\left[\bar{\varepsilon}\frac{\partial UH}{\partial y} + \bar{\varepsilon}\frac{\partial VH}{\partial x}\right]}_{8} \qquad (3.2)$$

$$\frac{\partial VH}{\partial t} + \beta \left[\frac{\partial VUH}{\partial x} + \frac{\partial V^2 H}{\partial y}\right]$$

$$= fUH - gH\frac{\partial \eta}{\partial y} - \frac{H}{\rho}\frac{\partial Pa}{\partial y} + \frac{\tau_{yw}}{\rho} - \frac{\tau_{yb}}{\rho} + 2\frac{\partial}{\partial y}\left[\bar{\varepsilon}\frac{\partial VH}{\partial y}\right]$$

$$- \frac{\partial}{\partial x}\left[\bar{\varepsilon}\frac{\partial UH}{\partial y} + \bar{\varepsilon}\frac{\partial VH}{\partial x}\right] = 0 \quad (3.3)$$

where β = momentum correction coefficient for non-uniform vertical velocity profile, τ_{xw}, τ_{xb}, and τ_{yw}, τ_{yb} = wind and bed shear stress components in the x and y directions respectively and $\bar{\varepsilon}$= depth averaged Eddy viscosity, f = Darcy-Weisbach resistance coefficient, P_a= local atmospheric pressure.

The terms 1 to 8 in Eq. (3.2) refer to: (1) local acceleration; (2) advective acceleration; (3) Coriolis acceleration; (4) pressure gradient (in terms of the water surface slope); (5) barometric pressure, generally negligible, except for very large lakes, seas or oceans; (6) wind stress; (7) bed resistance; and (8) diffusion transport of momentum by turbulence.

Studying each of these terms individually:

a. Momentum correction coefficient

$$\beta = \frac{\int u^2 \, dz}{U^2 H}(3.4)$$

where u = local velocity, U = depth average velocity, H = total water depth, and z = straight up coordinate.

In practical model studies, and in the absence of extensive field data, β is either set to unity or a vertical velocity profile is assumed. For an assumed Seven Power law profile, i.e.:

$$u = U_{max} \left(\frac{z}{H}\right)^{1/7} \quad (3.5)$$

Giving a value of β = 1.016.

For a logarithmic vertical velocity profile of the form:

$$u = \frac{u_*}{\kappa}\log_e(z) + u_* C_1 \quad (3.6)$$

where: u_* = shear velocity ($\sqrt{\frac{\tau_0}{\rho}}$ where τ_0 = boundary shear stress and ρ = fluid density), κ = von Karman's constant (=0.4) and C = constant of integration.

Then substitution gives:

$$\beta = \left[1 + \frac{g}{C^2\kappa^2}\right](3.7)$$

where C = Chezy bed roughness coefficient.

b. Eddy viscosity

Eddy is the swirling of a fluid and the reverse current created when the fluid past an obstacle. The moving fluid creates a space devoid of downstream flowing fluid on the downstream side of the object. Fluid behind the obstacle flows into the void creating a swirl of fluid on each edge of the obstacle, followed by a short reverse flow of fluid behind the obstacle flowing upstream, towards the back of the obstacle.

In fluid mechanics, an eddy is not a property of the fluid, but a violent swirling motion caused by the position and direction of turbulent flow. In the study of turbulence in

fluid, a common practical strategy for calculation is to ignore the small scale eddies in the motion and to calculate a large-scale motion with an eddy viscosity that characterizes the transport and dissipation of energy in the smaller-scale flow. Values of eddy viscosity used in modelling ocean circulation may be from 5×10^{-4} to 1×10^{6} Pa.s depending of the numerical grid.

For a logarithmic vertical velocity profile (i.e. Eq. 3.5), then:

$$\bar{\varepsilon} \approx \frac{\kappa}{6} U^* H \quad (3.8)$$

From field data by Fischer et. al. (1973), this valueis too low for natural rivers and estuaries and more typical values are:

$$\bar{\varepsilon} \approx 0.15 \, U^* H \quad (3.9)$$

This equation was obtained through laboratory experiments with dissolved tracer. The laboratory floating-particle experiments yield in an average surface dimensionless-mixing coefficient of $\varepsilon_z/du_* = 0.20$. An average of all the laboratory experiments with dissolved tracer, representing the depth-averaged transverse-mixing coefficient, is $\varepsilon_z/du_* = 0.15$. Okoye (1970) indirectly measured the variation of ε_z with depth in a number of experiments. His results, modified to match the surface and mean values $\varepsilon_z/du_* = 0.20$ and 0.15, suggestedan approximate variation of E_z.

c. Wind shear stress

For the surface wind shear stress components a quadratic friction law is again assumed giving for the x-direction:

$$\tau_{xw} = C_s \rho_a W_x W_s \quad (3.10)$$

where C_s= air-water resistance coefficient (typically 0.0026); ρ_a = air density (typically 1.292 kg/m³); W_x= wind velocity components in x-directions; and W_s= wind speed $= \sqrt{W_x^2 + W_y^2}$, with a similar equation as (3.38) for the y-direction.

d. Bed shear stress

For two-dimensional flow then the bed shear stress can be represented for the *x*-direction as:

$$\tau_{xb} = \rho g U \frac{V_s}{C^2} \quad (3.11)$$

where V_s = water flow speed = $\sqrt{U^2 + V^2}$, and C = Chezy roughness coefficient, with a similar equation for the *y*-direction.

To determine the Chezy value either a constant value can be specified directly for C, giving typically 30 m$^{1/2}$s^{-1}<C< 100 m$^{1/2}$s^{-1}, or C can be evaluated from the Manning equation, given as:

$$C = \frac{1}{n} H^{1/6} \quad (3.11)$$

where n=Manning roughness coefficient, with typical values for n being in the range of 0.015 to 0.04 over most tidal floodplains.

Alternatively, the Colebrook-White equation can be used (Henderson, 1966) giving:

$$C = \sqrt{\frac{8g}{f}} = -18 \log\left[\frac{k_s}{12H} + \frac{2.5C}{Re\sqrt{8g}}\right] \quad (3.12)$$

where f = Darcy-Weisbach resistance coefficient, k_s = Nikuradse equivalent sand grain roughness and Re = Reynolds number for open-channel flow (given as 4 V_sH/ν, where V_s is fluid speed and ν is kinematic viscosity).

In the numerical model DIVAST, the Colebrook-White equation has been used to calculate C, since the value of the roughness coefficient can be more closely related to bed features such as ripples and dunes. Furthermore, unlike the Chezy and Manning representation, this formulation includes the region of transitional turbulent flow (or non-fully developed turbulent rough flow). Recent numerical simulation refinements reported by Falconer and Owens (1987) and Falconer and Chen (1991) have shown

that this improved and more comprehensive representation of the bed friction coefficient can be particularly important when modelling flooding and drying over tidal floodplains, where Reynolds number effects may be significant due to shallow depths and low velocities.

3.1.2   Solute transport modelling

For a quasi-horizontal flowthe three-dimensional solute mass balance equation can be integrated over the water depth to give the two-dimensional depth integrated advective-diffusion equation (Adam & Baptista, 1987) as follows:

$$\frac{\partial HS}{\partial t} + \frac{\partial HUS}{\partial t} + \frac{\partial HVS}{\partial t}$$

$$= \frac{\partial}{\partial x}\left[D_{xx}H\frac{\partial S}{\partial x} + D_{xy}H\frac{\partial S}{\partial x}\right] + \frac{\partial}{\partial y}\left[D_{yx}H\frac{\partial S}{\partial x} + D_{yy}H\frac{\partial S}{\partial y}\right] + \Phi_s \quad (3.13)$$

where:

S = depth averaged solute concentration (unit/volume) or temperature;

D_{xx}, D_{xy}, D_{yx}, D_{yy} = depth averaged dispersion-diffusion coefficients in the x and y directions respectively (m^2/s), which were shown to be of the form:

$$D_{xx} = \frac{(\gamma U^2 + \delta V^2)H\sqrt{g}}{C\sqrt{U^2 + V^2}} \quad (3.14)$$

$$D_{yx} = D_{xy} = \frac{(\gamma - \delta)UV\sqrt{g}}{C\sqrt{p^2 + q^2}} \quad (3.15)$$

where: γ = depth average longitudinal dispersion constant; δ = lateral turbulent diffusion constant.

For values of and these can be set to minimum values assuming a logarithmic velocity distribution, wherein γ= 5.93 (Elder, 1959) and δ= 0.15 (Fischer, 1976). However, in

practical studies these values tend to be rather low (Fischer et al. 1979) with measured values of and ranging from 8.6 to 7500 and 0.42 to 1.61 for γ and δ, respectively.

3.1.3 Numerical solution

The finite difference scheme used to solve the governing equations is based on the Alternating Direction Implicit, or ADI, which involves the sub-division of each time step into two half steps. In this technique a two-dimensional implicit scheme is applied but considering only one dimension implicitly for each time step, without the solution of full two-dimensional matrix. On the first half time step the water elevation, the U velocity component (or the unit width discharge p) and the solute concentration are solved implicitly in the x-direction, whilst the other variables are solved explicitly. Similarly, for the second half time step, the water elevation, the V velocity component (or the unit width discharge q), and the solute concentration are solved implicitly in the y direction, and the other variables are solved explicitly. The resulting finite difference equations for each half time step are then solved using the method of Gauss elimination and back substitution (Gerald & Wheatly, 1992).

A space staggered grid system is used, with the variable η (water surface elevations) and S (concentrations) being located at the centre of the grid square and with U and V at the centre of the grid sides, as shown in Fig. 3.2. The depths are also located at the centre of the grid sides.

3.1.4 Initial and boundary conditions

At the start of the simulation period, the water level are set to a horizontal level everywhere, usually high or low water, the initial velocities are usually set to zero across the domain, the solute concentrations are set to a constant value, if the solute distribution is uniform initially. The model computes the velocities, elevations and solute concentrations at each time step so that eventually equilibrium is reached.
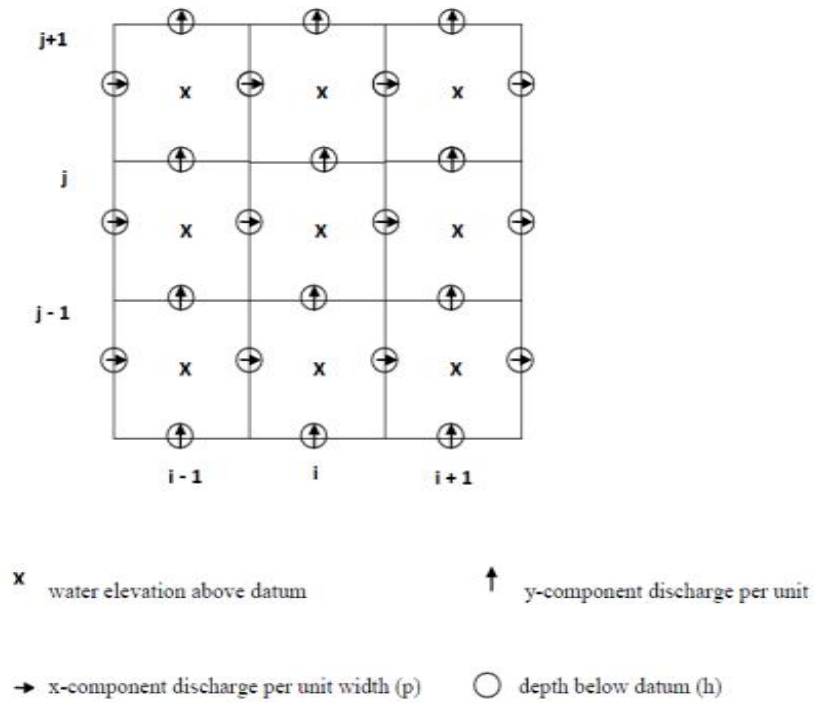
Fig. 3.2 Computational space staggered system

When solving the hydrodynamic and solute transport equations, boundary conditions of water elevations or velocities for the hydrodynamics and solute values for the solute transport processes need to be specified, throughout the simulation time, at both the lower and upper boundaries for each computational row and column, within the model domain. There are generally two types of boundary condition, the first being the closed boundary and the second the open boundary. For the identification of boundary values the velocity components in the x and y directions are not specified at the same points for the staggered grid, and solving equations tangential to the boundary requires values of the velocity just outside the boundary to be used.

A closed boundary can be regarded as a 'wall' boundary so that no flow or solute fluxes are allowed to cross the boundary. This type of boundary occurs along coastlines or adjacent to structures. Values outside the modelling domain are obtained

42

by assuming a 'no slip' condition (or zero flow velocity at the wall) parallel to the boundary and zero flow perpendicular to the boundary.

Unlike the closed boundary, along the open boundary the flow and solute fluxes are permitted to cross the boundary. Appropriate hydrodynamic and solute conditions need to be specified, such as measured water surface elevations, velocities and solute values. A free slip boundary condition is used by assuming zero gradient of a variable perpendicular to the open boundary.

3.1.5   Solution strategy

With the boundary conditions being included, the finite difference equations for momentum and continuity are solved for each half time step, using the method of Gauss elimination and back substitution (Gerald & Wheatly, 1992).After establishing the hydrodynamic field within the model domain, including the water surface elevations, velocity distributions, the solute, including water quality or sediment transport, parameters are computed during each half time step and again using the method of Gauss elimination and back substitution.

Various combinations of possible boundary conditions:
(a) conditions at both boundaries specified using flow;
(b) conditions at both boundaries specified using water elevations;
(c) flow specified at lower boundary, water elevation at upper boundary;
(d) elevations specified at lower boundary, flow specified at upper boundary;
when other combinations of the boundary conditions are considered, similar sets of equations can be obtained with reduced numbers of unknown variables.

Upon the completion of the above mentioned procedures for each half time step, the computation proceeds for the next time step until the time reaches the prescribed simulation time.

3.1.6   Application of the model on the study

In order to find the agreement between the physical model and the mathematical model, several steps were taken in this study, namely:

1. Plotting the bathymetry and boundary of the Severn estuary: The bathymetry data which was provided from the digitation of Admiralty Map was input to the Input File of the model. The domain was also input to the Input File (the file consisting values of parameters such as time step, grid numbers, Eddy viscosity value, n-Manning, etc).
    The size of the domain was 242 x 168 cells.
2. Fitting the geometry between the physical model and the mathematical model: Although the bathymetry data and domain block of the computer model and physical model were based on the same data, which is the Admiralty Map, there may still exists geometric disagreement between the two models. Therefore an adjustment need to be done between the the two models.

    Although both the computer model and physical models use the same data source for the bathymetry, there is possibility that both models are not in perfect agreement, especially for the reason of construction of the physical model which might contain error.

    Therefore an effort should be made to check whether the bathymetry of the computer model agrees with that of the physical model. This is done by checking several points which are obvious in the physical model (such as deep point and hump) and searching the corresponding point in the computer model. A correction in the computer model should be made if the depth of both model is not in agreement.

3. Hydrodynamic calibration: After the geometric fitting is done, the computer model is calibrated against the experimental data from the physical model. This data is consisted of water level and velocity data. Calibration is done using several parameters such as n-Manning roughness coefficient, Eddy viscosity

coefficient, and momentum correction coefficient. Each factor was used for the calibration of the model successively.

4. Boundary condition refinement: this is done in order provide the model the measured boundary condition from the tide instead of using a sinusoidal equation.

5. Bathymetry refinement: this is done to provide the model an accurate data of bathmetry so that the modelling result is expected to be more precise. The refinement was done using PIV (particle image velocitimetry, short description).

6. Dispersion calibration: to find the best value of dispersion coefficient. Like in the hydrodynamic modeling, calibration process is also carried out in the dispersion modeling.

3.2 Groundwater modelling

3.2.1 Darcy's law

Water flow in groundwater is commonly expressed by Darcy's law. The law is an equation that defines the ability of a fluid to flow through a porous media such as rock. It was formulated by Henry Darcy based on the results of experiments on the flow of water through beds of sand. It shows that the volumetric flow rate is a function of the flow area, elevation, fluid pressure, and a proportionality constant. Darcy's law can be expressed as follows:

$$Q = KA\frac{(h_1 - h_2)}{L} \ or \ q = \frac{Q}{A} = -K \ ^{dh}/_{dl} \ (3.16)$$

where Q is the flow rate, K is the termed permeability coefficient (this describes the porosity of the underground formation and depends on the material property), A is the cross sectional area, h_1 and h_2 constitute the height of the inlet head and outlet head respectively, and L is the length of flow.

In this study, Darcy equation is used to check whether the experiment results follow the equation. By knowing several parameters (discharge, water level, conduit length), the permeability of the groundwater model can be estimated. If the value of K has

been found before, then the accordance between the experiment results and the Darcy equation can be determined. If the experiment results agreed with the Darcy's equation, then the analysis on dispersion process in the groundwater can be further experiment of dispersion can be carried out assuming that the groundwater flow follows the Darcy's equation.

3.2.2 Advection and diffusion equation

The formulation for the advective-diffusion equation is as follow:

$$\frac{\partial \bar{c}}{\partial t} + \bar{u}\frac{\partial \bar{c}}{\partial x} + \bar{v}\frac{\partial \bar{c}}{\partial z} = \frac{\partial}{\partial x}\left(D_{tx}\frac{\partial \bar{c}}{\partial x}\right) + \frac{\partial}{\partial y}\left(D_{ty}\frac{\partial \bar{c}}{\partial y}\right) + \frac{\partial}{\partial z}\left(D_{tz}\frac{\partial \bar{c}}{\partial z}\right) \text{(3.17)}$$

where D_{tx}, D_{ty}, D_{tz} are the termed turbulent diffusion coefficients and are not necessarily the same in the three co-ordinate directions; the advective equations are along x direction and y direction; while the diffusion equation is along x direction, y direction, and z direction.

In the experiment of the present study, however, the 1-D model experiment of the advective-diffusion equation can be written in 1-D formula, as follows:

$$\frac{\partial \bar{c}}{\partial t} + \bar{u}\frac{\partial \bar{c}}{\partial x} = \frac{\partial}{\partial x}\left(D_{tx}\frac{\partial \bar{c}}{\partial x}\right) \text{(3.18)}$$

Here, if an ideal pulse of tracer is injected into the fluid entering a 1-D channel as with a vessel with an open-open boundary condition, the diffusion coefficient D represents the speed of the spreading of the tracer, a larger D therefore denotes a faster spreading of the tracer curve. In addition to this, D/uL indicates the dimensionless group characterizing the spread in the whole channel, and the values of D and (D/uL) depend on the shape of tracer curve as it passes the channel.

Ideally, the results of the experiment would be the only results from the advective and diffusion movement. However, because of the experiment's facilities and the model's limitations, the real experiment result is more inclined to dispersion than diffusion. Notwithstanding this, it also takes the defects of the physical model into

consideration; two types of boundary condition for the monitoring location are established in the experiment and these fit the experiment data separately with corresponding theoretical calculation results.

The curve expression for the open-open boundary condition is:

$$E_{\theta,00} = \frac{1}{\sqrt{4\pi\left(\frac{D}{uL}\right)}} e^{\left[\frac{(1-\theta)^2}{4\theta(D/uL)}\right]} (3.19)$$

Where is the normalized concentration of tracer and is the normalized time, and the tracer response curves for open boundary condition can have large deviations from the plug flow (Levenspiel, 1999). The family tracer curves of the open-open boundary condition are shown in Figure 3.5.

The expression for the close-open boundary condition is:

$$\bar{t} = \frac{\sum t_i C_i}{\sum C_i}; \ \sigma^2 = \frac{\sum t_i{}^2 C_i}{\sum C_i} - \bar{t}^2 = \frac{\sum t_i{}^2 C_i}{\sum C_i} - \left[\frac{\sum t_i C_i}{\sum C_i}\right]^2 (3.20)$$

$$\sigma_\theta{}^2 = \frac{\sigma^2}{\bar{t}^2} = 2\frac{D}{uL} - 2\left(\frac{D}{uL}\right)^2 \left(1 - e^{-\frac{uL}{D}}\right) (3.21)$$
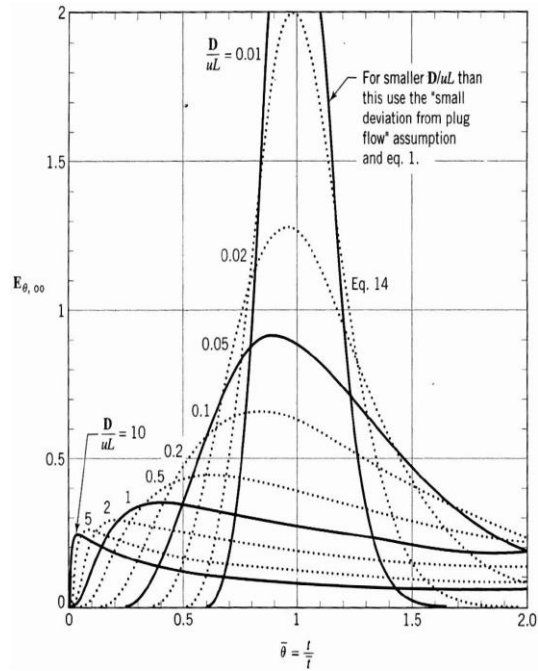
Fig. 3.3 Tracer response curve family for the open boundary condition

(after Levenspiel, 1999)

CHAPTER 4
EXPERIMENTAL METHODS OF
HYDRODYNAMICS AND DISPERSION

The purpose of the experiment is to provide sufficient data to support analysis of the problem being studied. In the present study, there are mainly two experiments, that are experiment in the Severn physical model and experiments in the groundwater physical model. Experiments in the estuary physical model are then used to calibrate computer model, while experiments in the groundwater are then analyzed using a mathematical model. Table 4.1 lists all the experiments delivered in the present study.

Table 4.1 Experiment sets

Experiment no.	Location	Sampling point	Purpose	Parameters
E-1	Estuary	P1, P2, P3 P4, P5, P6	Hydrodynamics Hydrodynamics	Water level Velocity
E-2	Estuary	P7, P8, P9, P10, P11, P12	Hydrodynamics	Water level and velocity
E-3	Estuary	P7, P8, P9, P10, P11, P12	Dispersion	Dye tracer concentration
G-1	Groundwater model	A, B, C, D, E, F, G	Calibration	Water level
G-2	Groundwater model	A, B, C, D, E, F	Effect of tide on groundwater	Water level
G-3	Groundwater model	A, B, C, D, E, F	Effects of tide and pump on groundwater	Water level
G-4	Groundwater model	A, B, C, D, E, F	Dispersion	Dye tracer concentration

The purpose of Expt. E-1 is to characterize the hydrodynamic process of the physical model, which contains water level and velocity experiments. Expt E-2 is to provide data for model calibration. Expt. E-3 is to characterize the dispersion process in the estuary model, and to provide data for dispersion model. Expt. G-1 is the experiment for calibration. Expt. G-2 is to establish the effect of tide on groundwater dynamics. Expt. G-3 is to explore the effects of tide and pump on groundwater hydrodynamics, and finally Expt. G-4 is to establish the dispersion characteristics of the groundwater model.

4.1 Experiments in the Severn Estuary Physical Model

4.1.1 Description and working principle

This study uses an estuary physical model namely the Severn Estuary physical model as its main tool, along with the DIVAST model described in Chapter 3. The physical model is located in the Hyder-Hydraulic Laboratory, Cardiff University. With 5.7 m long and 3.9 m wide, the physical model was built in a tidal basin constructed previously. It is a miniature of the Severn estuary (the prototype) with the ratio of 1:125 and 1:25,000 for vertical and horizontal dimensions, respectively. The scope of the model is shown in Fig. 4.1. An aerial view and a lay out of the physical model are shown in Fig. 4.2 and Fig. 4.3, respectively. Fig. 4.4 shows the bathymetry of the physical model.

The physical model simulates the water movement (hydrodynamics) in the estuary which is mainly affected by a simulated tide. Water is stored in a ground tank beneath the physical model, and when the model is operated the water is pumped and flowed through a pipe system and a perforated big pipe, before finally enters the physical model. The pump is operated at 1,400 rpm.

Fig. 4.1 Scope of Seven estuary physical model
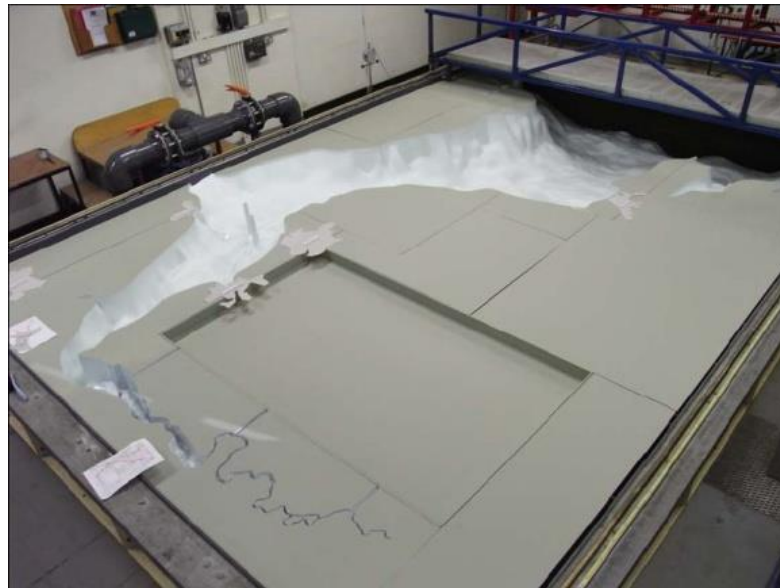
Fig. 4.2 An aerial view of the Severn estuary physical model
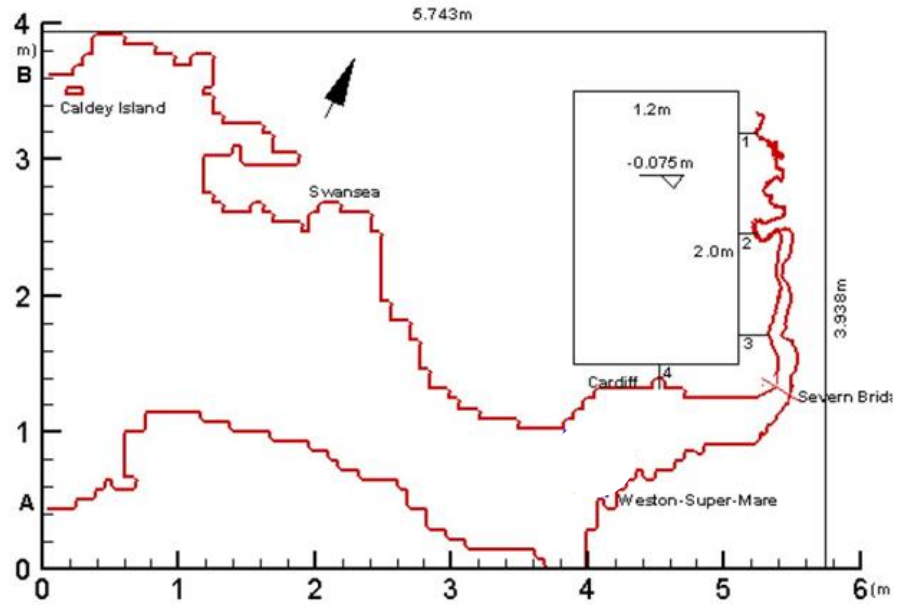
Fig. 4.3 A lay out of the Severn estuary physical model
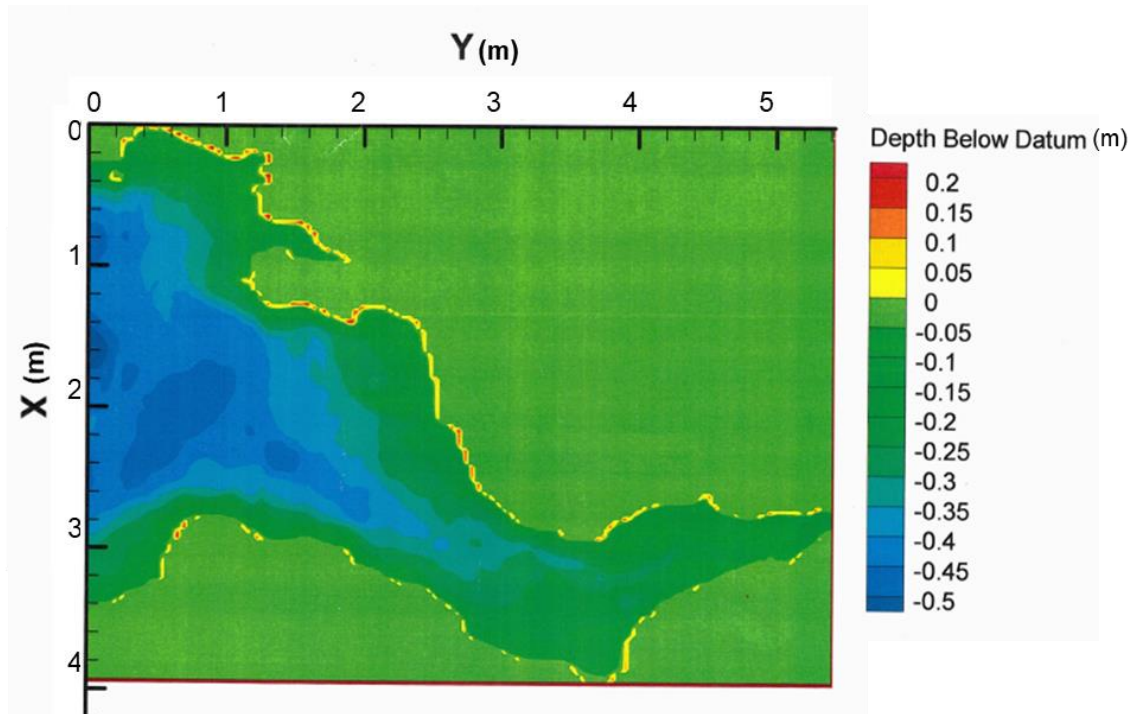
Fig. 4.4 A bathymetry map of the Severn estuary physical model

(datum: mean water level)

To simulate the tide, a weir is constructed in the sea boundary of the model (Fig. 4.4). Using a computer software, the weir is regulated in a control room. The frequency of the weir is 1/40 Hz (period: 40 seconds).

Fig. 4.5 The tide-generating weir

Due to the limitation of the laboratory space, the physical model was built with an angle from the north-south direction, as shown in Fig. 4.1.

4.1.2 Dimensional analysis

In order to represent the real estuary, the dimensions of the physical model were determined through a dimensional analysis. The analysis was based on the "Froude similitude". The Froude number is defined as:

$$F_r = \frac{v}{\sqrt{gL}} \quad (4.1)$$

where v = velocity, g = gravity acceleration, and L = linear dimension, such as depth or diameter.

The number is used generally for scaling free surface flows, open channels, and hydraulic structures. It is assumed that the Froude number of the physical model is the same with that of the prototype, hence Froude number can be used for the dimensional analysis.

Following is an example of dimensional analysis for determining the ratio between velocity of the physical model and the prototype.

Example: Dimensional analysis for velocity

The ratio between the prototype and the model for horizontal dimension:

$$\frac{l_p}{l_m} = \lambda_1 \qquad (4.2)$$

where l_p = length in the prototype, l_m= length in the model, λ_1 = horizontal scale (= 25,000).

And the ratio between the prototype and the model for vertical dimension:

$$\frac{h_p}{h_m} = \lambda_2 \qquad (4.3)$$

where h_p = height in the prototype, h_m= height in the model, λ_2= vertical scale (= 125).

Horizontal velocity is determined by assuming that the Froude number for the prototype is the same with that of the physical model:

$$F_{N_p} = F_{N_m} \qquad (4.4)$$

where F_{N_p}= Froude number of the prototype, and F_{N_m} = Froude number of the physical model.

$$\frac{V_p}{\sqrt{g_p h_p}} = \frac{V_m}{\sqrt{g_m h_m}} \qquad (4.5)$$

$$\frac{V_p}{V_m} = \frac{\sqrt{g_p h_p}}{\sqrt{g_m h_m}} = \frac{\sqrt{h_p}}{\sqrt{h_m}} = \left(\frac{h_p}{h_m}\right)^{1/2} = \lambda_2{}^{1/2} = \sqrt{125} \quad (4.6)$$

$$V_m = \frac{V_p}{\sqrt{125}} \approx 0.0894\, V_p \qquad (4.7)$$

As a conclusion, the ratio between velocity in the model and in the prototype is 1: 0.0894.

4.1.3   Water level measurement

a.   Water level probes

The main tool of water level measurement is a probe which has two parallel stainless-steel wires. The probe operates based on the conductivity principle. The water current flowing between the probe wires is proportional to the depth of immersion and this current is converted into an output voltage proportional to the instantaneous depth of immersion. The read data is then transferred and shown in a computer located in the control room, using a computer software namely "Advantech Genie". The water level data is then downloaded into spread sheet files for further processing.

Fig. 4.5 shows a water level probe as it was being used in the estuary physical model experiment.The water level probes are attached to an aluminium bar which lied on the physical model surface, enabling the probe wires to be submerged in the basin water.

The conductivity data which are read by the water level probes need to be calibrated and converted into the actual water level. The calibration is done by measuring the actual water levels, and then making an equation (calibration equation) relating the reading data and the actual water level. By this way all the read data is then converted to the actual water level data. There were two levels measure for this calibration, which are low and high water levels. They were measured relative to the mean water level.
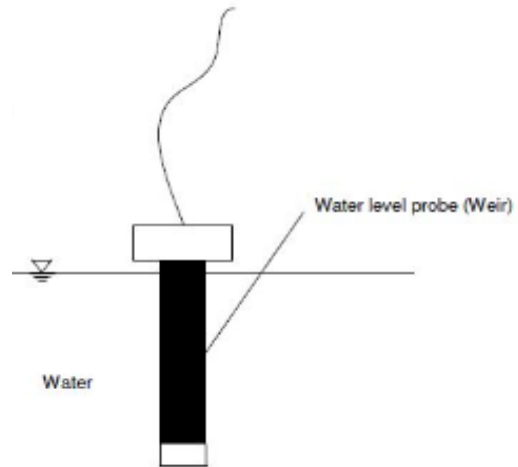
<center>(a)   (b)</center>

Fig. 4.6 (a) Water level probe (b) Position of WL probe

4.1.4 Velocity measurement

Water flow velocity is measured by the Acoustic Doppler Velocimeter (ADV) which works on the basis of Doppler effect principle. An ADV probe consisted of three main components: (i) one transmitter, (ii) three receivers, and (iii) conditioning module (see Fig. 4.7). First, a short acoustic pulse is emitted from the transmitter to the water. Particles (or scatterers) present in the water then reflect (or echo) the pulse and this echo is received in three ADV receivers, amplified in the conditioning module and digitized/analysed in the processing board. The frequency shift between the pulse transmission and its receiving is used to calculate the velocity of the particles, based on the Doppler principle.

There are three types of ADV probes, namely downlook, uplook and sidelook ADV probes. They can be used interchangeably depending on the situation of sampling points. For example, for the sampling points near the physical model bed the downlook ADV is used, while for the sampling points near the water surface the uplook ADV is used (Fig. 4.8).

<div align="right">56</div>

A special bridge is constructed in the physical model to attach and move the ADV probes and to help access all the points in the Severn estuary physical model. When the ADV probes were set in the physical model, the velocity measurement were started and monitored in the computer using the ADV software. The velocity measurement is applied on the particles contained in a virtual volume, called sampling volume, which is about 5 cm from the transmitter. (Fig. 4.7).
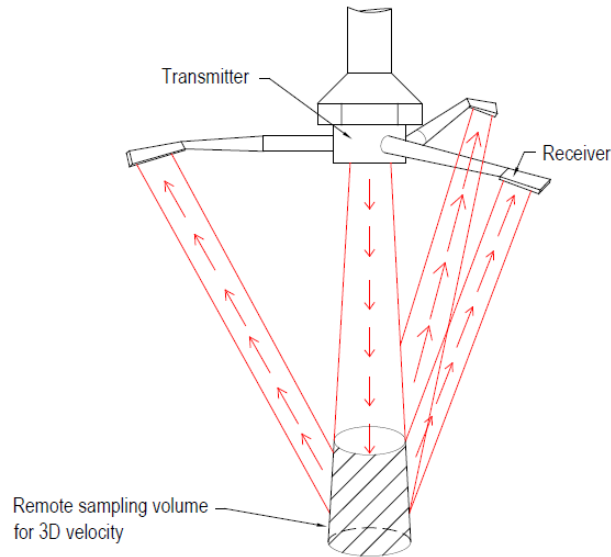
Fig. 4.7 Schematic representation of ADV

| (a) | (b) | (c) |
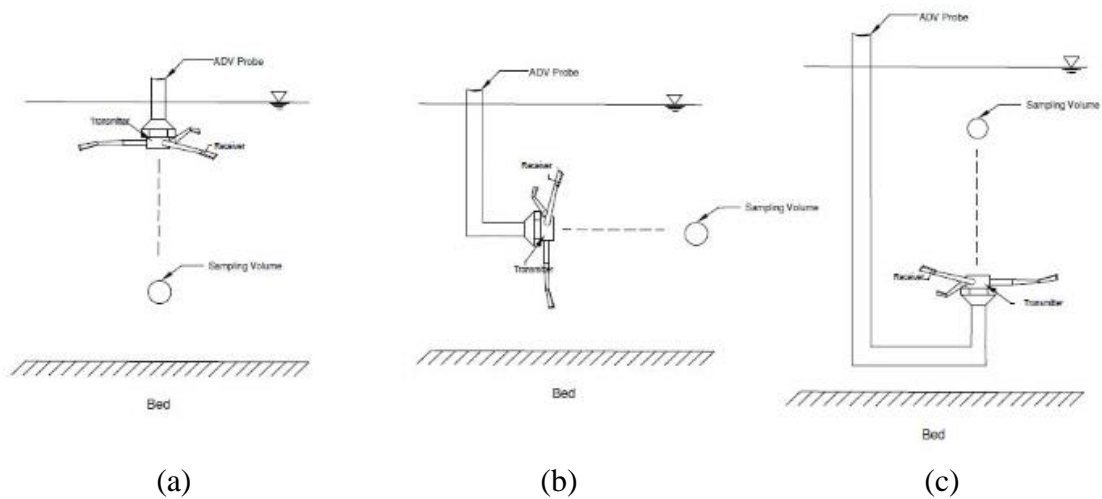
Fig. 4.8 Three types of ADV: (a) downlooking (b) sidelooking (c) uplooking

a. Accuracy

The measurement of the ADV has a range of $\pm$ 15 cm/s.To ensure the quality of measurement data, two parameters are set in this instrument. They are "Sound-to-Noise Ratio" (SNR) and Correlation (COR).SNR is the ratio between the sound of the pulse and noise from the surroundings. The SNR parameter indicates the relative density of acoustic scatterers in the flow and the resulting strength of the signal received compared to the noise level of the instrument. The formula of SNR is:

$$SNR = 20 \, log_{10} \left(\frac{Amplitude_{signal}}{Amplitude_{noise}} \right) \quad (4.8)$$

ADV manufacturers recommend an SNR of at least 5 when measuring average flow velocities, and 15 or higher when measuring instantaneous velocities and turbulence quantities.If the velocity data look "noisy", it may be due to a low concentration of scatterers in the water. This can be remedied by adding seeding material. A stagnant, clear basin or flumes are seeded with hollow spheres that have a density close to that of water and a size around 10 µm. Particle that are close to neutrally buoyant will remain in suspension without additional stirring and are ideal for low-flow experiments. The used seeding level is 10-50 grams per cubic meter.

The correlation parameters, COR, is an indicator of the relative consistency of the behaviour of the scatterers in the sampling volume during the sampling period. ADV's collect data at a higher sampling rate than the sample reporting period, and the COR parameter indicates the consistency of the multiple measurements that take place within each sampling period. The value varies from 0 to 100, and ADV manufacturers have typically recommended filtering to remove any samples with correlation scores below 70. WinADV offers such a filter, with the option to adjust the cutoff value. Samples with correlationmuch less than 70 can sometimes still provide good data, especially when the signal to noise ratio is high and the flow is relatively turbulent (a condition that seems to lead the generally lower correlation scores). COR indicates the correlation among the data. Ideally, COR should have values between 70 and 100.

The measurement resulted in three graphs in the computer control, namely Vx, Vy, and Vz, which represent longitudinal, transversal, and vertical velocities, respectively. The reading of the ADV was recorded in a computer using Win-ADV software, showing the three directions of velocity (Vx, Vy, and Vz).

4.1.5 Dispersion experiments

Dispersion study in the Severn Estuary physical model was carried out by injecting dye tracer in a certain point (called injection point) and measuring its concentration in several points. Later the measurement results will be compared to the modelling results in order to find the best value of dispersion coefficient.

a. Dye tracer preparation

The dye tracer used in this experiment is Rhodamine WT. The stock solution was 2 pph (2%) concentration. Dye tracer solution was prepared from the Rhodamine WT stock to obtain the solution for both fluorometer calibration and experiment. For the fluorometer calibrationa dye solution of 100 ppb was prepared, and for the experiment a solution of 250 ppm was prepared. Table 4.2 shows the preparation procedure for 250 ppm dye tracer solution.

Table 4.2 Dilution procedure for the 250 ppm dye tracer

Step	Initial conc.	Added volume (ml)	Flask volume (ml)	Dilution factor	Final concentration
1	20 pph	2	200	100	2 ppt
2	2 ppt	125	1000	8	250 ppm

b. Fluorometer setting

In order to measure the concentration of dye tracer, a type of fluoromer is used. The fluorometer used in this study is Cyclops-7 fluorometer, which consists of the following components:

1) fluorometer probe, which emits the fluorescence light and catch the reflected photon from the dye tracer;

2) data bank, which stores the measured data from the dye tracer returned back by the fluorometer;

3) fluid cell, functioning as the case for the fluorometer probe. The fluid cell is a package in which the flurometer probe is inserted so that the fluorometer does not necessarily submerged in the water. By this method the flurometer can be safely put outside the water body.

Fig. 4.9 shows the Cyclops-7 with all its components.
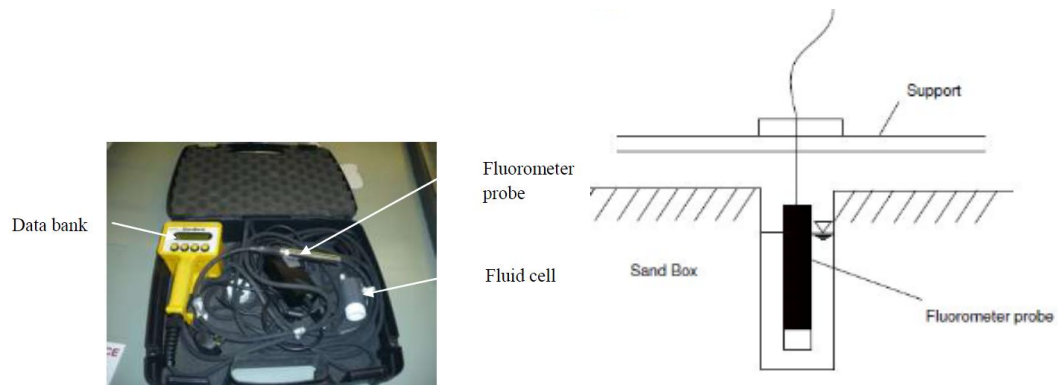
Fig. 4.9 Cyclops flurometer

The fluorometer along with the data bank is installed in the computer according to the installation manual from the manufacturing company.

Before it is used, the fluorometer needs to be calibrated against the standard solution. The calibration involves two main steps:

1) Calibration against the distilled water as the blank (zero concentration)

2) Calibration against 100-ppb dye tracer solution as the dye solution standard

The selection of the 100-ppb dye concentration was based on an expectation that the concentration of the dye tracer in the water system did not exceed 100 ppb.

The data collected from the dye tracer experiments are processed further with the data bank. The data is downloaded from the data bank to the computer using GUI software, and the result is converted to a spread sheet software.

4.1.6 Experiment setting

All the descriptions above (4.1.1 to 4.1.6) explain the working principle of the instruments used in this study. Those instruments are used for carrying out experiments in the Severn estuary physical model, which consist of:

(a) Experiment E-1 (Expt. E-1),which aims at obtaining a general characteristics of hydrodynamic in the physical model;

(b) Experiment E-2 (Expt. E-2), which aims at providing a more detail data for the the modelling of hydrodynamic and dispersion aspects.

For the Expt. E-1, the sampling points are shown in Table 4.3 and Fig. 4.10. As this experiment is an initial observation of the hydrodynamic condition, the water level and velocity experiments was carried out in different points.

Table 4.3 Coordinate of sampling points in Expt. E-1

Sampling point	Physical model coordinate (cm)	
	X	Y
Water level		
- Point P1	479	93
- Point P2	143	182
- Point P3	0	92
Velocity (ADV)		
- Point P4	320	86

Sampling point	Physical model coordinate (cm)	
	X	Y
- Point P5	160	178
- Point P6	0	225

For Expt. E-2, the sampling points are shown in **Table 4.4** and **Figure 4.10.** In this experiment the water level and velocity experiments were carried out in the same sampling points in order to enable the next modelling works to study the water level and velocity of the same location.

Table 4.4 Coordinate of sampling points in Expt. E-2

Sampling point	Physical model coordinate	
	X	Y
Point P7	435	90
Point P8	390	47
Point P9	335	54
Point P10	305	60
Point P11	258	108
Point P12	202	174

4.1.7   Bathymetry refinement

Bathymetry refinement was done using Particle Image Velocitymetry (PIV) method. PIV is an optical method usually applied for velocity measurements and related properties in fluids. In this method the fluid is seeded with tracer particles which, for sufficiently small particles, are assumed to faithfully follow the flow dynamics. The fluid with entrained particles is illuminated so that particles are visible. The motion of the seeding particles is used to calculate speed and direction (the velocity field) of the flow being studied.
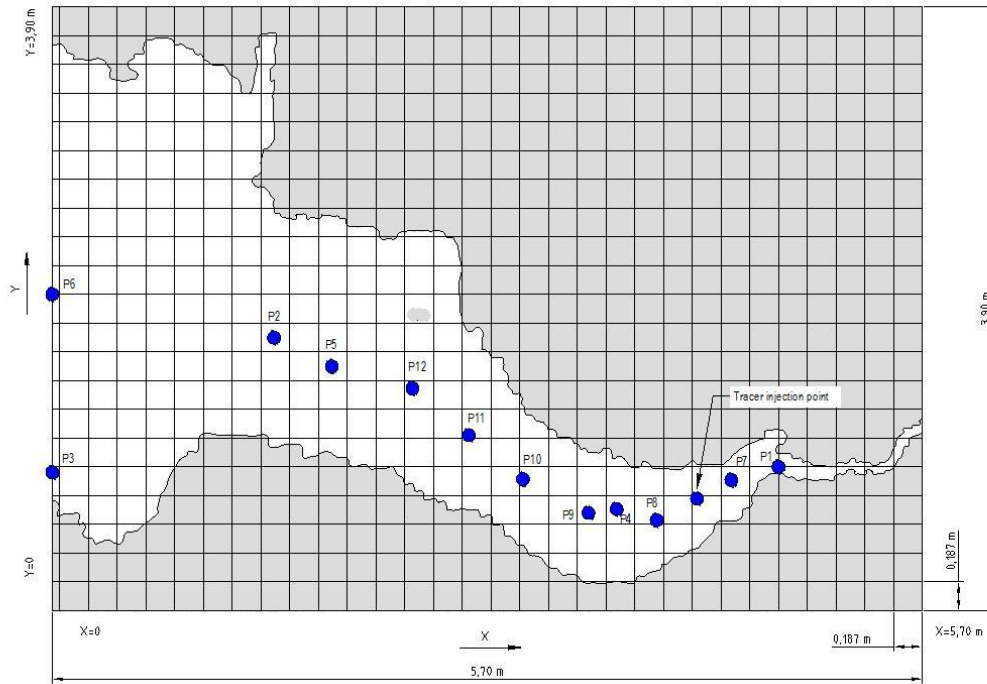
Fig. 4.10 Locations of sampling points in Expt. E-1 and Expt. E-2

PIV apparatus consists of a camera (normally a digital camera), a strobe or laser with an optical arrangement to limit the physical region illuminated, a synchronizer to act as an external trigger for control of the camera and light guide may connect the laser to the lens setup. PIV software is used to post-process the optical images.

In this study PIV method is used to measure the bathymetry.After the PIV measurement is done the bathymetry are measured manually to verify the results. Then the new bathymetry data is used to run the model.

4.1.8 Modelling of the results

As it has been described in Chapter 3, that the computer used in this is DIVAST model. The parameters used in this model is presented in **Table 4.5**.

Table 4.5 Parameters of the DIVAST model applied in this study

Parameter	Symbol	Value	Unit
Maximum number of grid points in I (or X) direction	IMAX	242	-
Maximum number of grid points in J (or Y) direction	JMAX	168	-
Time of simulation	TIMESM	0.2570	hr
Half time step	HFDT	0.005	second
Grid spacing in the physical model	DELX	0.024	m
Eddy viscosity coefficient	COED (ε)	0.30 (typical)	-
Momentum correction coefficient	β	1.031 (typical)	-
n-Manning roughness coefficient	MANNING'S n	0.035 (typical)	-
Longitudinal dispersion constant	γ	0.8 (typical)	-
Lateral turbulent diffusion constant	δ	0.6 (typical)	-

4.1.9 Error Analysis

The agreement between the computer model and the physical model is evaluated using several error analysis methods, in order to find the best parameters.

1. Mean square error (MSE)

$$MSE = \frac{1}{N}\left[\sum_{i=1}^{N}(X_p - X_m)^2\right](4.9)$$

(the less the *MSE* the better)

2. Root mean square error (RMSE)

$$RMSE = \frac{1}{N}\left[\sum_{i=1}^{N}(X_p - X_m)^2\right]^{\frac{1}{2}}(4.9)$$

(the less the *RMSE* the better)

3. Standard error (SE)

$$SE = \frac{1}{N}\left[\sum_{i=1}^{N} Abs\ (X_p - X_m)\right](4.10)$$

(the less the *SE* the better)

4. Normalized error (NE)

$$NE = \frac{1}{N}\left[\sum_{i=1}^{N} 100\frac{(X_p - X_m)}{X_m}\right](4.11)$$

(the less the *NE* the better)

5. α-coefficient

$$\alpha = X_m/X_p (4.12)$$

(the closer α to unity the better)

6. R^2 (coefficient of correlation) – obtained from the graphs (using trend-line in the Excel)
   (the closer R^2 to unity the better)

Where:

X_m = measured data, X_p = predicted data, N = number of data

4.2 Experiments in the groundwater model

Experiments study in the groundwater model consisted of hydrodynamic and dispersion experiments. Hydrodynamic experiment was done to analyse the flow condition in the groundwater model, while the dispersion experiments was done to analyse the flow of the dye tracer in the groundwater model. Both experiments will be compared to related models, i.e. Darcy's law for hydrodynamics and advection-diffusion equation for dispersion.

4.2.1   Description and working principle

The sandbox can be used in full dimension which is 2 dimension (2m x 1.2m x 0.075m), but can also be used in only 1 dimension (2 m x 0.16 m x 0.075 m). In this study only the 1 dimension model is used.

The idealized groundwater is located is a part of the Severn estuary physical model and located beside the estuarine physical model.

The groundwater model is connected to the estuarine physical model through four small channels. Water from the estuarine model flows into the idealized sandbox through those channels. The movements of the estuarine model therefore affect the condition of the groundwater model.

In this experiment five boreholes (B-C-D-E-F) are set in the sandbox as illustrated in Fig. 4.11. Point A is located in the connecting channel. The boreholes are perforated so that water can flow through them.
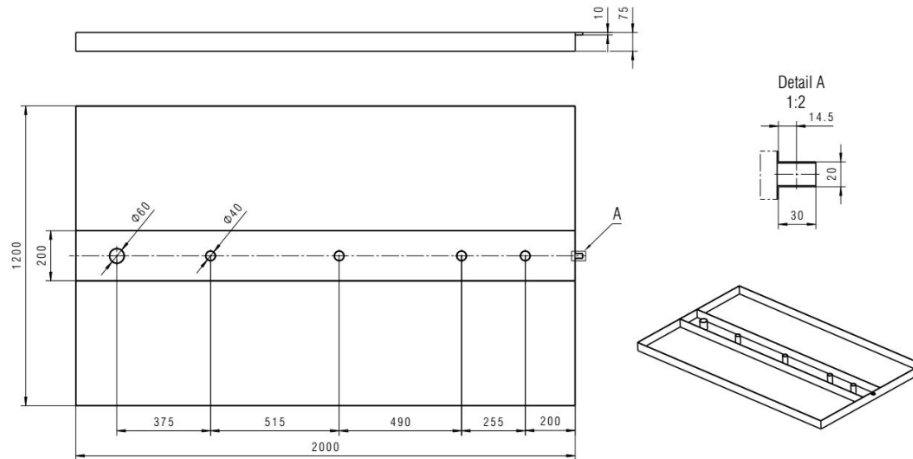
Fig. 4.11 Location of boreholes in the groundwater model

A pump is set in the upper boundary to be used in the experiments observing the effect of pumping on the groundwater flow. The pump is located in the upper boundary of the sandbox, close to point F (Fig. 4.11). The water from the pump is flowed on the borehole F, pushing the dye tracer injected into any borehole to flow to the estuary model direction.

The boundary of the idealized groundwater model is consisted of two boundaries: (1) the closed boundary in the upstream of the groundwater model, (2) the open boundary which is connected to the Severn estuary physical model (Fig. 4.12).

4.2.2   Water level measurement

The water level probes used in this experiment in the groundwater model is the same with the water level used in the estuarine physical model experiments.

In order to measure the water level in the groundwater, the water level probes were set in the borehole and attached to the velocity bridge. The base of the water level probes touched the base of the box in the borehole to ensure that the water depth is measured fully.

Water level probes used in this experiment were the same with those used in the estuarine experiments. In this experiment water level need to be calibrated as well.

However, the method of calibration is rather different. Here the water level was measured in four levels in order to find the relationship between the actual water level and the reading data. After this relationship (calibration equation) is found then it is used to transform the read data into the actual water level data.

4.2.3 Dispersion experiments

After the water level measurements have been done, the experiments of dispersion were carried out. Firstly the dye tracer was prepared in the same way with that in the estuarine experiments.

Firstly the dye tracer was prepared in the same method with that in the estuarine physical modelexperiments. There are two standard solutions, namely blank standard and solution standard. The concentration of the standard tracer was 100 ppb; this was used to calculate and to assist with the accuracy of the concentration range for the concentration measurement databank facility. For the experiment, the tracer concentration was 20 ppm, this being used for transporting the sandbox.

As has been describe in the previous chapter, there are two boundary conditions examined in this study:

(1) Open-open boundary conditions

The open-open boundary conditions mean that the both boundary of the groundwater model are open so that the water coming from the upper boundary does not change in term of flow and dispersion. This can be illustrated in Fig. 4.12.
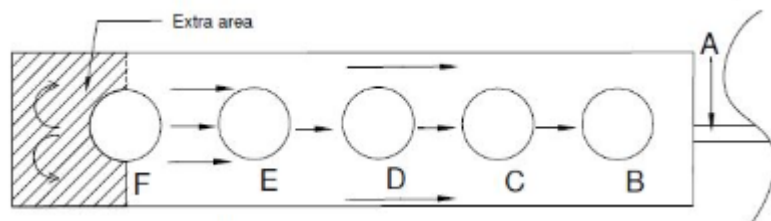
Fig. 4.12 Open-open boundary conditions

The upper boundary (F) is open without barrier. This affects on that the water pumped into borehole F flows first to the back side, filling an extra area before it flows downwards (to borehole E, etc.). This has an effect on the accuracy of model.

(2) Close-open boundary conditions

For close-open boundary conditions, this means that the upper boundary of the groundwater model is open, letting the water flow without any obstruction, while the lower boundary is open. This is illustrated in Fig. 4.13.
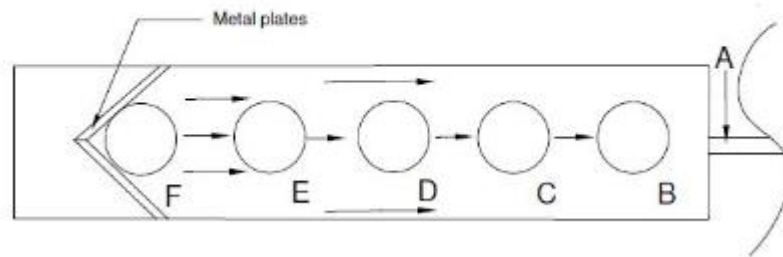
Fig. 4.13 Close-open boundary conditions

In this scenario, borehole F in which water is pumped in is restricted by a metal barrier, by which the water flow directly to borehole E, etc.

In this study, two kinds of boundary conditions were applied. The reason for this is that in order to find the best fit for the dispersion coefficient, the two conditions need to be looked for in order to find the best value of the dispersion coefficient.

The purpose of the study is to find the value of the dispersion coefficient in order to compare it with the dispersion coefficient in the estuary physical model, and to apply it to the prototype.

CHAPTER 5

HYDRODYNAMICS OF THE ESTUARY PHYSICAL MODEL

5.1 Experiment E-1

Expt. E-1 was carried out in order to assess the general hydrodynamics of the Severn estuary physical model. The experiments, undertaken at six sampling points in total, consistedof three sampling points (P1, P2 and P3) for water levels and three other points (P4, P5, and P6) for velocity measurement. The locations of the sampling points have been identified in Chapter 4. The sampling points were set as to represent the upper boundary, lower boundary, and the middle of the physical model. The cross sections where the sampling points were located are different in terms of width and depth. Fig. 5.1 shows an illustration of sampling point cross sections according to the bathymetry data used in the model.

Fig. 5.1 shows that the cross section of the sampling points was quite various. Cross sections P1 and P4 were shallow and simple, while cross sections P2, P3 and P5 were deep and complex. This affected the water velocity in those cross sections.

It is known that the hydrodynamics of a water body is significantly affected by its geometric parameters (such as width, depth, and cross sectional area). **Table 5.1** shows several geometric parameters of the Severn estuary physical model where the sampling points were located.

The following experiments were delivered in the tidal forcing condition as follow:

- Period: 40 seconds
- Amplitude: 85 cm
- Min water level: -70 mm
- Max water level: 100 mm
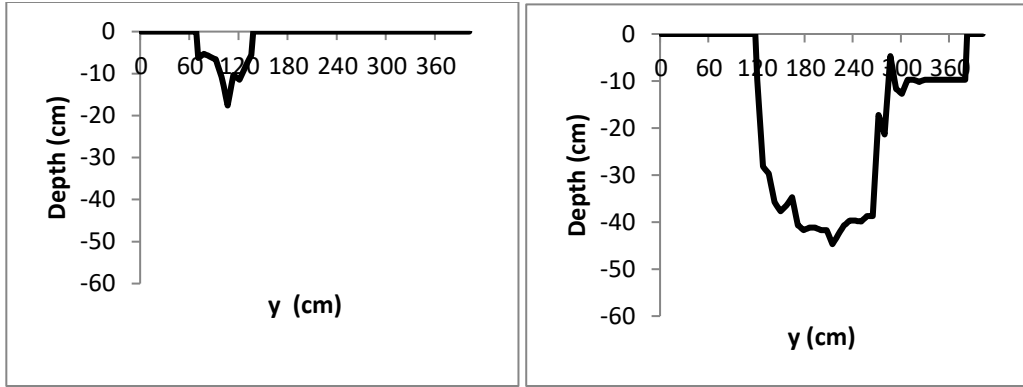
(a) Cross section P1

(b) Cross section P2
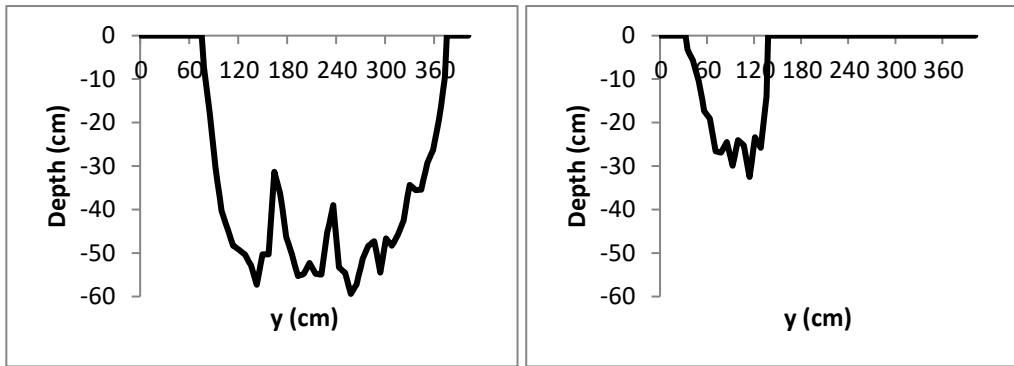
(c) Cross section P3 = P6

(d) Cross section P4
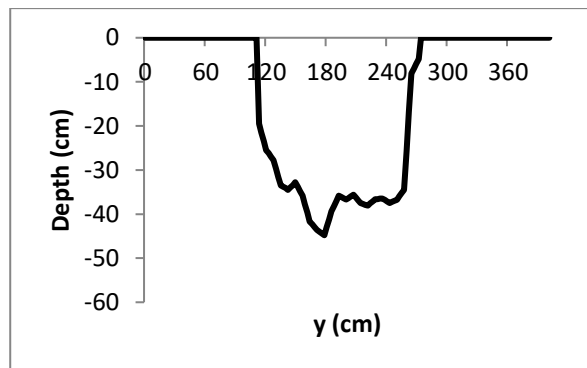
(e) Cross section P5

Fig. 5.1 Sampling point cross sections

Note: the cross section for water level measurement at P3 is the same with the velocity measurement of P6.

Table 5.1 Geometry of the sampling point cross section in the Expt. E-1

Parameter	P1	P2	P3	P4	P5	P6
Upper width, B (m)	0.37	1.67	3.14	0.97	1.63	3.14
Average depth, d_{avg} (m)	0.15	0.35	0.41	0.23	0.33	0.41
Maximum depth, d_{max} (m)	0.24	0.48	0.54	0.31	0.43	0.54
Cross section area, A (m^2)	0.058	0.586	1.284	0.225	0.535	1.284

Table 5.1 shows that the width, depth and cross section area increased from P1 to P3, and from P4 to P6, in accordance with Fig. 5.1.

5.1.1 Water level probe calibration

As explained in Chapter 4, the data shown from the water level probes were not the actual water level data, but values related to conductivity. In order to convert the data read from the water level probes, a calibration procedure needed to be carried out. Table 5.2 shows the results of the calibration exercise.

Table 5.2 Water level calibration in Expt. E-1

Point	x		y		Equation
	Max	Min	Max (cm)	Min (cm)	
P1	48.84	-92.99	5.30	-5.30	$y = 0.0747\,x + 1.652$
P2	82.71	-48.79	4.90	-4.90	$y = 0.0745\,x - 1.262$
P3	120.66	-13.95	4.35	-4.35	$y = 0.0646\,x - 3.448$

The calibration equation was obtained by assuming linear relationship, giving:

$$y_2 - y_1 = m\,(x_2 - x_1) \tag{5.1}$$

where: y_2 = maximum water level, y_1= minimum water level, x_2= maximum read data value, and x_1= minimum read data value.

For example, for Point P1: y_2= -5,3; y_1= 5.3, x_2= -92.985, x_1= 48.835

As a result, the calibration equation was found to be *y = 0.0747 x + 1.652*, as shown in Table 5.2. The same method was applied for the points P2 and P3, resulting in the calibration equations as given in the same table.

This procedure of calibration is critical for obtaining the correct measurement of water level.

5.1.2 Water level measurement results

Water level measurements were carried out at the three sampling points after the calibration of the water level probes. The measurements were undertaken simultaneously, using three water level probes. These measurements were done with the datum of the mean water level. By using these equations the read data were converted to actual water level data.

The overall water level measurement results are shown in Fig. 5.2.
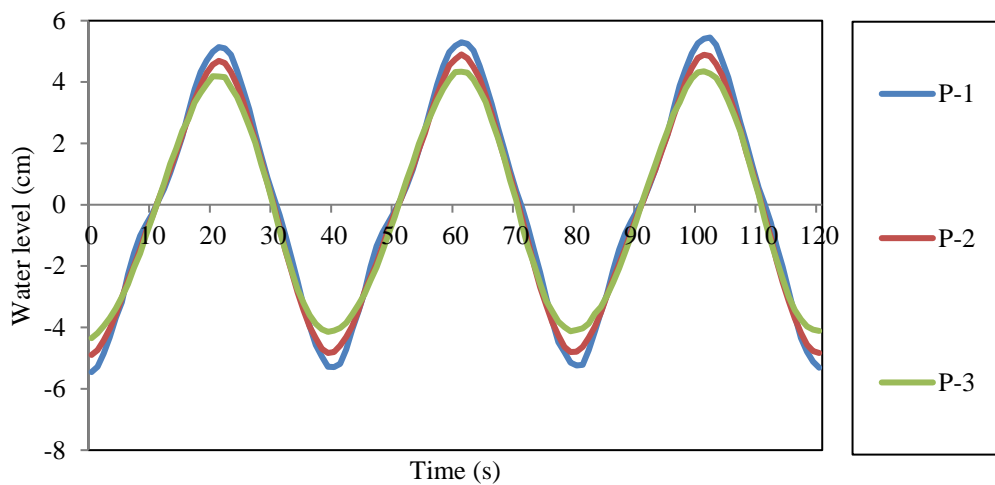
Fig. 5.2 Water level measurement results in the Expt. E-1

From Fig. 5.2 it can be seen that the water level range at the sampling points varied from 8 to 10 cm. The water level range was increasing in the following order: Points P3, P2, and P1. The water level range at each sampling point is shown in Table 5.3.

Table 5.3 Water level range at each sampling point in the Expt. E-1

Sampling point	Water level range (m)
P1	0.109
P2	0.098
P3	0.087

It is clear that the water level fluctuations at any point in the estuarine physical model were generated by the movement of the weir at the seaward boundary (i.e. lower boundary), and there was no other sources of water level change. Measurements of the water level fluctuations at the lower boundary, which were done after these experiments, revealed that the tidal range at the weir setting was 8.162 cm. This meant that the tide at the lower boundary had resulted in a larger water level range at the sampling points.

As can be seen in Table 5.3, the value of the tide range at the three sampling points was (from the biggest): Point P1, Point P2, and Point P3. Several aspects can be concluded from these results, as follow:

a.   Location of the sampling points

Theoretically the further the distance of the sampling point from the tidal weirthe smaller the water level range, with the water level range indicating the potential energy contained in the water column at that point. The further the location up the estuary meanta decrease in the potential energy. However, this theory was not always practical for this study, since there was a reflecting tide (ebb tide) from the upper boundary, which interacted with the incoming flood tide. The measured results in these experiments showed that the largest tide range occurred at Point P1, then P2, and

finally P3. This result did not agree with the energy theory, where the order should have been: P3, P2, and P1.

b. Cross sectional area at which the sampling point was located

According to the continuity principleand assuming that the velocity across the section is constant, then the larger the width of the channel, the smaller would be the tide range. From Table 5.1 it can be seen that cross section P3 is about 2.4 times greater than P2, and about 24 times greater than P1. According to the continuity principle, the decreasing water level range would be in the order (from the biggest): P1, P2, and P3.

c. Energy loss

There was energy loss in the water movement throughout the basin. The energy was generated from the potential energy of the tide weir. This potential energy is then converted to kineticenergy which causes water flow with a certain velocity. The water velocity measured in these experiments was therefore the representation of the kinetic energy (as the kinetic energy is formulated as $E_k = \frac{1}{2} mv^2$, where m = mass and v = velocity).

As stated in the energy conservation law, energy does not disappear, but is converted to other forms. Here the friction with the bed surface and the channel walls caused energy to be lost as heat. Theoretically, this energy loss should mean the reduction in the tidal range or a reduction in the velocity. The results show that the tide range in the physical model increased as the water flowed from the lower boundary (the sea boundary). Point P1 had the biggest tide range, succeeded by P2, and lastly P3. According to the law of continuity, fluid with a constant discharge which enters a narrower cross section will have a velocity increase.

5.1.3   Velocity measurement results

The next experiment was the experiment for measuring velocity. In order to obtain the velocity profiles, the velocity measurements were carried out in several levels in the water. The determination of those levels was based on the depth of the water in the sampling points.

The velocity measurements in each level were carried out using the suitable ADV probes. In general, for the levels near the physical model bed the downlooking ADV was used, while for the levels near the water surface the uplooking ADV was used.

After all the data was obtained, the velocities were then represented as the depth-average velocity using trapezoidal method.

Velocity was measured at the sampling points which were chosen as outlined above, and the velocity profiles were drawn, based on the velocity measurements at several levels at the sampling points. Fig. 5.3, 5.4 and 5.5 show the results of the velocity measurements for Point P4, P5 and P6, respectively.
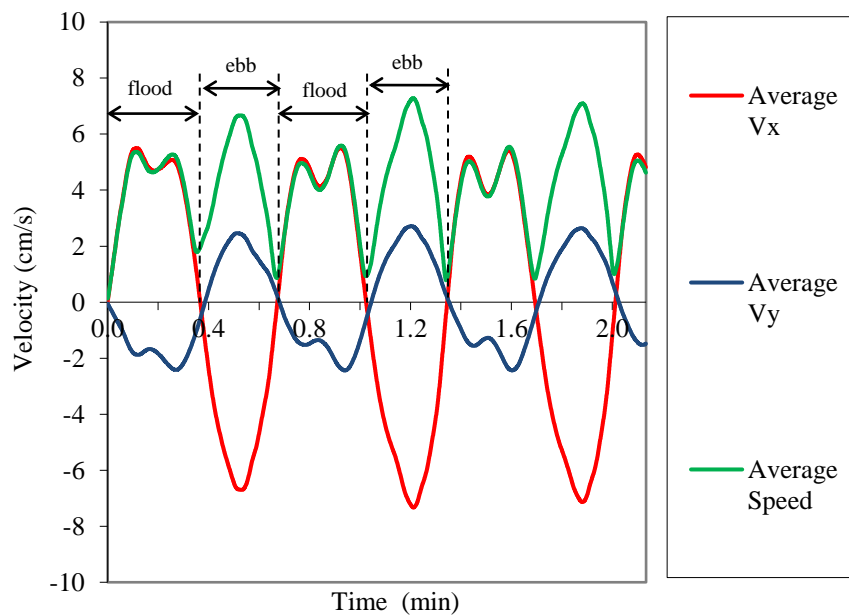
Fig. 5.3 Velocity measurement results at Point P4
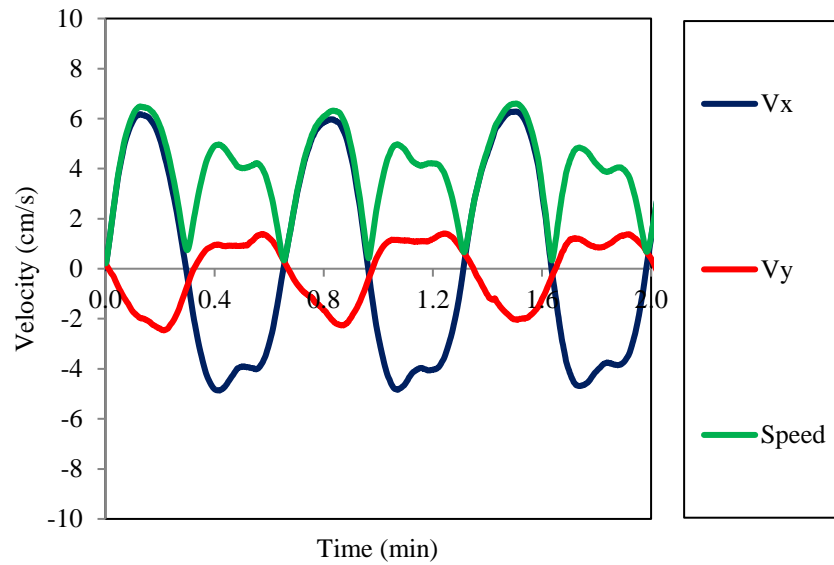
Fig. 5.4 Velocity measurement results at Point P5
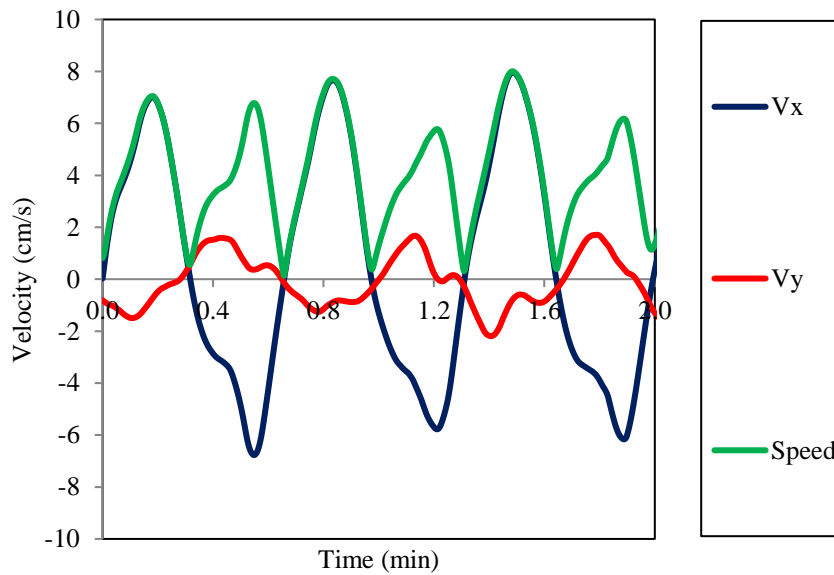
Fig. 5.5 Velocity measurement results at Point P6

Fig. 5.3, 5.4, and 5.5 show the velocity at Point P4, P5, and P6, respectively. At Point P4, Vx and Vy in the flood tide had two peaks, but in the ebb tide had only one peak. But at Points P5 and P6, Vx and Vy in the flood tide had only one peak, but in the ebb

tide had two peaks. This difference is due to geometrics of the physical model and the position of the sampling points relative to the weir which generated the tide.

For Points P4 and P6, maximum ebb Vx was larger than maximum flood Vx, but opposite situation happened at Point P5. For Points P4, maximum ebb Vy was larger than maximum flood Vy, but for P5 and P6 the opposite situation happened. These results were related to the position of the points and geometry of physical model.

Fig. 5.3 shows that there is a double peak in the flood tide at Point P4. But there is no double peak in the flood phase at Point P5. Instead, double peaks occur in the ebb phase of the graph. One possible reason that Vx only has one peak in the flood phase is that there is no obstruction from the reflecting wave from the upper boundary. This means that the reflecting wave came before the peak in the flood tide was achieved. Then, when the water level is forming the ebb phase, the reflecting wave came to Point P5 and hence double peaks are formed in the ebb phase.

The velocity graphs at Point P6 show a different shape from those at Point P4 and Point P5. At this point Vx is much more dominant. The velocity range of Vx (max-min) is about 13 cm/s, while Vy is about 3 cm/s. There is no double peak in the flood tide, but ebb tide shows double peaks although this is not obvious.

From the results shown above several data on velocity characteristics can be obtained, as shown in Table 5.4.

Table 5.4 Characteristics of velocity from the measurement

Sampling point	Vx-max flood (cm/s)	Vx-max ebb (cm/s)	Vy-max flood (cm/s)	Vy-max ebb (cm/s)	Speed-max flood (cm/s)	Speed-max ebb (cm/s)
P4	5.50	7.29	2.43	2.43	7.80	5.94
P5	6.28	4.84	2.46	1.41	6.60	4.94
P6	7.97	6.65	2.19	1.71	8.00	6.69

The hydrodynamics in the physical model can be analyzed generally by velocity graphs;

First is the speed comparison between flood tide and ebb tide. All points showed that maximum speeds in flood tide (7.80, 6.60 and 8.00 cm/s at P4, P5 and P6, respectively) were larger than maximum speed in ebb tide (5.50, 6.28 and 7.97 at P4, P5, and P6, respectively). This suggested that there was no obstruction from the reflected tide of the preceeding flood tide, since the location of Points P4, P5 and P6 were closer to the sea boundary than to the river boundary.

Second is the comparison between the speed from a point to the others (P4, P5 and P6). The maximum speed in flood tide decreased from 8.00 cm/s at P6 to 6.60 cm/s at P5, suggesting a decrease in energy as water flowed from sea boundary to river boundary. However at Point P4 the speed increased again to 7.80 cm/s, because of the effect of reflected tide from the preceeding flood tide as Point P4 was closer to the river boundary compared to the others.

Third is the comparison between Vx and Vy which indicates how velocity was diverted from longitudinal direction. Vx-max for flood increased from P4 to P6, or decrease from P6 to P4. This was because the flow was dominantly longitudinal at Point P6, then less longitudinal at Point P5 and P4. This can also be evaluated from the value of Vy-max flood. Vy-max at P6 was less than P5 and P4, suggesting that the transversal flow is minor compared to longitudinal flow at this point.

5.1.4   Velocity profile

In a water body, velocity of water particles are not usually homogenous, both vertically and horizontally. The velocity is distributed depending on the hydrodynamics of the water body. The distribution of velocity is usually represented by a velocity profile, and this profile is essential to identify the characteristics of the water body being studied.

DIVAST model represents velocity in three directions, namely longitudinal velocity (Vx), lateral or transversal velocity (Vy), and vertical velocity (Vz). Since this study approaches hydrodynamics of the Severn Estuary physical model as two dimensional,

that is water flows only in longitudinal and lateral directions, only Vx and Vy are analyzed.

At every point in the physical model, the magnitudes of Vx and Vy differed depending on the geometry of the model. For example, at Point P6 Vx is dominant as the water tended to flow straightly in longitudinal direction without obstacles or bends. However at Point P11 where the model bends, Vx was no longer dominant and Vy started to dominate the flow direction.

Considering this, velocity profile was analyzed in term of speed, that is the resultant betweenVx and Vy.

Fig. 5.6 to **Fig 5.8** show the vertical speed profiles at the sampling points in Exp. E-1 in flood and ebb tides, based on the velocity measurements undertaken during the experiments and a result of 3 (three) cycles averaging.

(a)   (b)
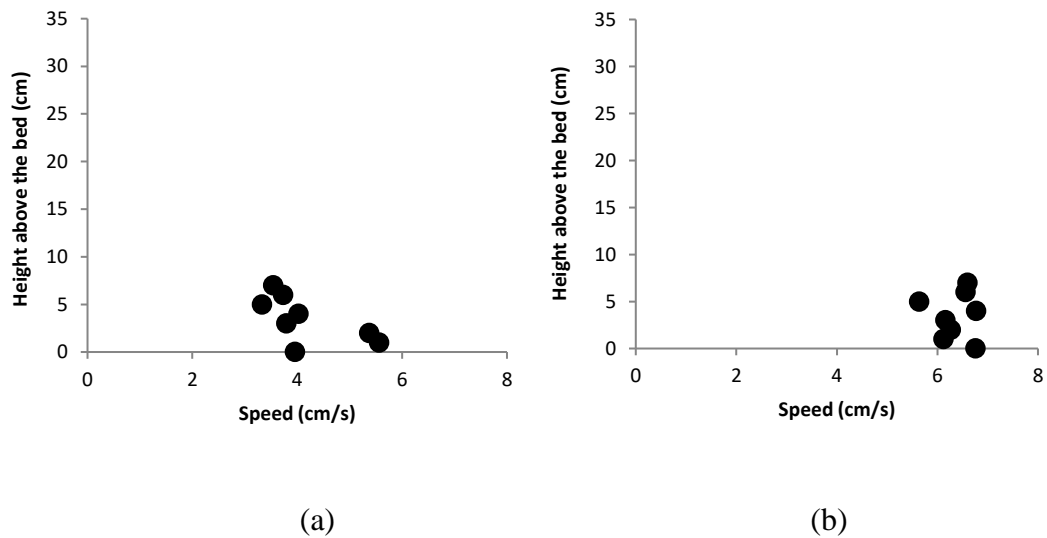
Fig. 5.6 Vertical speed profiles at Point P4 in Expt. E-1: (a) flood tide; (b) ebb tide

(a) (b)
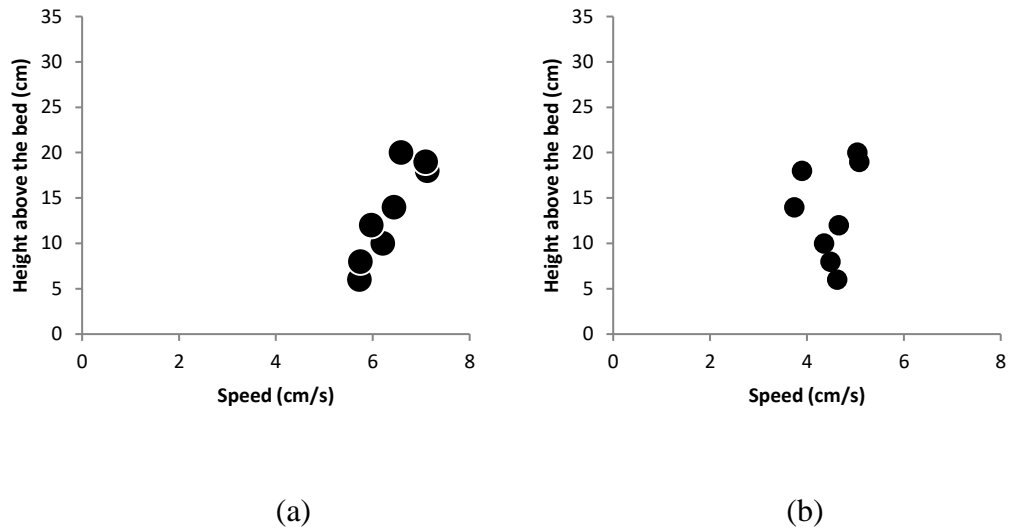
Fig. 5.7 Vertical speed profiles at Point P5 in Expt. E-1: (a) flood tide; (b) ebb tide

(a) (b)
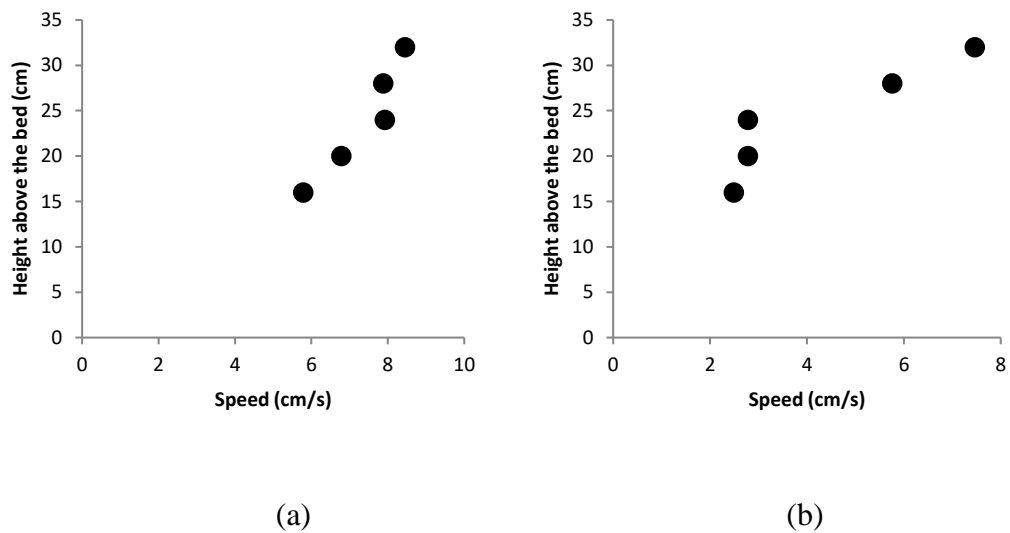
Fig. 5.8 Vertical speed profiles at Point P6 in Expt. E-1: (a) flood tide; (b) ebb tide

In this study the longitudinal flow happened in flood tide resulting in the flow going from the weir (or sea boundary), and ebb tide resulting in the flow coming to the weir. Flood tide happens when the physical model weir moves up, while ebb tide happens when the physical model weir moves down. Beside the two tides, there is also a flow

as the reflection of the flood tide to the river boundary. This flow is named reflected flow. Flood tide and reflectide flow may meet in a certain region of the physical model, meaning that the flood tide going from the weir may meet the reflected flow tide from the flood tide of the preceeding tide cycle. This region is predicted to be near the river boundary. As a result of this, the speed profile may not similar with the typical profiles for laminar flow, which start from zero velocity in the bed and maximum velocity in the water surface, as sketched in Fig. 5.9.
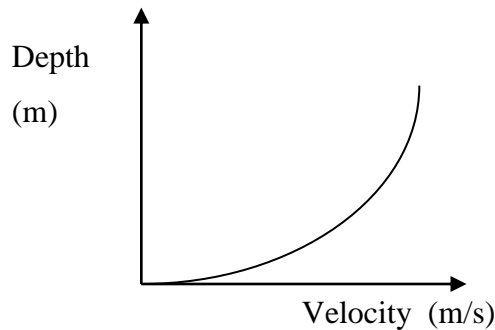
Fig. 5.9 Typical vertical velocity profile in laminar flow

Fig. 5.6 to 5.8 shows the vertical speed profiles at Point P4, P5 and P6, for flood and ebb tides. For Point P4, generally water speed in the flood tide was smaller than in the ebb tide. Five points showed close speed values, namely between 3.3 cm/s and 4.0 cm/s, and only two points showed rather far values, which were 5.4 cm/s and 5.6 cm/s.

Despite the two points which showed rather far velocity values, the remaining points showed close values of speed. This suggested that either the flow was turbulence (which tend to form a flatter velocity profile than laminar flow as illustrated in Fig. 5.9), or there was a disturbance from the reflected flow deterring the formation of normal velocity profile as illustrated in Fig. 5.9.

As for Points P5 and P6, more curved speed profile can be observed. This is closer to the ideal velocity profile in Fig. 5.9

As a contrast to Point P4, at Points P5 speed of flood tide was larger than speed of ebb tide. The speed profile shows tendency to ideal velocity profile, with the speed in the

top of the profile being the maximum speed and the bottom of the profile being the minimum. This suggests that the flow tended to be longitudinal, without significant disturbance from the reflected flow from the preceding flood tide. This is suggested to relate with the position of Point P5 which was much further from the river boundary than Point P4, making the effect of reflected flow insignificant.

At Point P6, the shape of speed profile clearly represented the ideal velocity profile depicted in Fig. 5.9. The top of the profile was the maximum speed, while the bottom of the profile was the minimum speed, and the other points formed a smooth curve from large speed value in the upper position to smaller ones in the lower position. This suggests that the flow tend to be laminar than the flow at the other points (P4 and P5). This also happened in the ebb tide, with a steeper profile. The top of the profile was the largest speed, while the bottom of the profile comprises the smallest speed. The value of speed decreased from upper to lower points, suggesting an ideal velocity profile such as depicted in Fig 5.9. However, there is a slack between the speed at third and forth level (from the bottom), suggesting that there is always possible disturbance to the profile by certain aspects, such as shape of the physical model which is irregular.j

5.2 Experiment E-2

The Expt. E-1 helped in obtaining some basic information on the hydrodynamics of the Severn estuary physical model. They described the hydrodynamic characteristics of the estuarine physical model, including the water levels, velocity and velocity profiles. These observations led to a first assessment of the hydrodynamics of the physical model, which can help in predicting the value of the dispersion coefficient for this water body. However, a more detail observation was needed to predict the dispersion coefficient, by undertaking more comprehensive experiments, assisted by a mathematical solution (including computer modeling). Expt. E-2 was designed to observe the change in the hydrodynamic conditions from point to point, which were quite close, so that the change in the hydrodynamic parameters could be evaluated more accurately.

As for the Expt. E-1, Expt. E-2 included:

- water level measurements
- velocity measurements

After the experiments were completed, the computer model was run and calibrated against the experimental results for the hydrodynamics.

5.2.1   Water level measurement results

As for the Expt. E-1, the first measurement was carried out for the water levels. The results can be seen in Fig. 5.10.

Change in slope of flood levels seems to be related to geometry – only starts occurring at P8.
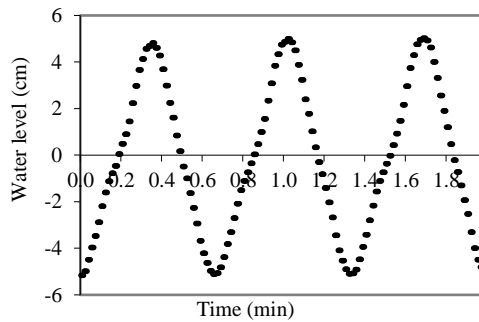
(a)
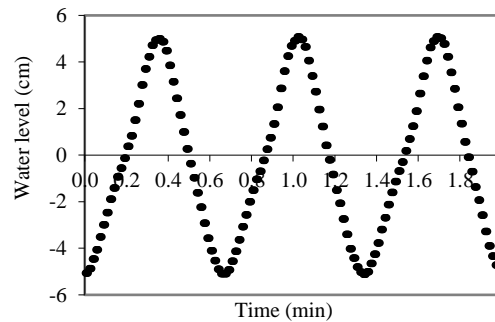
(b)
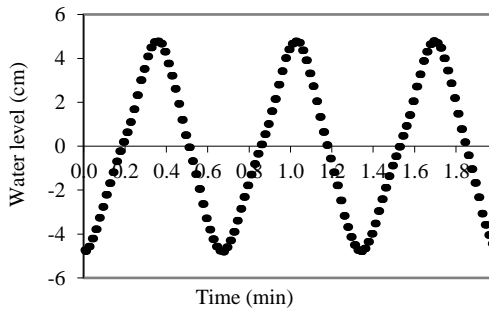
(c)
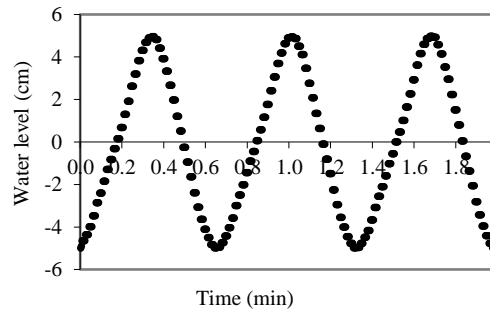
(d)
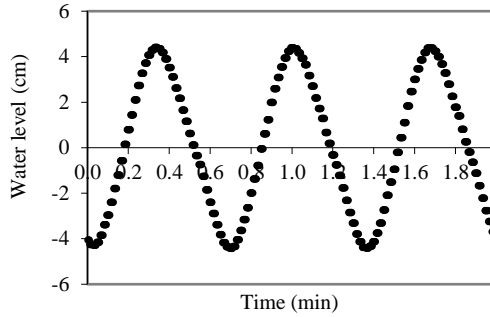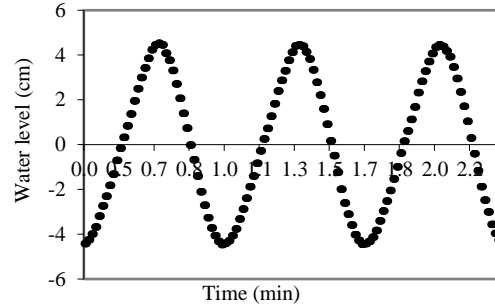
(e)   (f)

Fig. 5.10 Water level measurements for Expt. E-2 at (a) P7, (b) P8, (c) P9, (d) P10, (e) P11, and (f) P12

Fig. 5.10 shows that there are no significant differences for the water level measurement results at the six sampling points. This is rather different with the results in the Expt. E-1, where the differences in the water level range were quite significant.The reason of this is because in the second experiments the location of the sampling points were close to each other.

It was predicted that the water level and velocity in Expt. E-2 did not differ significantly. Figure 5.10 shows that the differences of tide range between the successive sampling points were small.

The small distance and small differences among the water level in Expt. E-2 was important so it was easier to discuss the dispersion process later.

5.2.2 Velocity measurement results

Velocity measurements were then undertaken for Expt. E-2, in the same manner as for Expt. E-1, taking several levels for the measurement in order to calculate the depth-averaged velocity and to establish the velocity profile at each sampling point. The depth at which measurements were taken is shown in Table 5.5.

Table 5.5 Data of levels for velocity measurements

Level	Point-7 H (cm)	Point-8 H (cm)	Point-9 H (cm)	Point-10 H (cm)	Point-11 H (cm)	Point-12 H (cm)
1	2.8	2.8	2.6	3.5	4	4
2	5.6	5.6	5.2	7	8	8
3	8.4	8.4	7.8	10.5	12	13
4	11.2	11.2	10.4	14	16	17
5	14	14	13	17.5	19.3	22
6	16.8	16.8	15.6	21	23.0	25
Total depth	19.2	20	18	25	28.5	29.2

Fig. 5.11 to 5.16 show the velocity measurement results at the six sampling points (P7 to P12). There are some differences in the velocity measurement results at each point. These differences includes the magnitude of the velocity and the shape of the velocity graphs.
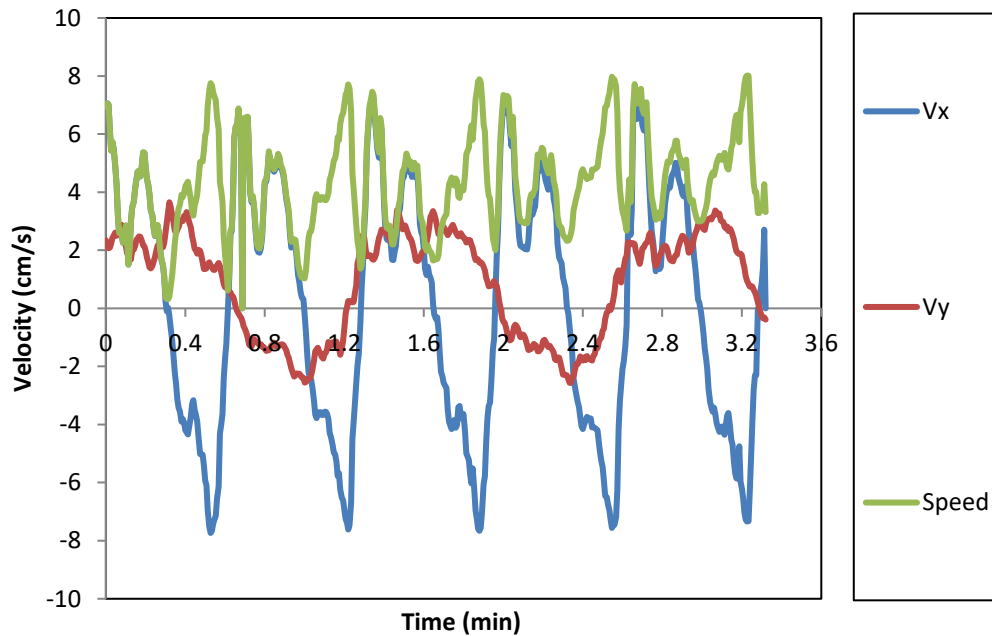
Fig. 5.11 Velocity measurement results (depth-averaged) at Point P7
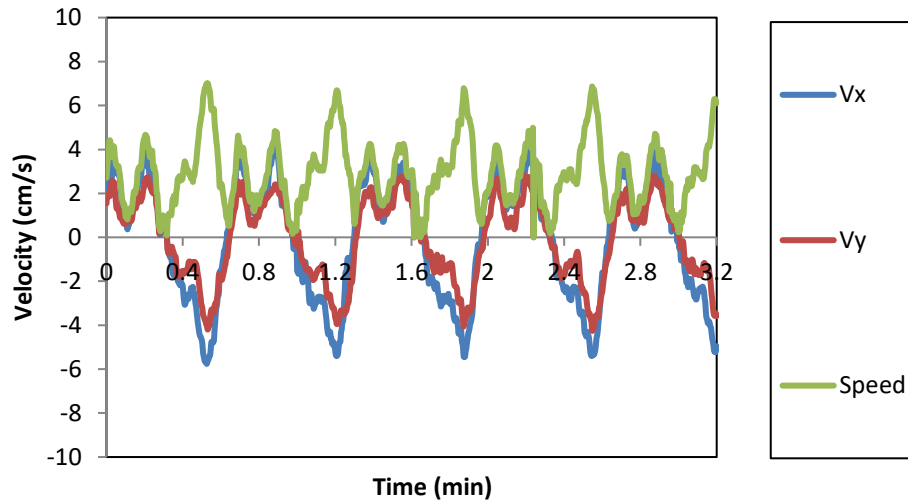
Fig. 5.12 Velocity measurement results (depth-averaged) at Point P8
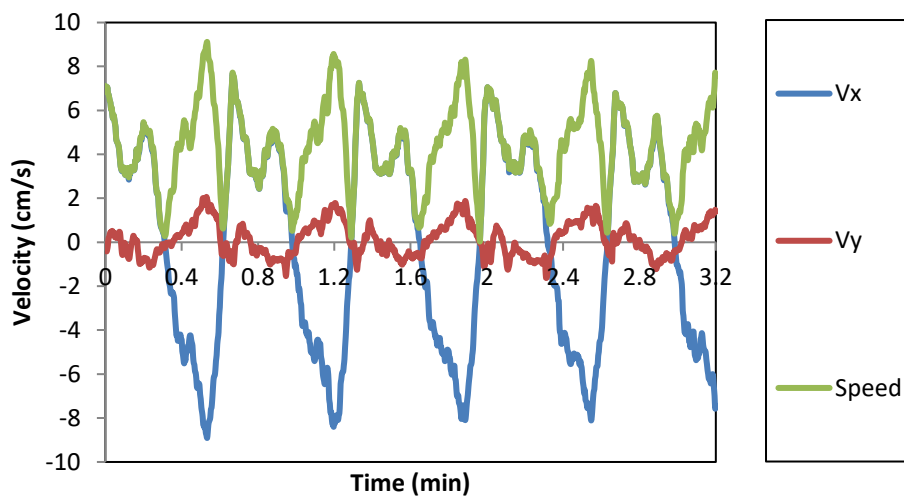
Fig. 5.13 Velocity measurement results (depth-averaged) at Point P9
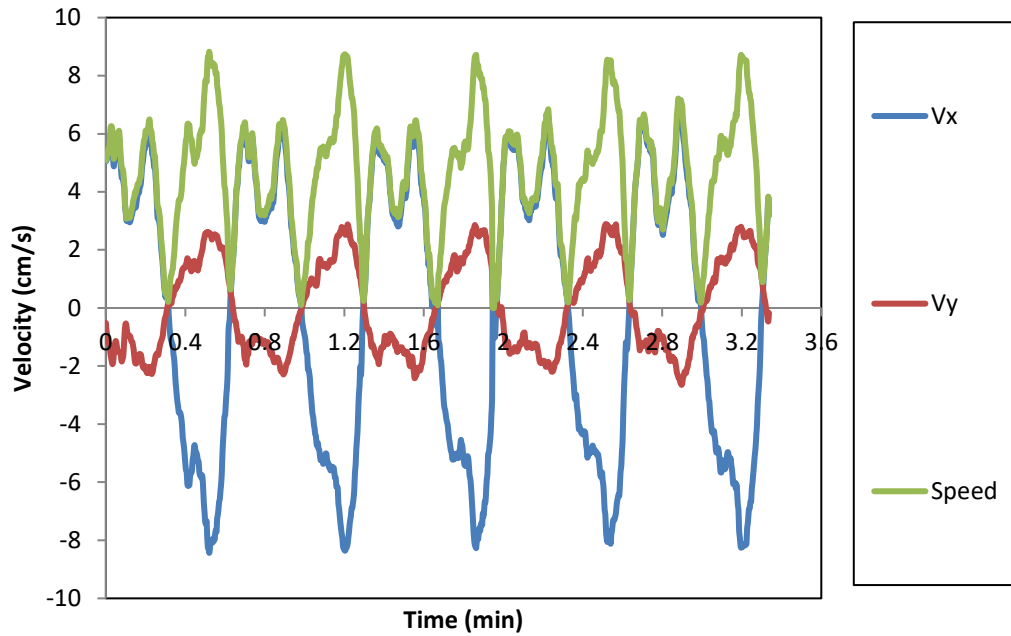
Fig. 5.14 Velocity measurement results (depth-averaged) at Point P10
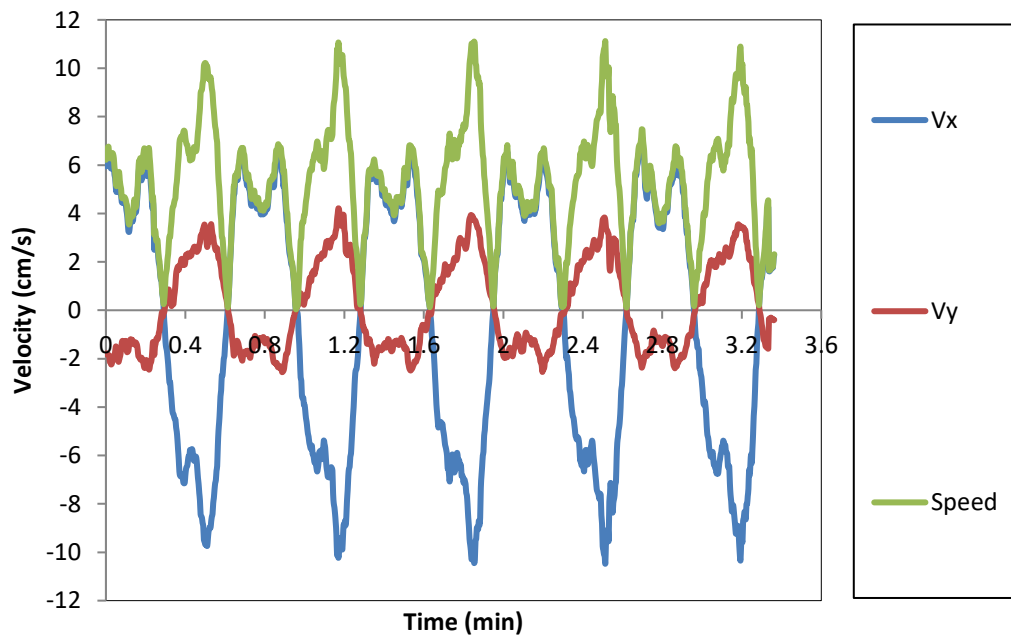
Fig. 5.15 Velocity measurement results (depth-averaged) at Point P11
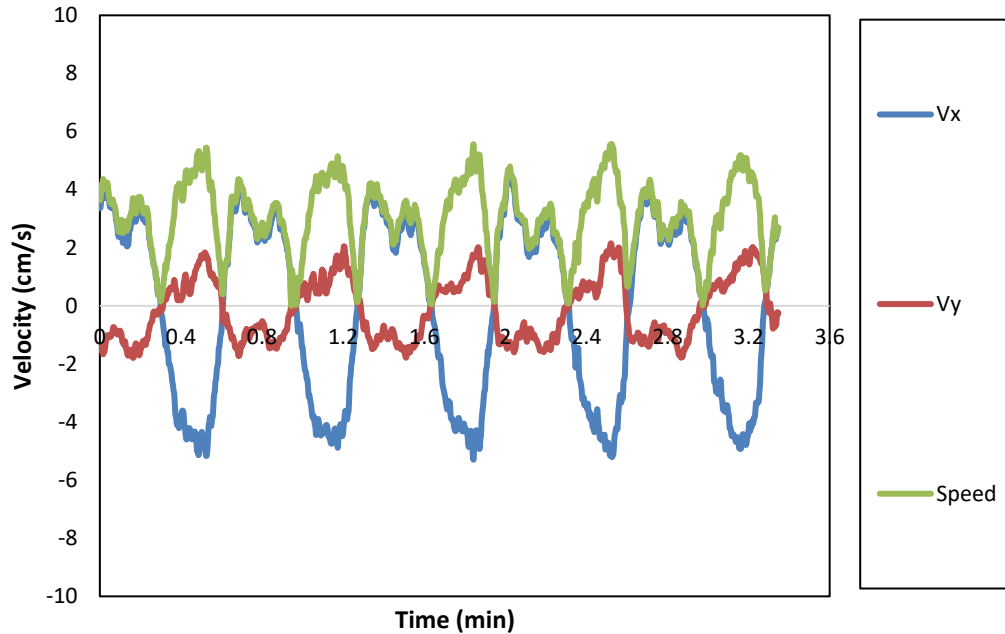
Fig. 5.16 Velocity measurement results (depth-averaged) at Point P12

Based on the results shown in Fig. 5.11 to Fig. 5.16, the maximum velocity can be identified as shown in Table 5.6.

Table 5.6 Maximum Vx, Vy and Speed in the Expt. E-2

	Vx-max-flood	Vx-max-ebb	Vy-max-flood	Vy-max-ebb	Speed-max-flood	Speed-max-ebb
P7	7.08	-7.66	3.65	-2.42	7.72	7.98
P8	4.12	-5.66	2.53	-3.99	7.84	6.96
P9	7.65	-8.67	-1.31	1.99	7.71	9.12
P10	6.47	-8.25	-2.23	2.43	7.21	8.83
P11	6.76	-10.46	-2.25	4.21	7.48	11.01
P12	4.49	-5.17	-1.72	2.22	4.69	5.54

There are several points which can be derived from the data above:

-The ratio between Vx and Vy: The more dominant Vx, the closer the flow to be dominantly longitudinal. In general, Vx is always larger than Vy according to the data in Table 5.6. This means that the longitudinal flow is dominant to lateral/transversal

flow. The comparison between Vx and Vy in flood tide, regardless the negative signs are as follow:

P7: 1.9   P10: 2.9

P8: 1.6   P11: 3.0

P9: 5.8   P12: 2.6

Based on the data above, the flood tide Vx was about 2-3 times than the flood Vy. These values have relationship with the positions of those sampling points which were in the bends, making Vx not dominant. Only P9 had significant value of this ratio, where its Vx was almost 6 times than Vy in flood tide. This can be explained by the position of the sampling points. For P7, and P8, the posision is north-east, making Vx positive and Vy positive. For P10, P11, and P12 the position of the sampling points were north-west, making Vx positive and Vy negative. As for P9, its position was between the two bends. Therefore it seemed that the velocity had dominant longitudinal, because this point was in the position where the flow altered. The value of Vy was therefore the smallest among the other points, that was only 17% of Vx.

This happened oppositely in the ebb tide. P7 and P8 had negative Vx and negative Vy, while P10, P11 and P12 had negative Vx and positif Vy. P9 tended to follow the other points in north-west, making it have negative Vx and positive Vy. Still among the other points, Vy at this point was the smallest, suggesting that this was a dominant longitudinal flow.

Other aspects which can be discussed is the comparison between flood tide and ebb tide in term of speed. Except for P8, flood tide had lower speed than flood tide. The ratio between flood tide and ebb tide in percent was: 97%, 112%, 85%, 81%, 68%, and 85% for P7, P8, P9, P10, P11 and P12, respectively. This is suggested to be related with the position of the sampling points, which were closer to the river boundary than to the sea boundary. These positions made the flood be detered by the fixed river boundary or by the reflected flow of the preceding flood tide, thus reducing

the velocity of the flood tide. On the other hand, ebb tide had no obstruction. It just flowed without obstruction towards the sea boundary and fall to the ground tank.

A comparison may be made between sampling points in this experiment with the Experiment E-1. In experiments E-1, at sampling points near river boundary (P1), speed in ebb tide was larger than speed in flood tide. However, at P2 and P3, speed in ebb tide was smaller than in flood tide. This was because flood tide was not detered by the fixed river boundary or by the reflected wave. The difference between flood tide speed and ebb tide speed is suggested to be related with the energy loss from the flood tide.

5.2.3 Velocity profile

Although the hydrodynamic conditions were predicted in the same manner and at certain phase of the tidal cycle, it was considered important to compare and assess the velocity profile at certain phases of the tidal cycle.

From the preliminary results it can be seen that Vy was in generalsmaller than Vx, and the speed graph was almost the same as the absolute value for Vx. Therefore for the further analysis, only the speed is regarded and drawn in the velocity (or speed) profiles.

The velocity profile is also used to evaluate the values of the momentum correction coefficient (β), which is an important parameter for more accurate modelling of the advective accelerations. In the analysis it is important to ensure that βis evaluated throughout the tidal cycle from the velocity graphs, and then averaged to obtain a tide averaged representative value of β. The formula for β is as follow:

$$\beta = \frac{1}{H}\left(\sum_{i=1}^{i_{max}} \frac{v_i + v_{i+1}}{2}\Delta h_i\right) (5.2)$$

where H = total water depth, v = velocity/speed, i = index for depth of velocity measurement, Δh_i = distance between two successeive point measured.

Fig. 5.17 to Fig. 5.22 show the speed profile for each sampling point, and Fig. 5.23 shows the value of average β at each point. Data were take in in the maximum (high) water level in five cycles.
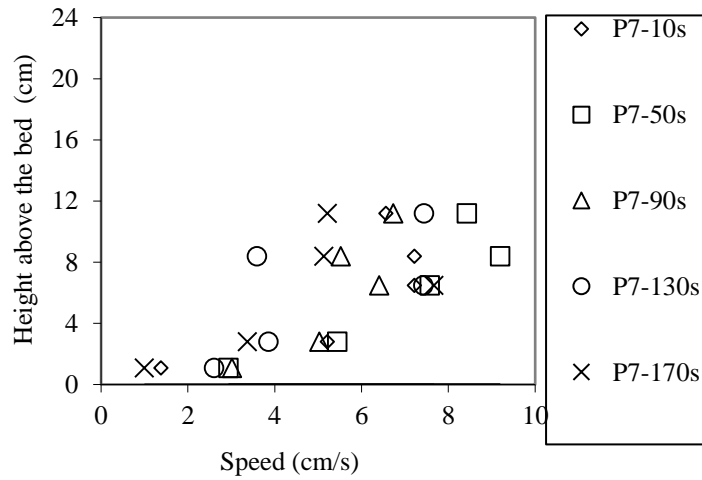
Fig. 5.17 Vertical speed profiles at Point P7
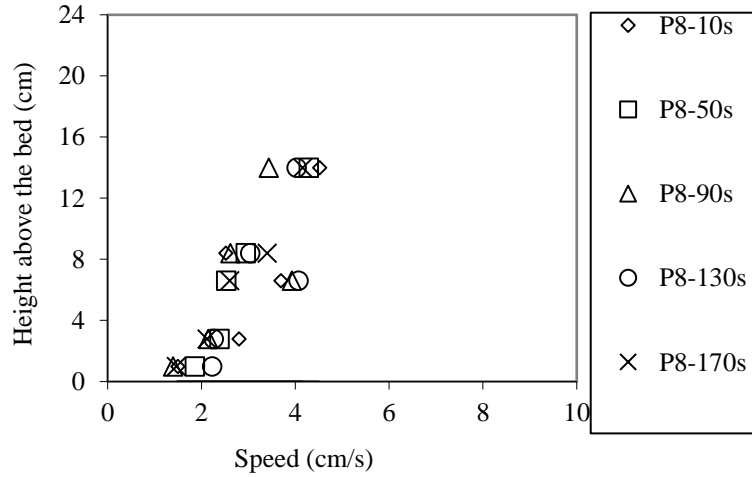
Fig. 5.18 Vertical speed profiles at Point P8
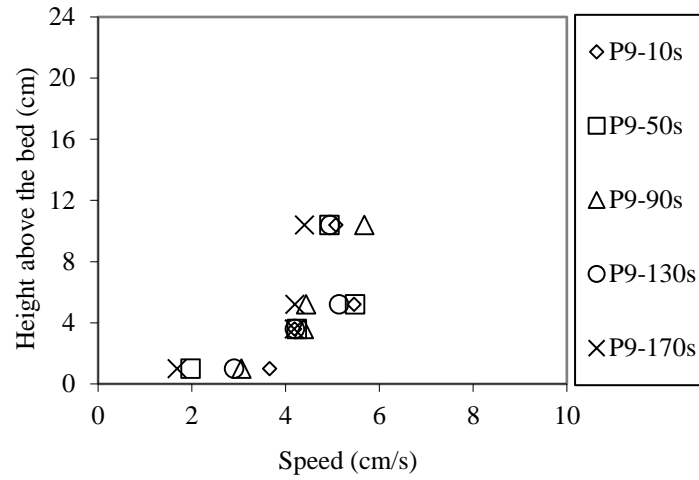
Fig. 5.19 Vertical speed profiles at Point P9
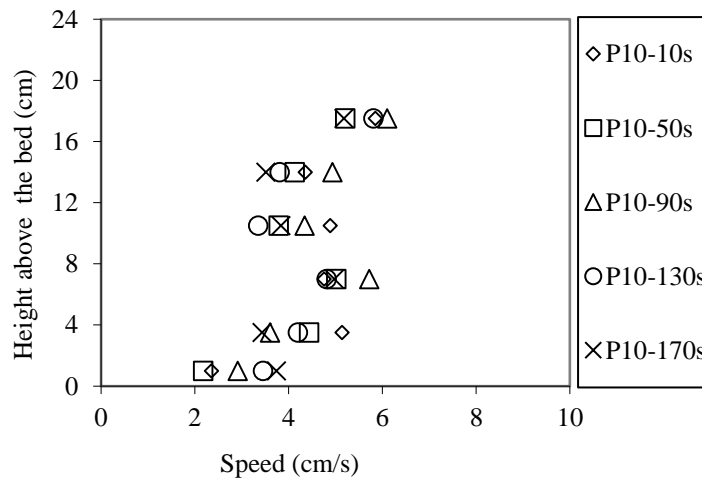
Fig. 5.20 Vertical speed profiles at Point P10
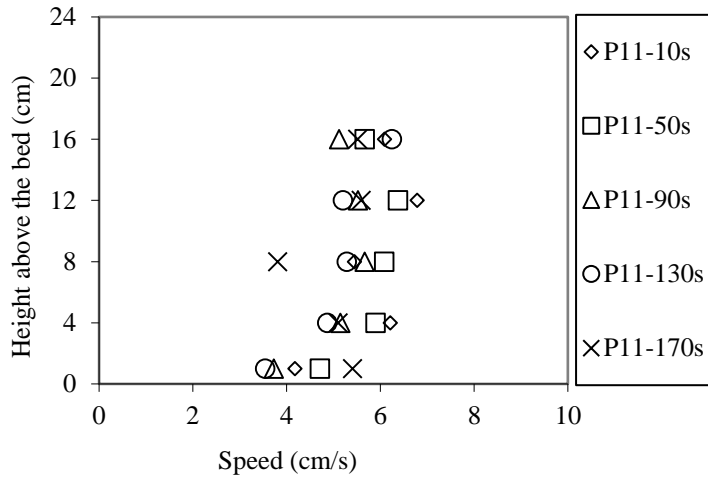
Fig. 5.21 Vertical speed profiles at Point P11
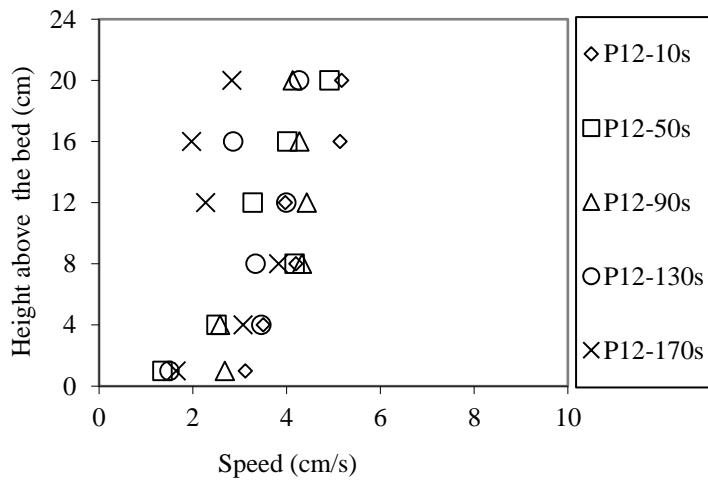
Fig. 5.22 Vertical speed profiles at Point P12
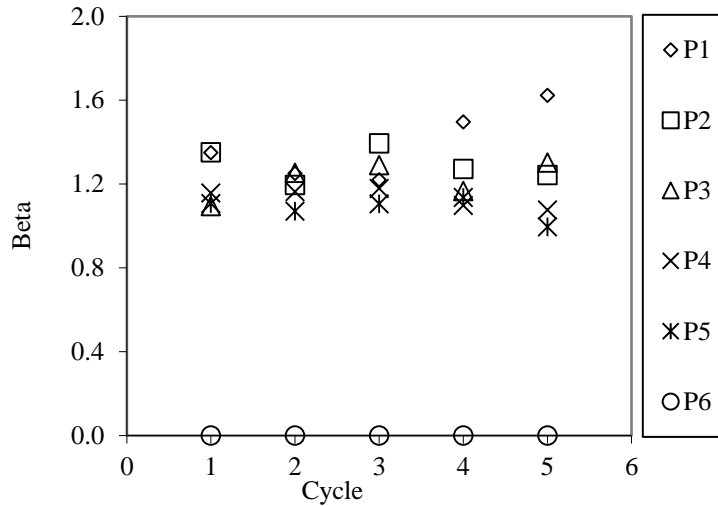
Fig. 5.23 Values of β per cycle at each point

For each point, the velocity profile was made for several cycles of the tide, that were 10, 50, 90, 130, and 170 seconds according to the period of the tide which was 40 second. This was done in order to evaluate whether the velocity profile was consistent in several cycles. The figures show that the velocity profiles at all sampling points were quite consistent.

Fig. 5.23 shows the β values at each sampling points in several cycle. This value of β will be then used in the modelling works in the next step.

5.3 Modelling results

After the hydrodynamic parameter data were obtained, the computer model needed to be calibrated against those data. The calibration steps consisted of: (i) geometric fitting, where the coordinates of the computer model were fitted to those of the physical model, (ii) parametric calibration, where the model was calibrated by varying the values of some parameters, namely the Manning roughness coefficient (n), the eddy viscosity coefficient (ε), and the momentum correction coefficient (β).

5.3.1   Water level modelling

The first step in model calibration is geometric fitting, namely checking the agreement between the geometry of estuary between the domain in the computer model and the physical model. This is done by checking the coordinates of several obvious points, such as angles, humps, and deep points. The results of this fitting was that the domain of the computer model should be shifted as many as 6 (six) rows. Results are not shown here.

After geometric fitting, the model was run and the predicted water level result were compared to the experimental data. The results can be seen in Fig. 5.24 to 5.29.
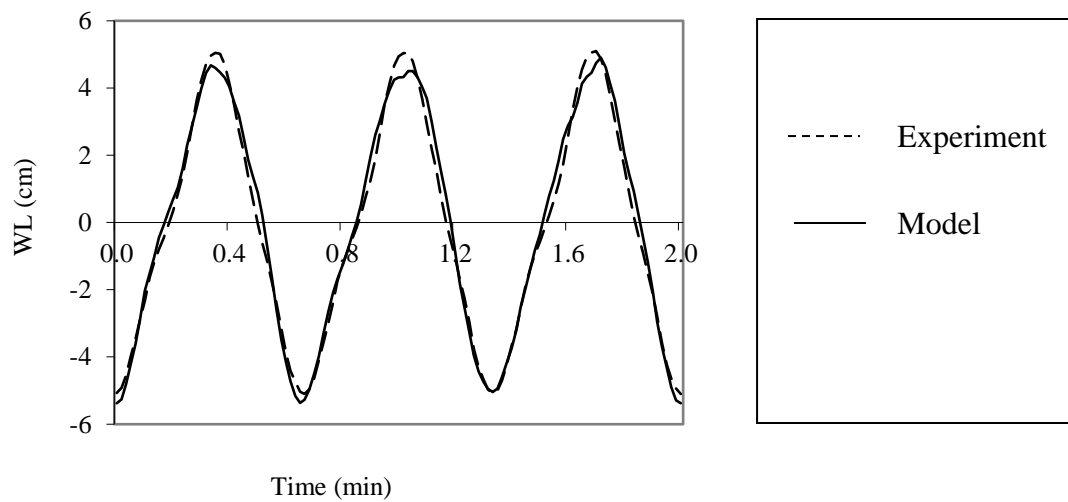
Fig. 5.24 Water level comparison at P7
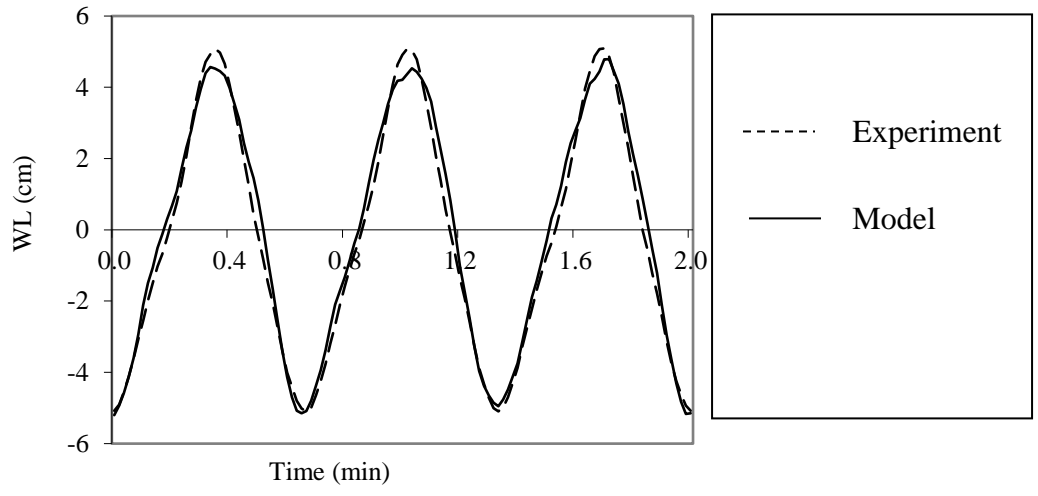
Fig. 5.25 Water level comparison at P8
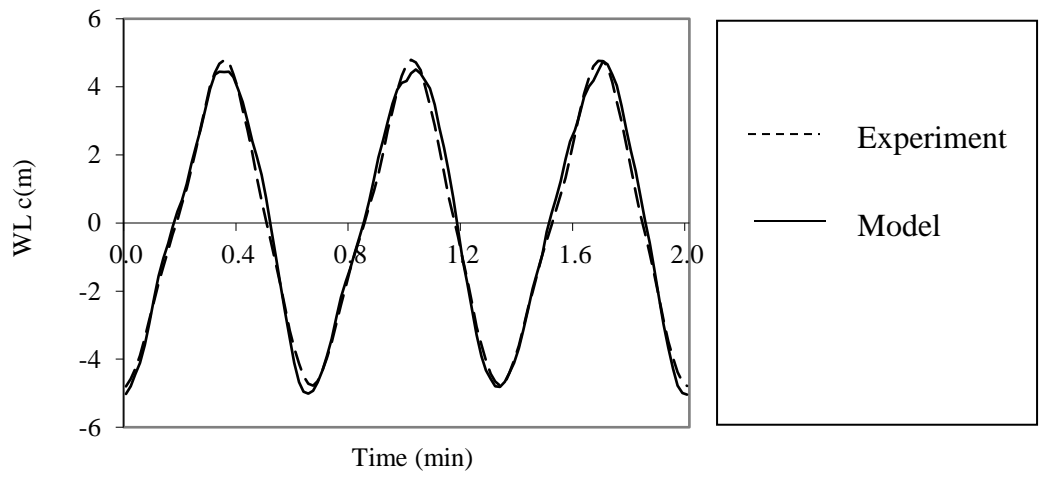
Fig. 5.26 Water level comparison at P9
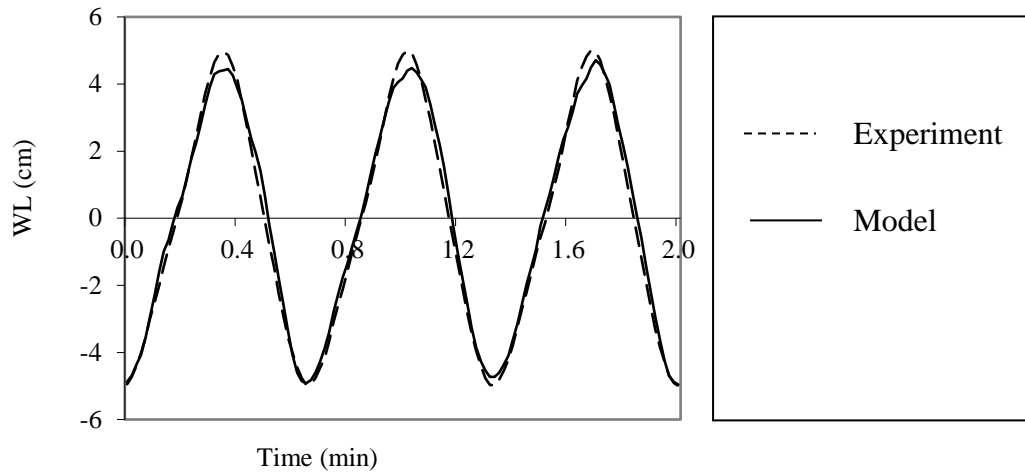
Fig. 5.27 Water level comparison at P10
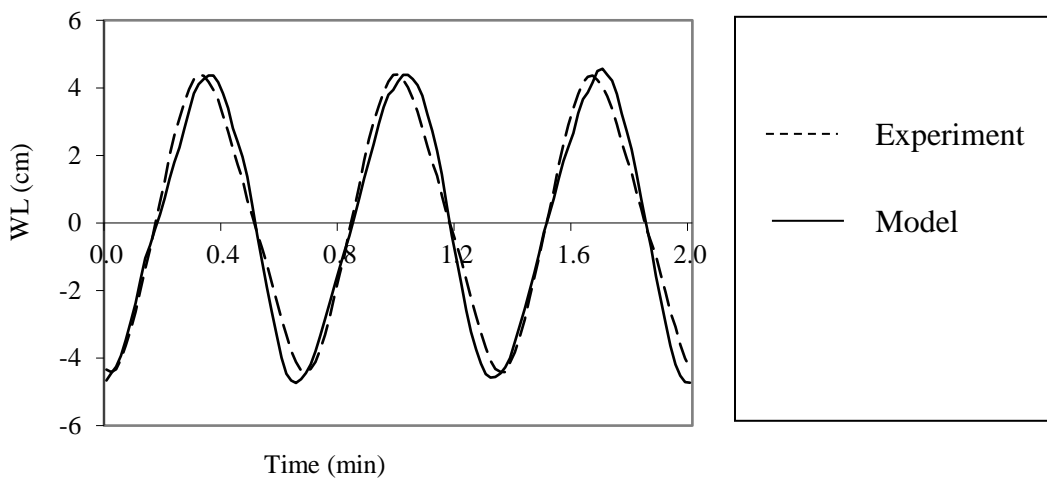
Fig. 5.28 Water level comparison at P11
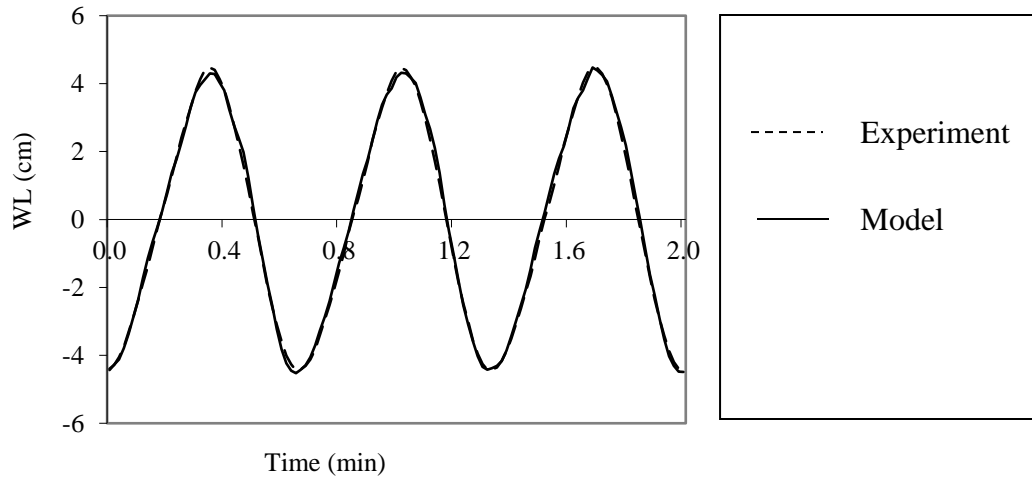
Fig. 5.29 Water level comparison at P12

The first attempt for addressing this problem was to fit the geometry of the domain block in the computer model with the physical model. This step was taken in order to make sure that the geometry of the computer model fit perfectly the geometry of the physical model. After this step had been done, the model was directly applied to Expt. E-2 results. The first calibration was to model the water level, the results of which is shown in Fig. 5.24 to Fig. 5.29.

From the figures it can be concluded that the model could fit the experimental results, except for Point 5. But for the other points, the model fit with the experimental results very well.

5.3.2   Velocity modelling

a.   Parametric calibration

After geometric fitting, the model was also calibrated against the experimental data by varying several parameters, namely: the Manning n roughness coefficient, the eddy viscosity coefficient, and the momentum correction coefficient (β). The condition of each run for these comparisons are shown in **Table 5.7**.

Table 5.7 Values of the parameter in the calibration

Run	COED	β	n-Manning
1	1.5	1.031	0.035
2	0.3	1.031	0.035
3	0.3	1.106	0.025

The value of β still used assumption, using a random value. Later in the next step an exact value of β using equation Eq. (5.2) will be used.

After trying those values and evaluated the model, three combinations were selected as they were shown in Table 5.7. Finally after error analysis using α, the best values of the parameters were selected, namely: COED = 0.3, n = 0.025, and β = 1.106. The complete results of the error analysis is shown in Table 5.8.
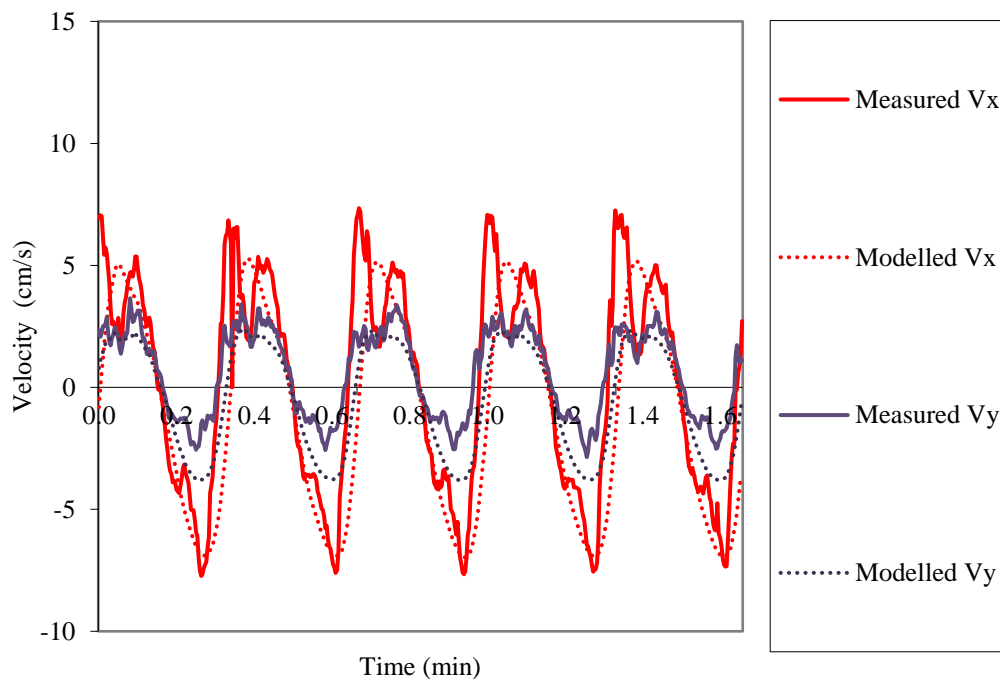
Fig. 5.30 Velocity model results at P7 (n = 0.025, ε = 0.3, β = 1.106)
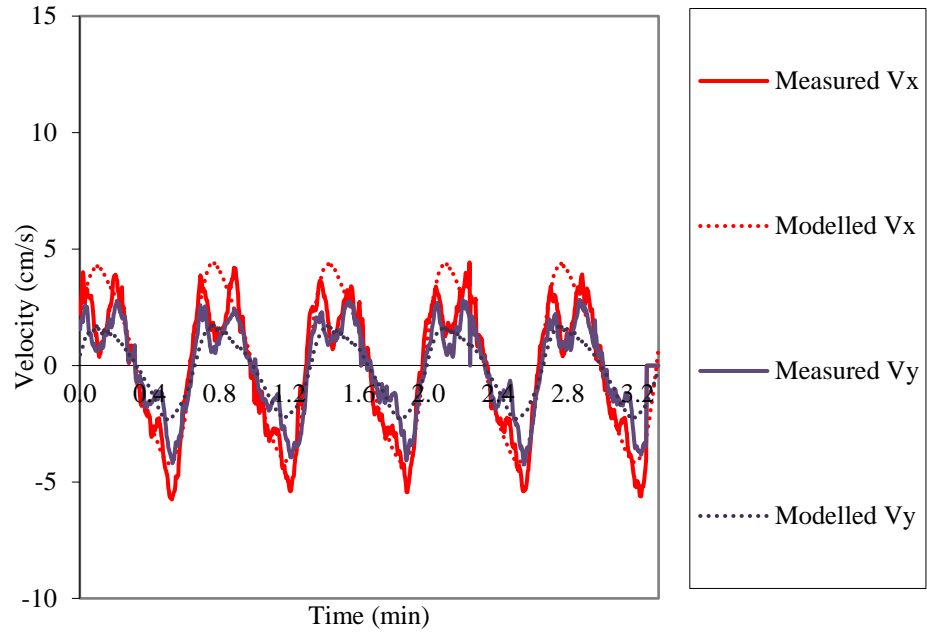
Fig. 5.31 Velocity model results at P8 (n = 0.025, ε = 0.3, β = 1.106)
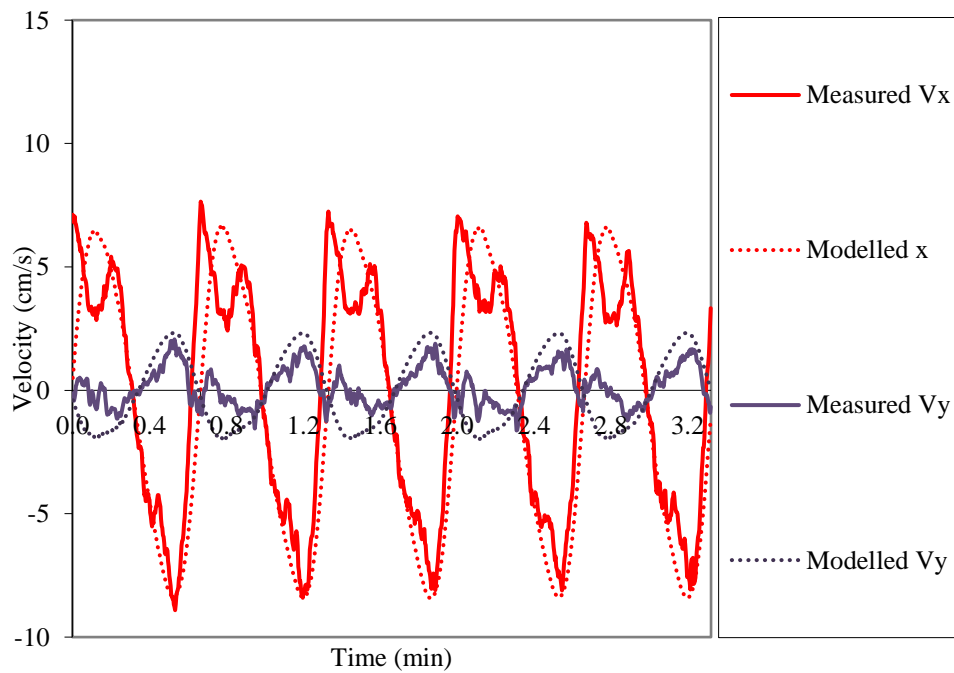
Fig. 5.32 Velocity model results at P9 (n = 0.025, ε = 0.3, β = 1.106)
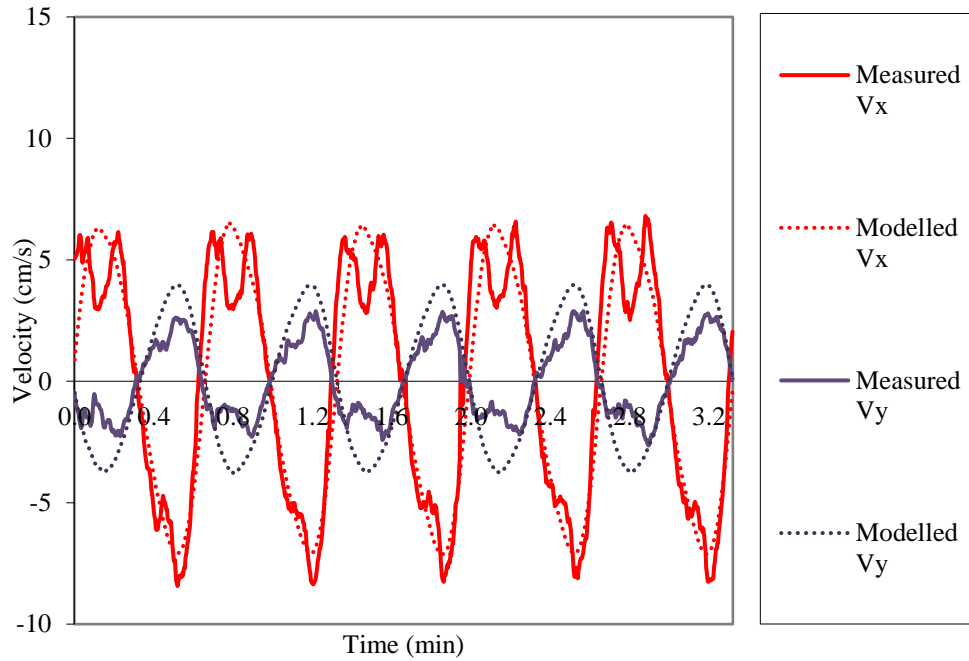
Fig. 5.33 Velocity model results at P10 (n = 0.025, ε = 0.3, β = 1.106)
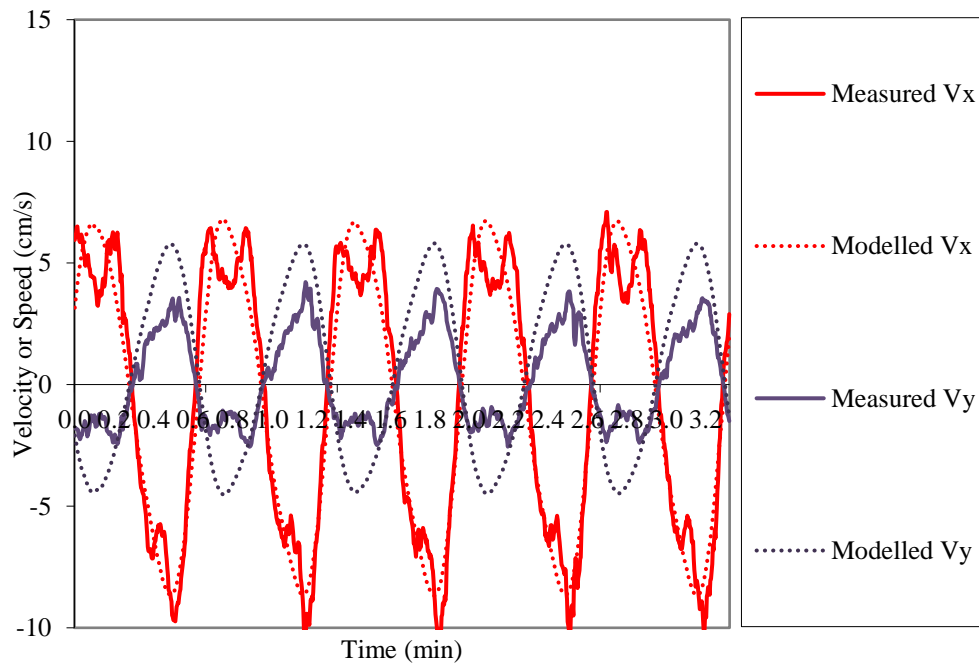
Fig. 5.34 Velocity model results at P11 (n = 0.025, ε = 0.3, β = 1.106)
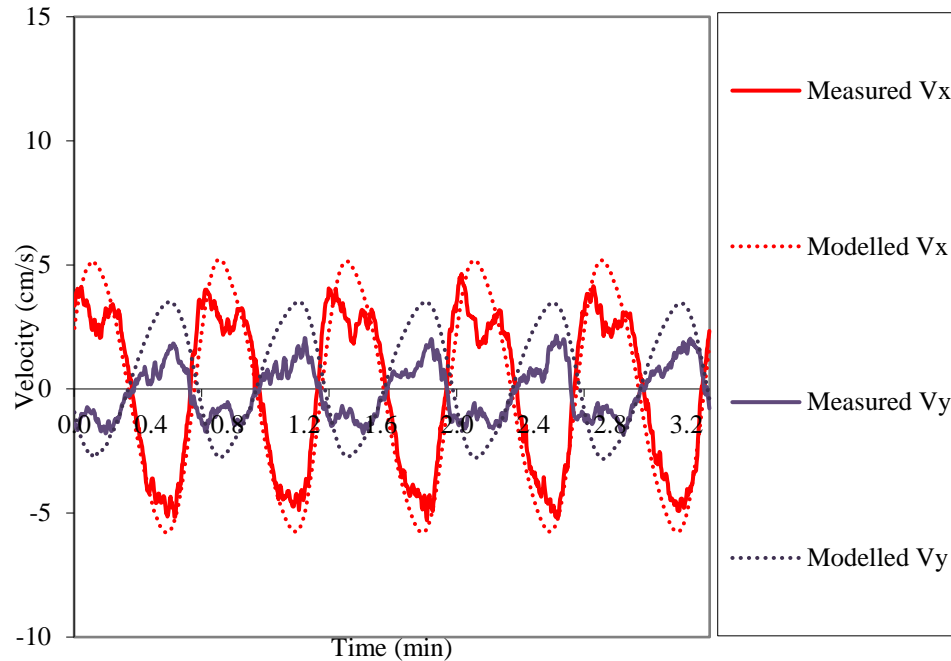
Fig. 5.35 Velocity modelresults at P12 (n = 0.025, ε = 0.3, β = 1.106)

The modelling results in Fig. 5.30 to 5.35 show that the models were quite close to the experimental results, only that the uneven lines of the experimental curve resulted from the water turbulencewasnot represented by the smooth model.Also, the double peaks in the velocity graphs at Points P7, P9, P10, and P11 (Figs. 5.11 to 5.16) was not represented by the computer model. This is probably due to boundary conditions which still use a simulated graphs (not an actual one) which will be discussed in the next section.

At Point P12 the degree of agreement was quite low except for Vx and Vy in Run-1. This is quite strange given that P12 is the closest point to the lower boundary, meaning that the model should have given the best result. However the turbulent condition generated by the weir may have affected the velocity making some deviation from the velocity predicted by the computer model.

103

Table 5.8 Error analysis for the parametric calibration (in term of α)

Vx	P7	P8	P9	P10	P11	P12
Run-1	0.655	0.855	0.596	1.038	1.409	0.944
Run-2	0.846	1.140	0.756	1.168	1.466	0.449
Run-3	0.542	0.816	1.002	1.612	0.613	0.267
Vy	P7	P8	P9	P10	P11	P12
Run-1	0.563	1.172	0.292	0.427	0.461	0.479
Run-2	2.115	1.360	0.250	0.649	0.629	0.778
Run-3	0.896	1.263	0.216	0.651	0.467	1.880
Speed	P7	P8	P9	P10	P11	P12
Run-1	1.049	1.100	1.054	0.964	1.021	0.909
Run-2	2.114	1.262	1.241	1.449	1.411	1.018
Run-3	1.664	1.269	1.301	1.351	1.309	1.122

b. Effect of boundary condition

The effect of the boundary conditions were then investigated and are reported in this section. The actual boundary condition was firstly measured using the water level probes, and then the data obtained was input directly into the model as the the corresponding seaward boundary conditions.

Comparison between the old and new boundary conditions can be seen in Fig. 36.
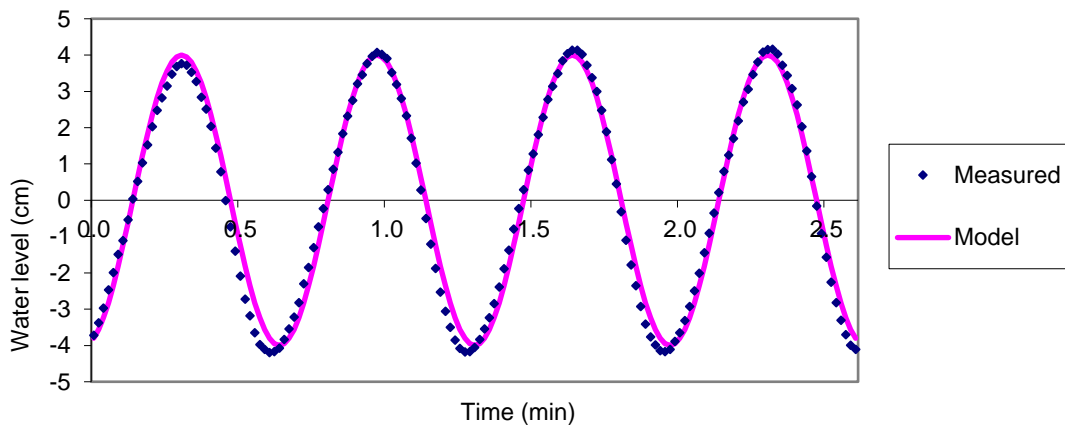
Fig. 5.36 Comparison between the old and new boundary conditions

It appears from Fig. 36 that the difference between measured and model data of boundary conditions were not significant. However, the model showed slightly smaller tidal range (after the first tide). The slope of the tide was also a bit different. This difference may be insignificant but the impact of this difference may significant, meaning that the model result is sensitive to boundary condition.

The parameter values used in this step was the best one obtained from the previous step (parametric calibration), namely: COED = 0.3, n = 0.025, and β = 1.106.

The results of the modelling using a new boundary condition are shown in Fig. 5.37 to 5.42.
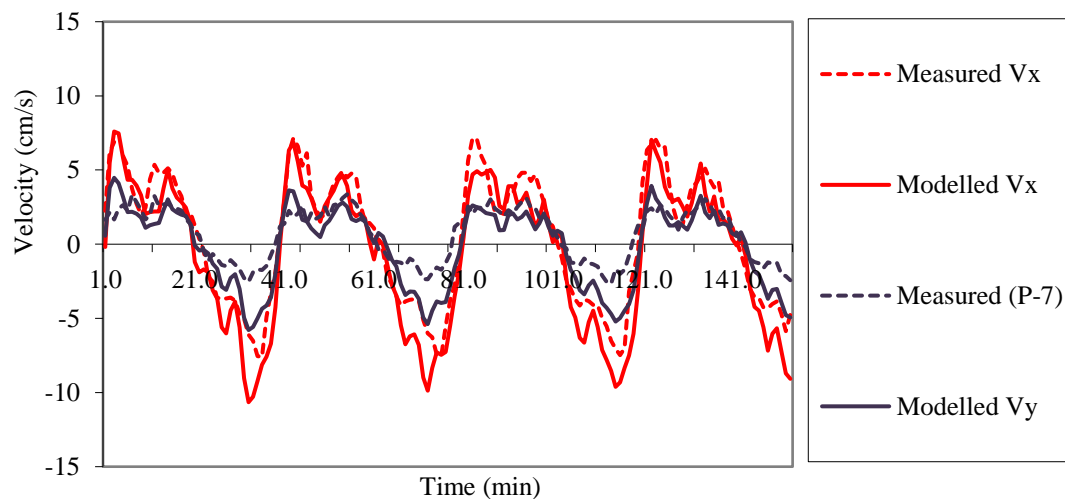
Fig. 5.37 Velocity modelling – boundary condition calibration Point P7
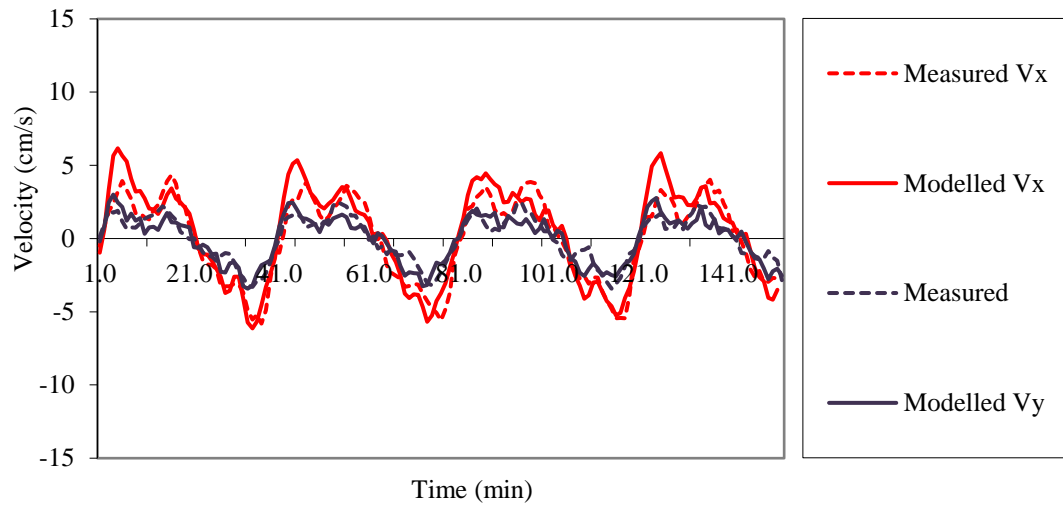
Fig. 5.38 Velocity modelling – boundary condition calibration Point P8
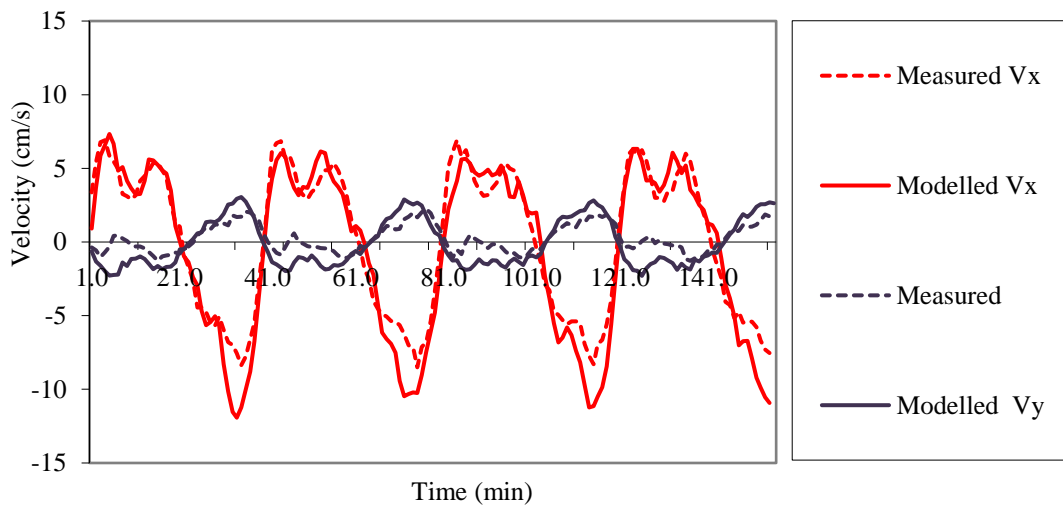
Fig. 5.39 Velocity modelling – boundary condition calibration Point P9
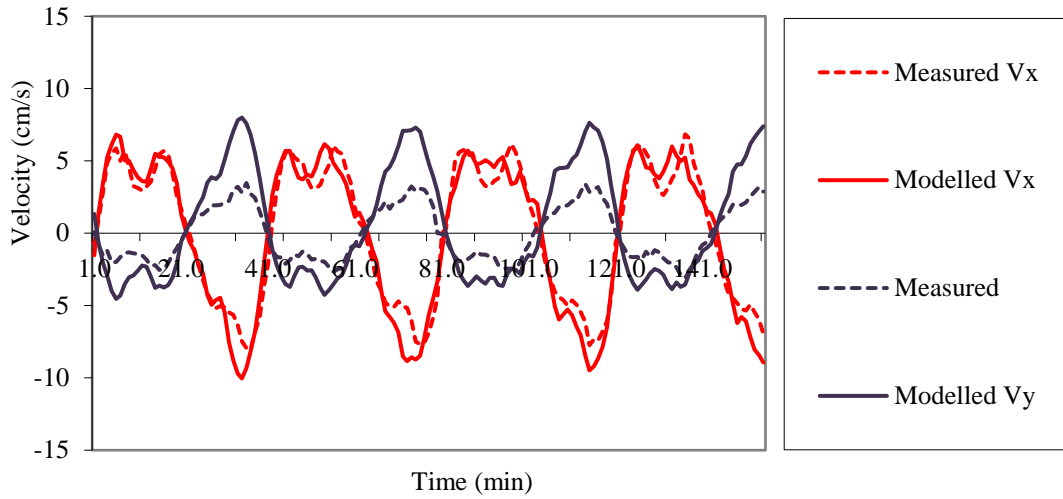
Fig. 5.40 Velocity modelling – boundary condition calibration Point P10
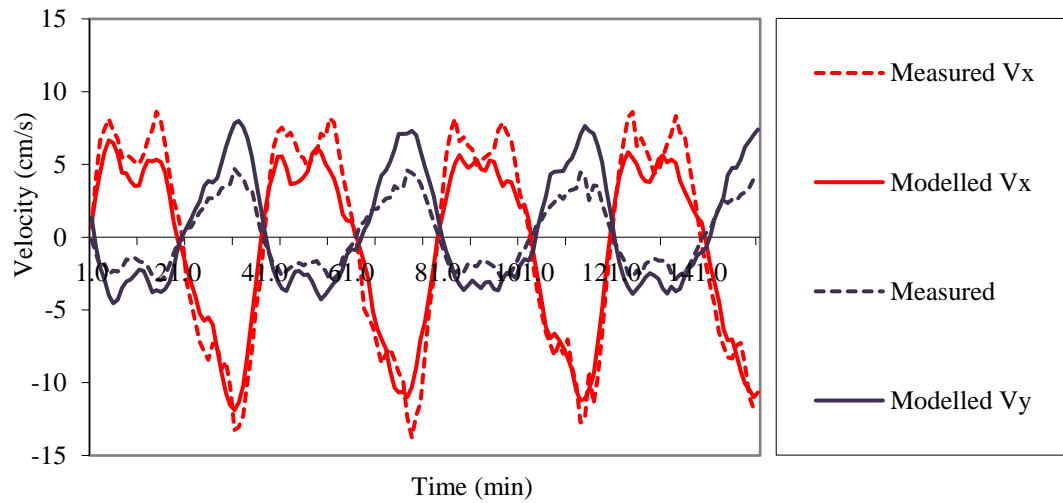
Fig. 5.41 Velocity modelling – boundary condition calibration Point P11
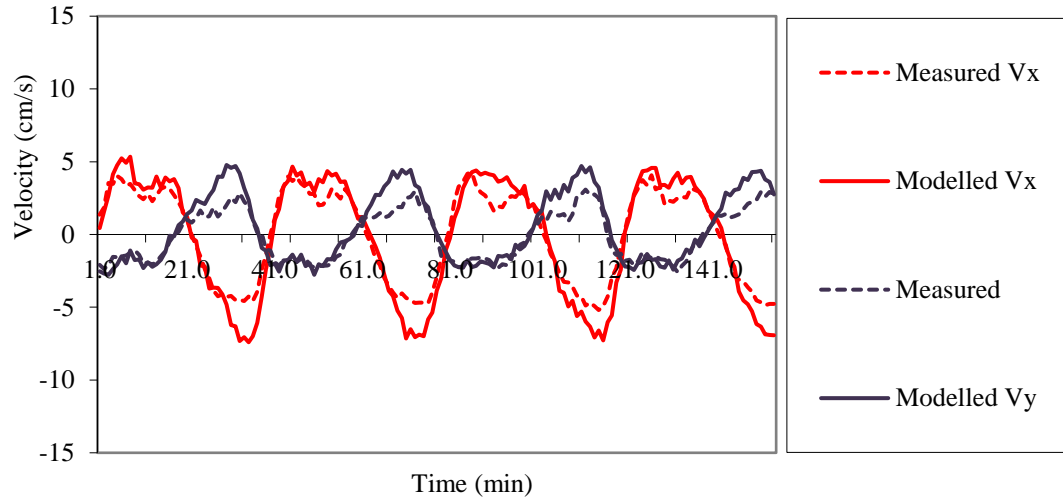
Fig. 5.42 Velocity modelling – boundary condition calibration Point P12

As it can be seen from Fig. 5.37 to Fig. 5.42 the model were significantly changed by the change of boundary conditions, compared to the change by the parameters (n-Manning, COED, etc).

Error analysis was carried out to evaluate the effect of the boundary condition change on the modelling results, and the results are shown in Table 5.9.

Table 5.9 Analysis after boundary condition refinement (in term of "α")

	P7	P8	P9	P10	P11	P12
Vx	0.98	1.18	1.04	1.30	0.76	0.82
Vy	0.84	0.91	0.57	0.61	1.15	0.82
Speed	1.07	1.06	1.02	0.92	1.15	0.79

From Table 5.9 it can be seen that the value of α is nearer to unity than those in Table 5.8. This means that refinement of boundary condition has improved the model.

c. Effect of bathymetry refinement

As described in the Chapter 4, bathymetry measurements were carried out following the hydrodynamic and dispersion modellingusing the old bathymetry. The method used for the bathymetry measurement was PIV, of which working principle has been described in Chapter 4.

After the bathymetry measurements had been completed, a verification step wasundertaken to make sure that the refined measurements were correct. This was done by measuring the bathymetry manually, using a level gauge.

The verification step was done for several cross sections, with points in each cross section. The list of the cross section is shown in the Appendix. By obtaining these improved bathymetric results it was expected that the accuracy of the hydrodynamic model would be improved relative to the data of the physical model.The new bathymetric data were used in the model, and the model was again run to obtain predictions of the water levels and velocities.

Results of the bathymetry refinement can be seen in Fig. 4.3
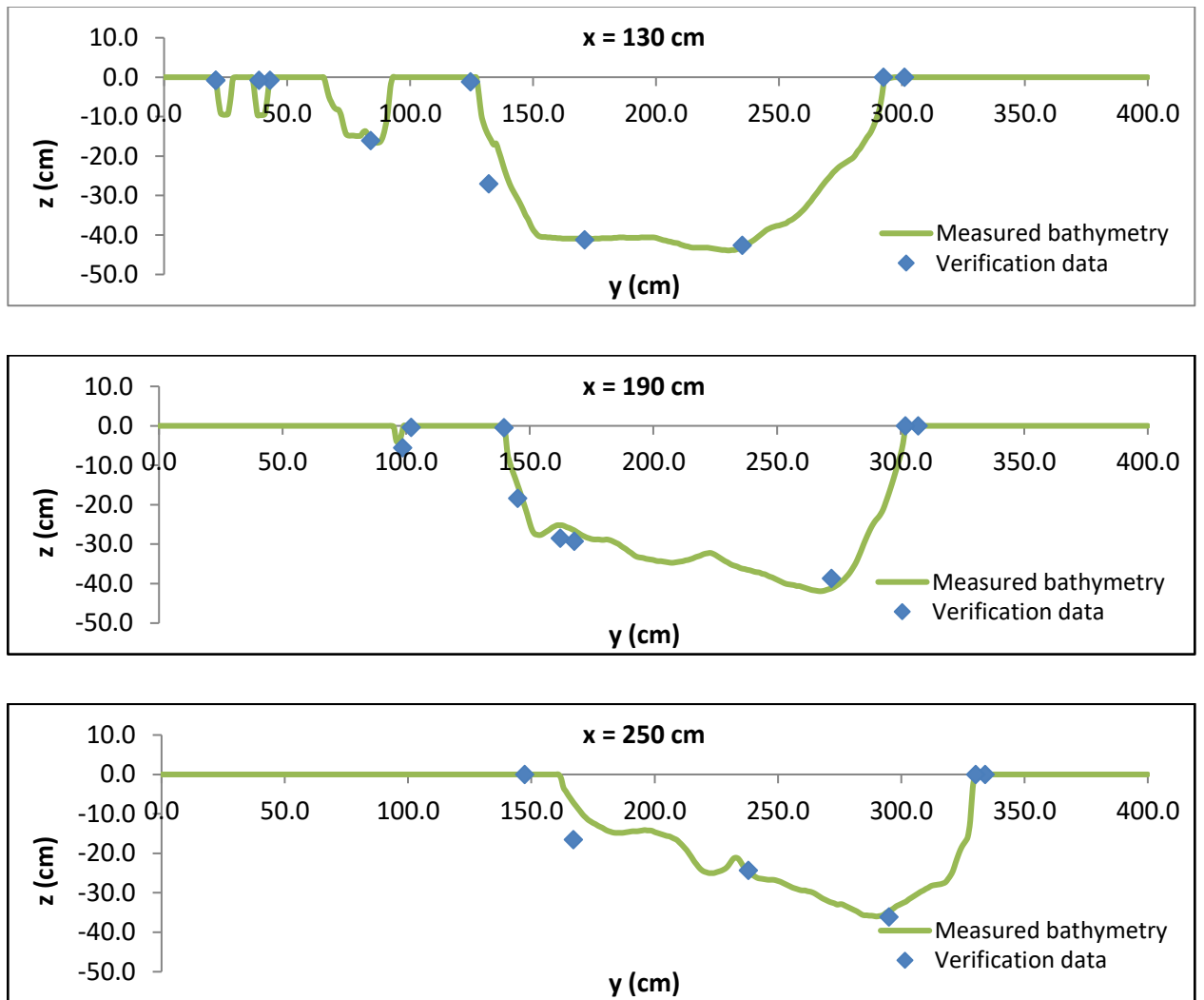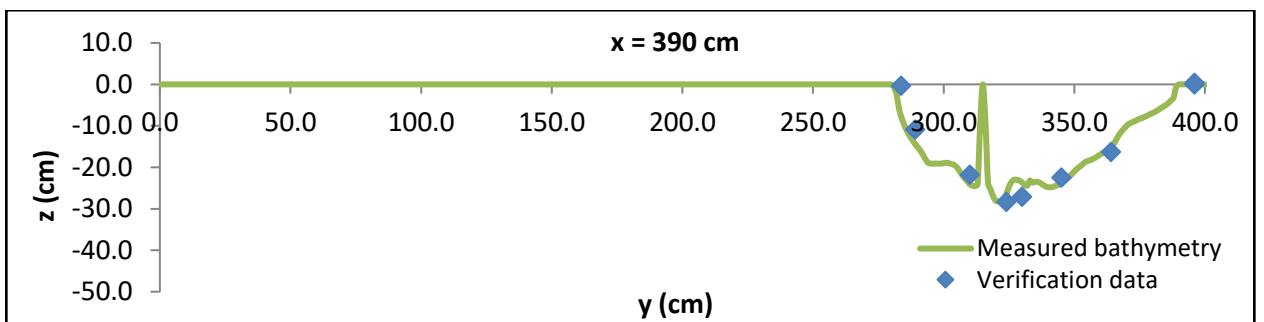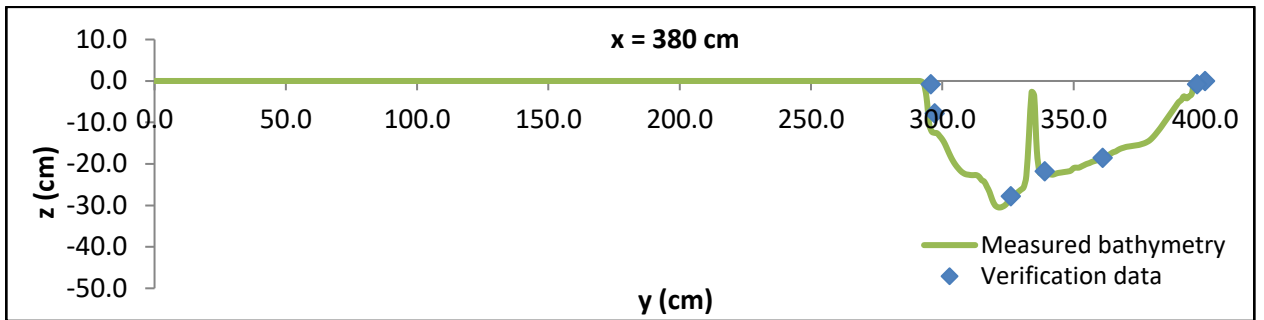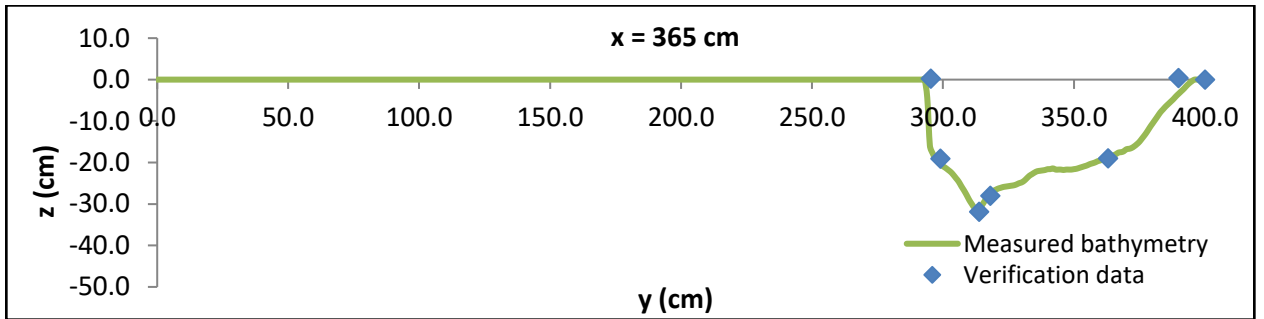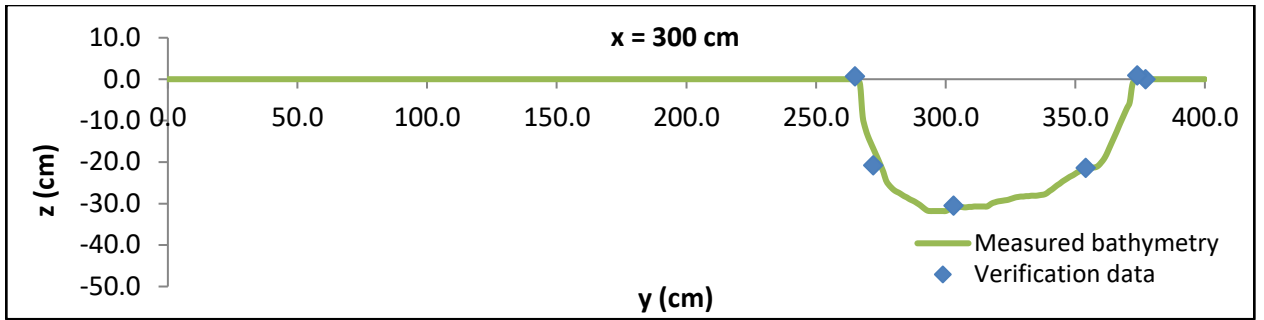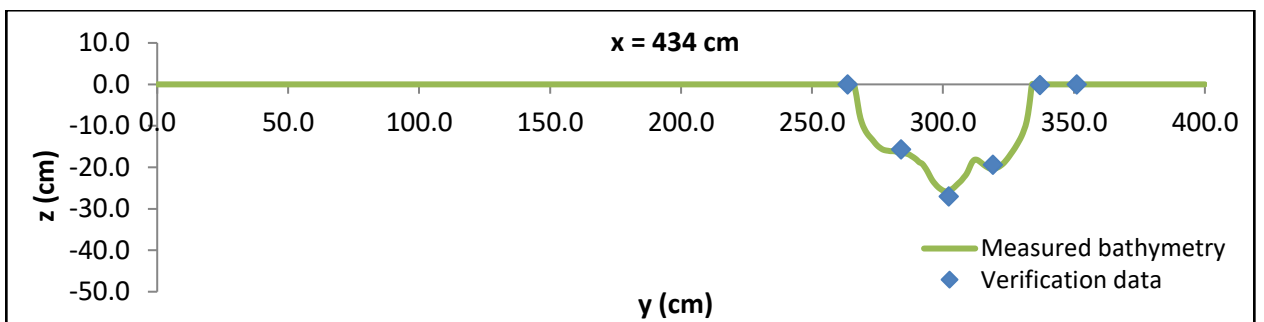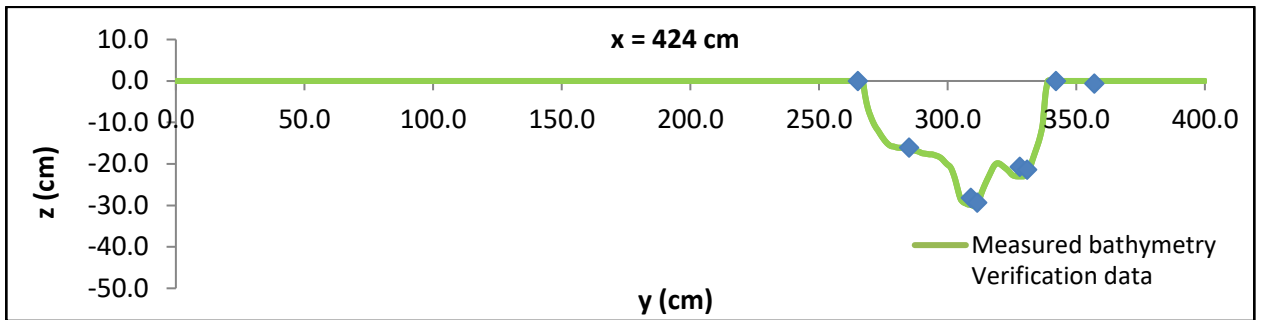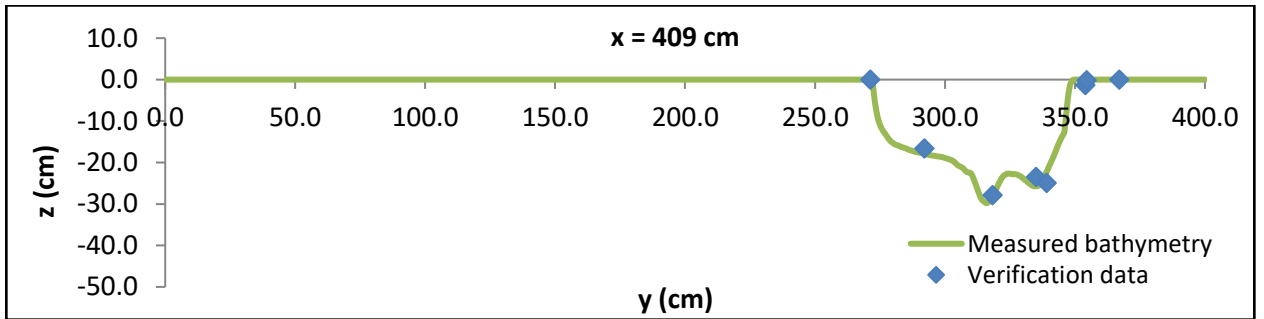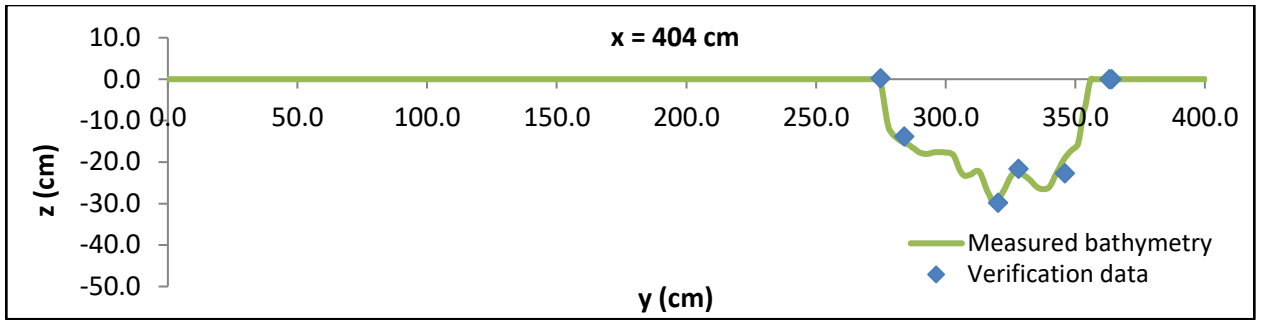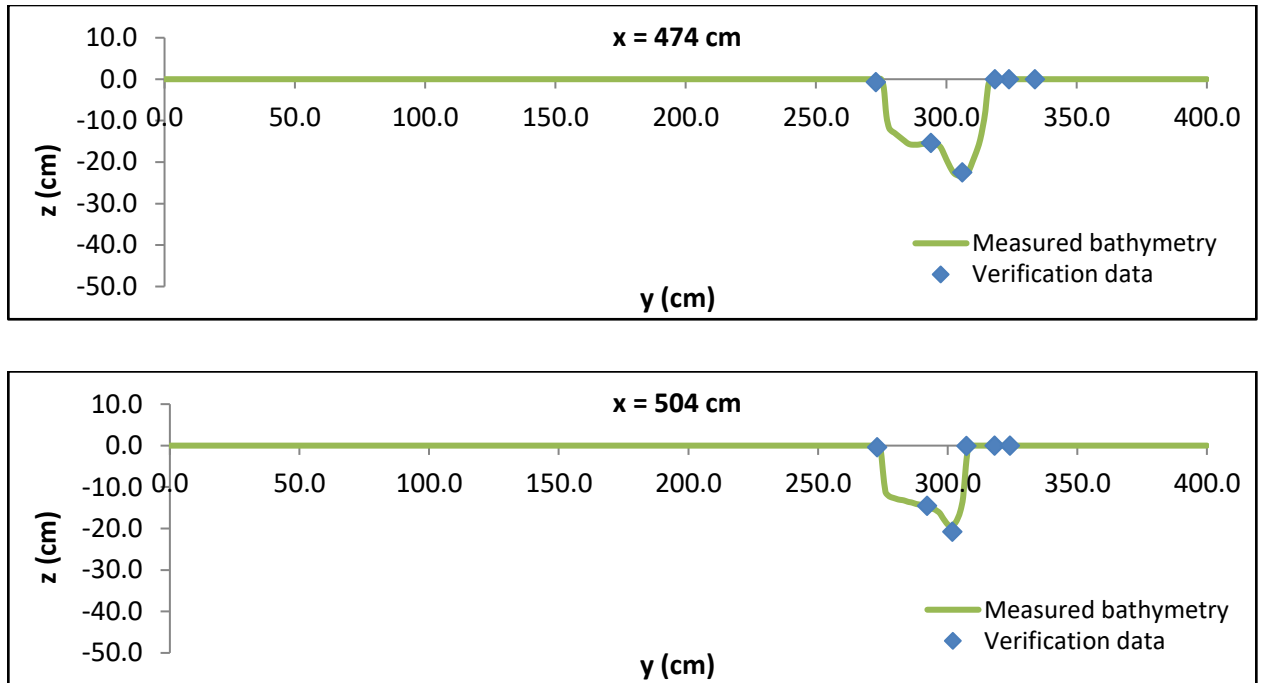
Fig. 5.43 Bathymetry verification results in the Severn estuary physical model

Using the new bathymetry, the model was then re-run several times using different values of parameters, i.e. n-Manning and COED.

Detail steps and results are as follow:

1. Selection of n-Manning

    - Using β = 1.218 (which was the result of calculation using Eq. 5.2), the model was run using different n-Manning coefficient values, which were: 0.015, 0.025, and 0.035. Those values were selected on common range of the coefficient. After running the model using those values, error analysis was conducted using all the error analysis methods described in Sect. 4.1.9, namely: MSE, RMSE, SE, NE, α, and R^2. All sampling points (P7 to P12) were analysed in terms of water level, Vx and Vy.

    - Based on the results of each error analysis, the three options were scored for each parameter and each sampling point, using the following values (from the highest): 3, 2, and 1.

    - The total of the score were then calculated, and the results are as follow:

    n = 0.015 : 145

n = 0.025 : 254

n = 0.035 : 243

Therefore the best n value was 0.025.

- Detail calculation of the above error analysis is presented in Appendix-3.

2. Selection of COED

- Using n-Manning = 0.025 (based on the procedure 1 above), the model was run with different COED values, which were: 0.3, 0.5, 1.5 and 3.0

- All procedures for the selection of n-Manning above were also carried out for COED.

-The total score are as follow:

COED = 0.3 : 139

COED = 0.5 : 184

COED = 1.5 : 191

COED = 3.0 : 207

Therefore the best COED value was 3.0.

Detail calculation is presented in Appendix-4.

From the results above, the best model values for the new bathymetry were: $\beta = 1.218$, n-Manning = 0.025, and COED = 3.0

Fig. 5.44 to Fig. 5.46 shows the results of water level modelling using the new bathymetry data and best parameter values.
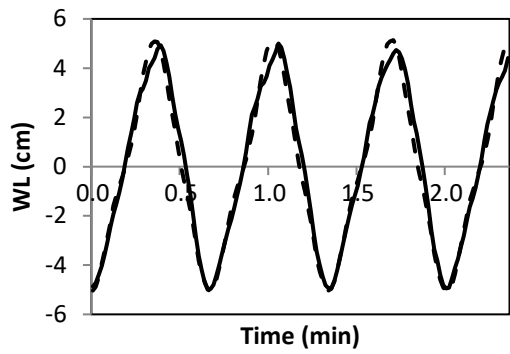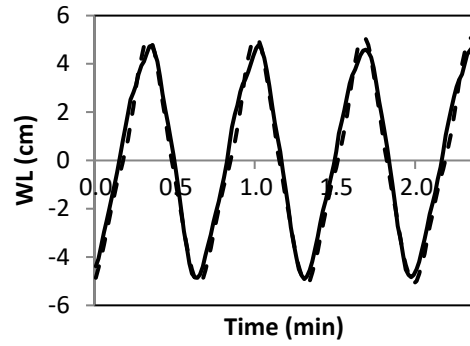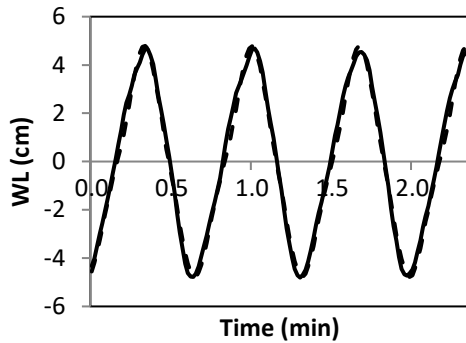
(a)

(b)

(c)

(d)

(e)
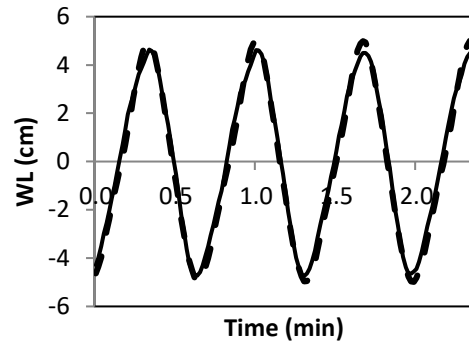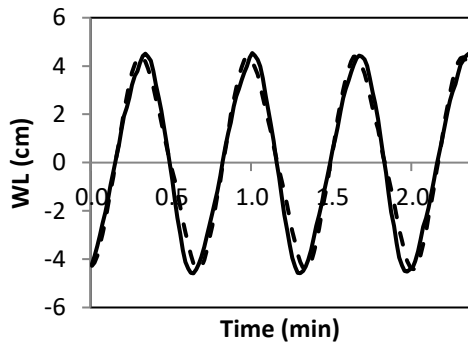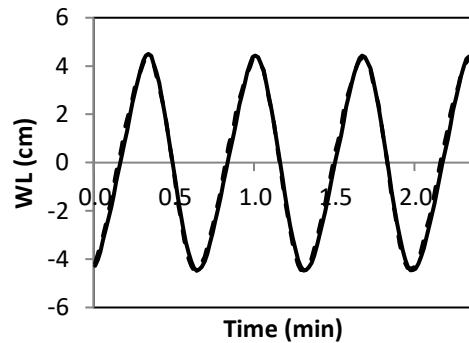
(f)

Fig. 5.44 Water level modelling after bathymetry refinement: (a) P7, (b) P8, (c) P9, (d) P10, (e) P11, (f) P12
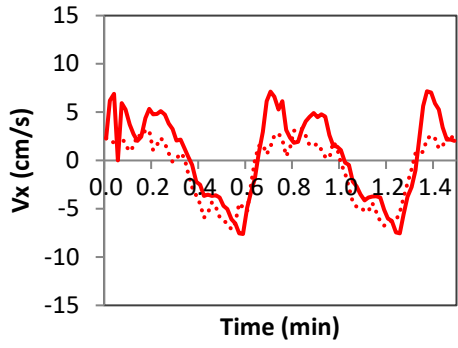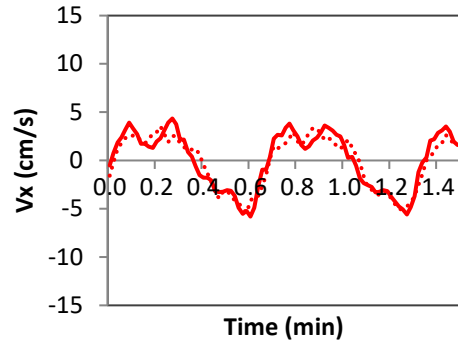
114

(a)

(b)

(c)

(d)

(e)
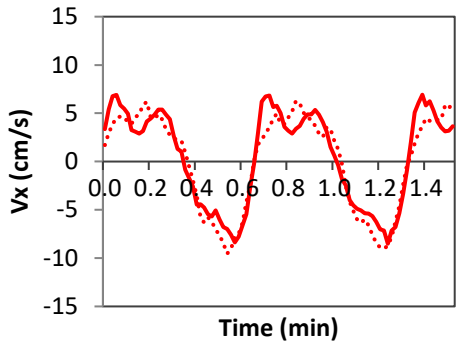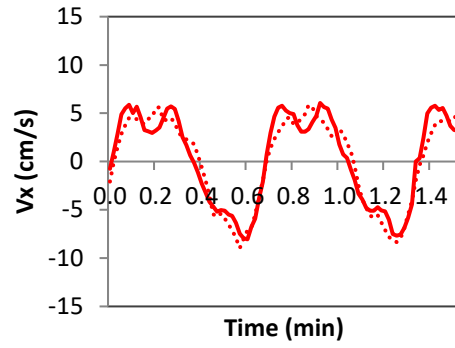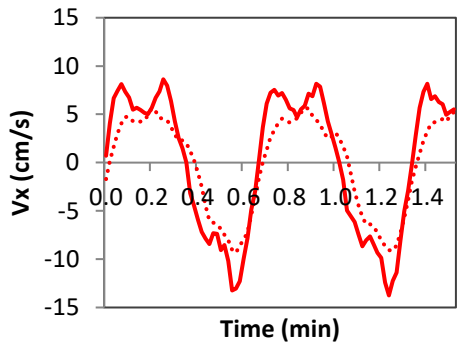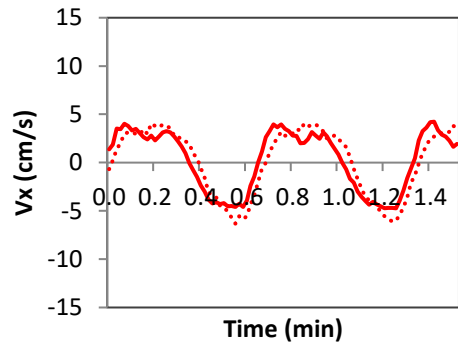
(f)

Fig. 5.45 Vx modelling after bathymetry refinement
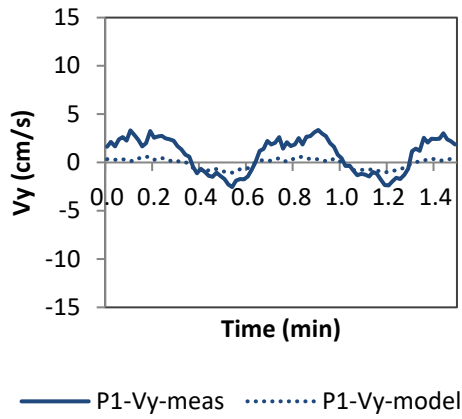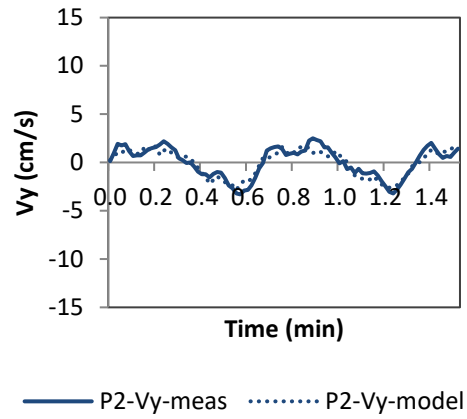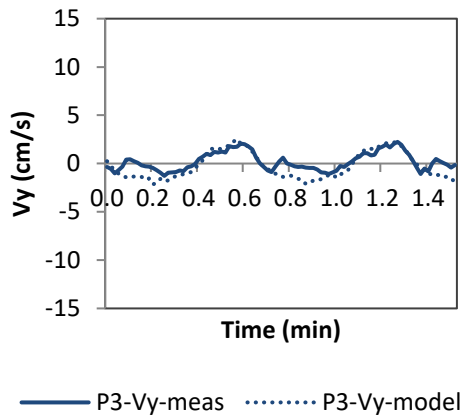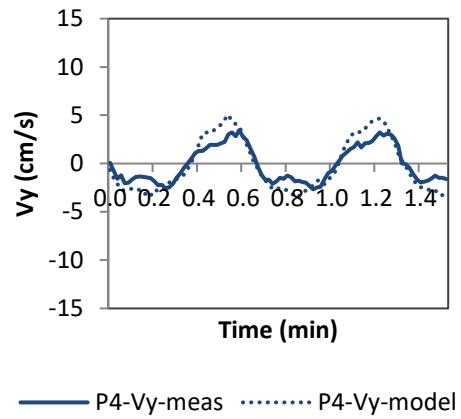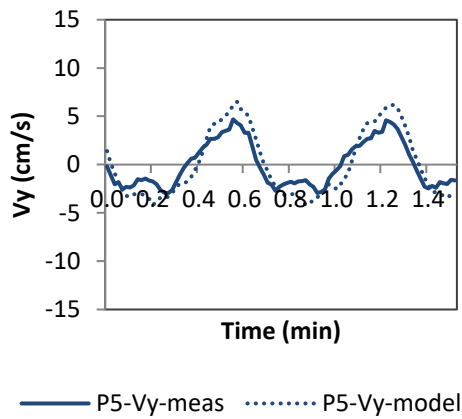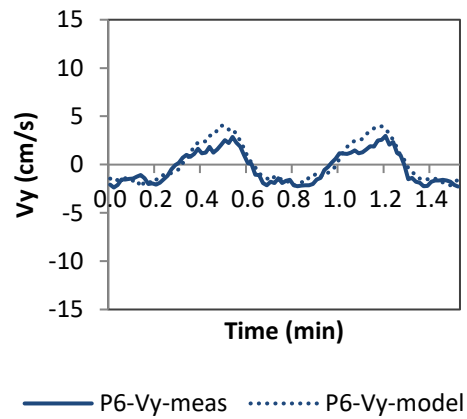
Fig. 5.46 Vy modelling after bathymetry refinement: (a) P7, (b) P8, (c) P9, (d) P10, (e) P11, (f) P12

In order to compare between model results before and after refinement, an error analysis was again conducted. The same procedures for n-Manning and COED above were also conducted for comparing the old and new bathymetry. The results are shown in Appendix-3.

The total score was as follow:

- Old bathymetry: 180

- New bathymetry: 146

From the results above it can be concluded that the model result is sensitive to the change of bathymetry. Although in this study the model using old bathymetry showed better results than the model using new bathymetry, it does not mean that using correct bathymetry is not important. The results above show that the old bathymetry was quite precision, and that that by chance in overall the old bathymetry is more precsion than the new one.

As a conclusion for the best practice in building a physical model, two approaches can be followed:

a. The physical model can be build based on available bathymetry map.
b. After the physical model is built, verification of the bathymetry should be carried out by measuring the depth using PIV method.

After having two bathymetry, the computer model is run using two bathymetry, and then the results of both are to be compared. If the results show that the difference is quite close, then the verification results should be used as it is the results of the real measurement to the physical model. However, if the difference is quite far, than the best one should be used, as the other may contain error.

CHAPTER 6

DISPERSION PROCESSES IN THE SEVERN ESTUARY BASED ON A PHYSICAL MODEL

6.1 Introduction

Dispersion studies have been undertaken as an extension of the hydrodynamic studies reported in Chapter 5. Calibration of the model against the dispersion data was undertaken only after the model had been calibrated against the hydrodynamic data.

After the fluorometer had been calibrated, and the dye tracer prepared, the dispersion experiments were undertaken. The main experiments were carried out by injecting the dye tracer at the injection point and then monitoring the tracer concentration at a number of sampling points. Six sampling points were selected in the experiments. The location of the sampling points were the same as the sampling points used for the water level and velocity measurements. The coordinates of the tracer injection point were (X = 410, Y = 280), with the location shown in Fig. 4.9 in Chapter 4.

The aim of this study was to establish the best representation of the dispersion coefficient for this estuary physical model and to investigate the influence of the various hydrodynamic parameters on the dispersion process.

According to Eqs. (3.55) and (3.56) in Chapter 3 which represent dispersion and diffusion processes, there are two dispersion constants which need to be determined in order to describe the dispersion process. These are:

1. Longitudinal dispersion constant, which is henceforth termed "γ" (*gamma*) - this is theconstantcomponent of the longitudinal dispersion coefficient, which is defined as: $D = \gamma u_* h$, where D is dispersion coefficient, and $\gamma$is the longitudinal dispersion constant, u_* is shear velocity, and h is water depth.

2. Lateral turbulent diffusion constant, which is henceforth termed "δ" (*delta*) - this is a constant component of the lateral turbulent diffusion coefficient, which is defined as: $D* = \delta\, u_* h$, where $D*$ is diffusion coefficient due to lateral turbulent diffusion.

The combined dispersion coefficient is therefore $(\gamma + \delta)\, u_* h$ (Elder, 1958).

The model was calibrated against the experimental data by trying to find the best values of γ and δ. The agreement between the model and the experimental data wasevaluated by an error analysis. This analysis used a coefficient,namely coefficient α, which wasdefined in Chapter 4 as follow:

$$\alpha = X_m / X_p \quad (6.1)$$

where: X_m = experimental/measured data and X_p = predicted/model data.

The modelling resultswere assessed to be in agreement withthe measurement data ifαwas equal to, or close to, unity. There were several steps in the modelling carried out in this study, including:

1. Study of the individual effects of γ and δ on the dispersion model – this was done by applying various values for each parameter (i.e. γ or δ), while setting the other parameter to zero, to assess the sensitivity of the model to each constant.
2. Search for the best combination between γ and δ – this was done by running the model for a wide range of combinationsforγ and δ and then carrying out the error analysis for each each modeling result to find the best fit with the data.
3. Comparison between constant and variable dispersion coefficients - this was done by trying some constant dispersion coefficient and comparing the results against the model results which used the variable dispersion coeffient. The variable dispersion coefficient was obtained by setting the dispersion to be a function of the velocity, depth and the dispersion constant.

4. Evaluation about the effect of bathymetry refinement on dispersion modelling – as undertaken for the hydrodynamic modelling in Chapter 5, this was done by running the model using the new bathymetry data and then comparing the results with those results obtained using the old bathymetry.

6.2 Experimental results

After the dye tracer was injected at the selected point, the concentration of the dye tracer was monitored at the sampling points using the fluorometer. The tracer was injected at a point between between P7 and P8 as shown in Fig. 4.10 in Chapter 4 and for the purpose of clarity it is showed again below.
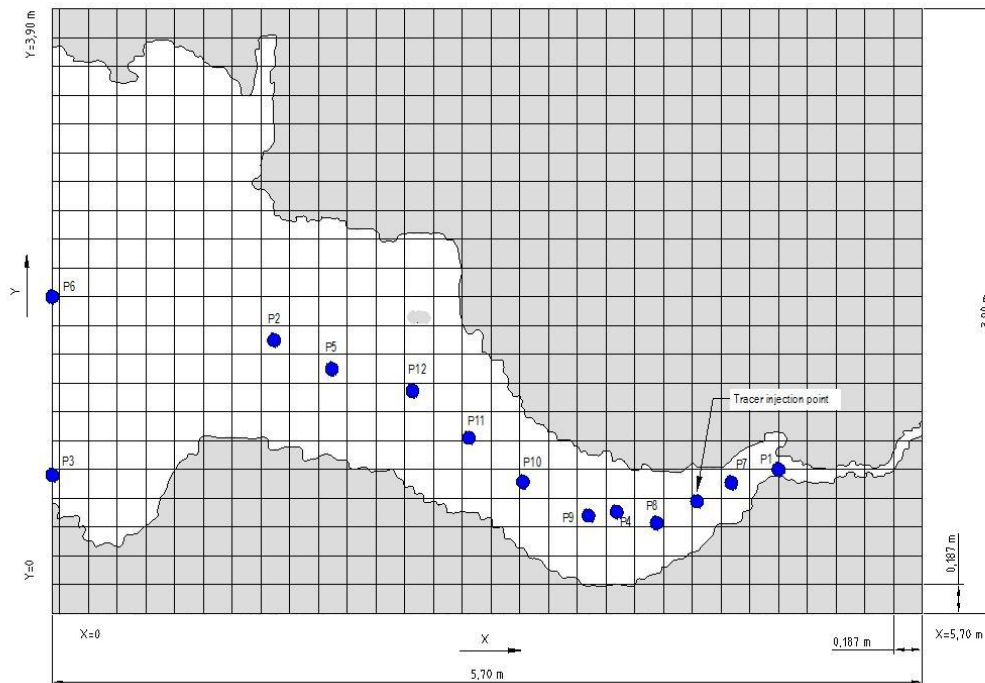
Typical monitoring results are shown in Fig. 6.1.
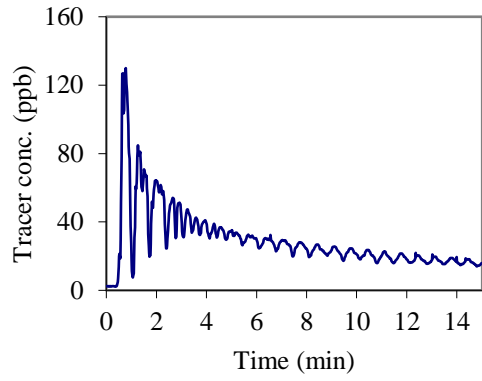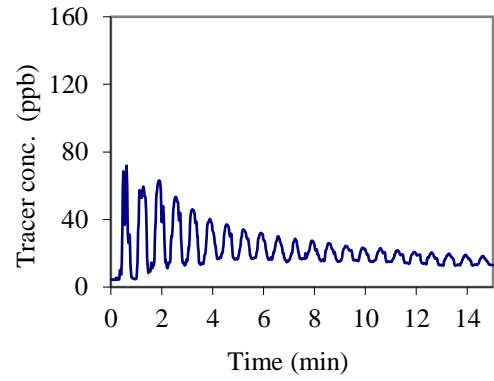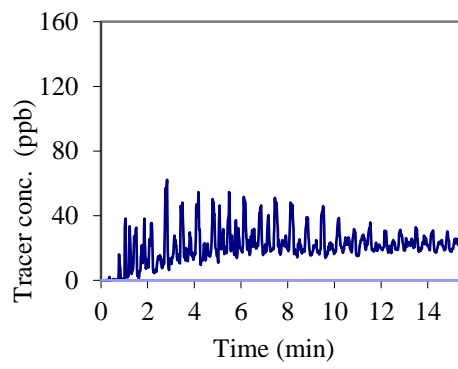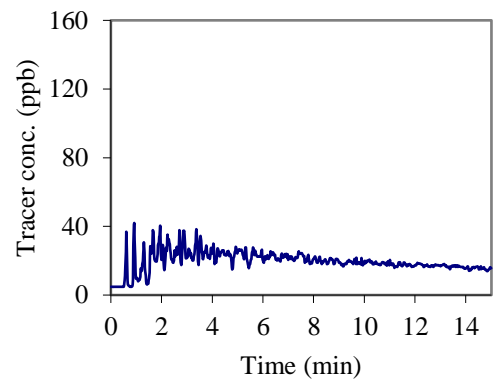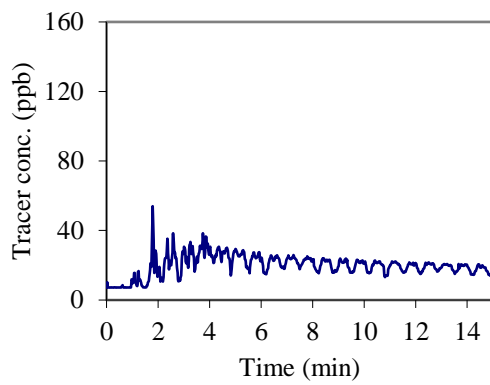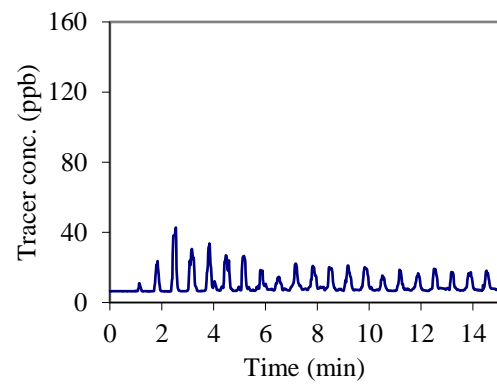
Fig. 6.1 Dispersion experiment results at: (a) Point P7, (b) Point P8, (c) Point P9, (d) Point P10, (e) Point P11, and (f) Point P12

Fig. 6.1 shows that the dispersion curves are different for such factors as: the maximum concentration (which happened in the initial stages of the experiments), the graph slopes, the shapes of the spike, and the height of each spike, etc.

For the maximum concentration, Fig. 6.1 shows the tracer decrease from Point P7 to Point P12. The maximum and average concentrations of the tracer at each sampling point are shown in Table 6.1.

Table 6.1 Maximum and average tracer concentrations at each sampling point

Sampling point	Maximum conc. (ppb)	Average conc. (ppb)
P7	127.60	26.51
P8	67.08	17.13
P9	62.19	21.17
P10	37.08	14.64
P11	46.77	12.67
P12	36.46	3.90

At points P7, P8 and P9, the first spike passing the point was the highest spike or the maximum tracer concentration, but at points P10, P11 and P12 the highest spike was not the first, but the second or third spike. This was the effect of flood and ebb tide occurrences. After the tracer injection, the dye tracer plume was advected by the ebb tide towards the seaward boundary. On the subsequent flood tide, the front of the plume was diluted by the flood tide, as the tide propagated towards the head of the basin. For the second ebb tide the plume flowed again towards the seaward boundary. This mixing of the tracer plume front by the flood and ebb tides caused the dilution of the front zone, so the tracer plume front did not necessarily represent the maximum concentration of the dye tracer. This process does not happen in such one-direction flow channel as rivers.

The other observation from Table 6.1 was that the maximum tracer concentration at a point was logically higher than the maximum concentration at another point,located

downstream (i.e. further from the injection point). This is because the tracer dilution increases further away from the injection point. However, according to the data in Table 6.1, the maximum tracer concentration at Point P10 was lower than the maximum concentration at Point P11. This was also probably due to the tracer dilution being increased by the flood tide. The dilution of the plume was the cause of the maximum concentration at one point being lower than that at the other point,which was located further from the injection point (in this case, between point P10 and Point P11).

The other possibility is since the plume did not follow a straight path, it is possible that the concentration of a point is lower than that of the point further from the injection point. This can be seen in Fig. 6.2 which describe the trajectory of the plume.
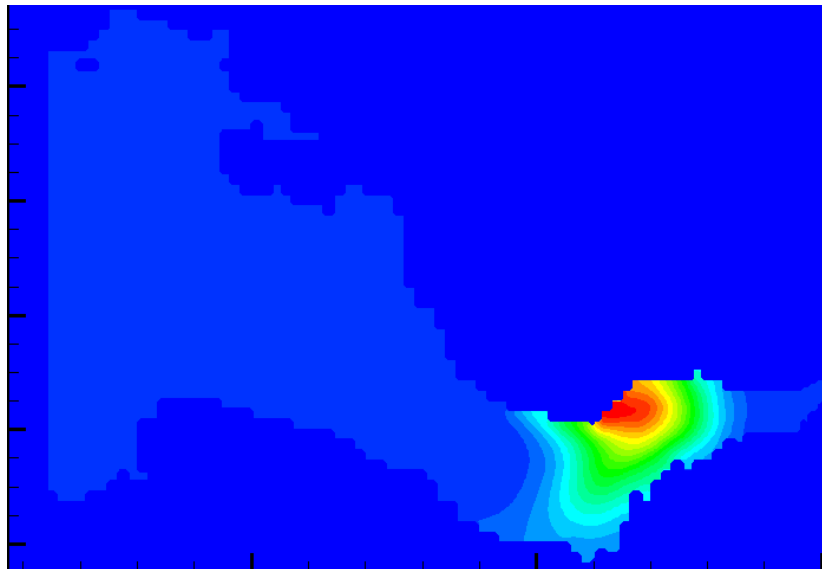
(a) $D_{xx} = 0.00123$ - High water level – 2nd cycle (t = 58 s)
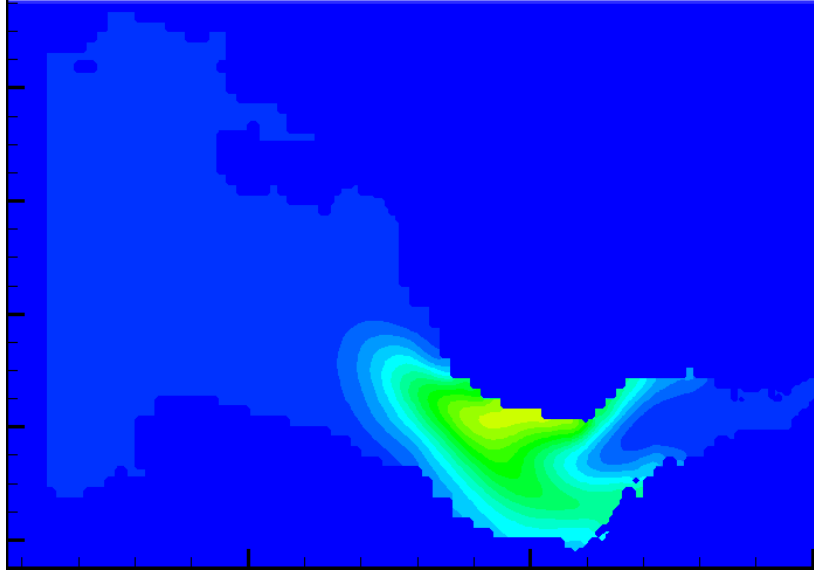
(b) $D_{xx} = 0.00123$ - Low water level – 2nd cycle (t = 76 s)

Fig. 6.2 Typical plume trajectory of the tracer dye in the Severn estuary physical model

Figure 6.2 (a) was produced as a snapshot of the condition of dye plume at the high water level at 58 second, while Figure 6.2 (b) was a snapshot of the condition of dye plume at the low water level at 78 second. This is in accordance with the tidal period which is 40 s, therefore the time distansce between the high water level and low water level was 20 s (78-58 second).

The above plots were produced in the following conditions: COED = 0.3, Manning's n=0.035, $\gamma = 0.8$, $\delta = 6$, β (momentum correction coefficient) = 1.031. This condition is before the calibration of the model, just to show the irregular form of the plume resulting in the unpredictable results.

From both picture it can be seen that the trajectory of the plume did not follow a straight path, rather it has a certain pattern where about the centre of the cross section the flume reaches its peak. But this also depends on the shape of the channel boundary.

The experimental results above were then used to calibrate the computer model, in order to find the best value for γ and δ . First, both experimental model and computer model were plotted in a graph such as shown in Fig. 6.3.
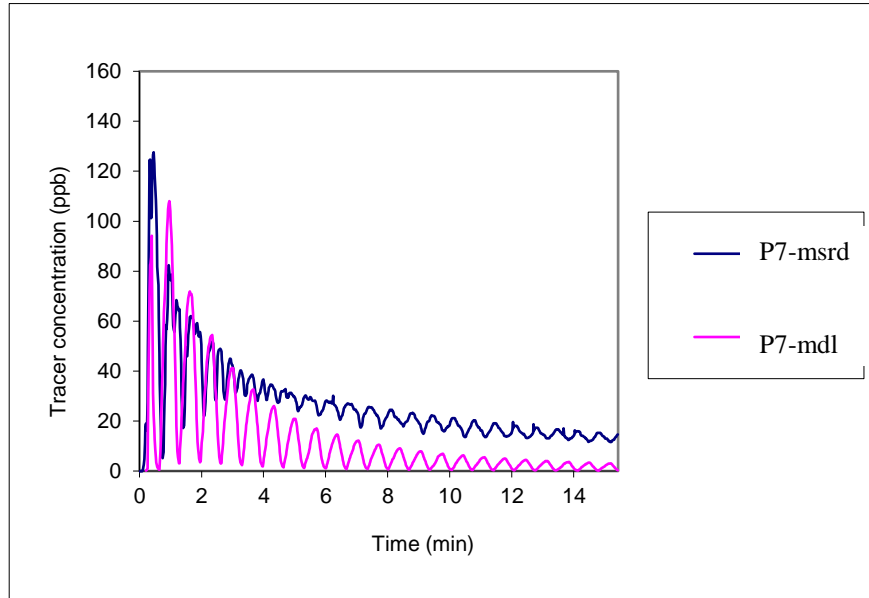
Fig. 6.3 Typical graph comparing experimental results and computer model
$(\gamma = 0.8 - \delta = 6)$

In order to evaluate the agreement between both results, error analysis using α were carried out. Firstly the analysis was carried out using the rough data as Fig. 6.3. However, there is a problem in this method because the cycle of both results is not always in agreement in a time. For example, at minute 8, the measured result show a peak while the model result show lowest concentration.

Due to this problem, another approach was taken, that is by averaging the tracer concentration so that both results are more comparable. The time period used in the averaging was 40 s. This is the same period with the tidal period, as it is expected that the average can represent the all concentration values during the related period. There is a concequence of this averaging that some peaks in the original graph (before averaging) will not appeared in the avaraged graph. But it is also not possible to determine a certain period for averaging which can accomodate all possible peak as the peaks appeared at any time. In addition, the purpose of this averaging was to

compare the models and the experimental data and then find the best parameter of the model. Therefore it was decided that the tide period which is 40 s is taken as the averaging time.
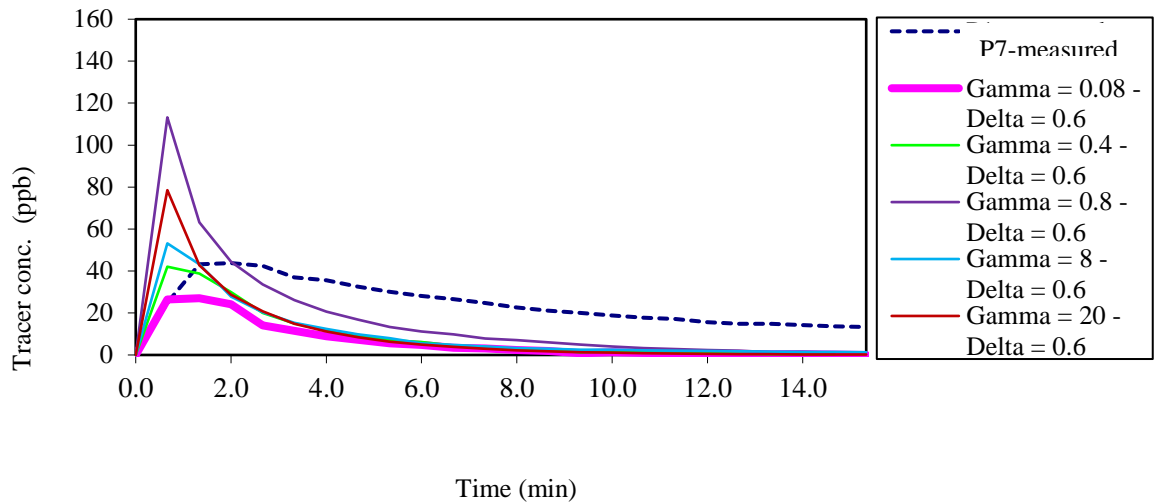
Fig. 6.4 Typical graph comparing the average of model and experimental results

The graphs seemed to be different with the actual graph before averaging (**Fig. 6.3**), as the actual graph show a peak at ... s. This was caused by the averaging of the concentration data, which possibly diminished any peak appeared in the original data. This has been explained before.

6.3 The Effect of γ and δ on Dispersion

6.3.1 The Effect of δ

The values of γ which were used in this modelling step were: 0.8, 4, 8, 10, 20. These values wereselected as follow: typical value of γ is 0.8. Then it was expected that by multiplying it for example by 5, 10, 12.5, and 25 times, there will be a significant difference resulted from the model. Hence the above values were selected.After the result of a model run using a particular γ value was evaluated in terms of its agreement

with the experimental data, the next γ value was chosen as a trial to get a better modelling result.

As can be seen from Fig. 6.1, the tracer graphs consisted of many spikes, and therefore comparing the measured graphs with the model graphs was not practical. Therefore it was decided to average the tracer data in order to smooth the graphs and make it easier for comparisons. The averaging was made 40 times, thereby changing the time step from 1 s to 40 s. The figures shown henceforth were the results of averaging.

Fig. 6.2[a-f] shows the modelling results using the γ values while δ was set zero. In general, the model almost resembles the experimental results at all points. The graphs dramatically increased up to the maximum concentration, and then decreased with different slopes.

(a)   (b)

127
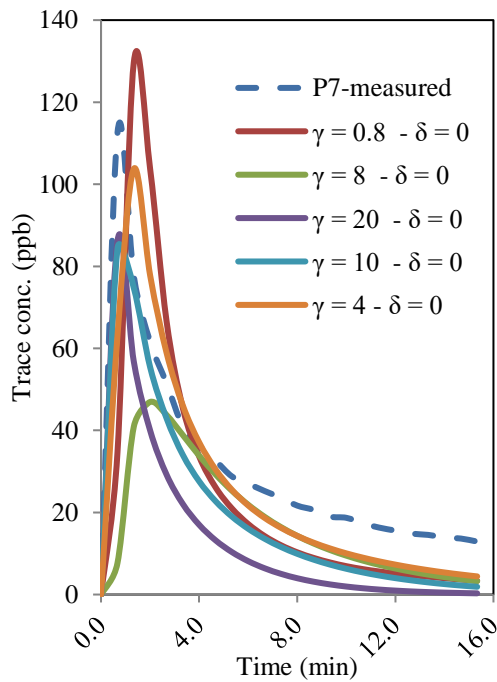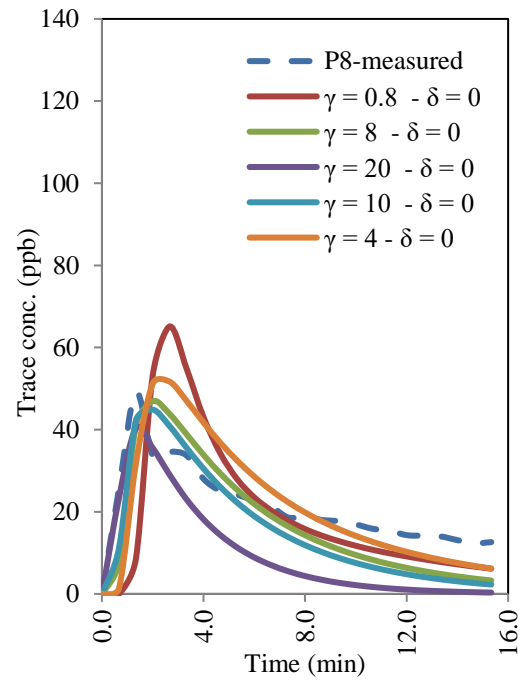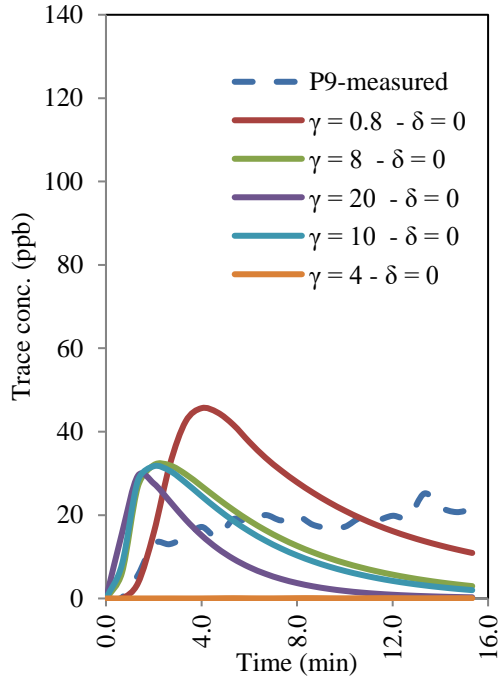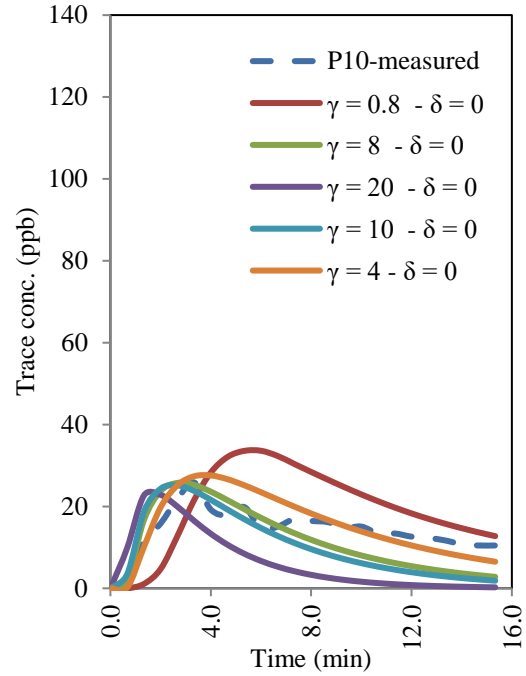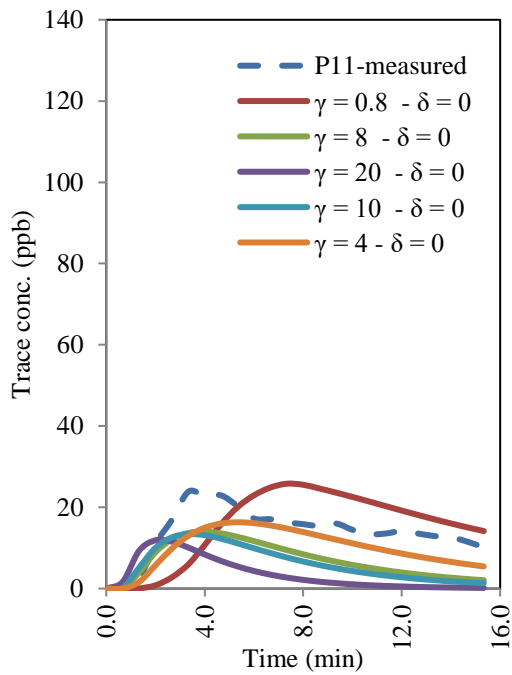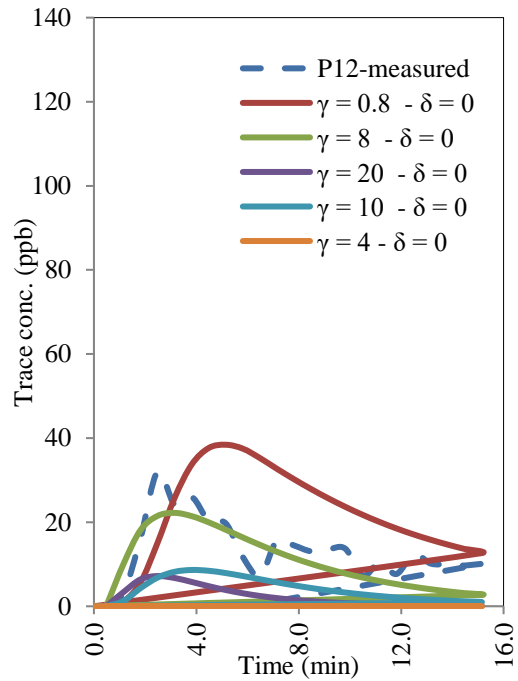
Fig. 6.5 Effect of γ on dispersion modelling at: (a) Point P7, (b) Point P8, (c) Point P9, (d) Point P10, (e) Point P11, and (f) Point P12

Fig. 6.5 [a] shows that all the models resulted in similar shapes with the experimental curve, but they differed in the maximum (or peak) concentration. The highest peakof the model corresponded to a value of$\gamma = 0.8$.The order of γ values according to the increasing peak produced in the model was: 8, 10, 20, 4, 0.8. Theoretically, the smaller the value of γ, the lower the peak of the dispersion graph. This is because low γ value means low dispsersion coefficient, thus low dispersion process happens, resulting in high concentration of dye tracer remaining in a point under study. Fig. 6.5 shows that there was an increasing trend of dye tracer peaks from $\gamma = 20$, 4, to 0.8. For $\gamma = 10$ and 20 the peak were not so different. The exception was only for $\gamma = 8$, where it should have a higher peak than 10 and 20. But overall it can be suggested that the lower the γ value the higher the graph peak. With regard to the agreement between the model and experimental curve, the closest model predictions to the experimental curve was obtained when the model value of $\gamma = 4$.

Like Point P7, at Point P8 (Fig. 6.5 [b]) all models were close to the experimental curve. The order of the γ value with increasing model peak was: 20, 10, 8, 4, and 0.8. Therefore it can be concluded that at this point the level of tracer concentration increased with a decreasing value of γ. The models which fit the experimental graph best were those with $\gamma = 4$, 8, and 10.

At point P9 (Fig. 6.5 [c]), it seemed that the model did not really simulate the experimental results that well. The order of the γ value with the increasing model peak was: 20, 10, 8, and 0.8.

All of the model results were similar with the experimental curve at Point P10 (Fig. 6.5 [d]). The models which were closest to the experimental results were those with $\gamma = 4$, 8, and 10. The order of γ value with the increasing model peak was: 20, 10, 8, 4, and 0.8. It was therefore apparent that at this point the tracer concentration level of the model increased with a decrease in the γ values.

At Point P11 (Fig. 6.5 [e]), again all the model results were close to the experimental results. The model with γ of 0.8 had a close concentration level with the experimental

result, but it had a longer lag time. The other models, with γ = 4, 8, 10, were also close to the experimental results but had lower concentration levels. The order of the γ value with the increasing model peak was: 20, 10, 8, 4, and 0.8, meaning that the smaller the γ value the higher the tracer concentration level.

Fig. 6.5 [f] shows that the model which was closest to the experimental curve was the model with γ= 8.The order of the γ value with the increasing concentration level was: 20, 10, 8, and 0.8. This meant that the level of the tracer concentration of the model increased with a decrease in the γ value.

In general, the model predictions resembled the experimental curves. The difference between the model and the experimental curves were primarily in the peak occurrence. Also, the model seemed smoother than the experimental curve. The model with different parameter values differed in the peaks, the concentration levels, and the time lag. The selection of γ values therefore affected those aspects of the model. From Fig. 6.5 it can be seen that the higher the γ value the lower the concentration levels, as shown at P8, P9, P10, P11, and P12. The exception was for Point P7, where the trend was not consistent, probably because of the position of this point which was upstream from the injection point. However because there was only one point in this position, this assumption needed more evidence.

Table 6.2 shows the analysis results of the γ effect on dispersion modelling in the estuary physical model. The value of "α"is the average over the full simulation time.

Table 6.2 Error analysis of the γ effect on dispersion modelling

Sampling point	α from the error analysis				
	0.8	4	8	10	20
P7	2.22	1.58	2.04	2.74	10.88
P8	1.45	0.85	1.78	2.20	9.24
P9	0.95	-	2.25	3.05	15.63
P10	1.29	1.23	1.64	2.16	10.18
P11	4.19	1.51	2.53	3.29	16.59
P12	0.87	-	1.84	4.96	24.92

Note: - : Too large values due to comparison between the experimental and model data where the model data was near zero.

From Table 6.3 it can be seen that in general the α value increased with increasing values of γ. The optimum value of α seemed to occur when γ = 0.8. The large numbers of α at P9 and P12 were due to the small values of the model data, therefore since α is the ratio between the measured and the model data the α values werevery large. The values of α were good at γ = 0.8, 4, and 8, that was around 1-2. From $\gamma = 10$ and 20 the best α value was around 2-3. It can be seen from Table 6.3 that the α values tended to increase from γ = 0.8 to 20.

The longitudinal dispersion coefficient is the main component of dispersion. Therefore many studies have been undertaken on this topic, as described in Chapter 2. Dispersion is a complex phenomenon, and it is influenced by many factors, including geometrical and hydraulic factors.

The equation used in this study is the two-dimensional depth integrated advective-diffusion equation i.e. Eqs. (3.55), (3.55), and (3.56) in Chapter 3, where the longitudinal dispersion coefficient and the lateral turbulent diffusion coefficient were included. As the other factors depend on the experimental data, only γ and δ remain to be determined, and their values cannot be determined except by trial and error to find their best values.

Because only two parameters are evaluated, it is important to know the effect of each parameter individually in the absence of the other parameter, so that the effect of each parameter on the concentration level can be evaluated.

The results shown in Fig. 6.5 indicated that the concentration level of the model tracer increased with a decrease in γ values. Beside from the results shown in Fig. 6.5, this can be seen from the α values in Table 6.2, where an increase in the α value occurred for an increase in the γ values.

However, it is not easy to quantify the effect of the dispersion constant on the dye concentration level. The order of the concentration level affected by γ was not always consistent. This was thought to be due to the geometric aspects of the physical model, which were not homogeneous (in term of depth, width, etc). Therefore it was not easy to quantitatively relate the effect of γ on dispersion.

The difference between the model and the experimental curve primarily arose in the peak of the graphs and the rate of decrease of the concentration. The model decreased very rapidly and hence its concentration was much lower than the experimental curve. Besides, the assumption of full mixing in the computer model may have not occurred in the physical model causing differences between both results.

The possible causes of this difference are:

-there were some parameters in the physical model which did not match with the computer model.

-some assumption beside the γ and δ values did not match the experiments, for example: the eddy viscosity, β coefficient, etc.

-in this experiment turbulent diffusion was not included, thus it was assumed that dispersion was only caused by the shear dispersion.

6.3.2   Effect of δ

The values of *γ* which were used in this modelling step were: 0.06, 0.6 and 6. The typical value is 6, and therefore variation of this value for example by dividing it by 10 or 100 (to 0.6 and 0.06) may give significant differences for model calibration.

Fig. 6.6 shows the effect of *δ* on dispersion modelling at Point P9-P12. In general, the patterns of the models were quite similar to the experimental curves, except for Point P9.

(a)

(b)

(c)

(d)

133
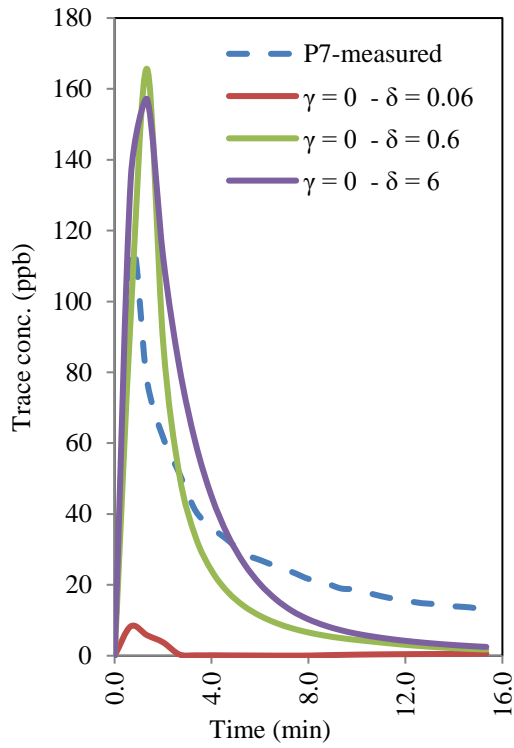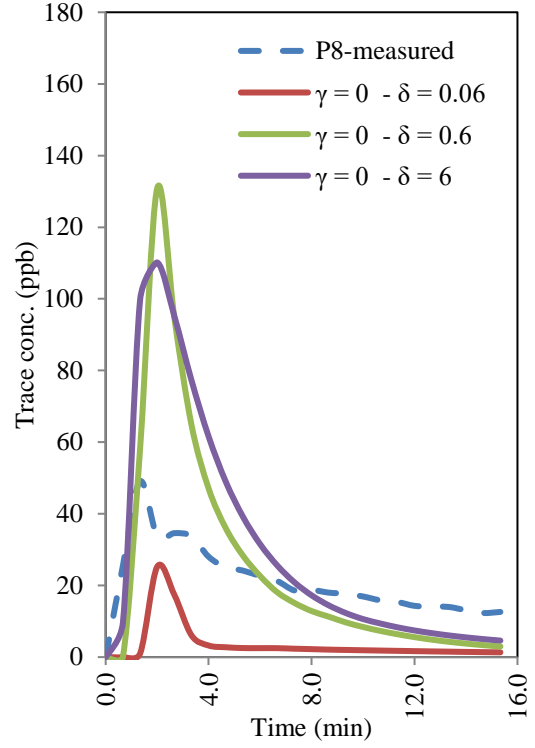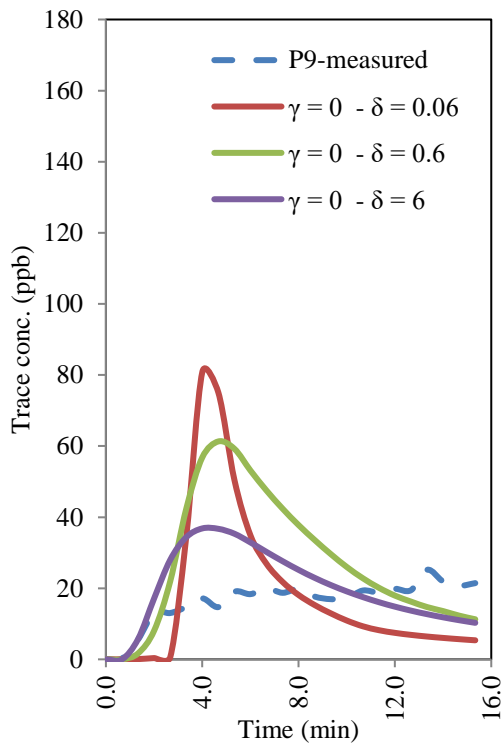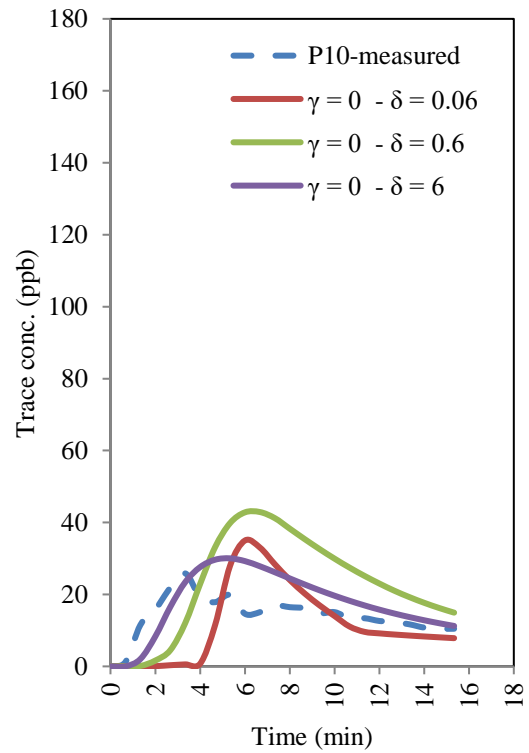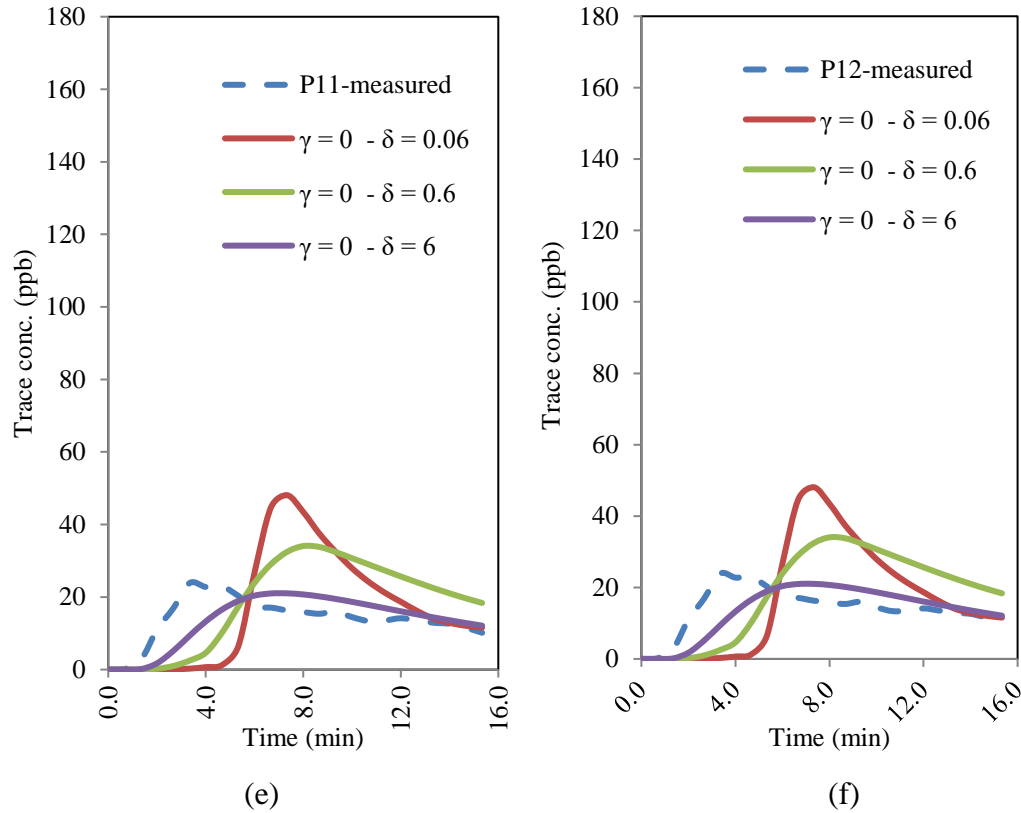
Fig. 6.6 Effect of δ on disperson modelling in estuary at: (a) Point P7, (b) Point P8, (c) Point P9, (d) Point P10, (e) Point P11, and (f) Point P12

Fig. 6.6 [a] shows the effect of the value of δ on dispersion process modelling at Point P7. The shapes of the model results with δ = 0.6 and 6 were similar to the shape of the experimental curve, except that their peaks were higher than those for the experiment. It seemed that increasing the value of δ from 0.06 to 0.6 significantly increased the peak concentration from about 10 ppb to about 160 ppb, but increasing the δ value from 0.6 to 6 did not increase the peak.

Fig. 6.6 [b] shows the effect of δ on dispersion modelling at Point P8. The model with a δ value of 0.06 was quite similar to the experimental results, but the concentration level was much lower. The modelresultsfor the other δ values (i.e. 0.6 and 6) had a very high concentration level. At Point P7, the concentration level increasedsignificantlyfrom δ = 0.06 to δ = 0.6, but from δ = 0.6 to δ = 6 there was a slight decrease in the peak concentration.

134

At Point P10, all the model results were similar to the experimental curve as shown in Fig. 6.6 [d]. The model setup which agreed best with the experimental curve was the one with δ of 6. The model with δ of 0.6 had higher concentration levels, and the model with δ of 0.06 had a rather long time lag.

For Point P11, the most suitable model setup was the one with δ of 6 as shown in Fig. 6.6 [e], but there was a lag time in the beginning compared to the experimental curve. The order of the γ value which resulted in the increasing concentration level of the model was: 6, 0.6, and 0.06. It seemed that at this point the concentration level increased with the decrease in the δ value.

Table 6.3 shows the error analysis of the δ effect on dispersion modelling in the estuary physical model.

Table 6.3 Error analysis of the δ effect on dispersion modelling

Sampling	α from the error analysis		
point	0.06	0.6	6
P7	-	3.48	2.37
P8	9.93	1.78	1.35
P9	8.20	0.97	1.00
P10	-	5.46	1.05
P11	78.90	4.47	2.23
P12	78.90	4.47	1.37

Note: - : Too large values due to comparison between the experimental and model data where the model data was near zero.

According to Table 6.3, there was a trend of decreasing in the α value with an increase in δ. It can be seen from Table 6.3 that the δ value which resulted in the best α was 6.

δ is the lateral transverse diffusion coefficient. From the modelling results about the effect of δ on dispersion model it can be seen that the effect of δ was different with the effect of γ. For γ, an increase in γ resulted in a decrease of the model concentration

level. On the other hand, an increase in δ resulted in an increase of themodel concentration level at Points P10, P11, and P12.

Turbulence is the other process affecting dispersion beside shear. The effect of turbulent diffusion can be evaluated from these results. Like the effect of γ, the differences between the model and the experimental results depended upon the following factors:

- the peak of the graph
- the rate of decrease of the concentration

The effect of γ and δ can be compared, for example at the same point, thereby indicating how δ affected the concentration level in the model results, compared to the effect of γ.

For example, at Point P7, the peak of the model decreased from 80 to 60 by an increase in δ from 0.06 to 0.6. This meant that by increasing the value of δ 10 fold, the peak of the model decrease by 25%. For γ at the same point, the increase in γ from 4 to 8 decreased the concentration level from about 100 to about 45. This means that an increase of γ by two fold decreases the concentration level by 55%. Therefore the effect of γ was about two times bigger than the effect of δ.

The increase in γ from 0.8 to 4 decreased the peak from about 130 to about 105. This means that an increase by 5 fold decreases the peak by about 20%, with an increase of γ from 0.8 (130 ppb) to 10 (85 ppb) resulting inadecreasein the peak by about 35%. Likewise, when γ is decreased from 10 (85 ppb) to $\gamma = 8$ (45 ppb), i.e. a reduction of 20%, then the peak concentration is decreased by 47%.

From the two examples above, the trend was not consistent. Therefore this change in the peak cannot be related quantitatively to the change in either δ or γ.

6.4 Effect of various γ and δ combinations on dispersion

The values for γ and δ were chosen when the model results best matched the experimental curves. After the results were obtained and trials undertaken sufficiently for evaluation, the results were then grouped according to the parameter. One model result (run) could be included in more than one group. Group-1 consisted of all the modeling runs with δ = 0.6. Here the γ constant was varied from 0.08, 0.4, 0.8, 8, 20. Group-2 consisted of all the modeling runs with δ = 6 and with the γ values varying through 0.4, 0.8, 1.6, 16, and 20, which were not exactly the same with those with δ = 0.6. Group-3 consisted of two modelling runs with γ =0.8, and δ being varied for values of 0.6 and 6. Group-4 consisted of three model runs with γ = 20, and δ being varied by 0.6, 3.2 and 6. Group-5 consisted of three model runs with specific γ and δ values, that were $\gamma = 5.93$, and $\delta = 0.07$, $\gamma = 8$ and $\delta = 0.06$, and $\gamma = 13$ and $\delta = 1.6$. Finally Group-6 consisted of two constant dispersion coefficients, namely 0.00123 m^2/s and 0.00524 m^2/s.

The reason of the parameter value selection has been explained previously. For γ = 5.93 and γ = 0.07, they were taken from Elder (1959). For D = 0.00123 and D = 0.00524, they are the averaged dispersion coefficient troughout the physical model in transversal and longitudinal direction, respectively. They were computed using the computer model. Table 6.4 shows the list of all γ and δ combinations.

As mentioned before, one run may be included in more than one group. For example, γ = 0.8 – δ = 0.6 is included in group 1 and group 3. This does not mean that the model was run twice, but this is only to ease the analysis of the effect of one parameter on model while the other parameter was kept constant. For example, group 1 is based on δ = 0.6 and γ is varied by 0.08, 0.4, 0.8, 8 and 20. While group 3 was based on γ = 0.8 and δ is varied by 0.6 and 6.

Table 6.4 List of γ–δ combinations used in the dispersion modelling

No.	Group	Values
1	$\delta = 0.6$	$\gamma = 0.08, \delta = 0.6$
		$\gamma = 0.4, \delta = 0.6$
		$\gamma = 0.8, \delta = 0.6$
		$\gamma = 8, \delta = 0.6$
		$\gamma = 20, \delta = 0.6$
2	$\delta = 6$	$\gamma = 0.4, \delta = 6$
		$\gamma = 0.8, \delta = 6$
		$\gamma = 1.6, \delta = 6$
		$\gamma = 16, \delta = 6$
		$\gamma = 20, \delta = 6$
3	$\gamma = 0.8$	$\gamma = 0.8, \delta = 0.6$
		$\gamma = 0.8, \delta = 6$
4	$\gamma = 20$	$\gamma = 20, \delta = 0.6$
		$\gamma = 20, \delta = 3.2$
		$\gamma = 20, \delta = 6$
5	Variation of γ and δ	$\gamma = 5.93, \delta = 0.07$
		$\gamma = 8, \delta = 0.06$
		$\gamma = 13, \delta = 1.6$
6	Constant disp. coeff.	$Dxx = 0.00123$
		$Dxx = 0.00524$

Fig. 6.7 [a-f] shows the modelling results at Point P7 using various combinations of γ and δ. In general the models show similar shapes with the experimental curve, but the peak of the models were higher and the model concentrations decreased more rapidly than the experimental result.
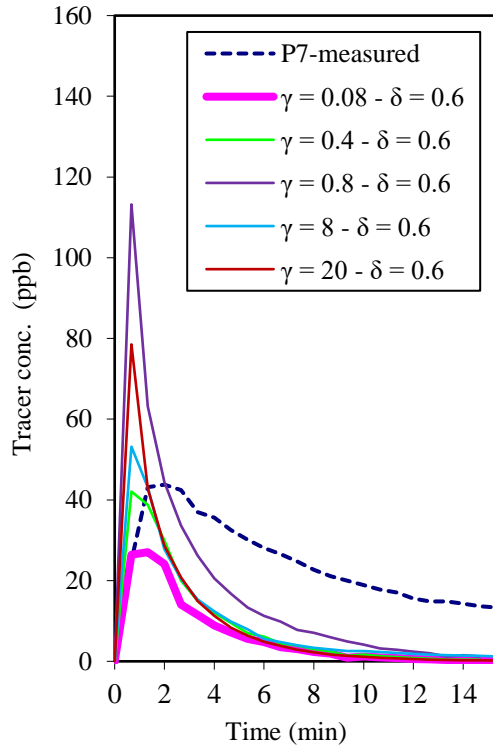
(a)
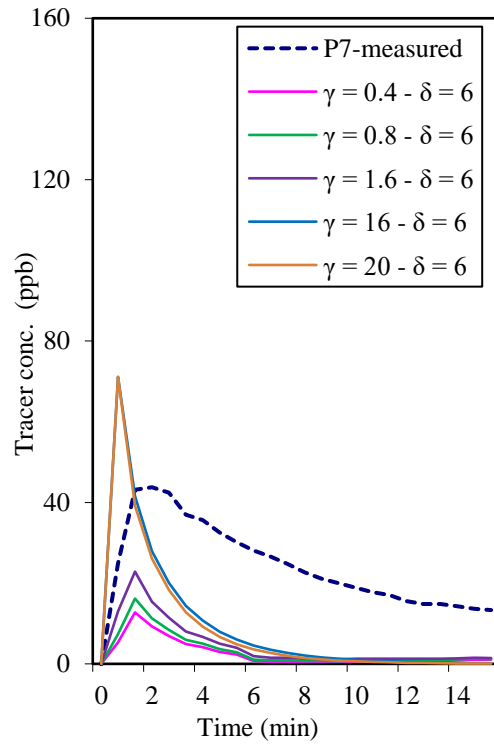
(b)
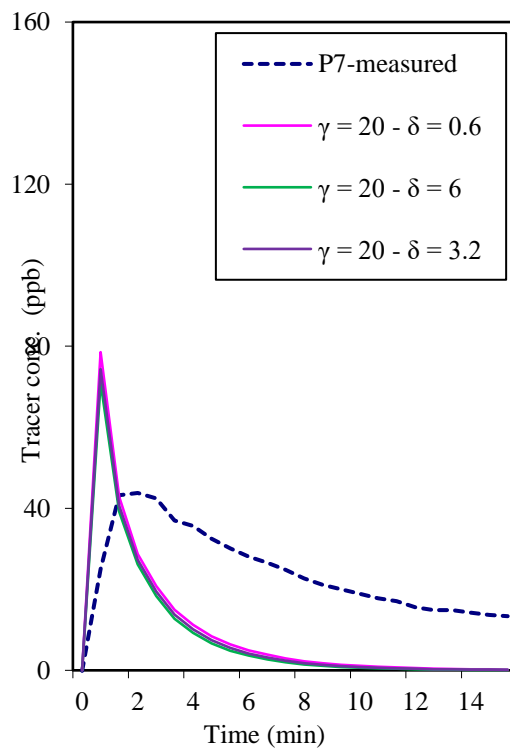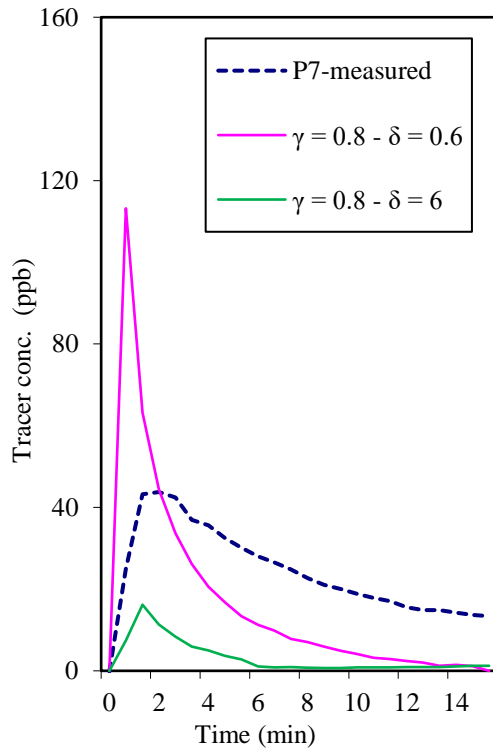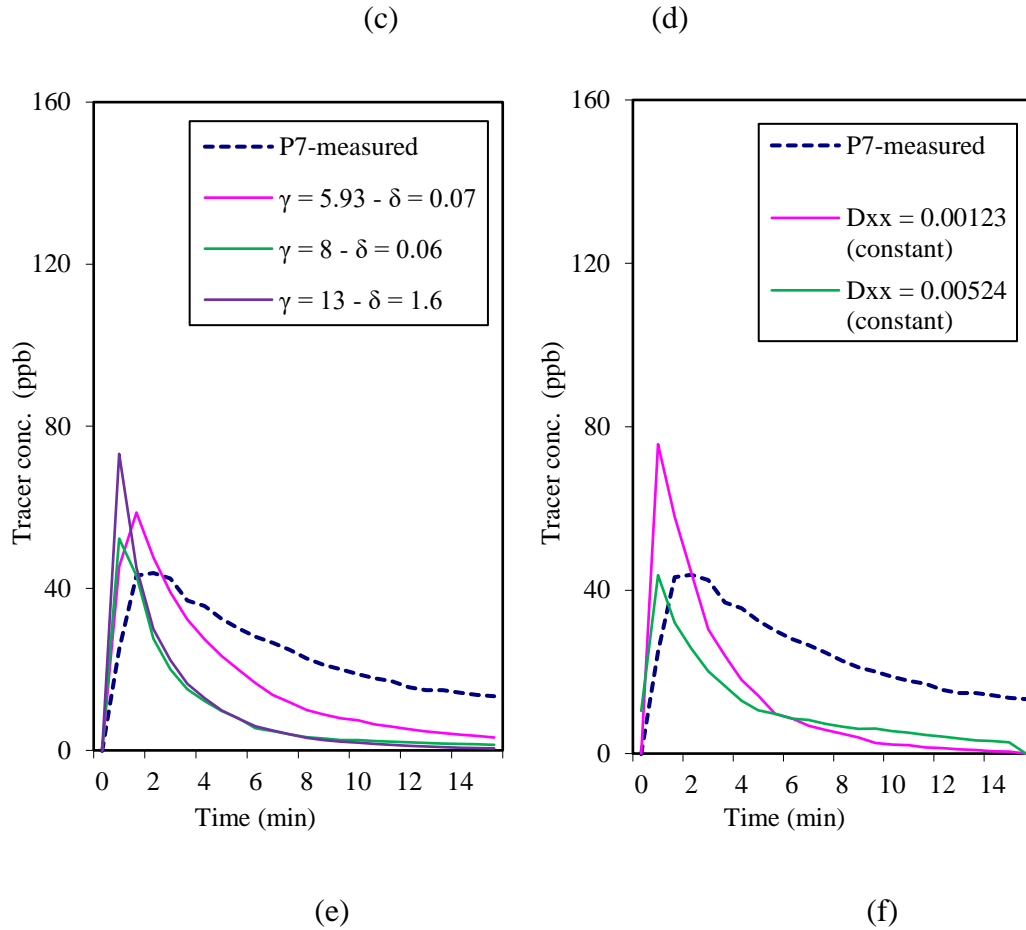
Fig. 6.7 Dispersion modelling with various combinations of γ and δ at Point P7: (a) Group-1, (b) Group-2, (c) Group-3, (d) Group-4, (e) Group-5, and (f) Group-6

The results above lead to the following conclusions:

Table 6.5 Trends of dispersion graph at Point P7

POINT	GROUP	VALUES	TREND
P7	1	δ = 0.6	γ increases, conc. increases
	2	δ = 6	γ increases, conc. increases
	3	γ = 0.8	Conc. with δ = 0.6 > conc. with δ = 6
	4	γ = 20	All coincident
	5	Variation of γ & δ	γ = 5.93, δ = 0.07 the highest conc.
	6	Constant Dx	Conc. with Dx = 0.00123 > conc. with Dx = 0.00524

Table 6.6 shows the error analysis in the modelling results at Point P7.

Table 6.6 Error analysis of dispersion modelling with various combinations of γ and δ at Point P7

Group 1		
γ	δ	α
0.08	0.6	15.61
0.4	0.6	11.41
0.8	0.6	4.23
8	0.6	5.97
20	0.6	18.77

Group 2		
γ	δ	α
0.4	6	22.65
0.8	6	16.19
1.6	6	10.56
16	6	20.52
20	6	39.38

Group 3		
γ	δ	α
0.8	0.6	4.23
0.8	6	16.19

Group 4		
γ	δ	α
20	0.6	18.77
20	6	39.38
20	3.2	28.51

Group 5		
γ	δ	α
5.93	0.07	2.22
8	0.06	5.76
13	1.6	9.14

Group 6			
γ	δ	Cons	α
-	-	0.00123	7.57
-	-	0.00524	3.16

According to Table 6.6, the best value for γ in each group was as follows: Group-1: ($γ$ = 0.8 and $δ$ = 0.6) with α = 4.24, Group-2: ($γ$ = 1.6 and $δ$ = 6) with $α$ = 10.56, Group-3: ($γ$ = 0.8 and $δ$ = 0.6) with α = 4.23, Group-4: ($γ$ = 20 and $δ$ = 0.6) with $α$ = 18.77, Group-5: ($γ$ = 5.93 and $δ$ = 0.6) with $α$ = 2.22, Group-6: constant dispersion coefficient of 0.00524 m^2/s ($α$ = 3.16).

Fig. 6.8[a-f] shows the modelling results compared with the experimental results at Point P8,for various combinations of $γ$ and $δ$ values. In general, the models resembled the experimental curves, except that the model results decreased more rapidly.

(Group-1)

(Group-2)

(Group-3)

(Group-4)

(Group-5)   (Group-6)
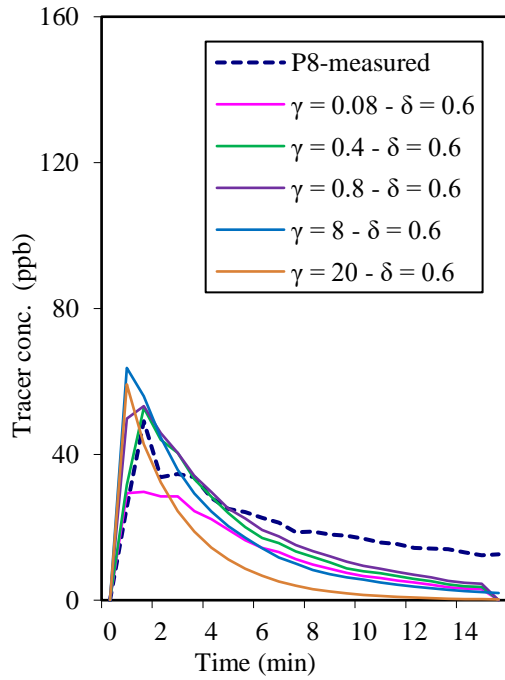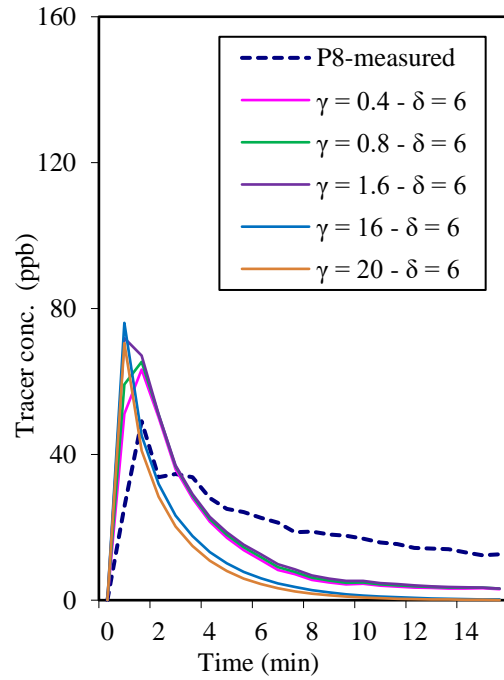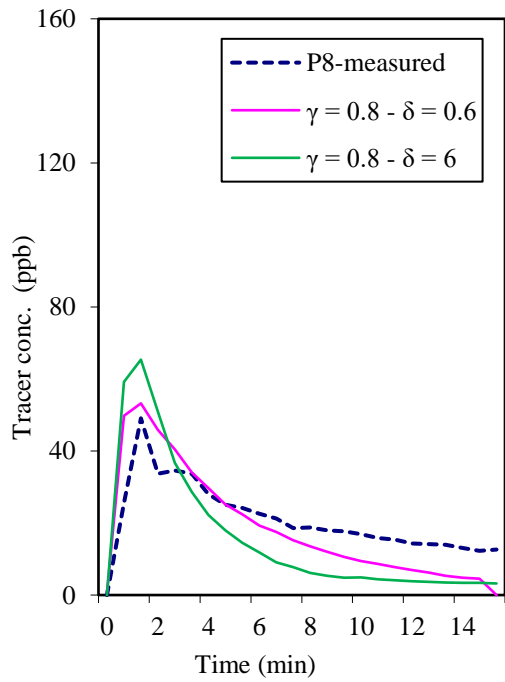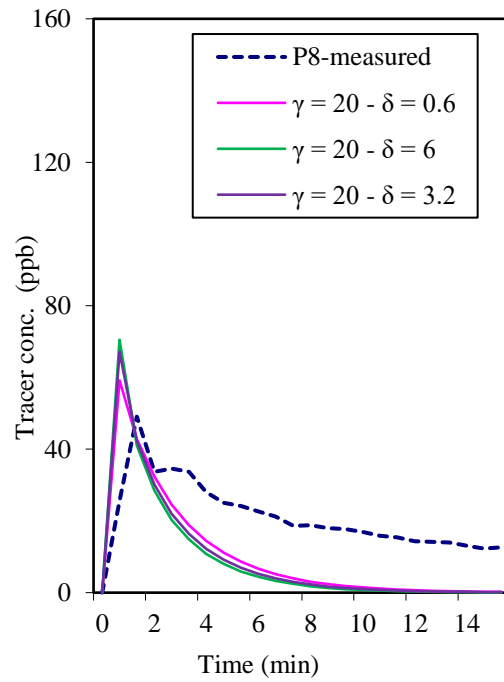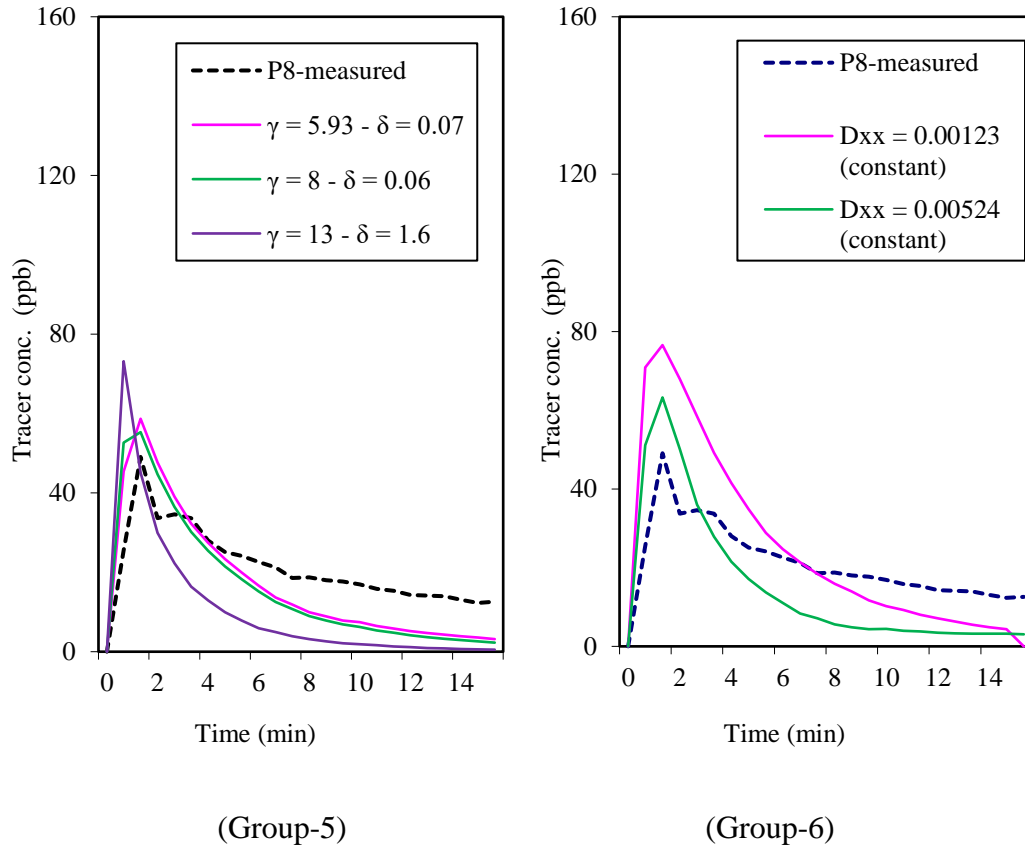
Fig. 6.8 Dispersion modelling with various combinations of γ and δ at Point P8

The results above lead to the following conclusions:

Table 6.7 Trends of dispersion graph at Point P8

POINT	GROUP	VALUES	TREND
P8	1	δ = 0.6	γ decreases, conc. increases
	2	δ = 6	γ decreases, conc. increases
	3	γ = 0.8	Conc. with δ = 0.6 > conc. with δ = 6
	4	γ = 20	All coincident
	5	Variation of γ & δ	-
	6	Constant Dx	Conc. with Dx = 0.00123 > conc. with Dx = 0.00524

Table 6.8 shows the error analysis of modelling results at Point P8.

Table 6.8 Error analysis of dispersion modelling with various combinations of γ and δ at Point P8

Group 1		
γ	δ	α
0.08	0.6	2.18
0.4	0.6	1.76
0.8	0.6	1.51
8	0.6	2.65
20	0.6	13.85

Group 2		
γ	δ	α
0.4	6	2.77
0.8	6	2.56
1.6	6	2.42
16	6	15.69
20	6	32.10

Group 3		
γ	δ	α
0.8	0.6	1.51
0.8	6	2.56

Group 4		
γ	δ	α
20	0.6	13.85
20	3.2	22.38
20	6	32.10

Group 5		
γ	δ	α
5.93	0.07	1.97
8	0.06	2.39
13	1.6	9.14

Group 6			
γ	δ	Cons	α
-	-	0.00123	1.34
-	-	0.00524	2.77

From Table 6.8 it can be seen that the best combination for each group was: Group-1: ($\gamma = 0.4$ and $\delta = 0.6$) with $\alpha = 1.51$, Group 2: ($\gamma = 1.6$ and $\delta = 6$) with $\alpha = 2.42$, Group-3: ($\gamma = 0.8$ and $\delta = 0.6$) with $\alpha = 1.51$, Group-4: ($\gamma = 20$ and $\delta = 0.6$) with $\alpha = 13.85$, Group-5: ($\gamma = 5.93$ and $\delta = 0.07$) with $\alpha = 1.97$, and Group 6: D = 0.00123 with $\alpha = 1.34$.

Fig. 6.9 [a-f] shows the effect of several combinations of γ and δ on dispersion modelling at Point P9. In general the concentration levels of the models were higher than those obtained in the experimental curves in the beginning, but then decreased rapidly over the remaining measuring time.

(Group-1)

(Group-2)

(Group-3)

(Group-4)

(Group-5)   (Group-6)
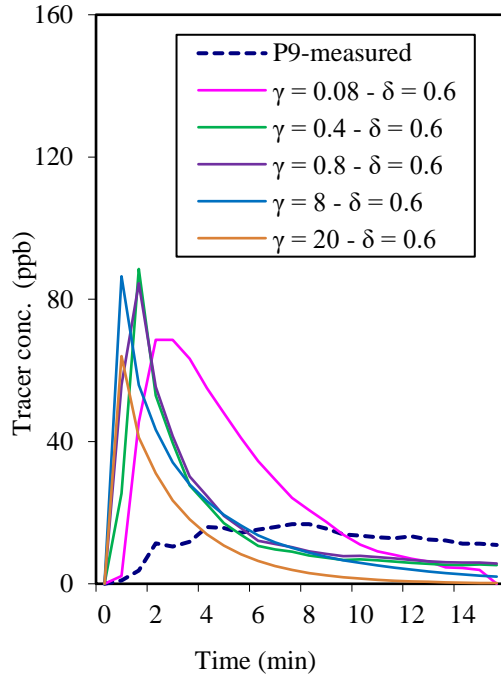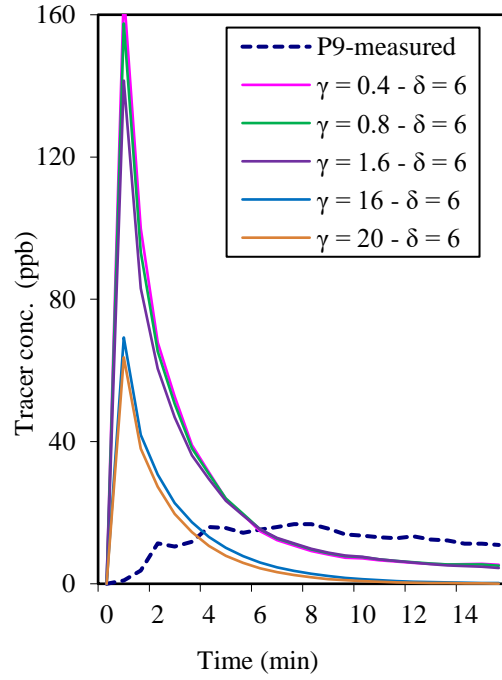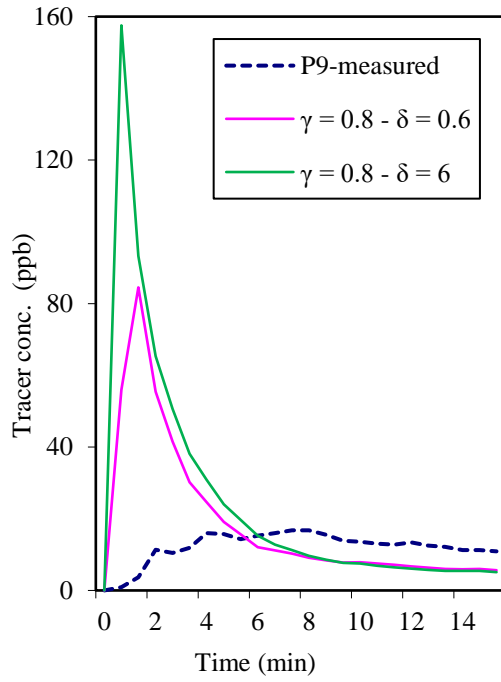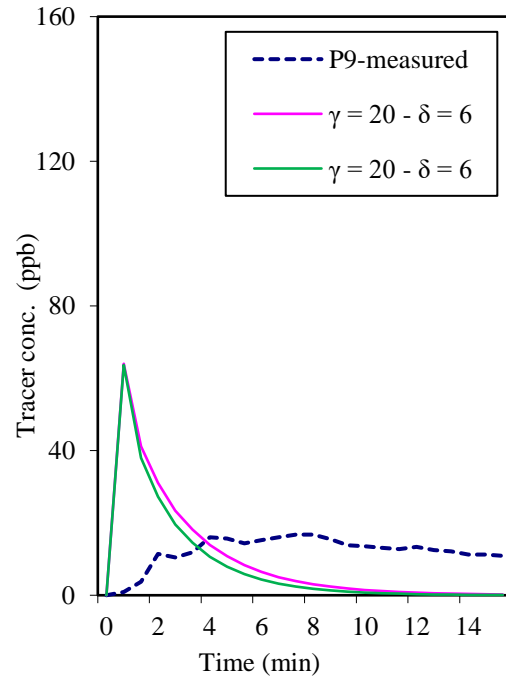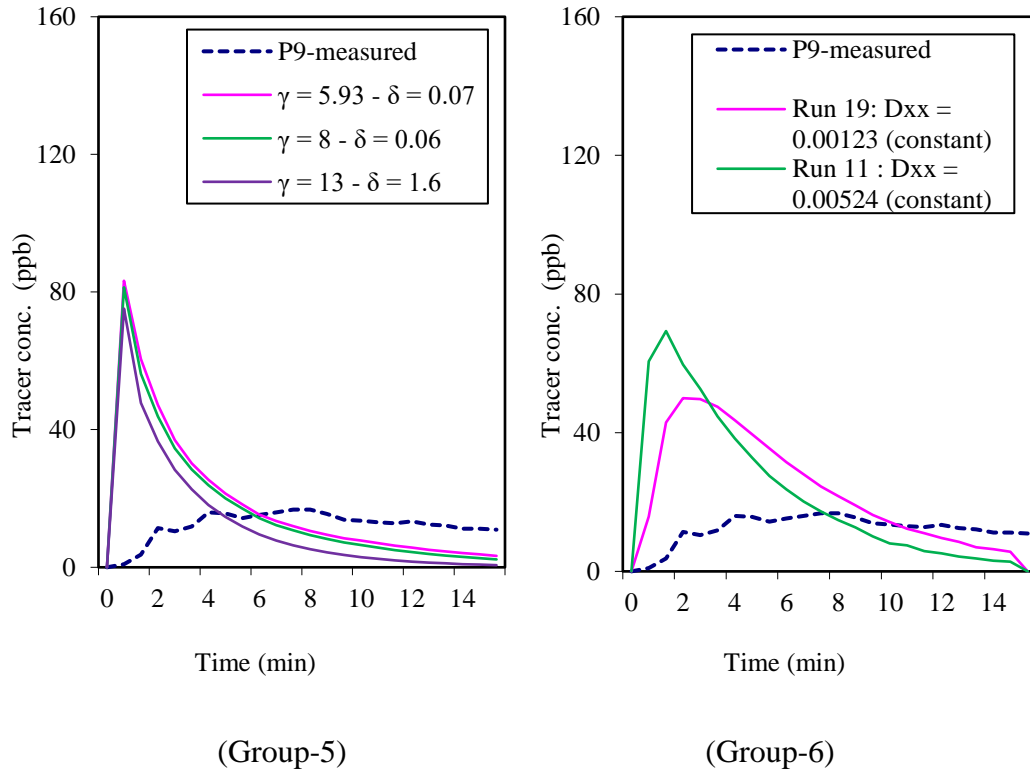
Fig. 6.9 Dispersion modelling for various combinations of γ and δ at Point P9

The results lead to the following conclusions:

Table 6.9 Trends of dispersion graph at Point P9

POINT	GROUP	VALUES	TREND
P9	1	δ = 0.6	γ decreases, conc. increases
	2	δ = 6	γ decreases, conc. increases
	3	γ = 0.8	Conc. with δ = 6 > conc. with δ = 0.6
	4	γ = 20	All coincident
	5	Variation of γ &δ	-
	6	Constant Dx	Conc. with Dx = 0.00524 > conc. with Dx = 0.00123

Table 6.10 shows the error analysis results of the models at Point P9.

Table 6.10 Error analysis of dispersion modelling with various combinations of γ and δ at Point P9

Group 1		
γ	δ	α
0.08	0.6	1.30
0.4	0.6	1.48
0.8	0.6	1.30
8	0.6	2.03
20	0.6	11.96

Group 2		
γ	δ	α
0.4	6	1.34
0.8	6	1.32
1.6	6	1.36
16	6	13.56
20	6	28.61

Group 3		
γ	δ	α
0.8	0.6	1.30
0.8	6	1.32

Group 4		
γ	δ	α
20	0.6	11.96
20	6	28.61

Group 5		
γ	δ	α

Group 5		
5.93	0.07	1.46
8	0.06	1.84
13	1.6	4.79

Group 6			
γ	δ	Cons	α
-	-	0.00123	0.80
-	-	0.00524	1.38

According to Table 6.10, the best combination for each group was as follow: Group-1: ($\gamma = 0.08$ and $\delta = 0.6$) and ($\gamma = 0.8$ and $\delta = 0.6$) with $\alpha = 1.30$, Group-2: ($\gamma = 0.8$ and $\delta = 6$) with $\alpha = 1.32$, Group-3: $\gamma = 0.8$ and $\delta = 0.6$ with $\alpha = 1.30$, Group 4: ($\gamma = 20$ and $\delta = 0.6$) with $\alpha = 11.96$, Group-5: ($\gamma = 5.93$ and $\delta = 0.07$) with $\alpha = 1.46$, Group-6: D = 0.00123 with $\alpha = 0.80$.

Fig. 6.10 [a-f] shows the effect of several combinations of γ and δ on the dispersion modelresults at Point P10 At Point P10, the model reached concentration levels which were close to the experimental curve after some time.

(Group-1)

(Group-2)

(Group-3)

(Group-4)

(Group-5)   (Group-6)
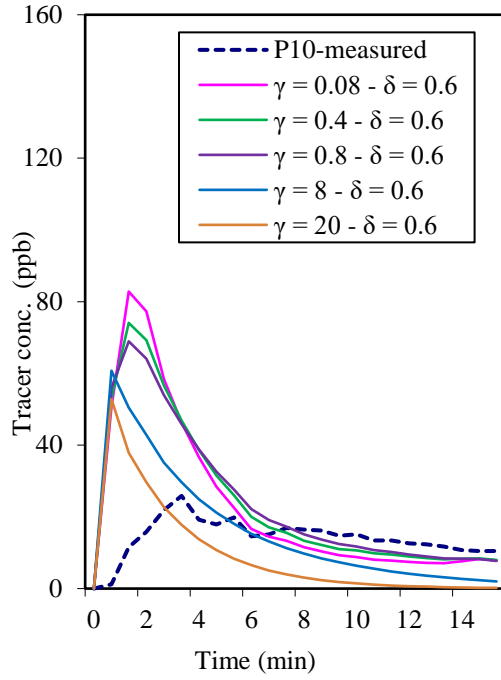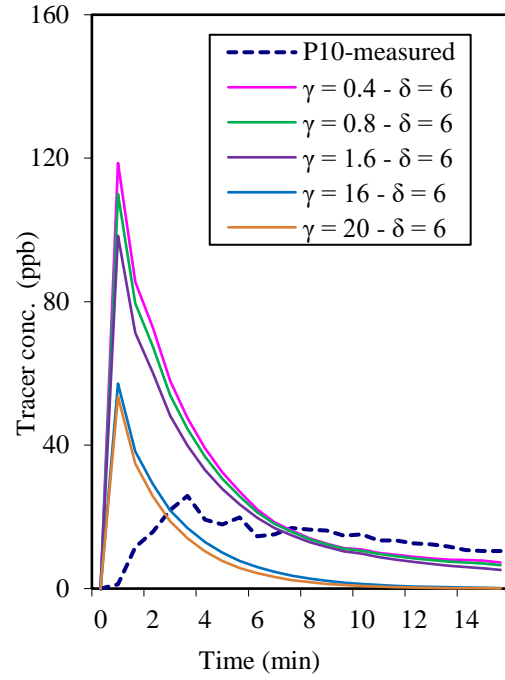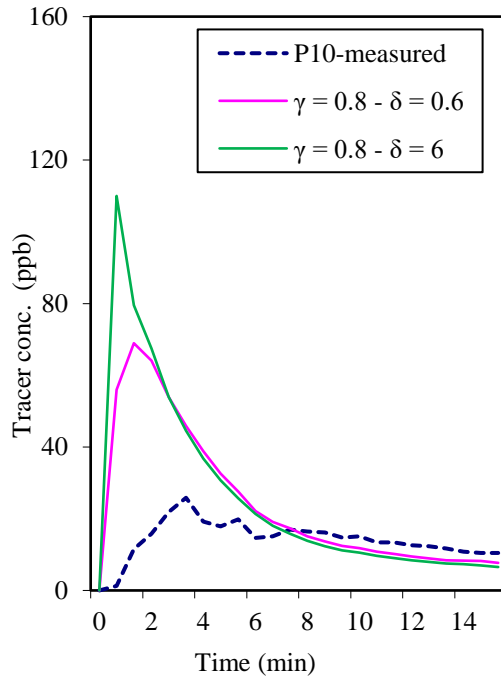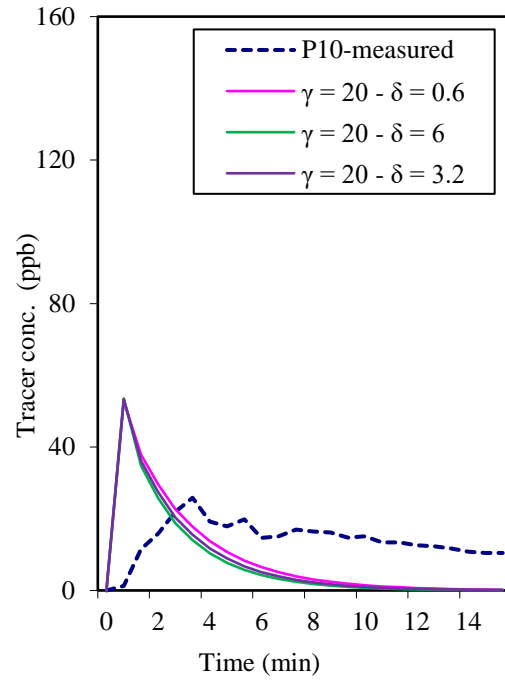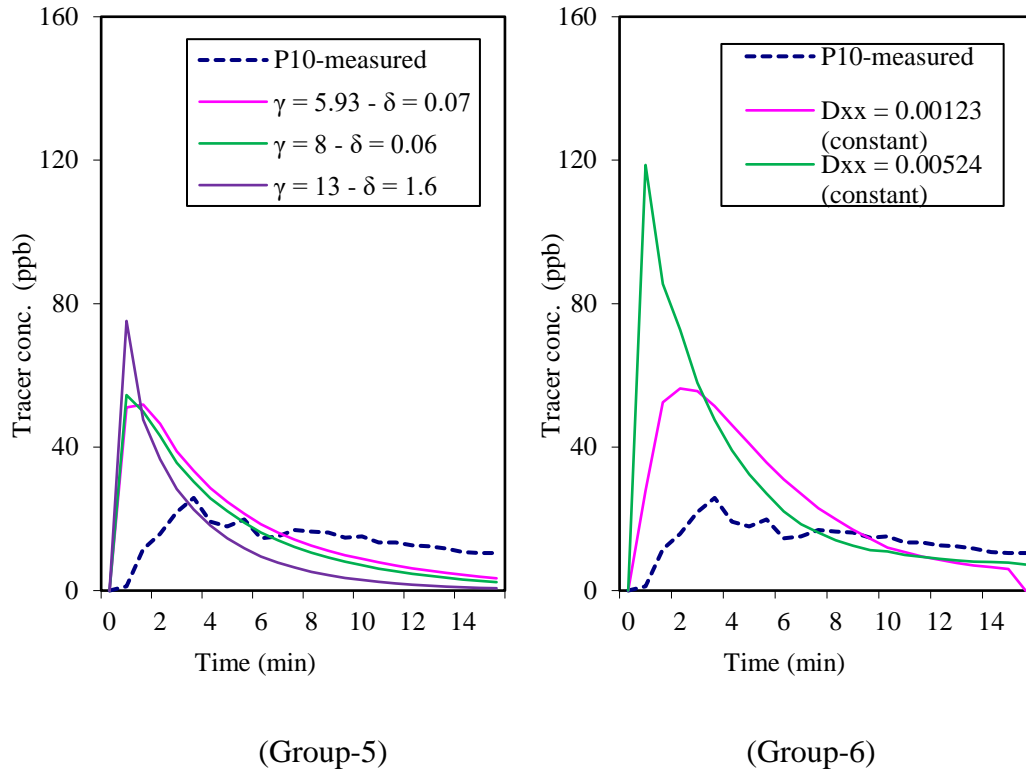
Fig. 6.10 Dispersion modelling with various combinations of γ and δ at Point P10

The results above can be concluded as follow:

Table 6.11 Trends of dispersion graph at Point P10

POINT	GROUP	VALUES	TREND
P10	1	δ = 0.6	γ decreases, conc. increases
	2	δ = 6	γ decreases, conc. increases
	3	γ = 0.8	Conc. with δ = 6 > conc. with δ = 0.6
	4	γ = 20	All coincident
	5	Variation of γ &δ	-
	6	Constant Dx	Conc. with Dx = 0.00524 > conc. with Dx = 0.00123

Table 6.12 shows the error analysis results of the models at Point P10.

Table 6.12 Error analysis of dispersion modelling with various combinations of γ and δ at Point P10

Group 1		
γ	δ	α
0.08	0.6	1.10
0.4	0.6	0.96
0.8	0.6	0.91
8	0.6	1.97
20	0.6	12.05

Group 2		
γ	δ	α
0.4	6	0.95
0.8	6	1.01
1.6	6	1.14
16	6	13.82
20	6	29.15

Group 3		
γ	δ	α
0.8	0.6	0.91
0.8	6	1.01

Group 4		
γ	δ	α
20	0.6	12.05
20	6	29.15
20	3.2	19.89

Group 5		
γ	δ	α
5.93	0.07	1.37
8	0.06	1.78
13	1.6	4.79

Group 6			
γ	δ	Cons	α
-	-	0.00123	0.88
-	-	0.00524	0.95

According to Table 6.12, the best combination of γ and δ for each group was as follows: Group-1: (γ = 0.4 and δ = 0.6) with α = 0.96, Group-2: (γ = 0.8 and δ = 6) with α = 1.01, Group-3: (γ = 0.8 and δ = 6) with α = 1.01, Group-4: (γ = 20 and δ = 0.6) with α = 12.05, Group-5: (γ = 5.93 and δ = 0.07) with α = 1.37, and Group-6: D = 0.00524 m^2/s with α = 0.95.

Fig. 6.11 [a-f] shows the modelling results using various combinations of γ and δ at Point P11. Like most of the previous results, the models had higher peaks than the experimental curve at the beginning, but then approached the concentration level of the experimental curve after some time.
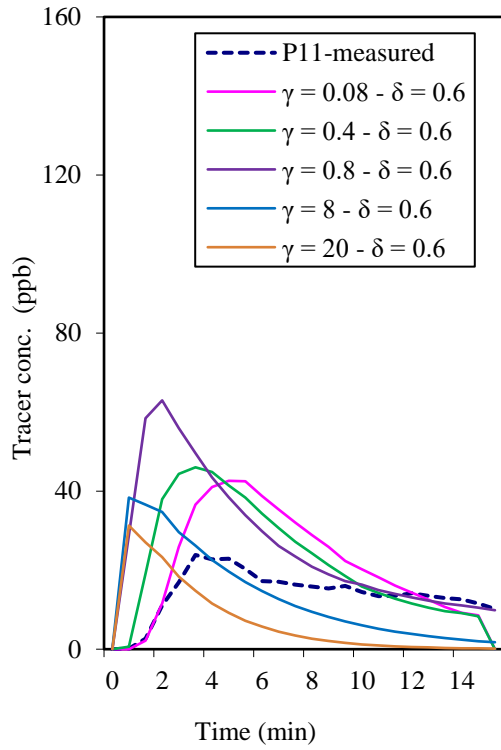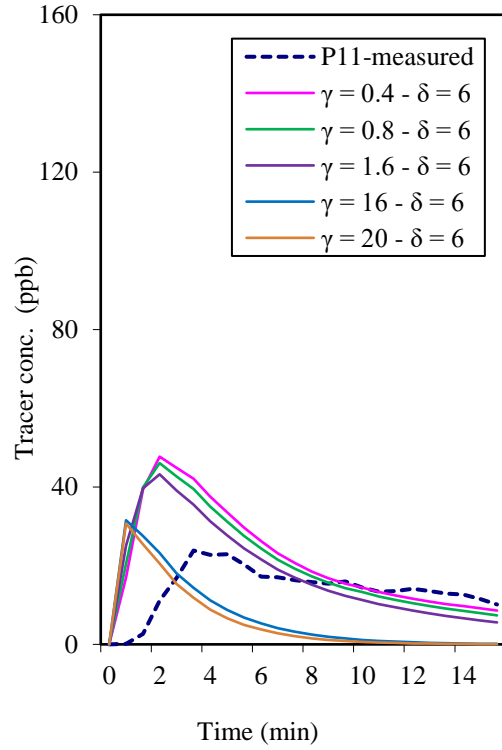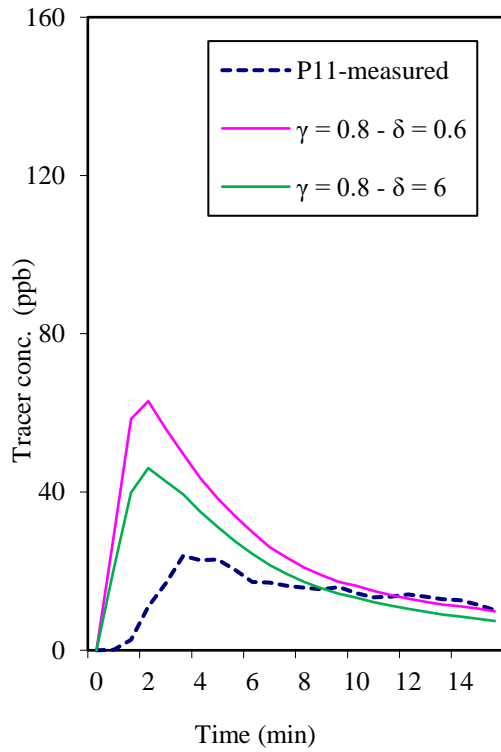
(Group-1)
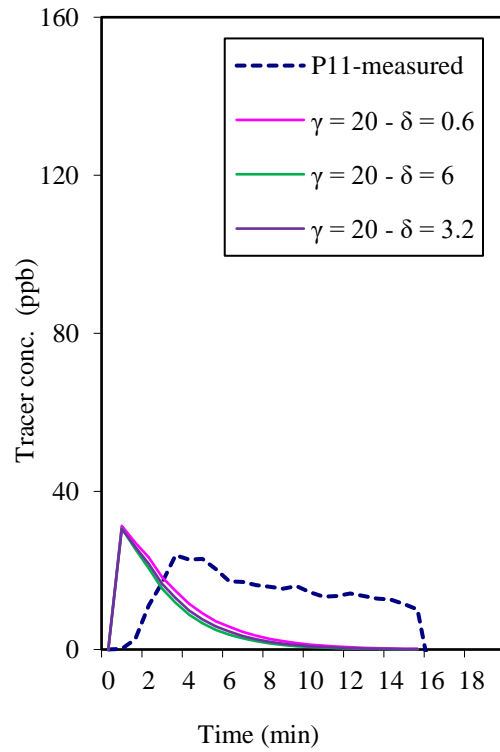
(Group-2)
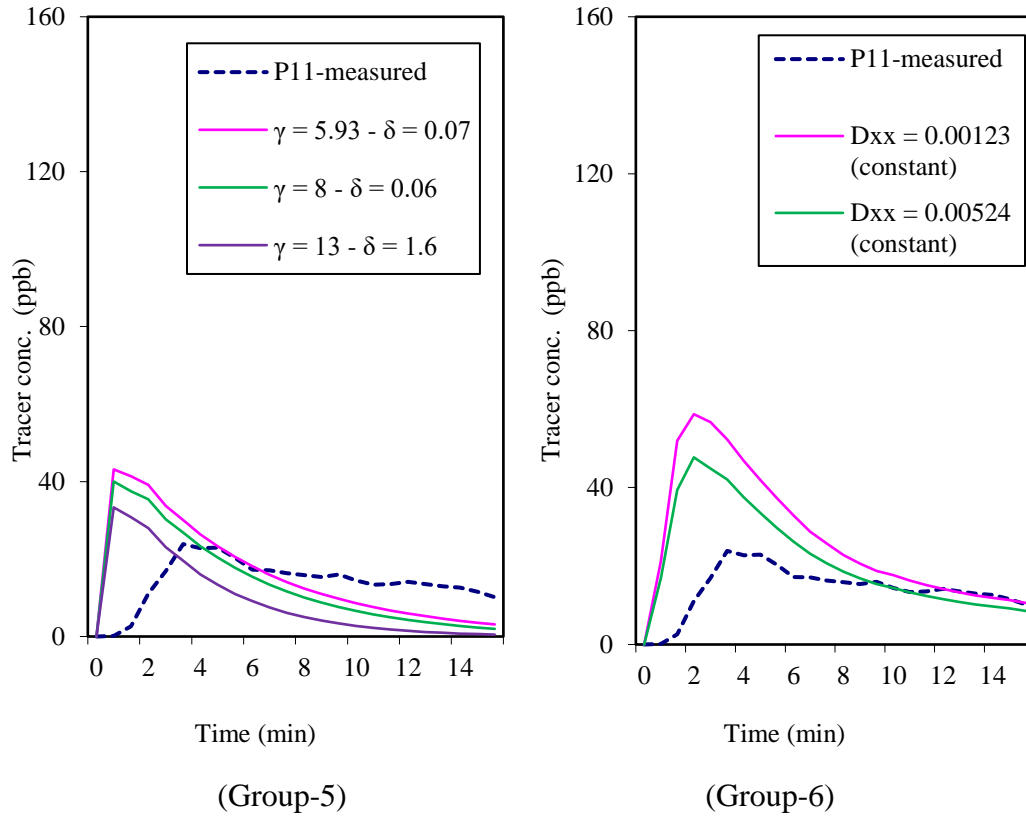
(Group-3)

(Group-4)

Fig. 6.11 Dispersion modelling with various combinations of γ and δ at Point P11

The results above can be summarized as follow:

Table 6.13 Trends of dispersion graph at Point P11

POINT	GROUP	VALUES	TREND
P11	1	δ = 0.6	γ decreases, conc. increases
	2	δ = 6	γ decreases, conc. increases
	3	γ = 0.8	Conc. with δ = 0.6 > conc. with δ = 6
	4	γ = 20	All coincident
	5	Variation of γ & δ	-
	6	Constant Dx	Conc. with Dx = 0.00123 > conc. with Dx = 0.00524

Table 6.14 shows the error analysis results of the models at Point P11.

Table 6.14 Error analysis of dispersion modelling with various combinations of γ and δ at Point P11

Group 1		
γ	δ	α
0.08	0.6	3.03
0.4	0.6	0.75
0.8	0.6	0.72
8	0.6	2.27
20	0.6	1.51

Group 2		
γ	δ	α
0.4	6	0.82
0.8	6	0.90
1.6	6	1.08
16	6	17.55
20	6	37.94

Group 3		
γ	δ	α
0.8	0.6	0.72
0.8	6	0.90

Group 4		
γ	δ	α
20	0.6	15.83
20	6	25.92
20	3.2	37.94

Group 5		
γ	δ	α
5.93	0.07	1.51
8	0.06	2.06
13	1.6	5.93

Group 6			
γ	δ	Cons	α
-	-	0.00123	0.66
-	-	0.00524	-0.21

According to Table 6.14, the best combination for each group is as follows: Group-1: (γ = 0.4 and δ = 0.6) with α = 0.75, Group-2: (γ = 1.6 and δ = 6) with α = 1.08, Group-3: (γ = 0.8 and δ = 6) with α = 0.90, Group-4: (γ = 20 and δ = 0.6) with α = 15.83, Group-5: (γ = 5.93 and δ = 0.07) with α = 1.51, and Group 6: D = 0.00123 m^2/s with α = 0.66.

Fig. 6.12 [a-f] shows the modelling results with various combinations of γ and δ at Point P12.

(Group-1)

(Group-2)

(Group-3)

(Group-4)

159

(Group-5)   (Group-6)
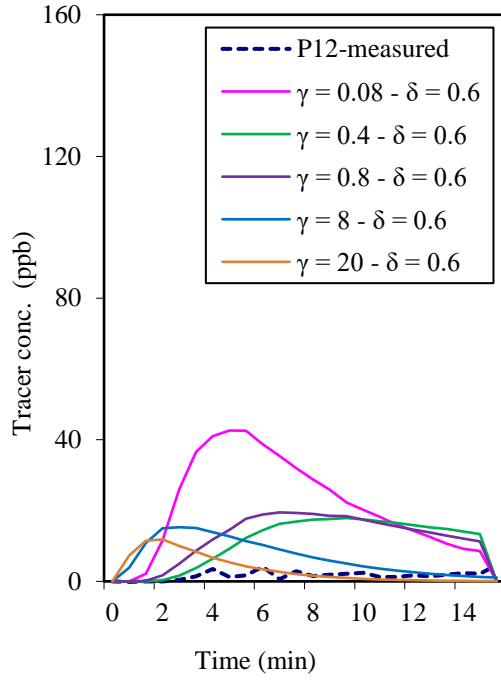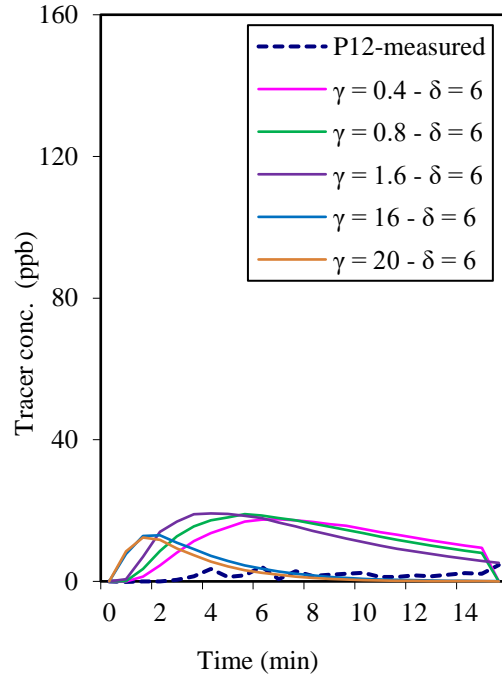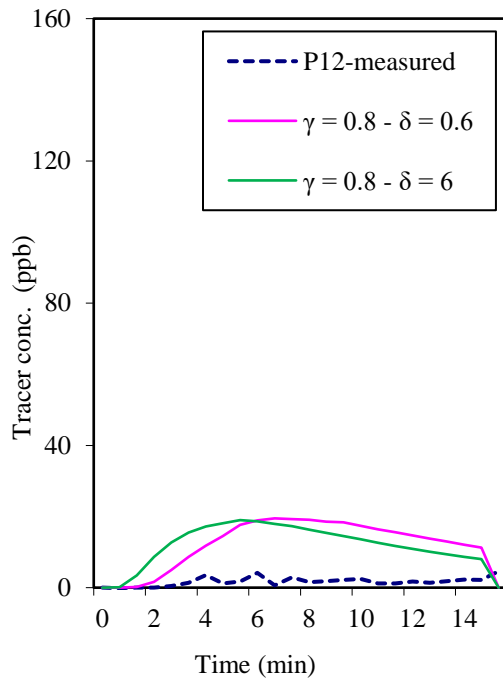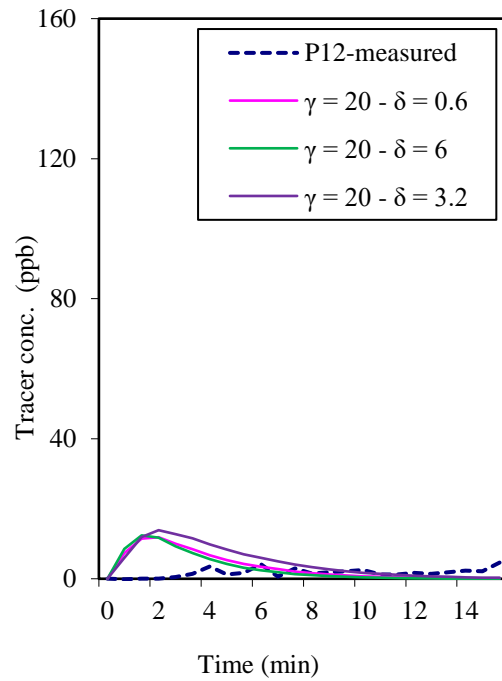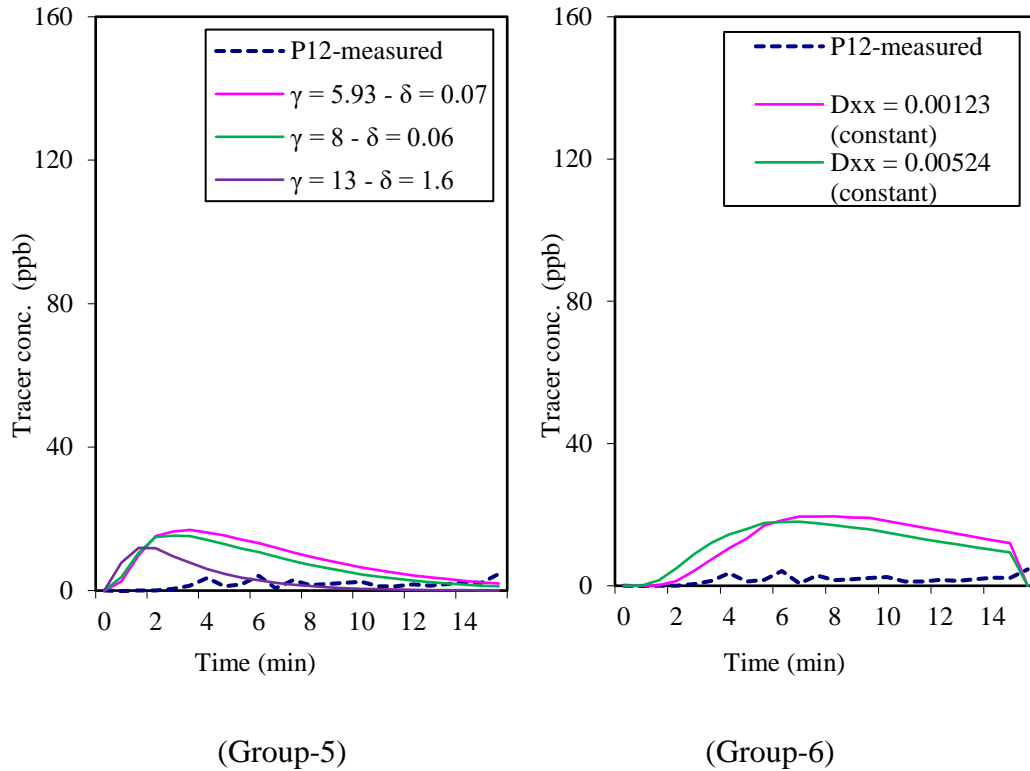
Fig. 6.12 Dispersion modelling with various combinations of γ and δ at Point P12

The results above lead to the following conclusions:

Table 6.15 Trends of dispersion graph at Point P12

POINT	GROUP	VALUES	TREND
P12	1	δ = 0.6	γ decreases, conc. Increases
	2	δ = 6	γ decreases, conc. Increases
	3	γ = 0.8	Conc. with δ = 0.6 > conc. with δ = 6
	4	γ = 20	All coincident
	5	Variation of γ &δ	-
	6	Constant Dx	Conc. with Dx = 0.00123 > conc. with Dx = 0.00524

Table 6.16 shows the error analysis results of the models at Point P12.

160

Table 6.16 Error analysis of dispersion modelling with various combinations of γ and δ at Point P12

Group 1		
γ	δ	α
0.08	0.6	-2.19
0.4	0.6	0.15
0.8	0.6	0.12
8	0.6	0.60
20	0.6	0.35

Group 2		
γ	δ	α
0.4	6	-0.26
0.8	6	0.05
1.6	6	0.17
16	6	5.95
20	6	0.35

Group 3		
γ	δ	α
0.8	0.6	0.12
0.8	6	0.05

Group 4		
γ	δ	α
20	0.6	6.26
20	6	9.88
20	3.2	14.15

Group 5		
γ	δ	α
20	0.6	0.35
20	6	0.55
13	1.6	1.91

Group 6			
γ	δ	Cons	α
-	-	0.00123	0.12
-	-	0.00524	-0.21

According to Table 6.16, the best combination of γ and δ for each group is as follows: Group-1: ($\gamma = 8$ and $\delta = 0.6$) with $\alpha = 0.60$, Group-2: ($\gamma = 20$ and $\delta = 6$) with $\alpha = 0.35$, Group-3: ($\gamma = 0.8$ and $\delta = 0.6$) with $\alpha = 0.12$, Group-4: ($\gamma = 20$ and $\delta = 0.6$) with $\alpha = 6.26$, Group-5: ($\gamma = 20$ and $\delta = 6$) with $\alpha = 0.55$, and Group-6: D $= 0.00123$ m^2/s with $\alpha = 0.12$.

From the results in this section (6.4) some patterns can be seen for each group of γ and δ combinations, as follow:

a) Group-1 (effect of γ for $\delta = 0.6$): the concentration levels predicted using the model increased with a decrease in the γ value, except at Point P7, which showed the opposite tendency, due to the position of this point being upstream from the injection point.

b) Group-2 (effect of γ at $\delta = 6$): the models in this group showed a similar trend to those of Group-1. The concentration levels from the model results tended to increase with a decrease in the value of γ, except for Point7 which showed an opposite tendency as for Group-1. The modelresultsfor $\gamma = 0.4$, 0.8, and 1.6 were coincident and the model results with γ values of 16 and 20 were also coincident.

c) Group-3 (effect of δ at $\gamma = 0.8$): the trend was not so consistent. At some points (P7, P8, P11 and P12) the models with $\delta = 0.6$ had higher concentration levels

than the model results with δ = 6. However,at the other points (i.e. P9 and P10) the trend was opposite.

d) Group-4 (effect of δ at γ = 20): in this group three values of δ were considered, namely 0.6, 3.2, and 6. All of the model results were coincident, meaning that for the values of δ considered therewas no change in the relative concentration levels.

e) Group-5 (effect of several combinations of γ and δ): there were three combinations of γ and δ values used in this group, namely: (γ = 5.93 and δ = 0.07), (γ = 8 and δ = 0.06), and (γ = 13 and δ = 1.6). Generally the model with (γ = 5.93 and δ = 0.07) had lower concentration levels than those predicted for the other two model scenarios, with the two other model results being generally coincident.

f) Group-6 (effect of constant dispersion coefficient): there were two constant dispersion coefficients used in this group, including: 0.00123 m^2/s and 0.00524m^2/s. In general, the models with D = 0.001235 m^2/s had higher concentration levels than the model with D = 0.00524 m^2/s. Only at Points P9 and P10 did the model with D = 0.00524 m^2/s have higher concentration levels than the other model results.

The graphs were coincident in several places:

1.   γ = 20, δ = 0.6, 3.2 and 6.

When the value of γ was 20, all the graphs were coincident. This meant that the change in the δ value did not affect the tracer concentration. There is a possibility that the value of γ was so high that the change in δ value was insignificant.

2.   δ = 6, γ = 16 and 20.

At all points, the value of γ = 16 and 20 gave coincident graphs. In this case the δ value was 6. This suggested that the change of γ value was insignificant in this range.

3. $\delta = 6$, $\gamma = 0.4$, 0.8 and 1.6

This also suggested that in this value of δ, the change of δ value in this range was insignificant to the tracer concentration.

It should be noted that the value of longitudinal dispersion coefficient (D) and lateral turbulent diffusion (D*) are both determined by u_* and h. Therefore, for the same value of u_* and h, magnitudes of D and D* are only determined by γ and δ. According to Elder (1958), the value of 5.93. And the value of δ is ….. Therefore, taking the value above both seemed to be insignificant to the change of tracer concentration.

6.5 Comparison between constant and variable dispersion coefficients

It can be evaluated from the results in Section 6.4 that there was no definitive combination of γ and δ values which represented the best match for the dispersion with the experimental results. The best combination of values for γ and δ was different for each point. Therefore in order to compare between the variable and constant dispersion coefficient, the error analysis results of some γ-δ combinations and the two constant dispersion coefficients were compared. The results of these comparisons are shown in Table 6.11.

Table 6.17 Comparison of α values from error analysis between variable and constant dispersion coefficients

Values	P-7	P-8	P-9	P-10	P-11	P-12	Average
$\gamma = 0.8$ - $\delta = 0.6$	4.23	1.51	1.30	0.91	0.72	0.12	1.47
$\gamma = 0.8 - \delta = 6$	16.19	2.56	1.32	1.01	0.90	0.05	3.53
$\gamma = 8 - \delta = 0.6$	5.97	2.65	2.03	1.97	2.27	0.60	2.58
$\gamma = 5.93 - \delta = 0.07$	2.22	1.97	1.46	1.37	1.51	-	1.706
$D = 0.00123$	7.57	1.34	0.80	0.88	0.66	0.12	1.90
$D = 0.00524$	3.16	2.77	1.38	0.95	-0.21	-0.21	1.30

From Table**6.11** it appeared that the constant dispersion coefficient of 0.00524 m^2/s gave the best value for α.

6.6 Effect of bathymetry refinement on dispersion modelling

In Chapter 5, the bathymetry refinement has been shown to improve the accuracy of the hydrodynamic modelling. It was concluded from the corresponding results that the model predictions were very sensitive to the accuracy of the bathymetry. The effect of bathymetry refinements on dispersion modelling was also observed in this study. The modelling results using the new bathymetry were compared with those obtained for the old bathymetry, and in term of the degree of agreement with the measured results. Fig. 6.13 [a-f] show the results of this comparison. From the figures it was clear that the bathymetry refinement improved the model considerably. In the past little analysis has been undertaken on the effect of the bathymetry on the numerical model results. However, this is considered crucial as the bathymetry is the basis for the model accuracy. In the previous chapter, the bathymetry refinements proved to improve the hydrodynamic modelling results. In this part of the study the effect of the bathymetry refinements were also applied to improve the dispersion model.The values of γ and δ used were (γ = 8 and δ = 0.6). Fig. 6.13 shows the modelling results using the old and new bathymetry data, and Table 6.13 summarizes the results of error analysis.

(a)

(b)

(c)

(d)

166

(e)   (f)
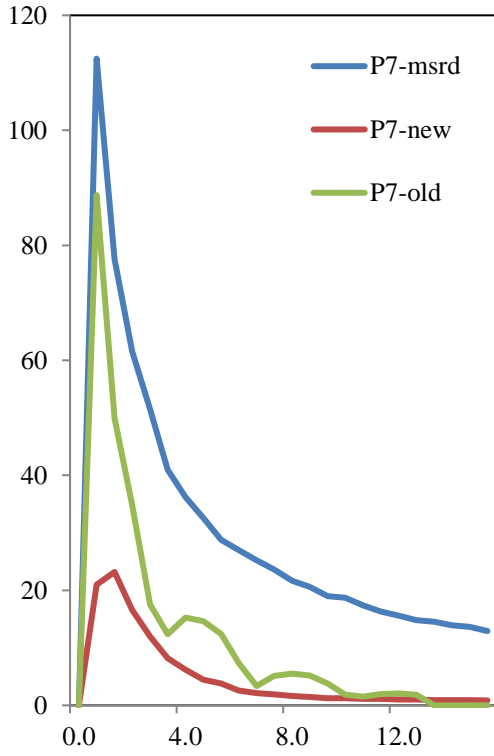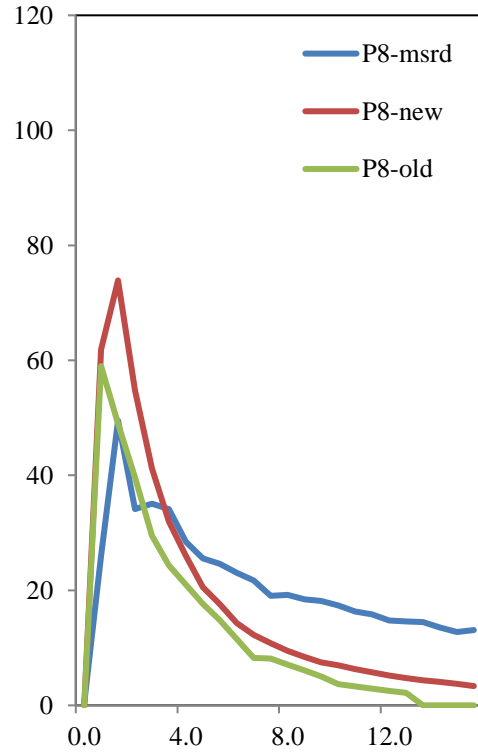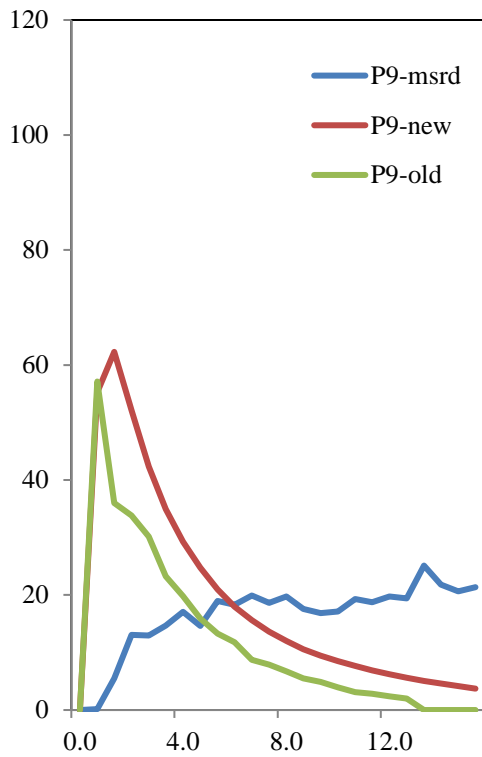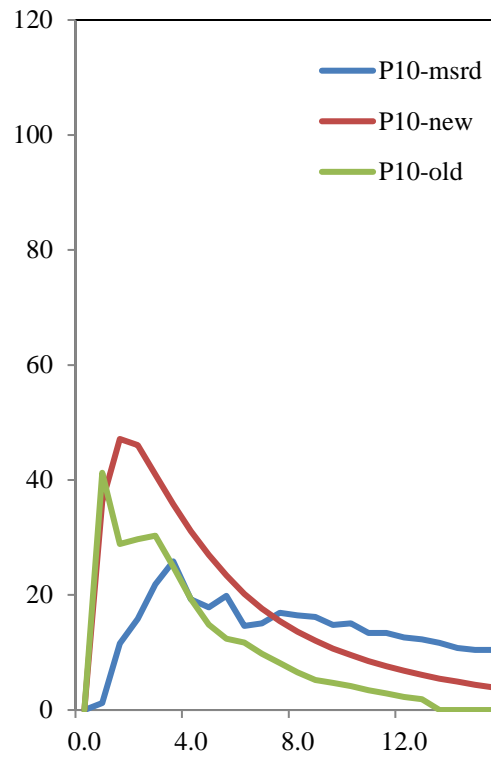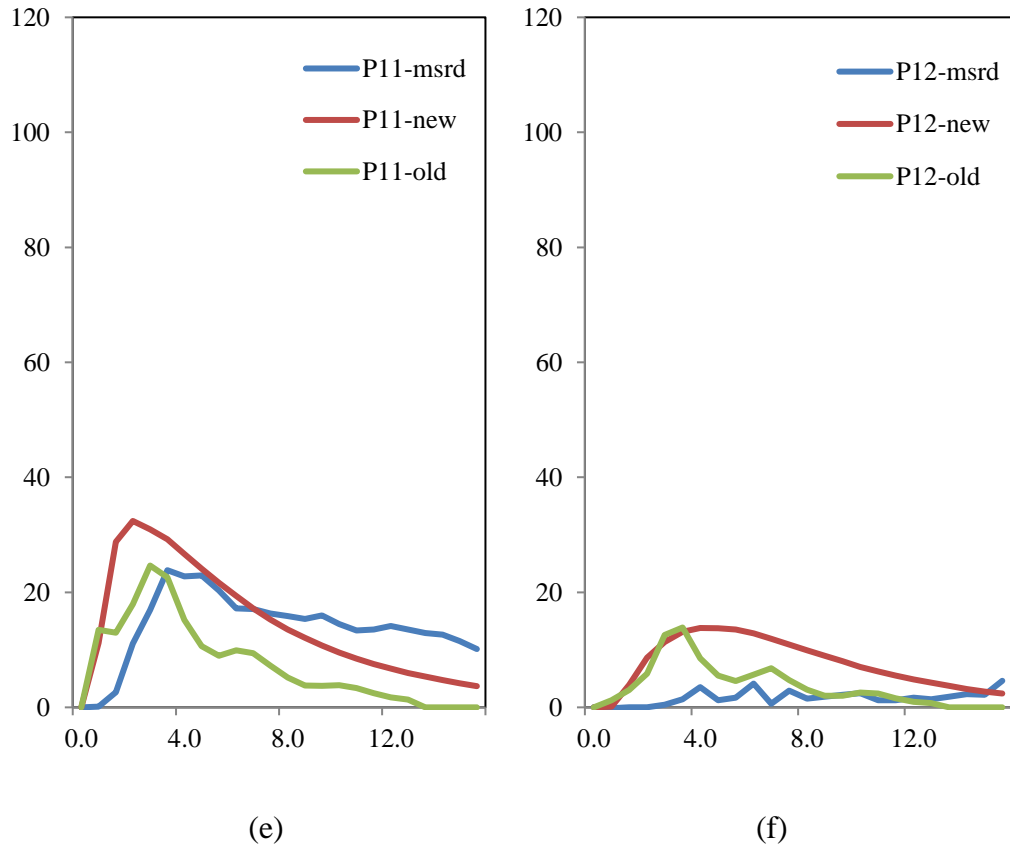
Fig. 6.13 Effect of bathymetry refinement on dispersion modelling

Table 6.18 Error analysis of bathymetry effect on dispersion modelling

Point	P7		P8		P9		P10		P11		P12	
	New	old	new	old	new	old	new	old	new	old	new	old
A	10.240	4.838	1.732	2.811	1.358	2.940	1.021	2.343	1.089	2.997	0.115	0.567

From these results it seemed that the new bathymetry data gave a better dispersion model. This conclusion is drawn because despite there are two points where the new bathymetry show worse model results (which were P7 and P12), the new bathymetry gave better results than the old one at the remaining sampling points.

CHAPTER 7

STUDIES IN THE GROUNDWATER MODEL

The Severn estuary physical model incorporates a sandbox which represents a groundwater environment, enabling investigations to be undertaken on surface water-groundwater interactions, both for the hydrodynamic and dispersion processes. The hydrodynamics of surface water (in this case the estuary) affects the surrounding groundwater, and vice versa.

Unlike the hydrodynamic study in the estuarine physical model, which consisted of water level and velocity measurements, the hydrodynamic study for the groundwater only consisted of water level measurements, since the size of the ADV did not allow velocity measurements to be performed in the small groundwater boreholes. However, for the dispersion experiments, it was possible to perform dye tracer measurement using fluorometers, since the fluorometer probes could be inserted inside the boreholes.

In order to analyze the results, the scaling factors for the estuary physical model were also applied for the groundwater study.

As it has been described in Chapter 4, the purpose of the experiments in the groundwater model is to simulate dispersion in groundwater. However a set of water level study were carried out to establish hydrodynamic characteristics of the groundwater and the effects of tide and pumping on groundwater level. A calibration steps need to be done first to enable water level readings.

Therefore, the experiments in the groundwater consist of:

1. Calibration of water level, in order to enable the reading of water level from the conductivity data of the water level probes
2. Effect of tide

3. Combined effect of tide and pump

4. Dispersion study with open-open boundary scenario

5. Dispersion study with close-open boundary scenario

7.1 Hydrodynamic experiments

7.1.1 Calibration of water level probes

Because there were only three water level probes available, the probes were used in turn to carry out the measurements at 7 points, with 3 points measured in a time. The measurements were therefore carried out in three groups, as follow:

1) Group ACD, including points A, C, and D

2) Group ABE, including points A, B, and E

3) Group AFG, including points A, F, and G

Point A was measured at each time as the reference to control the consistency of each measurement, and was also taken as the datum for the measurements.

Fig. 7.1 shows the layout of the sandbox and the position of the sampling points.
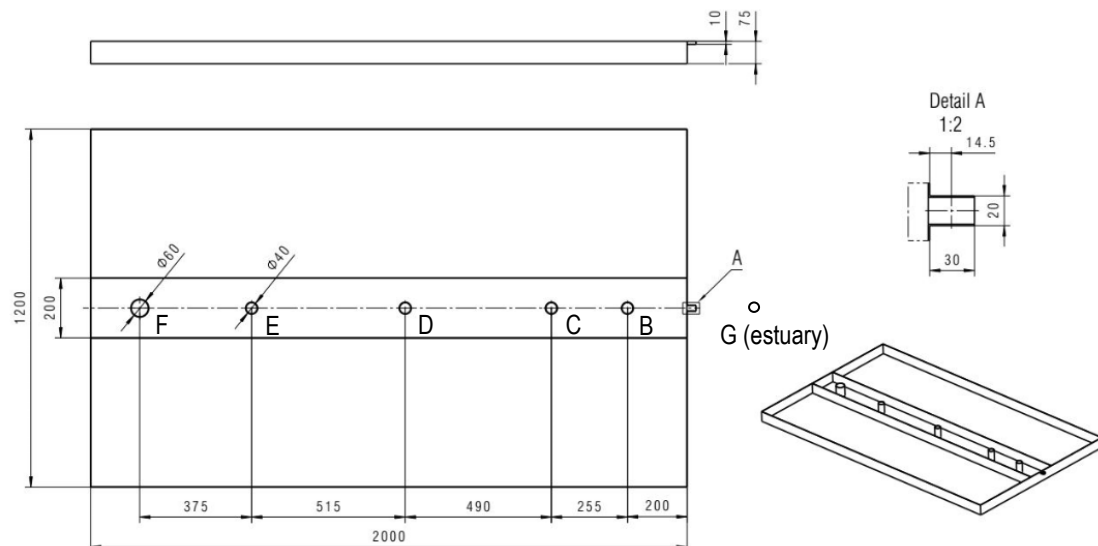
Fig. 7.1 Sandbox and the position of the sampling points

As for the experiments in the estuarine physical model, the water level measurements in the sandbox were preceded by calibration of the water level probes, in order that the read data could be converted to actual water level data. In this case the calibrations were done by setting several weir levels, and then measuring the actual water level for each weir level. This resulted in several points relating the read data and actual water level data, from which the calibration equations could be developed.

The weir setting consisted of minimum and maximum water weir levels, which can be seen in Table 7.1.

Table 7.1 Weir settings for the water level calibration

Weir setting no.	Minimum weir level	Maximum weir level
1	40	100
2	50	100
3	60	100
4	70	100

The tide was set off, so the weir stayed in the minimum level during the running period.For each setting, measurements were taken after the water level stabilized, which took about 20 minutes. Once this has been completed, the weir was changed to the next setting.

7.1.1.1   Water level calibration for group ACD

The water level calibration was firstly carried out for group ACD, with measured results being given in Table 7.2.

170

Table 7.2 The average readdata of ACD and the corresponding depth of point A

Weir setting	Probe-1 (D)		Probe-2 (C)		Probe-3 (A)		Water level at point A (mm)
	Read data	Water level (mm)	Read data	Water level (mm)	Read data	Water level (mm)	
40-100	-131.58	65.6	-144.68	65.6	-57.84	65.6	65.6
50-100	-115.44	74.5	-134.16	74.5	-45.49	74.5	74.5
60-100	-99.18	84.6	-123.06	84.6	-32.32	84.6	84.6
70-100	-87.86	94.5	-114.01	94.5	-19.098	94.5	94.5

Graphs were then produced to show the relationship between the read data and the water level data, with the calibration equations then being established. From the regression analysis of the graphs, the calibration equation for each point was made and they are shown in Table 7.3.

Table 7.3 Calibration equations for group ACD

Probe (borehole)	Calibration equation
Probe-1 (D)	$y = 0.6516x + 150.51$
Probe-2 (C)	$y = 0.9368x + 200.63$
Probe-3 (A)	$y = 0.7482x + 108.74$

The calibration equations in Table 7.3 were then used to convert all of the read data into the water level data, and the results are plotted in Fig. 7.1.
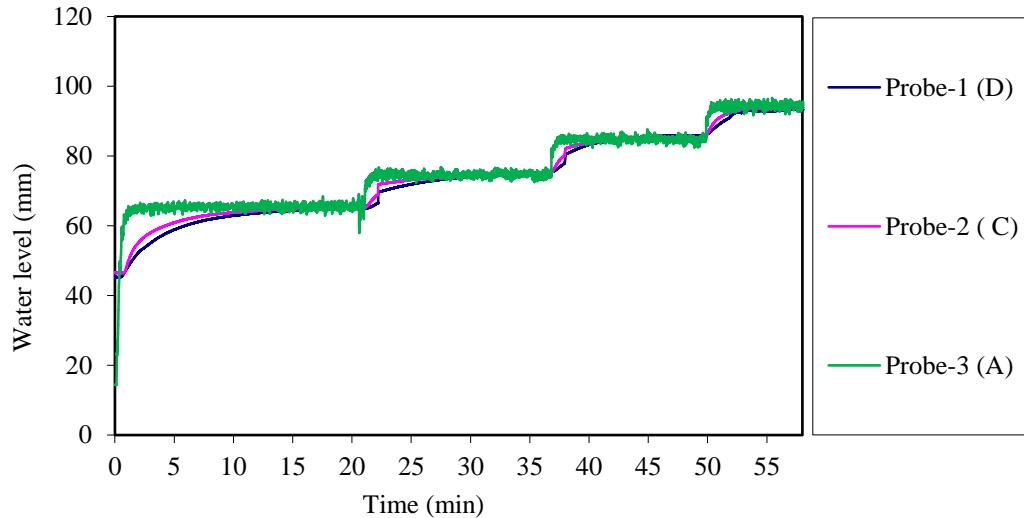
Fig. 7.2 Calibration graph of group ACD

From Fig. 7.1 it can be seen that the water level in the sandbox increases consistently with the changes in the weir setting. The figure also shows that there was a lag time for each borehole before the water level was stable, and this lag time depended on the distance between the borehole and the estuary. In Fig. 7.1 the shortest time lag was at borehole A, succeeded by C, and finally borehole D. This result is consistent with the distance between each borehole and the estuary, i.e. the further the distance between the borehole and the estuary, then the longer the lag time. Furthermore, the average water level in this group could also be obtained, as shown in Table 7.4.

Table 7.4 Average water level of group ACD in the calibration step

Weir setting	Average water level (mm)		
	Probe-1 (D)	Probe-2 (C)	Probe-3 (A)
40-100	60.400	61.605	64.294
50-100	73.300	73.913	74.641
60-100	84.038	84.201	84.836
70-100	92.117	93.009	94.314

Table 7.4, as well as Fig. 7.1, shows that the average water levels at A, C, and D for the same period (setting) were virtually identical. This showed that the water was stable throughout the sandbox. However, the average water level at Point A for all cases was higher than at Point C and D, as explained above with regard to the larger time lag at Points C and D, resulting in lower average water levels at these two boreholes.

7.1.1.2   Water level calibration for group ABE

The same procedure was undertaken for group ABE. The water level at the weir was set to the same program as listed in Table 7.1. The physical model was run in that setting and then the actual water levels were measured after the water level had stabilized. Table 7.5 shows the relationship between the read data and the actual water level data, and Fig. 7.2 shows the resulting graphs.

Table 7.5 The average read data of ABE and the corresponding depth of point A

| Weir setting | Probe-1 (E) | | Probe-2 (B) | | Probe-3 (A) | | Water level at point A (mm) |
	Read data	Water level (mm)	Read data	Water level (mm)	Read data	Water level (mm)	
40-100	-131.863	61.5	-145.802	61.5	-56.435	61.5	61.5
50-100	-110.137	71.3	-132.829	71.3	-43.349	71.3	71.3
60-100	-84.727	81.9	-118.474	81.9	-28.700	81.9	81.9
70-100	-63.049	92.3	-106.466	92.3	-14.870	92.3	92.3

The relationship between the read data and the water level data was established to make the calibration equation, the results of which are shown in Table 7.6.

Water level graphs were obtained after the conversion of the read data to the water level data was used through the calibration equations in Table 7.6, as shown in Fig. 7.2.

Table 7.6 Calibration equations for group ABE

Probe (borehole)	Calibration equation
Probe-1 (E)	y = 0.4439 x + 120.01
Probe-2 (B)	y = 0.7774 x + 174.62
Probe-3 (A)	y = 0.7391 x + 103.24
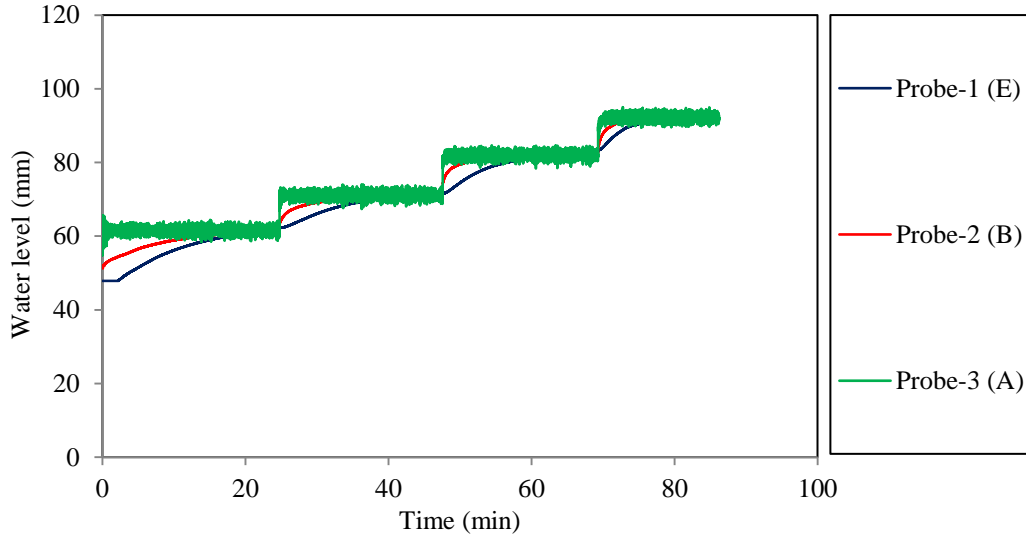
Fig. 7.3 Calibration graph of group ABE

Fig. 7.2 shows the different lag time in the three boreholes. Point A shows no time lag, Point B shows moderate lag time, and Point E shows longer lag time. This is consistent with the positions of the boreholes, that is the further the borehole is located away from the estuary then the longer the lag time.

The average water level for group ABE is shown in Table 7.7.

Fig. 7.2 and Table 7.7 show that the water level in boreholes A, F, and G are identical, indicating that the water level in the sandbox is stable. However differences can also be seen in that the average water level for Point A is higher than the corresponding level for the other points, as the time lag at this point is the smallest, resulting in the bigger average water level at this point.

Table 7.7 Average water level of group ABE in the calibration step

Weir setting	Average water level (mm)		
	Probe-1 (E)	Probe-2 (B)	Probe-3 (A)
40-100	56.094	58.630	61.508
50-100	67.953	69.542	70.678
60-100	79.292	81.339	81.958
70-100	89.772	90.660	91.551

7.1.1.3   Water level calibration for group AFG

The last group for the calibration is group AFG. The same procedure was applied, resulting in Table 7.8 and Fig. 7.3 for the establishment of calibration equations.

Table 7.8 The reading data of AFG and the corresponding depth of point A

Setting	Probe-1 (F)		Probe-2 (G)		Probe-3 (A)		Water level at point A (mm)
	Read data	Water level (mm)	Read data	Water level (mm)	Read data	Water level (mm)	
40-100	-114.028	62.5	0.79617	62.5	-52.517	62.5	62.5
50-100	-93.819	72.3	16.682	72.3	-39.201	72.3	72.3
60-100	-71.387	82.4	33.789	82.4	-24.277	82.4	82.4
70-100	-53.822	92.4	49.215	92.4	-9.408	92.4	92.4

From the regression analysis, the calibration equation for each point can be established as shown in Table 7.9.

Table 7.9 Calibration equations for group AFG

Probe (borehole)	Calibration equation
Probe-1 (F)	y = 0.4905x + 118.24
Probe-2 (G)	y = 0.6145x + 61.964
Probe-3 (A)	y = 0.6915x + 99.078

The water level graphs can be drawn as shown in Fig. 7.3.
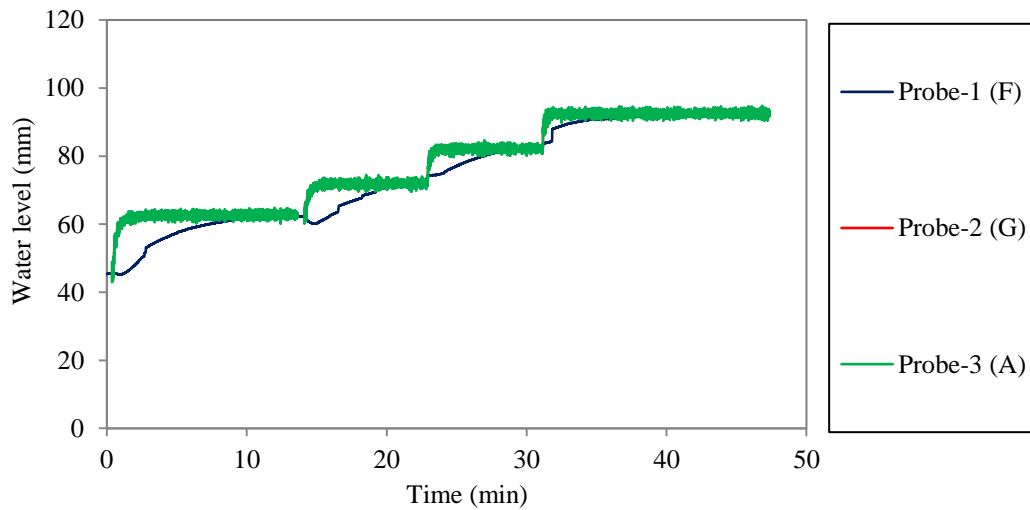
Fig. 7.4 Water level measurement of group AFG in the calibration step

From Fig. 7.3it can be seen that the water levels in all boreholes are identical, indicating the stability of the water level. The graphs of Point A and Point G are identical, as both points are located at the surface water (A being in the groundwater entrance and G in the estuary). Table 7.10 shows the average water level of group AFG.

Table 7.10 Average water level of group AFG in the calibration step

Weir setting	Average water level (mm)		
	Probe-1 (F)	Probe-2 (G)	Probe-3 (A)
40-100	56.977	61.768	62.190
50-100	66.963	71.128	71.093

Weir	Average water level (mm)		
setting	Probe-1 (F)	Probe-2 (G)	Probe-3 (A)
60-100	79.205	82.365	81.985
70-100	90.556	91.655	91.988

7.1.2   The effect of tide on water level

After the calibration and static water level measurements were completed, an experiment was carried out to measure the water levels for a dynamic condition. The weir was set to generate full tide (consisting of flood and ebb tides) with the water level varying from (-70 cm to 100 cm above datum). The first measurements were carried out for group ACD.

Point A showsa significant water level variation affected by the tide. This is because this point is located in the entrance tothe sandbox, resulting in no resistance to the water flow by the sandbox. However, the graph shows a minimum level at 14.6 mm, because below this level the water level in the estuary is too low for flow to enter the sandbox, i.e. point A becomes dry likewise.

Point C shows bigger fluctuation than point D, since Point C is closer to the estuary.

As was undertaken for group ACD, the hydrodynamics within the sandbox as a result of the effect of the tide was examined for group ABE. The fluctuations in the water levels in borehole E can be seen to show little variation which confirm that the estuarine hydrodynamic is very small at this distance from the estuary. Point B has much bigger fluctuation as affected by the tide, because its location is much nearer to the estuarine model.

The water level fluctuations as affected by the tide were also examined for group AFG, where G is located in the estuarine physical model. At point G the tide was complete (unlike Point A), since this point was located in the estuary, in comparison

with Point A which was located at the sandbox entrance. Point F shows small fluctuations, as this point was the farthest away from the estuary.

All the measurement results discussed above were undertaken separately for the three groups ACD, ABE, and AFG. In order to compare all of the results, all of the measurements needed to be combined so that the effect of the tide on the water levels could be evaluated. Fig. 7.4 shows the combined water level measurement results for all of the points, i.e. points A-G. The stepping (unsmooth) graphs were due to the frequency of the reading and not due to the tide. The frequency of the reading was 1/5 second, meaning that every second the WL probes read 5 data which was the same, and then when it shifted to the next second the data changed, and therefore there was a jump in the data resulting stepping graphs. This has nothing to do with the water level change, where actually the water changed smoothly.
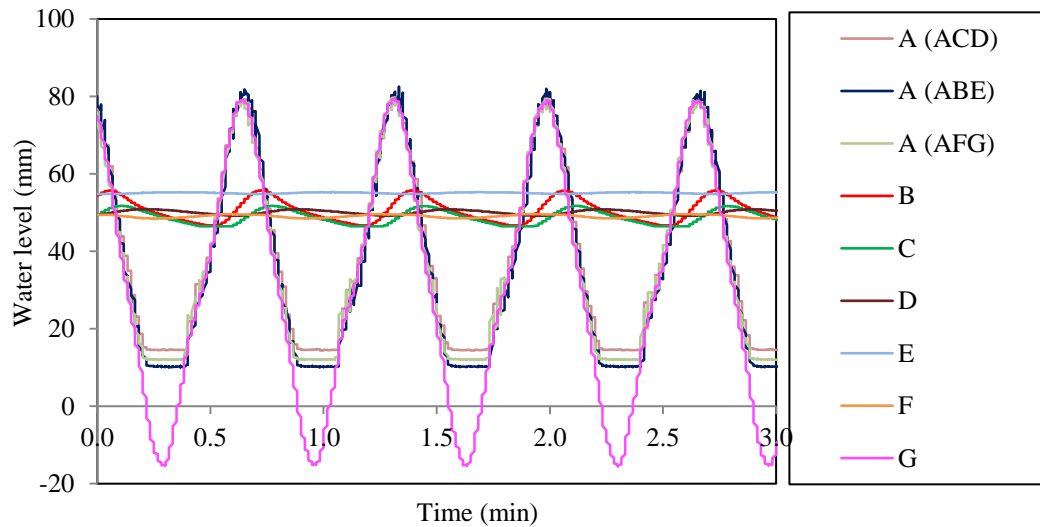
Fig. 7.5 Water level variations for the points (A to G)

In general, water level fluctuations were identified for all of the boreholes, with the one closer to the estuary having the biggest variation. However, from Fig. 7.4 it can be seen that point A shows some inconsistency among the groups ACD, ABE, and AFG, in particular at the lower water level, about 12 mm. This inconsistency was probably caused by a slight instability in the physical model when the tide was included. To compare all of the graphs, it was decided to normalize the water levels,

178

and then make all of the water levels at point A the same. This would enable all of the measured results at the other points to be corrected.

The formula of normalization is as follow:

$$normalized\ result = \frac{original}{[(max - min) - {min}/{(max - min)}]} \quad (7.1)$$

The normalized water level does not have dimension, because it is a comparison against the full tide (max WL - min WL) or the tide range at Point G.   By this formulation the water level data for all the points were corrected, and the results are shown in Fig. 7.5.
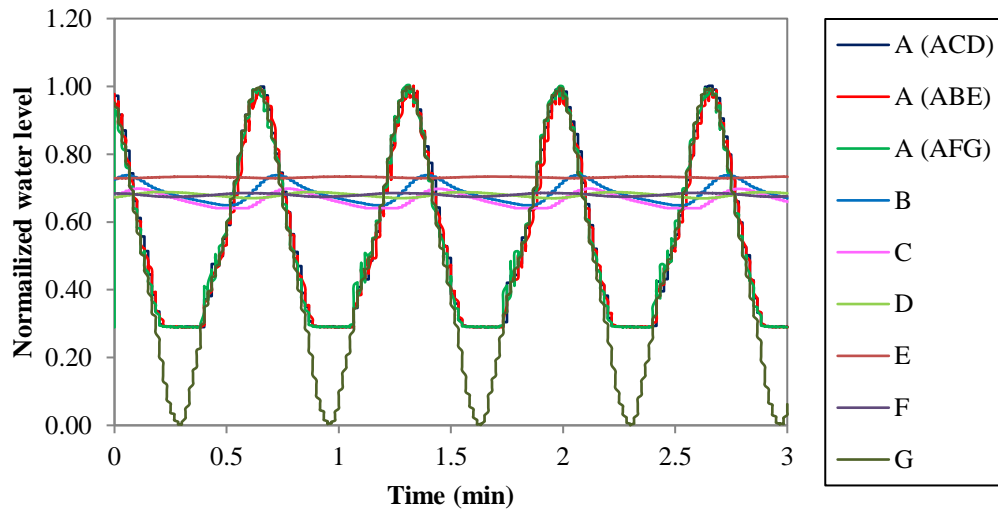
Fig. 7.6 Normalised water levels for all the points

After normalization, all points can be compared in term of the tidal range, with the results being show in Fig. 7.6.
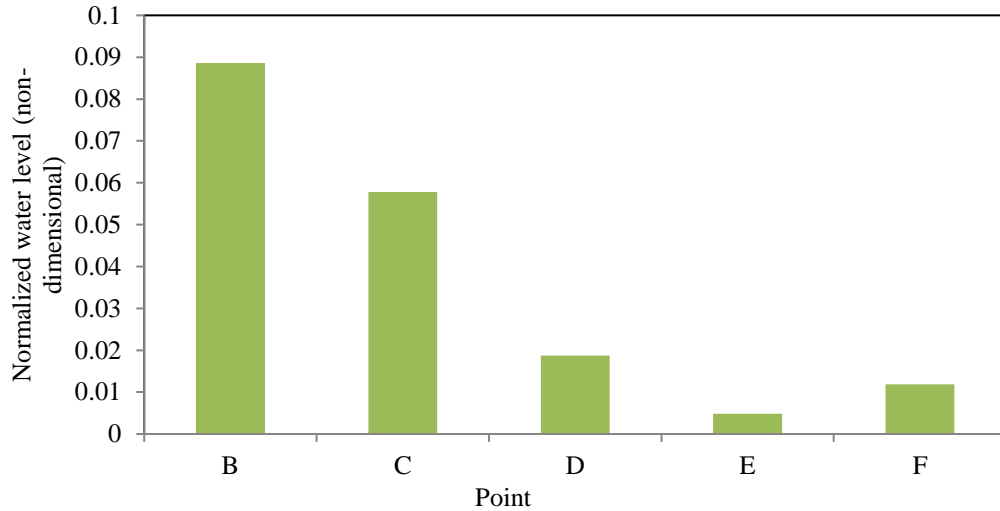
Fig. 7.7 Normalised tidal range for each borehole

From Fig. 7.6 it can be seen that the tidal range decreases from point B to point F. However, point F shows an increase from point E. This may be caused by the water accumulating at borehole F, since this is the borehole farthest away from the estuary and at this point the water is assumed to reflect back toward the estuary. The water need time to flow back from Point F, and hence the water level there was an accumulation between the water which was reflected from the upper boundary with the water flowing from the estuary. This was the reason of the larger tide range than point E.

From Fig. 7.6 it can also be seen that there is a phase shift in the fluctuations, which means that the maximum water level in each borehole does not occur at the same time. This is related to the time needed by the water to travel through the sandbox. The phase shift can be calculated, and it is shown in Fig. 7.7, relative to Point G.
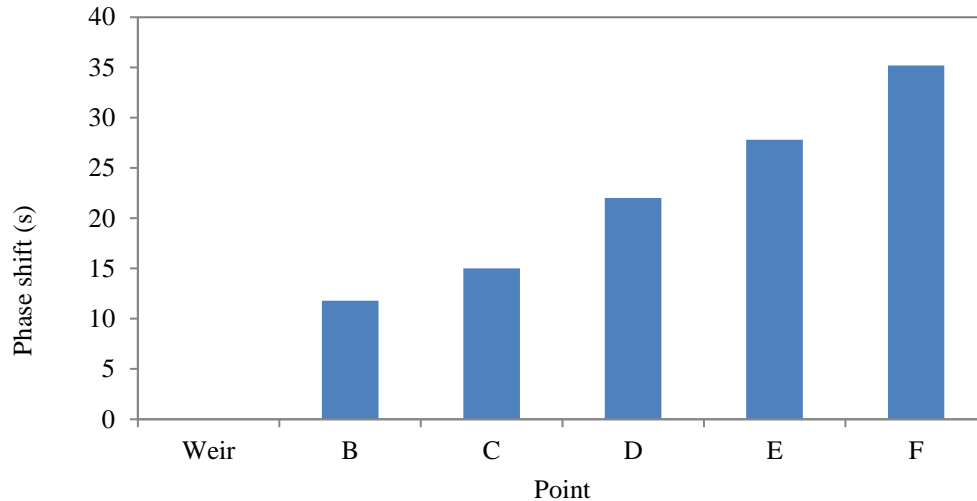
Fig. 7.8 Phase shift at each borehole relative to Point G

According to Fig. 7.7, the phase shift is consistently increasing from point B (11.8 s) to point F (35.2 s).

7.1.3   *The effect of tide and pump on water level*

So far the water levels conditions in the borehole have been shown to be affected by the tide. This tide constitutes the lower boundary condition of the groundwater. It is also of interest to study the effect of the upper boundary. The hydrodynamics of flow in the groundwater, connecting with the surface water (i.e. the estuary) is affected by both boundaries, which can be regarded as the upper and lower boundaries. For this purpose a pump was located near the upper boundary, with the average discharge being 2.85 x 10^6 m^3/s (obtained by measuring the volume of water discharged in a determined time interval). This pump was in inflow pump, which flowed the water into the borehole F.

In order to investigate the effect of both boundary conditions on the flow, a series of experiments were undertaken for three different conditions:

1)   The pump was operated, the weir was set at a constant level (pump on, tide off), where the pump is operated in the average discharge and the weir is set constant at (40, 100).

2) The pump was operated, the weir was set for a tide at [-70, 100], with the pump and tide both being on.

3) The pump was not operated, the weir was set for a tide at [-70,100], with the pump being switched off and the tide on

This series of experiments included boreholes C, E, and F as the sampling points for water level measurements. The experiments were preceded by the calibration procedure as undertaken previously with the measured data being used to refined the tidal boundary condition. In this experiment, the weir was taken as the reference level instead of Point A. Table 7.11 shows the water level measurement results used to develop the calibration equations, with the regression results being shown in Fig. 7.12.

Table 7.11 The average readdata of CFE and the corresponding depth of the weir

Setting	Probe-1 (C)		Probe-2 (F)		Probe-3 (E)		Water level at point A (mm)
	Read data	Water level (mm)	Read data	Water level (mm)	Read data	Water level (mm)	
40-100	-142.726	39.959	-151.371	39.959	-93.217	39.959	39.959
50-100	-132.704	50.000	-144.756	50.000	-84.844	50.000	50.000
60-100	-121.651	60.005	-136.948	60.005	-75.065	60.005	60.005
70-100	-108.521	69.958	-129.572	69.958	-65.838	69.958	69.958

The calibration equations resulting from the graphs shown in Fig. 7.12 are given in Table 7.12.

Table 7.12 Calibration equations for group CFE

Probe (borehole)	Calibration equation
Probe-1 (C)	$y = 0.8763x + 165.74$
Probe-2 (F)	$y = 1.3645x + 246.92$
Probe-3 (E)	$y = 1.0869x + 141.65$

The water level graphs as shown in Fig. 7.8 were then reproduced using the read data and the calibration equations given in Table 7.12.
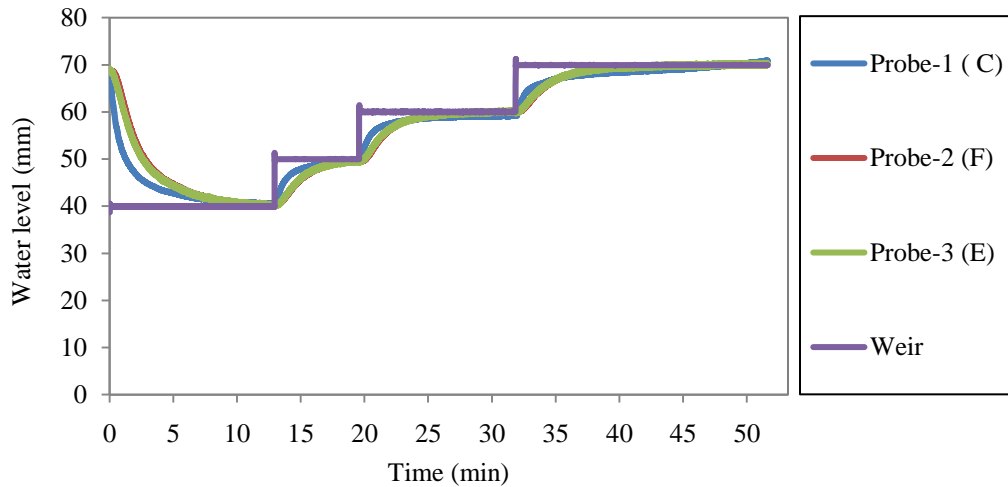
Fig. 7.9 Water level measurement of group CFE in the calibration step

7.1.3.1   Water level measurements for the first condition (pump on, tide constant 40-100)

For the first condition, i.e. with the pump on and the tide constant at (40,100), the measured water levels at Points C, F, and E can be seen in Fig. 7.9.

From Fig. 7.9 it can be seen that the water levels were constant because both the pump and weir were set to constant values. Point C shows a very low water level, which is at about 56.1 mm, while the water levels at points E and F are similar to one another, that is at 80.6 and 85.5 mm, respectively.

7.1.3.2 Water level measurements for the second condition (pump on, tide on)

For this condition, the tide was turned on and set for a flood condition, that is (-70, 100). This meant that there was another input beside the pump, i.e the tidal variations in the water level. The measurement results can be seen in Fig. 7.10 with the average water level at boreholes C, E and F being 47.3, 79.0, and 72.5 mm, respectively.

183
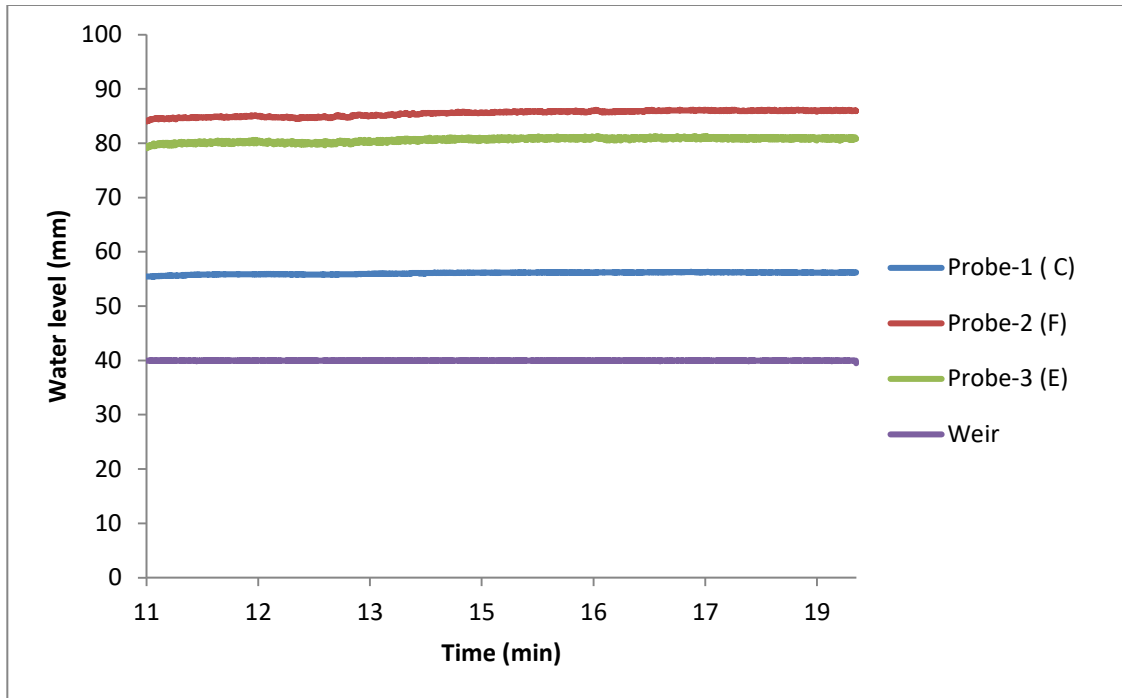
Fig. 7.10 Water level measurementsfor group CFE for the first condition, i.e. pump on and tide constant
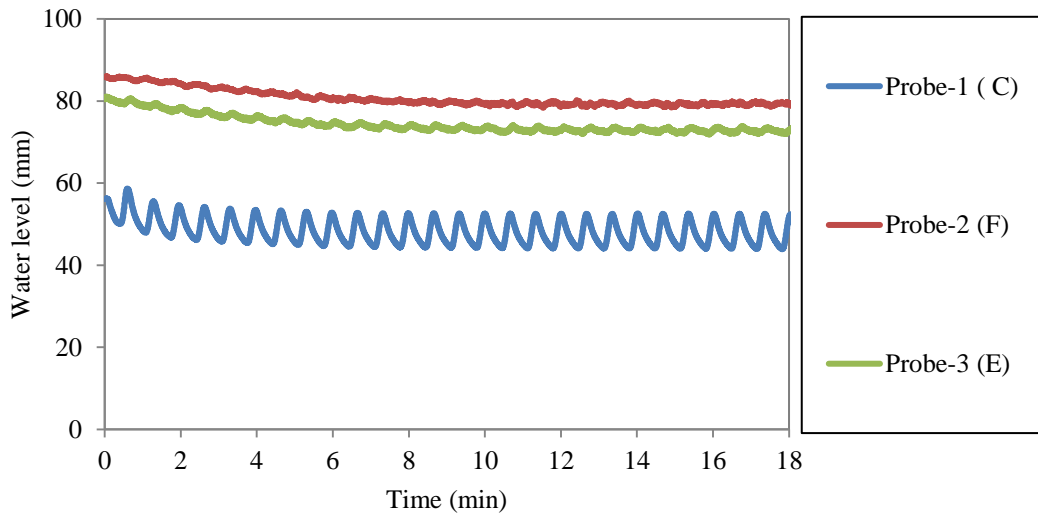
Fig. 7.11 Water level measurement for group CFE for the second setting, i.e. with the tide on and the pump on

184

7.1.3.3 Water level measurements for the third condition (pump off, tide on)

For the third condition the pump was turned off, while the weir was kept on and set again for a flood condition (-70,100). This meant that only the tide affected the water levels. For this case the results could be compared to the other two conditions to determine the impact of the tide. The result is shown in Fig. 7.10. The average water levels for C, E and F are 27.4, 27.0, and 25.9 mm, respectively. This clearly shows that without pumping, the water level in the sandbox decreased.
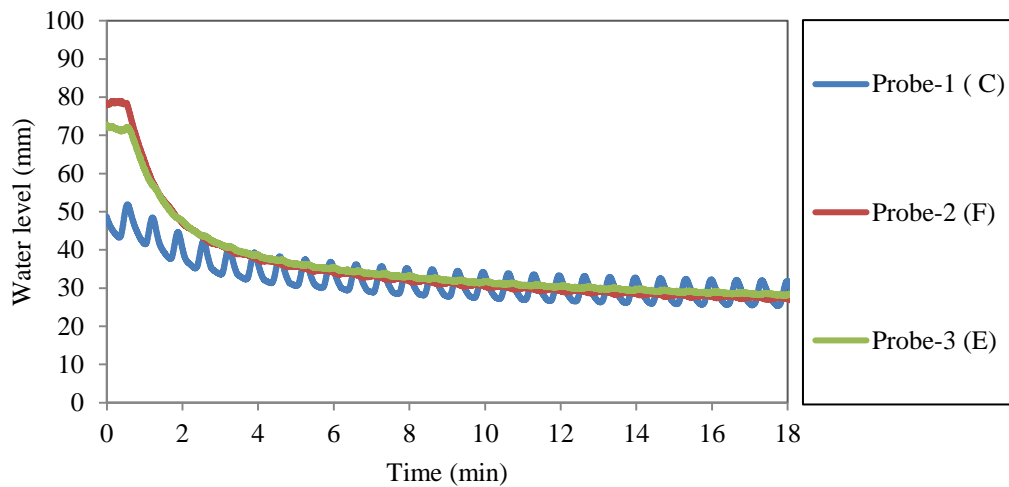
Fig. 7.12 Water level measurement for group CFE for the third condition (tide on, pump off)

Table 7.13shows the overall average water level values in boreholes C, F, and E,for the three conditions.

Table 7.13 Average water level for the three conditions

Condition	Probe-1 (C)	Probe-2 (F)	Probe-3 (E)
Pump on, tide constant	56.1	85.5	80.6
Pump on, tide on	47.3	79.0	72.5
Pump off, tide on	26.7	25.6	22.6

From Table 7.13, it can be seen that the highest average water level was achieved in the first condition, i.e. with the pump off and the tide off, followed by the second

condition, i.e. with the pump and tide both on, and the last condition being the third condition, i.e. with the pump off and the tide on.

A comparison can also be made between the points for each condition. For the first condition, Probe-2 (F) is the highest, followed by Probe-3 (E), and lastly Probe-1 (C). This is as expected since borehole F is the closest point to the pump and hence its water level is the most increased. This also occurs for the second condition (i.e. pump and tide both on). However, for the third condition, Probe-1 (C) is the highest, followed by Probe-2 (F), and Probe-3 (E). This result occurs as the pump was not operated.

7.1.4 Hydrodynamic analysis using Darcy's equation

The water level measurement results were then to apply Darcy's equation using the available data. As a reference it was found by Spark in his thesis that the value of k (i.e. the permeability coefficient) in the sandbox was 0.04 m. Using Darcy's analysis it was attempted to establish whether or not the measurement results were consistent with Darcy's equation.

Table 7.14 shows the application of Darcy's equation to analyze the experimental data and to estimate the value of k. The water level data was taken from the experiment described in Section 7.1.3.1, namely the first condition (pump on, tide constant).

Table 7.14 Calculation of the permeability coefficient using Darcy's equation

Parameter	Value	Unit	Description
SEGMENT: EF			
H at E	0.0739	m	Water level (WL)
H at F	0.0789	m	WL
dH	0.0050	m	WL difference
L	0.375	m	Channel length
B	0.16	m	Channel width
H(avg)	0.0764	m	Averaged WL
A	0.0122	m^2	Channel cross area
i	0.0133	m/m	Hydraulic slope (dH/L)
q	2.16E-06	m^3/s	Disharge
k = q / (i.A)	0.01331	m/s	Permeability coefficient

Parameter	Value	Unit	Description
SEGMENT: EF			
SEGMENT: CE			
H at C	0.0492	m	WL
H at E	0.0739	m	WL
dH	0.0247	m	WL difference
L	1.005	m	Channel length
B	0.16	m	Channel width
H(avg)	0.0615	m	Averaged WL
A	0.0098	m^2	Channel cross area
i	0.0246	m/m	Hydraulic slope (dH/L)
q	2.16E-06	m^3/s	Discharge
k = q / (i.A)	0.00891	m/s	Permeability coefficient
SEGMENT: CF			
H at C	0.0492	m	WL
H at F	0.0789	m	WL
dH	0.0297	m	WL difference
L	1.38	m	Channel length
B	0.16	m	Channel width
H	0.0640	m	Averaged WL
A	0.010245075	m^2	Channel cross area
i	0.0215	m/m	Hydraulic slope (dH/L)
q	2.16E-06	m^3/s	Discharge
k = q / (i.A)	0.00979	m/s	Permeability coefficient
Average 'k' of all segments	0.0107	m/s	

From Table 7.14 it can be seen that Darcy's analysis shows that the permeability coefficient is consistent in the three segment of the sandbox, with the average value being 0.0107. This value is close to reference value of *k*, which is 0.01 (Twumasi, 2010). This shows that the Darcy's equation is applicable in this experiment.

7.2 Dispersion experiments

As described in Chapter 3, the dispersion experiments undertakenin the groundwater model were classified into two types, according to the boundary conditions. Fig. 7.12 describes the two vessels, which are an open-open vessel and a closed-open vessel.

(a)   (b)
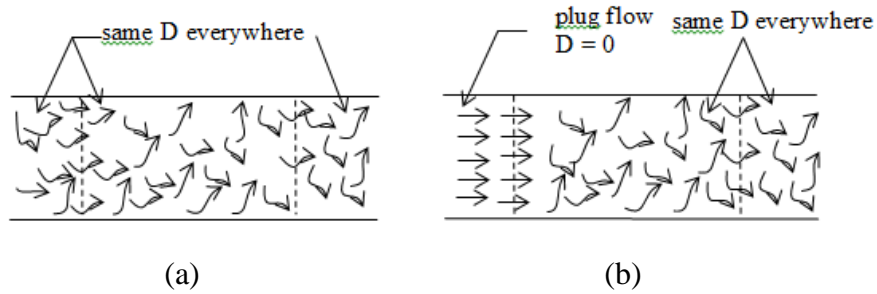
Fig. 7.13 Two types of boundary conditions used with the dispersion model: (a) Open-open vessel, (b) close-open vessel

Source: Levenspiel (1998)

The experiments were carried out for the condition where the pump and tide were both set on. The water level was measured at Points B, F, and D, as shown in Fig. 7.13.
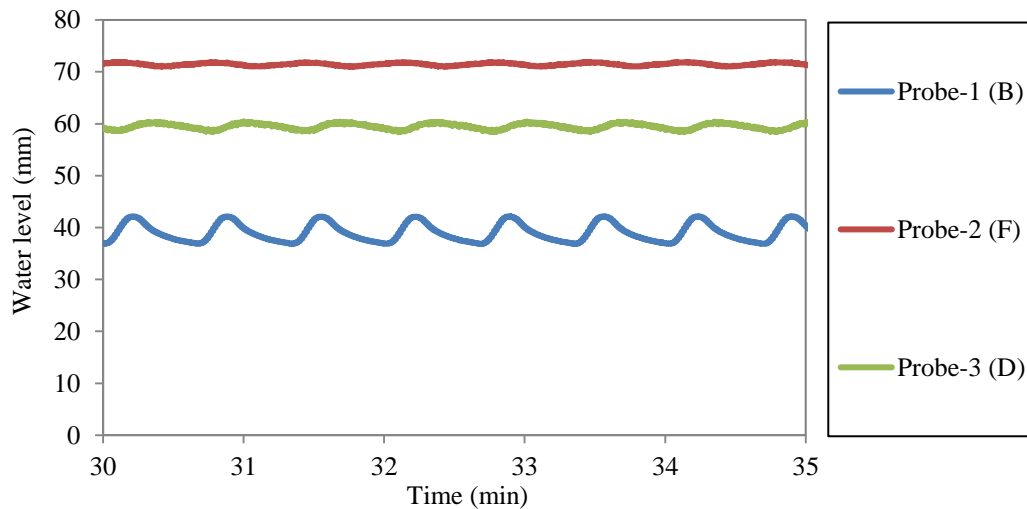
Fig. 7.14 Water levels for the dispersion experiments

7.2.1 Dispersion experiment with the open-open boundary condition

In the first type, the boundary condition were open. This meant that there was no change in the flow of water.

Dye tracer with a concentration of 20 ppmwas injected at Point F, and then its concentration was monitored at Point C and E. The results of the monitoring are shown in Fig. 7.14.
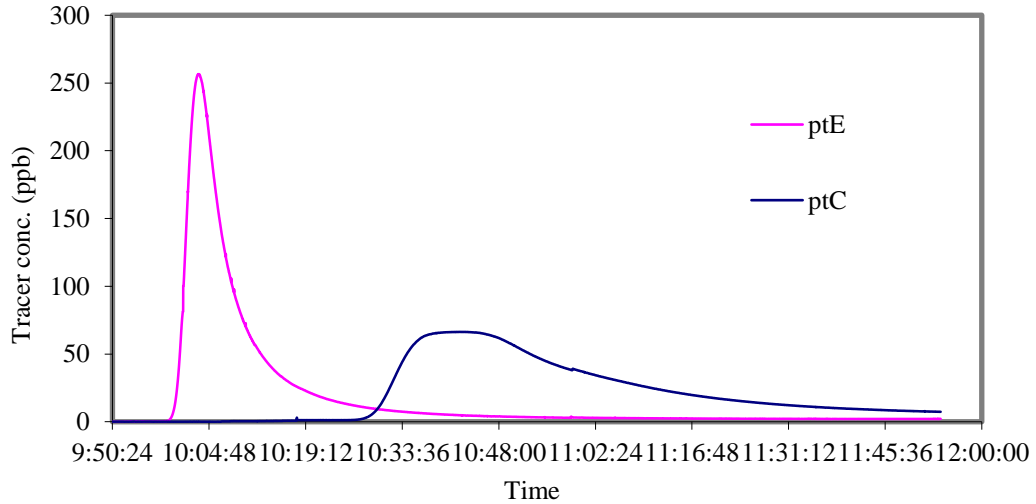
Fig. 7.15 Dye tracer measurement results at Points C and E at the open boundary

Fig. 7.14 shows that the dye concentration is different between point E and C.For Point E, the graphicalresults show that the peak is 254.4 ppb, while at Point C the results show a phase lag and a peak of 60.62 ppb.

As it has been described in Chapter 3, the study of dispersion, particularly in terms of determiningthe dispersion coefficient, requires that the dispersion curve be normalized, so that it can be compared to the standard curve.

The standard curve is based on the following equation:

$$E_{\theta,oo} = \frac{1}{\sqrt{4\pi(\frac{D}{uL})}} e^{\left[\frac{(1-\theta)^2}{4\theta(D/uL)}\right]} \qquad (7.1)$$

The dispersion curves were normalized using the available experimental data, and the results are shown in Fig. 7.15 and Fig. 7.16 for Points E and C, respectively.
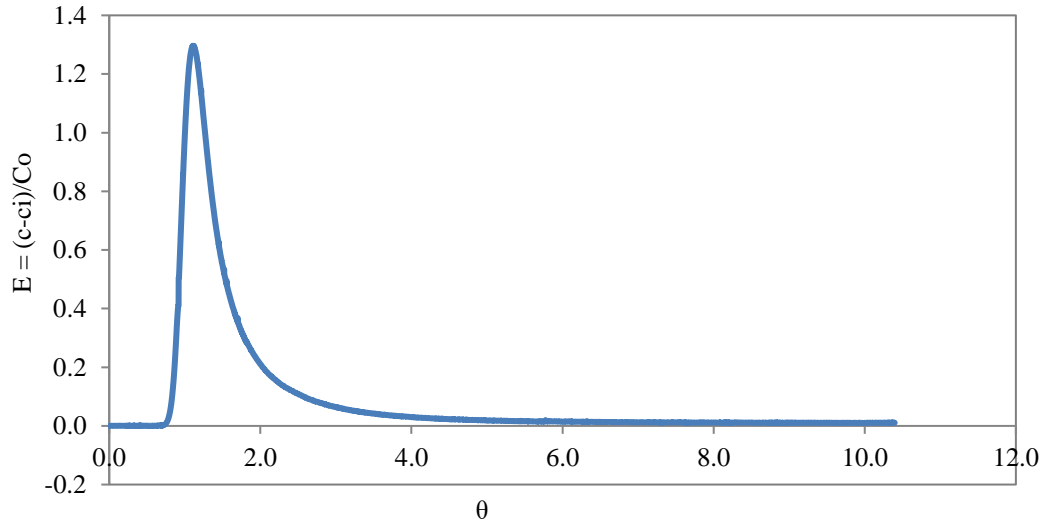
Fig. 7.16 The normalised dispersion curve at Point E
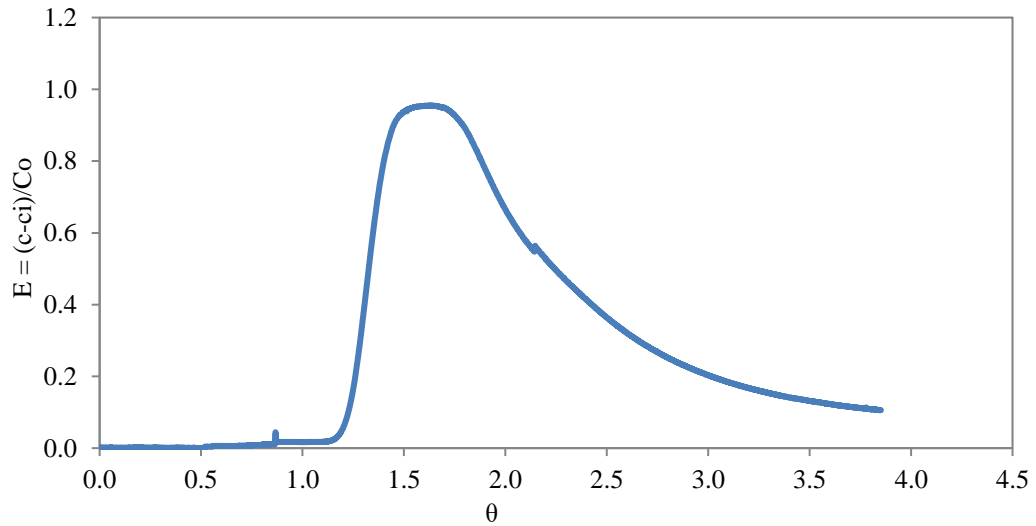
Fig. 7.17 The normalised dispersion curve at Point C

The standard family of dispersion curve can be seen in Fig. 7.17. This family of dispersion curves was established using equation (7.1) and varying the value of d as 0.01, 0.02, 0.05, 0.10, 0.30 and 1.00.
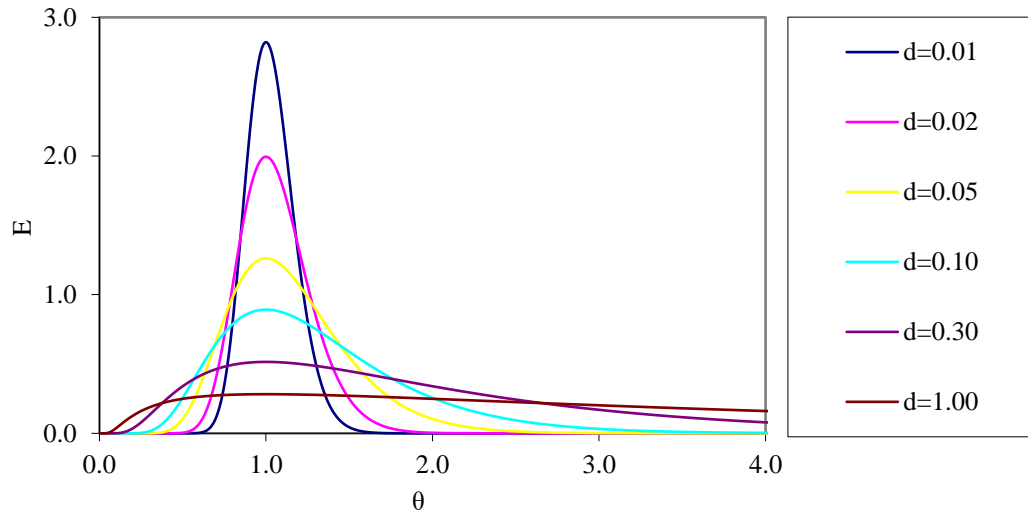
Fig. 7.18 Tracer response curves for open vessels with different d values

To obtain the value of dispersion coefficient, the dispersion curve at Fig. 7.17 needs to be compared with the dispersion family curve to find the closest fitting curve. The result is shown in Fig 7.18.
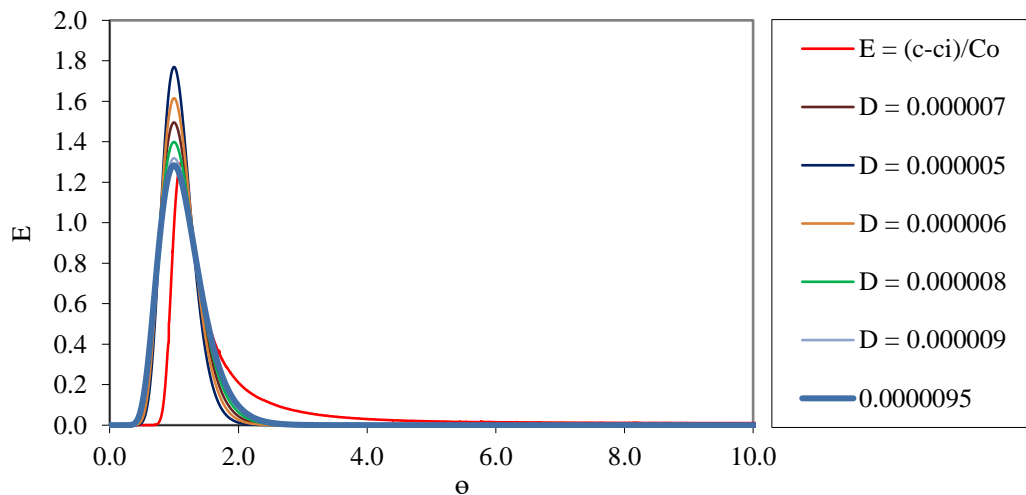
Fig. 7.19 Experiment curve for Point E in the standard cuve groups

The dispersion coefficient (D) was then calculated using Eq. (7.1) resulting in various graphs which depend on the value of the assumed d input.

Using the following data: L=0.375 m, H=0.0627 m, B=0.16 m, porosity=0.41, and Q=2.159x10^{-6}m^3/s (see Table 7.14), the most suitable D value is 0.000009 m^2/s .

The same procedure was applied to Point C. Using the following data: L=1.38 m, H=0.0518 m, B=0.16m, porosity=0.41, and Q=2.159x10^{-6} m^3/s, the most suitable valuefor D was again 0.00009 m^2/s.
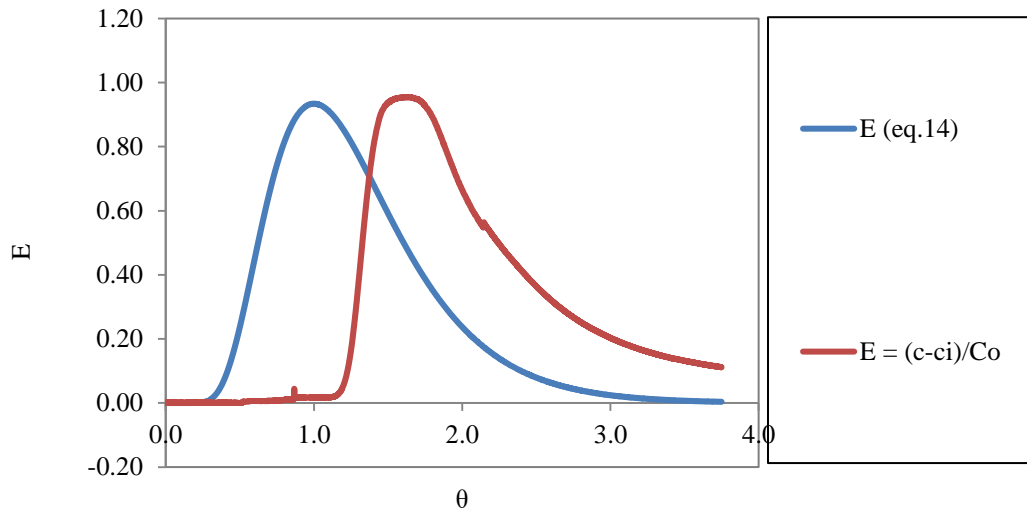
Fig. 7.20 The tracer respons curve for Point C with D = 0.00009

This results show that the D value for the two different experiments had different values, namely 0.000009 m^2/s for Point E and 0.00009 m^2/s for Point D, or the D value for Point C was ten times larger than that for Point E.

7.2.2 *Dispersion experiment with the close-open boundary condition*

From the results in Fig. 7.18 and Fig. 7.19 it appears that the model gives different values of D, instead of the same D value at every point. Therefore it is considered necessary to try the other model, that is the closed-open boundary condition. In this case the boundary of the sandbox was modified by setting a pair of platesat the upper boundary, so that water can flow directly without flowing back to the upstream direction.

The condition for water flow in this experiment is "pump on-tide on", and as shown in Fig. 7.20.
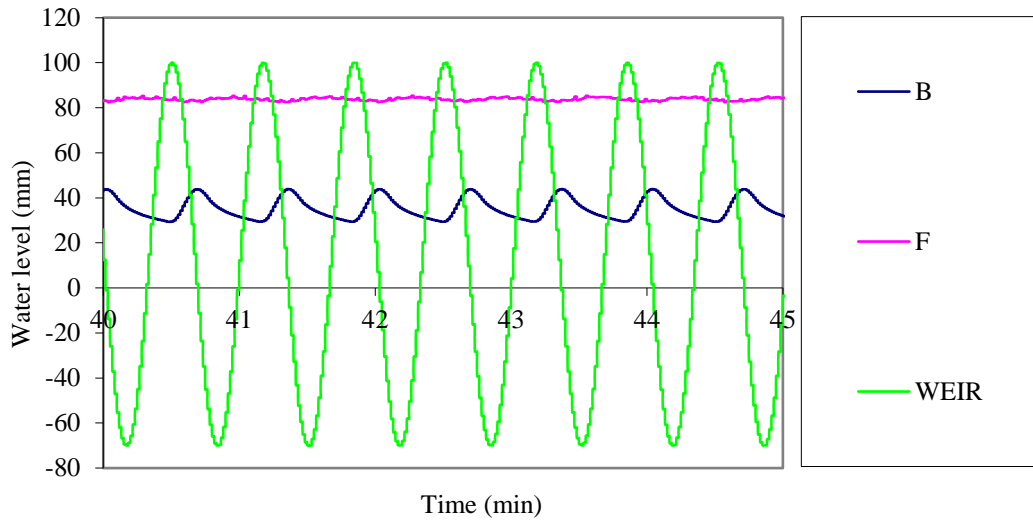
Fig. 7.21 Water level in the dispersion experiment using "close-open" boundary

Dye tracer was then injected at the same point, i.e. Point F, but in this experiment Points D and E were selected as the monitoring points. The result of dye tracer monitoring at Point E is shown in Fig. 7.21.
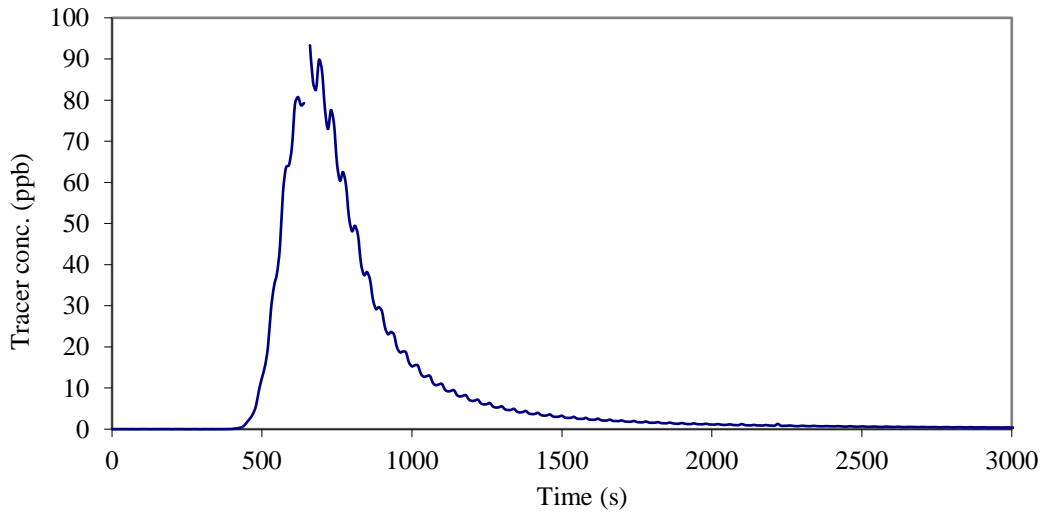
Fig. 7.22 Concentration-time curve at point E for a close-open boundary condition

To find the value of D at this point, the dispersion data at Point E was analyzed using Eq. (7.2) and Eq. (7.3), as given below.

$$\bar{t} = \frac{\sum t_i C_i}{\sum C_i}; \quad \sigma^2 = \frac{\sum t_i^2 C_i}{\sum C_i} - \bar{t}^2 = \frac{\sum t_i^2 C_i}{\sum C_i} - \left[\frac{\sum t_i C_i}{\sum C_i}\right]^2 \quad (7.2)$$

$$\sigma_\theta^2 = \frac{\sigma^2}{\bar{t}^2} = 2\frac{D}{uL} - 2\left(\frac{D}{uL}\right)^2 (1 - e^{-uL/D}) \quad (7.3)$$

Using the experimental data, the dispersion coefficient (D) in this experiment was calculated based on Eq. (7.2) and Eq. (7.3). The experimental data used were: B=0.16 m, H=0.0709 m, L=0.375 m, porosity= 0.41, and Q=2.852x10^{-6} m^3/s. The D value obtained from this set of conditions was 0.0002794 m^2/s.

The same analysis was carried out for Point D, with Fig. 7.22 showing the dispersion curve at Point D.
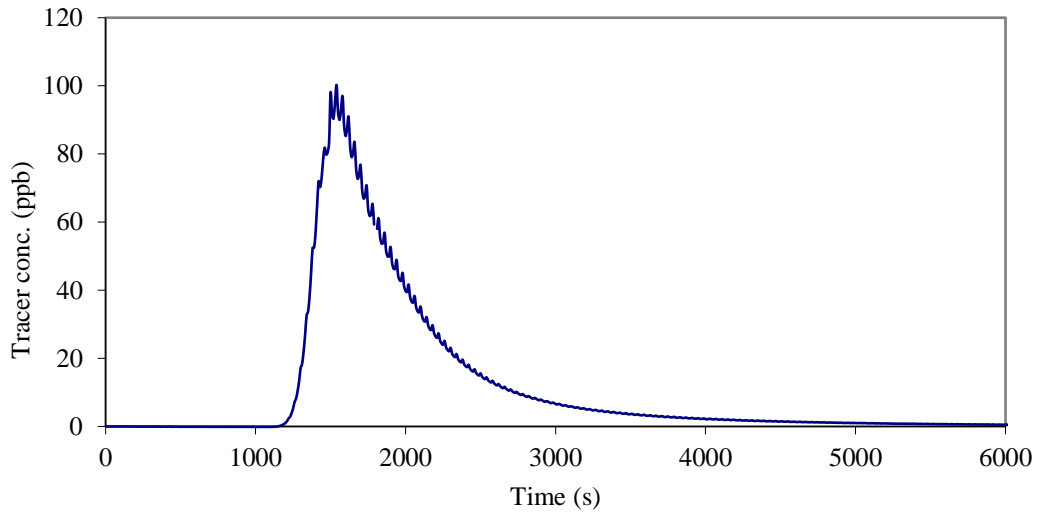
Fig. 7.23 Concentration-time curve of point D for a closed-open boundary condition

Using the same analysis as above, i.e. using Eq. (7.2) and (7.3), and the following data: B=0.16 m, H=0.0679 m, L=0.89 m, porosity=0.41, and Q=2.852E-06 m^3/s, then the resulting value for D was found to be 0.002198 m^2/s.

These results shows that the "closed-open" boundary setting also gave different values of D, which were 0.0002794 m^2/s for Point E and 0.002198 m^2/s for Point D, or D value for Point D was about ten times greater than that at Point E.

7.3 Summary

This chapter has discussed the interaction between surface water and groundwater. This includes water levels in the static and dynamic conditions, the effect of pumping and a tide on the groundwater hydrodynamics, and the application of Darcy's equation. Furthermore, a dispersion study analysis as the main topic of this work has revealed that the dispersion coefficient values change for different boundary conditions.

CHAPTER 8

CONCLUSIONS AND RECCOMENDATIONS

8.1 Conclusions

This study has explored the hydrodynamic and dispersion aspects of the Severn estuary physical model, using both experiment and modelling methods. Studies have also been undertaken in an idealized groundwater incorporating the estuary physical model, involving both hydrodynamic and dispersion aspects.

1. Water level in the estuary physical model have been measured.The analysis results showed that the tide range was larger in the point near the upper boundary than the sea boundary (lower boundary). This is related to the interaction between the flood and ebb tide and continuity principle where the narrower the channel the higher the tide range in the constant discharge assumption.
2. Calibration of hydrodynamic model showed that there were no significant effect of parameter changes (which were roughness coefficient, eddy viscosity coefficient, and momentum correction factor). The best values for each are: n-Manning = 0.025, Eddy viscosity coefficient (COED) = 0.3, and momentum correction (β) = 1.016.
3. By using the real boundary condition, that was by measuring the boundary condition in the physical model, the model has improved significantly, especially where the double peaks of velocity measurement graph were represented in the computer model.
4. Refinement of the bathymetryhas also changed the model significantly, by representing the turbulence appeared in the experimental results.
5. The increase of γ decreased the tracer concentration. This is logical because the higher the value of γ the higher the value of dispersion coefficient. This means

that the dye tracer disperse more rapidly, resulting in the lower level of dye tracer concentration.

6. The best combination between γ and δ was $\gamma = 0.8$ and $\delta = 0.6$.

7. Comparing two values of constant dispersion coefficient, the best value was 0.00524.

8. The refinement of bathymetry proved to increase the level of concentration, and thus improved the model.

9. In the hydrodynamic study of groundwater, the results show that there was a lag time before water reached the target water level at each sampling points. The results showed that the water level at each sampling point was different in term of phase and the tidal range. The further the sampling point from the estuary, the smaller the tide range.

10. Experiments on the effect of tide and pump have revealed that both influenced the groundwater level significantly.

11. The study on dispersion process in the groundwater using two scenarios of boundary condition, namely open-open and close-open boundary conditions have revealed that dispersion coefficient in the groundwater was much lower than that in the estuary.

12. This study contributes on following topic of research and enriches the previous studies summarized in Chapter 2, as follow:

-effect of bathymetry on hydrodynamic and dispersion modeling, which is quite new study and hence the novelty of this study

-effect of boundary condition on modeling

-comparison between constant and variable dispersion coefficient, enriching the study by Hunt (1999)

-effect of bed roughness and Eddy viscosity on modelling, enriching the studies done by Abd El-Hadi and Daver (1976), Magazine et al. (1988), and Schulz and Priegnitz (2011)

-groundwater-surface water interaction and its effects on groundwater hydrodynamic and dispersion

Those all aspects of study can be expected to contribute and enrich the field of water resource modeling and management.

8.2 Recommendations

1. It will be much easier if the procedure of model calibration is embedded in the computer model, so that one should not give too much effort in the calibration, and effort can be spend more in the analysis and interpretation of the results.
2. It will be beneficial if we can establish the method of water level calibration.
3. Also for the calibration of dispersion, it will be easier to make a routine in the computer model.

REFERENCES

Adarsh, S. 2010. Prediction of longitudinal dispersion coefficient in natural channels using soft computing techniques. *Scientia Iranica, Transaction A: Civil Engineering*. 17 (5), 363-371.

Ahsan, N. 2008. Estimating the coefficient of dispersion for a natural stream. *World Academy of Science, Engineering and Technology*. 44, 131-135.

Ani, E.-C., S. Wallis, A. Kraslawski, and P.S. Agachi. 2009. Development, calibration and evaluation of two mathematical models for pollutant transport in a small river. *Environmental Modelling & Software*. 24, 1139-1152.

Aris, R. (1956). On the dispersion of a solute in a fluid flowing through a tube. Proceedings of Royal Society of London Series A. 235, 67-77.

Asai, K. and K. Fujisaki. 1991. Effect of aspect ratio on longitudinal dispersion coefficient. Proceedings of the International Symposium on Environment and Hydrolog. A. A. Balkema, Rotterdam, The Netherlands. 493-498.

Azamathulla, H.M. and A.A. Ghani. 2011. Genetic programming for predicting longitudinal dispersion coefficient in streams. *Water Resource Management*. 25, 1537–1544.

Azamathulla, H.M. and F.-C. Wu. 2011. Support vector machine approach for longitudinal dispersion coefficients in natural streams. *Applied Soft Computing*. 11(2), 2902-2905.

Azevedo, I.C., A.A. Bordalo, and P.M. Duarte. 2010. Influence of river discharge patterns on the hydrodynamics and potential contaminant dispersion in the Douro estuary (Portugal). *Water Research.* 44(10), 3133-3146.

Baek, K.O. and I.W. Seo. 2010. Routing procedures for observed dispersion coefficients in two-dimensional river mixing. *Advances in Water Resources*. 33(12), 1551-1559.

Bansal, M.K. 1971. Dispersion in natural streams. *Journal of Hydraulic Division*. 97(11), 1867-1886.

Boxall, J.B. and I. Guymer. 2007. Longitudinal mixing in meandering channels: New experimental data set and verification of a predictive technique. *Water Research*. 41(2), 341-354.

Barros, F.P.J. and R.M. Cotta. 2007. Integral transforms for three-dimensional steady turbulent dispersion in rivers and channels. *Applied Mathematical Modelling*. 31(12), 2719-2732.

Barros, F.P.J., W.B. Mills, and R. M. Cotta. 2006. Integral transform solution of a two-dimensional model for contaminant dispersion in rivers and channels with spatially variable coefficients. *Environmental Modelling & Software*. 21(5), 699-709.

Brady, J.A. and P. Johnson. 1981. Predicting times of travel, dispersion and peak concentrations of pollution incidents in steams. *Journal of Hydrology*. 53, 135-150.

Burnett, W.C. and H. Dulaiova. 2003. Estimating the dynamics of groundwater input into the coastal zone via continuous radon-222 measurements. *Journal of Environmental Radioactivity*. 69, 21-35.

Chapman, B.M. 1978. Dispersion of soluble pollutants in non-uniform rivers: I. Theory. *Journal of Hydrology*. 40, 139-152.

Chapman, B.M. 1979. Dispersion of soluble pollutants in non-uniform rivers: II. Application to experimental results. *Journal of Hydrology*. 40(1–2), 153-163.

Chatwin, P.C. and C.M. Allen. 1985. Mathematical models of dispersion in rivers and estuaries. *Annual Review on Fluid Mechanics*. 17, 119-149.

Chatwin, P.C. and P.J. Sullivan. 1982. The effect of aspect ratio on longitudinal diffusivity in rectangular channels. *Journal of Fluid Mechanics*. 120, 347-358.

Day, T.J. 1977. Longitudinal dispersion of fluid particles in mountain streams: 2. Similarity of the mean motion and its application. *Journal of Hydrology*.16(1), 26-52.

Day, T.J. and I.R. Wood. 1976. Similarity of the mean motion of fluid particles dispersing in a natural channel. *Natural Resources Research*, 12(4), 655-666.

Davinroy, R.D. 1994. Physical sediment modeling of Mississippi river on a micro scale. MSc. Thesis. University of Missouri-Rolla.

Deng, Z.-Q. and H.-S. Jung. 2009. Scaling dispersion model for pollutant transport in rivers. *Environmental Modelling &Software*. 24(5), 627-631.

Deng, Z.-Q, V.P. Singh, and L. Bengtsson. 2001. Longitudinal dispersion coefficient in straight rivers. *Journal of Hydraulic Engineering*. 127(11), 919-927.

Deng, Z.-Q, V.P. Singh, and L. Bengtsson. 2002. Longitudinal dispersion coefficient in single-channel streams. *Journal of Hydraulic Engineering*. 128(10), 901-916.

Duarte, A.A.L.S. and J.M.P. Vieira. 2009. Estuarine hydrodynamic as a key-parameter to control eutrophication processes. *WSEAS Transactions and Fluid Mechanics*. 4, 137-147.

Elder, J.W. 1959. The dispersion of a marked fluid in turbulent shear flow. *Journal of Fluid Mechanics, Cambridge, UK*. 5(4), 544-560.

El-Hadi, N.D.A. and K.S. Davar. 1976. Longitudinal dispersion for flow over rough beds. *Journal of Hydraulic Division, ASCE*. 102(4), 483-498.

Fischer, H.B. 1966. Longitudinal dispersion in laboratory and natural streams. PhD thesis. California Institute of Technology, Pasadena, California.

Fischer, H.B. 1975. Discussion of simple method for prediction dispersion in streams by R.S. McQuivey and T.N. Keefer. *ASCE Journal of Environmental Engineering Division.* 101, 453-45.

Ghivehchi, M., M.F. Maghrebi, and J. Abrishami. 2009. New method for determination of depth-averaged velocity for estimation of longitudinal dispersion in natural rivers. *Journal of Applied Sciences.* 9(13), 2408-2415.

Gofrey, R.G. and B.J. Frederick. 1970. Dispersion in natural streams. *United States Geological Survey (USGS) Profl. Paper.*

Guymer. 1998. Longitudinal dispersion in sinuous channel with changes in shape. *Journal of Hydraulic Engineering.* 124(1), 33-40.

Guymer, I and J.R. West. 1992. Longitudinal dispersion coefficients in estuary. *Journal of Hydraulic Engineering.* 118, 718-734.

Han, Y., Z. Chen, X. Luo, and X. Wang. 2013. Physical modeling researches on the improvement project of the deep-draft channel of the Yangtze estuary. Proceedings of the 7th International Conference on Asian and Pacific Coasts (APAC 2013) Bali, Indonesia.

Hays, J.R. 1966. Mass transport phenomena in open channel flow. Ph.D. thesis. Vanderbilt University, Nashville. 138 p.

Heller, V. 2011. Scale effects in physical hydraulic engineering models. *Journal of Hydraulic Research.* 50(2), 244–246.

Ho, D.T., P. Schlosser, and T. Caplow. 2002. Determination of longitudinal dispersion coefficient and net advection in the tidal Hudson River with a large-scale, high resolution SF6 tracer release experiment. *Environmental Science and Technology.* 6, 3234-3241.

Gleick, P.H., ed. 1993. Water in Crisis: A Guide to the World's Freshwater Resources. Oxford University Press.

Hunt, B. 1999. Dispersion model for mountain streams. *Journal of Hydraulic Engineering.* 125(2), 99-105.

Iwasa, Y. and S. Aya. 1991. Predicting longitudinal dispersion coefficient in open-channel flows. Proceedings of Symposium on Environmental Hydraulics, Hong Kong. 505-510.J

Jamali, M., G.A. Lawrence, and K. Maloney. 2005. Dispersion in varying-geometry rivers with application to methanol releases. *Journal of Hydraulic Engineering.* 131(5): 390-396.

Jay, A. 2004. Estimating effective longitudinal dispersion in the Chesapeake Bay. *Estuarine, Coastal and Shelf Science.* 60(3), 359-368.

Jayawerdana, A.W. and P.H. Lui. 1984. Numerical solution of dispersion equation using a variable dispersion coefficient: method and applications. *Hydrological Science Journal.* 29(3), 293-309.

Jobson, H.E. 1997. Predicting travel time and dispersion in rivers and streams. *Journal of Hydraulic Engineering.* 123(11), 971-978.

Kashefipour, S.M. and R.A. Falconer. 2002. Longitudinal dispersion coefficients in natural channels. *Water Research.* 36(6), 1596-1608.

Koussis, A.D. and J.R. Mirasol. 1998. Hydraulic estimation of dispersion coefficient for streams. *Journal of Hydraulic Engineering.* 124(3), 317-319.

Li, Z.H., J. Huang, and Li, J. 1998. Preliminary study on longitudinal dispersion coefficient for the gorges reservoir. Proceedings of the Seventh International Symposium Environmental Hydraulics, Hong Kong, China.

Li, X., L. Sun, and X. Meng. 2003. Research and model constructing of the Yellow river estuary. International Conference on Estuaries and Coasts, Hangzhou, China.

Li, L., H. Liao, and T. Li. 2005. A hybrid model for simulating velocity field of a river with complex geometry plunged by multiple jets. *Journal of Hyrodynamics.* 18(6), 752-759.

Liu, H. 1977. Predicting dispersion coefficient of stream. *Journal of Environmental Engineering Division.* 103(1), 59-69.

Liu, H. 2011. Fate of three major rivers in the Bohal sea – a model study. *Continental Shelf Research.* 31:1490–1499.

Lloyds, J.W. 1994. Estuarine barrages and their influence on groundwater. *Journal of Hydrology.* 162, 247-265.

Montani, S., P. Magni, M. Shimamoto, N. Abe, and K. Okutani. 1998. The effect of a tidal cycle on the dynamics of nutrient in a tidal estuary in the Seto Inland Sea, Japan. *Journal of Oceanography. 54,* 65-76.

Nordin, C.F., Jr., and G.V. Sabol. 1974. Empirical data on longitudinal dispersion in rivers. *U.S. Geological Survey,Water-Resources Investigations.* 20-74.

Pritchard, D. W. 1967. *What is an estuary: physical viewpoint* [in: Lauf, G. H. *Estuaries.* A.A.A.S. Publ. 83. Washington, DC. 3–5].

Ross, D.A. 1995. *Introduction to Oceanography.* Harper Collins College Publishers, New York.

Ruesta, J.C.G., J.R. Salazar, and C. J. Schexnayder. Constructing a Physical Model of the Piura River.*Practice Periodical on Structural Design and Construction.* 10 (4), 253-259.

Ryckbost, P. 2005. *Redeveloping urban waterfront property.* USA: University of Michigan, USA.

Savage, B.M. and M.C. Johnson. 2001. Flow over Ogee spillway – physical and numerical model case study. *Journal of Hydraulic Engineering.* 127(8), 640-649.

Schiller, R.V., V.H. Kourafalou. 2010. Modeling river plume dynamics with the Hybrid Coordinate Ocean Model. *Ocean Modelling.* 33, 101–117.

Schubel, J.R., 1971. *The estuarine environment: estuaries and estuarine sedimentation.* AGI Short Course Lecture Notes, Wye Inst., Md. Washington DC : Am. Geol. Inst. [in: Fischer. 1976. Fischer, Mixing and Dispersion in Estuaries].

Schulz, M., J. Priegnitz, S. Heller, S. Meinecke, and M. Feibicke. 2011. Effect of bed surface roughness on longitudinal dispersion in artificial open channels. *Hydrological Processes.*

Seo, I.W. and K.O. Baek. 2004. Estimation of the longitudinal dispersion coefficient using the velocity profile in natural streams. *Journal of Hydraulic Engineering.* 130, 227-236.

Seo, I.W. and T.S. Cheong. 1998. Predicting longitudinal dispersion coefficient in natural steams. *Journal of Hydraulic Engineering.* 124(1), 25-32.

Shaha, D.C., Y.-K. Cho, M.-T. Kwak, S. R. Kundu, and K. T. Jung. 2011. Spatial variation of the longitudinal dispersion coefficient in an estuary. *Hydrology and Earth System Sciences Discussions.* 8, 7757-7780.

Shen, C., J. Niu, E.J. Anderson, and M.S. Phanikumar. 2010. Estimating longitudinal dispersion in rivers using Acoustic Doppler Current Profilers. *Advances in Water Resources.* 33(6), 615-623.

Sheppard C, M. Al-Husiani M, F. Al-Jamali, F. Al-Yamani, R. Baldwin, J. Bishop, F. Benzoni, E. Dutrieux E, et al. 2010. The Gulf: A young sea in decline. *Marine Pollution Bulletin.* 60, 13–38.

Sooky, A. 1969. Longitudinal dispersion in open channels. *Journal of Hydraulic Division*, ASCE. 95(4), 1327-1346.

Smith, R. 1976. Longitudinal dispersion of a buoyant contaminant in a shallow channel. *Journal of Fluid Mechanics.* 78(4), 677-688.

Smith, R. 1983. Longitudinal dispersion coefficients for varying channels. *Journal of Fluid Mechanics.* 130, 299-314.

Sparks, T.D., B.N. Bockelmann-Evans, and R.A. Falconer. 2013. Laboratory Validation of an Integrated Surface Water-Groundwater Model. *Journal of Water Resource and Protection*. 5, 377-394.

Stacey, M.T., S.G. Monismith, and J.R. Burau. 1997. Observations of turbulence in a partially stratified estuary. *Journal of Physical Oceanography.* 29.

Swamee, P.K., S.K. Pathak, and M. Sohrab. 2000. Empirical relations for longitudinal dispersion in streams. *Journal of Environmental Engineering.* 126(11), 1056-1062.

Tang, H., C. Chen, C. Hong, and J. Huang. An improved PTV system for large-scale physical river model. *Journal of Hydrodynamics*. 20(6), 669-678.

Tayfur, G. and V.P. Singh. 2005. Predicting longitudinal dispersion coefficient in natural streams by artificial neural network. *Journal of Hydraulic Engineering*. 131(11), 991-1000.

Taylor, G. 1953. Dispersion of soluble matter in solvent flowing slowly through a tube. Proceedings of the Royal Society of London Series A. 219, 186-203.

Toprak, Z.F., Z. Şen, and M.E. Savai. 2004. Comment on "Longitudinal dispersion coefficients in natural channels". *Water Research.* 38(13), 3139-3143.

Vale, L.M. and J. M. Dias. 2011. The effect of tidal regime and river flow on the hydrodynamics and salinity structure of the Lima Estuary: Use of a numerical model to assist on estuary classification. *Journal of Coastal Research.* 64: 1604-1608.

Teuchies J, Vandenbruwaene W, Carpentier R, Bervoets L, Temmerman S, et al. 2013. Estuaries as filters: the role of tidal marshes in trace metal removal. PLoS ONE 8 (8): e70381. Doi: 10.1371/journal.pone.0073081, Plymouth University, United Kingdom

Voroglue, E. and W.D.L. Finn. 1978. A finite element method for the diffusion-convection equation with constant coefficients. *Advances in Water Resources*. 1: 337-343.

Vermeulen, B.M.P. Boersema, A.J.F. Hoitink, J., Sieben, C.J. Sloff, and M. van der Wal. 2013. River scale model of a training dam using lightweight granulates. *Journal of Hydro-environment Research*. 1-7.

Wang, S. and W. Wu. 2004. River sedimentation and morphology modeling – the state of the art and future development. Proceedings of the Ninth International Symposium on River Sedimentation, Yichang, China.

Westbrook, S.J., J.L. Raynerb, G. B. Davis, T. P. Clementa, P.L. Bjerd, and S.J. Fisher. 2005. Interaction between shallow groundwater, saline surface water and contaminant discharge at a seasonally and tidally forced estuarine boundary. *Journal of Hydrology.* 302, 255-269.

Wood, R. and J. Handley. 1999. Urban waterfront regeneration in the Mersey Basin, North West England. *Journal of Environmental Planning and Management.* 42(4), 565-580.

Wu, X., J. Deng, R. Cheng, and T. Wu. 2003. A super-large tidal physical model for the Pearl river estuary. International Conference on Estuaries and Coasts, Hangzou, China.

Wu, L. 2010. Experimental investigation of effect of tide on coastal groundwater table. *Journal of hydrodynamics*. 22(1):66-72.

APPENDIX-1

DATA OF BATHYMETRY MEASUREMENTS

BATHYMETRY CHECK

3-Nov-11

Datum: 75.0   cm   (metal rod by the model, which the white bridge runs along)

All measurements are in cm

DATA   REAL   Ave Ztop   ACTUAL POSITION

                                                                          65.831   of land or deepest/highest points

Point	X (cm)	Y (cm)	Z (cm)	Description	X (cm)	Y (cm)	Z (cm)	Top of model (cm)	Depth Below Datum (cm)	Depth Below Top of model (cm)	Difference of depth between DATA and REAL (cm)	X (cm)	Y (cm)	Z (cm)	Difference of Y between DATA and REAL (cm)
11	180	21	-0.2	land	130	21	65	65.5	-10.0	-0.8	0.6	130	21	65	0
12	180	43	-0.2	land	130	43	65		-10.0	-0.8	0.6	130	38.5	65	-4.5
13	180	84	-17.6		130	84	49.7		-25.3	-16.1	-1.5				
14	180	132	-0.2	land	130	132	38.8		-36.2	-27.0	26.8	130	124.5	64.6	-7.5
15	180	171	-47.7		130	171	24.6		-50.4	-41.2	-6.5				
16	180	235	-50.4		130	235	23.2		-51.8	-42.6	-7.8				
17	180	301	-0.1	land	130	301	66	66.1	-9.0	0.2	-0.3	130	292.5	66	-8.5
18	240	102	-4.2	deepest point	190	102	65.4	65.7	-9.6	-0.4	-3.8	190	98.5	60.2	-3.5
19	240	145	-1.4		190	145	47.4		-27.6	-18.4	17.0	190	139.5	65.3	-5.5
20	240	168	-24.6	highest point	190	168	36.5		-38.5	-29.3	4.7	190	162.3	37.3	-5.7
21	240	272	-41.9		190	272	27.1		-47.9	-38.7	-3.2				
22	240	307	-0.5	land (boundary)	190	307	66.1	65.8	-8.9	0.3	-0.8	190	301.9	65.9	-5.1
23	300	167	-0.9	land	250	167	49.3	65.4	-25.7	-16.5	15.6	250	147.2	65.9	-19.8
24	300	238	-20.4		250	238	41.5		-33.5	-24.3	3.9	250			
25	300	295	-36	deepest point	250	295	29.7		-45.3	-36.1	0.1	250	290.7	66	-4.3
26	300	334	-3.4	land	250	334	66	66.1	-9.0	0.2	-3.6	250	330.1	66	-3.9

208

Point	X (cm)	Y (cm)	Z (cm)	Description	X (cm)	Y (cm)	Z (cm)	Top of model (cm)	Depth Below Datum (cm)	Depth Below Top of model (cm)	Difference of depth between DATA and REAL (cm)	X (cm)	Y (cm)	Z (cm)	Difference of Y between DATA and REAL (cm)
27	350	272	-2.7	land	300	272	45	65.7	-30.0	-20.8	18.1	300	265	66.5	-7
28	350	303	-31.7	highest point	300	303	35.3		-39.7	-30.5	-1.2	300			
29	350	354	-23.2		300	354	44.4		-30.6	-21.4	-1.8	300			
30	350	377	-1.4	land	300	377	66.7	66.4	-8.3	0.9	-2.3	300	373.9	66.7	-3.1
31	415	299	-4.4	land	365	299	46.7	65.7	-28.3	-19.1	14.7	365	295.3	66	-3.7
32	415	318	-31.3	deepest point	365	318	37.8		-37.2	-28.0	-3.3	365	313.7	33.9	-4.3
33	415	363	-20		365	363	46.8		-28.2	-19.0	-1.0	365			
34	415	400	-0.4	land (boundary)	365	400	n/a	66.3	n/a	n/a	n/a	365	389.9	66.2	n/a
35	430	297	-0.1	land	380	297	58	65.8	-17.0	-7.8	7.7	380	295.6	65	-1.4
36	430	326	-29.7		380	326	38		-37.0	-27.8	-1.9	380			
37	430	339	0	island	380	339	44		-31.0	-21.8	21.8	380			
38	430	361	-20		380	361	47.3		-27.7	-18.5	-1.5	380			
39	430	400	-3.1	land	380	400	n/a	65	n/a	n/a	n/a	380	397	65	n/a
40	440	289	-0.1	land	390	289	54.9	65.9	-20.1	-10.9	10.8	390	283.6	65.5	-5.4
41	440	310	-15.8		390	310	44		-31.0	-21.8	6.0	390			
42	440	324	0	island	390	324	37.5		-37.5	-28.3	28.3	390			
43	440	330	-23.5	deepest point	390	330	38.7		-36.3	-27.1	3.6	390			
44	440	345	-21.1	deepest point	390	345	43.3		-31.7	-22.5	1.4	390			
45	440	364	-15		390	364	49.5		-25.5	-16.3	1.3	390			
46	440	396	-0.5	land	390	396	66.2	66.2	-8.8	0.4	-0.9	390	396	66.2	0
47	454	284	-1.6	land	404	284	52	65.6	-23.0	-13.8	12.2	404	274.8	66	-9.2
48	454	328	-24.9	deepest point	404	328	44.2		-30.8	-21.6	-3.3	404	320.2	36	-7.8
49	454	346	-22.1	deepest point	404	346	43.1		-31.9	-22.7	0.6	404			
50	454	364	-0.1	land	404	364	65.7	66.2	-9.3	-0.1	0.0	404	363.1	65.8	-0.9
51	459	292	-2.2		409	292	49.2	65.5	-25.8	-16.6	14.4	409	271.2	65.9	-20.8
52	459	335	-24.7	deepest point	409	335	42.3		-32.7	-23.5	-1.2	409	318.2	67.9	-16.8
53	459	354	-21.4	deepest point	409	354	64.5		-10.5	-1.3	-20.1	409	339.1	40.9	-14.9
54	459	367	-0.7	land	409	367	65.7	66.1	-9.3	-0.1	-0.6	409	354.5	65.6	-12.5
55	474	285	-1.1	land	424	285	49.7	65.6	-25.3	-16.1	15.0	424	265.1	65.8	-19.9

209

Point	X (cm)	Y (cm)	Z (cm)	Description	X (cm)	Y (cm)	Z (cm)	Top of model (cm)	Depth Below Datum (cm)	Depth Below Top of model (cm)	Difference of depth between DATA and REAL (cm)	X (cm)	Y (cm)	Z (cm)	Difference of Y between DATA and REAL (cm)
56	474	309	-14.5		424	309	37.6		-37.4	-28.2	13.7	424	311.5	36.5	2.5
57	474	328	-25.1	deepest point	424	328	45.1		-29.9	-20.7	-4.4	424	330.8	44.4	2.8
58	474	357	-0.1	land	424	357	65.2	65.9	-9.8	-0.6	0.5	424	342.1	65.8	-14.9
59	484	284	-0.3	land	434	284	50.1	65.5	-24.9	-15.7	15.4	434	363.6	65.8	79.6
60	484	319	-21.5	deepest point	434	319	46.4		-28.6	-19.4	-2.1	434	302.2	38.8	-16.8
61	484	351	-1.5	land	434	351	65.7	65.8	-9.3	-0.1	-1.4	434	337	65.6	-14
62	524	294	-0.6	land	474	294	50.4	65.6	-24.6	-15.4	14.8	474	272.9	65.1	-21.1
63	524	324	-19.4	deepest point	474	324	65.7		-9.3	-0.1	-19.3	474	306.1	43.3	-17.9
64	524	334	-2.7	land	474	334	65.6	66.3	-9.4	-0.2	-2.5	474	318.6	65.8	-15.4
65	554	292	-2.9	land	504	292	51.3	65.5	-23.7	-14.5	11.6	504	272.7	65.4	-19.3
66	554	318	-16.1	deepest point	504	318	65.5		-9.5	-0.3	-15.8	504	301.8	45	-16.2
67	554	324	-6.1	land	504	324	65.3	66.4	-9.7	-0.5	-5.6	504	307.2	65.7	-16.8

APPENDIX-2

BATHYMETRY MEASUREMENT RESULTS

Legend:
- -5.0-0.0
- -10.0--5.0
- -15.0--10.0
- -20.0--15.0
- -25.0--20.0
- -30.0--25.0
- -35.0--30.0
- -40.0--35.0
- -45.0--40.0
- -50.0--45.0
- -55.0--50.0

Verification data				Verification data		
x (cm)	y (cm)	z (cm)		x (cm)	y (cm)	z (cm)
130	21	-0.8		380	297	-7.8
130	43	-0.8		380	326	-27.8
130	84	-16.1		380	339	-21.8
130	132	-27		380	361	-18.5
130	171	-41.2		380	400	0
130	235	-42.6		380	295.6	-0.8
130	301	0		380	397	-0.8
130	21	-0.8		390	289	-10.9
130	38.5	-0.8		390	310	-21.8
130	124.5	-1.2		390	324	-28.3
130	292.5	0		390	330	-27.1
190	102	-0.4		390	345	-22.5
190	145	-18.4		390	364	-16.3
190	168	-29.3		390	396	0
190	272	-38.7		390	283.6	-0.3
190	307	0		390	396	0.4
190	98.5	-5.6		404	284	-13.8
190	139.5	-0.5		404	328	-21.6
190	162.3	-28.5		404	346	-22.7
190	301.9	0		404	364	0
250	167	-16.5		404	274.8	0.2
250	238	-24.3		404	320.2	-29.8
250	295	-36.1		404	363.1	0
250	334	0		409	292	-16.6
250	147.2	0		409	335	-23.5
250	330.1	0		409	354	-1.3
300	272	-20.8		409	367	0
300	303	-30.5		409	271.2	0
300	354	-21.4		409	318.2	-27.9
300	377	0		409	339.1	-24.9
300	265	0.7		409	354.5	-0.2
300	373.9	0.9		424	285	-16.1
365	299	-19.1		424	309	-28.2
365	318	-28		424	328	-20.7
365	363	-19		424	357	-0.6
365	400	0		424	265.1	0
365	295.3	0.2		424	311.5	-29.3
365	313.7	-31.9		424	330.8	-21.4
365	389.9	0.4		424	342.1	0

Verification data		
x (cm)	y (cm)	z (cm)
434	284	-15.7
434	319	-19.4
434	351	0
434	263.6	0
434	302.2	-27
434	337	-0.2
474	294	-15.4
474	324	0
474	334	0

Verification data		
x (cm)	y (cm)	z (cm)
474	272.9	-0.7
474	306.1	-22.5
474	318.6	0
504	292	-14.5
504	318	0
504	324	0
504	272.7	-0.4
504	301.8	-20.8
504	307.2	-0.1

APPENDIX-3

SELECTION OF n-MANNING COEFFICIENT

Water level

POINT	MSE			RMSE			SE			NE			α			R^2		
	n = 0.035	n = 0.015	n = 0.025	n = 0.035	n = 0.015	n = 0.025	n = 0.035	n = 0.015	n = 0.025	n = 0.035	n = 0.015	n = 0.025	n = 0.035	n = 0.015	n = 0.025	n = 0.035	n = 0.015	n = 0.025
1	2.84E-05	5.05E-05	3.16E-05	5.78E-04	7.71E-04	6.10E-04	4.45E-03	5.99E-03	4.74E-03	-2.19	-2.91	-2.20	2.138	2.184	2.143	0.9763	0.9577	0.9734
2	3.36E-05	5.01E-05	3.40E-05	6.29E-04	7.67E-04	6.32E-04	4.54E-03	5.53E-03	4.66E-03	-2.31	-2.79	-2.41	2.082	2.117	2.087	0.9774	0.9637	0.9771
3	1.85E-05	2.98E-05	1.83E-05	4.66E-04	5.92E-04	4.64E-04	3.40E-03	4.30E-03	3.35E-03	-1.48	-1.88	-1.52	2.014	2.039	2.017	0.9834	0.9733	0.9837
4	1.85E-05	2.77E-05	1.84E-05	4.66E-04	5.71E-04	4.65E-04	3.47E-03	4.21E-03	3.49E-03	-0.66	-0.98	-0.69	2.017	2.038	2.020	0.9883	0.9799	0.9881
5	3.47E-05	3.86E-05	3.45E-05	6.39E-04	6.74E-04	6.37E-04	4.82E-03	5.06E-03	4.80E-03	0.48	0.23	0.46	1.931	1.943	1.934	0.9647	0.9607	0.9651
6	8.33E-06	1.02E-05	7.07E-06	3.13E-04	3.46E-04	2.88E-04	2.45E-03	2.58E-03	2.19E-03	-0.88	-1.32	-0.89	1.908	1.921	1.908	0.9919	0.9904	0.9932
												average	2.015	2.040	2.018			

Vx

POINT	MSE			RMSE			SE			NE			α			R^2		
	n = 0.035	n = 0.015	n = 0.025	n = 0.035	n = 0.015	n = 0.025	n = 0.035	n = 0.015	n = 0.025	n = 0.035	n = 0.015	n = 0.025	n = 0.035	n = 0.015	n = 0.025	n = 0.035	n = 0.015	n = 0.025
1	7.69E-04	9.35E-04	8.99E-04	3.01E-03	3.32E-03	3.25E-03	2.15E-02	2.46E-02	2.40E-02	-27.56	-34.59	-17.25	-0.318	-3.662	-0.226	0.7888	0.7495	0.7198
2	1.82E-04	1.95E-04	1.55E-04	1.46E-03	1.52E-03	1.35E-03	1.11E-02	1.20E-02	1.03E-02	-27.16	-36.02	-12.14	0.799	0.784	0.764	0.8033	0.7859	0.8342
3	3.63E-04	4.11E-04	3.73E-04	2.07E-03	2.20E-03	2.09E-03	1.59E-02	1.73E-02	1.57E-02	-23.58	-25.17	-26.94	0.927	2.876	0.604	0.8764	0.8677	0.8740
4	2.96E-04	3.53E-04	2.51E-04	1.87E-03	2.04E-03	1.72E-03	1.43E-02	1.58E-02	1.32E-02	-43.07	-48.95	-34.70	0.213	0.125	0.755	0.8692	0.8502	0.8956
5	1.99E-03	1.50E-03	6.04E-04	3.64E-03	3.71E-03	3.60E-03	2.96E-02	2.97E-02	2.94E-02	-1078.96	-732.68	-292.96	0.125	0.152	1.727	0.8755	0.8708	0.8940
6	1.12E-04	2.15E-04	1.14E-04	1.15E-03	1.59E-03	1.16E-03	2.88E-02	1.15E-02	9.06E-03	255.53	-367.75	-248.08	-0.341	-0.621	0.490	0.9052	0.8285	0.9014
												average	0.234	-0.058	0.686			

Vy

POINT	MSE			RMSE			SE			NE			α			R^2		
	n = 0.035	n = 0.015	n = 0.025	n = 0.035	n = 0.015	n = 0.025	n = 0.035	n = 0.015	n = 0.025	n = 0.035	n = 0.015	n = 0.025	n = 0.035	n = 0.015	n = 0.025	n = 0.035	n = 0.015	n = 0.025
1	2.61E-04	2.66E-04	2.60E-04	1.752E-03	1.77E-03	1.748E-03	1.37E-02	1.38E-02	1.36E-02	-91.10	-99.11	-72.99	1.682	5.601	1.466	0.7897	0.7219	0.7675
2	7.36E-05	8.08E-05	8.16E-05	9.31E-04	9.75E-04	9.80E-04	7.19E-03	7.56E-03	7.60E-03	32.74	46.40	-13.69	0.005	0.025	0.091	0.7765	0.7556	0.7482
3	4.31E-05	4.78E-05	4.72E-05	7.12E-04	7.50E-04	7.45E-04	1.05E-02	5.62E-03	1.07E-02	-60.36	-57.97	-59.22	0.648	-0.406	-0.008	0.7612	0.7099	0.7302
4	9.32E-05	1.17E-04	1.34E-04	1.05E-03	1.18E-03	1.26E-03	8.00E-03	8.80E-03	9.76E-03	747.07	768.03	482.99	-0.033	0.102	0.043	0.8154	0.7593	0.7173
5	1.23E-04	1.20E-04	8.93E-05	1.20E-03	1.19E-03	1.02E-03	9.15E-03	8.70E-03	8.10E-03	13.96	-14.50	-7.07	0.048	-0.554	0.491	0.8762	0.8652	0.9116
6	7.36E-05	9.68E-05	6.43E-05	9.30E-04	1.07E-03	8.70E-04	6.95E-03	7.67E-03	6.39E-03	8.46	10.25	1.52	0.448	0.367	19.415	0.8581	0.8111	0.8632
												average	0.466	0.856	3.583			

Note - score:

	3
	2
	1

Total score:

	n = 0.035	n = 0.015	n = 0.025
TOTAL	243	145	254

Conclusion: the best fit is n = 0.025

219

APPENDIX-4

SELECTION OF EDDY VISCOSITY COEFFICIENT

Vx

POINT	MSE				RMSE				SE				NE				α				R^2			
	COED = 0.5	COED = 1.5	COED = 0.3	COED = 3.0	COED = 0.5	COED = 1.5	COED = 0.3	COED = 3.0	COED = 0.5	COED = 1.5	COED = 0.3	COED = 3.0	COED = 0.5	COED = 1.5	COED = 0.3	COED = 3.0	COED = 0.5	COED = 1.5	COED = 0.3	COED = 3.0	COED = 0.5	COED = 1.5	COED = 0.3	COED = 3.0
1	8.23E-04	6.99E-04	8.99E-04	6.26E-04	3.11E-03	2.87E-03	3.25E-03	2.71E-03	2.31E-02	2.23E-02	2.40E-02	2.11E-02	-15.44	-10.54	-17.25	-10.93	1.83	11.52	0.63	-0.19	0.740	0.775	0.720	0.807
2	1.37E-04	1.08E-04	1.55E-04	9.78E-05	1.27E-03	1.13E-03	1.35E-03	1.07E-03	9.78E-03	8.49E-03	1.03E-02	8.04E-03	-8.83	1.07	-12.14	7.89	2.93	1.30	1.42	1.44	0.858	0.884	0.834	0.890
3	3.22E-04	2.88E-04	3.73E-04	2.70E-04	1.95E-03	1.84E-03	2.09E-03	1.78E-03	1.49E-02	1.42E-02	1.57E-02	1.37E-02	-25.07	-15.38	-26.94	-5.83	0.55	1.78	0.82	1.12	0.889	0.891	0.874	0.904
4	2.18E-04	1.98E-04	2.51E-04	1.90E-04	1.60E-03	1.53E-03	1.72E-03	1.49E-03	1.24E-02	1.18E-02	1.32E-02	7.97E-03	-31.44	-24.67	-34.70	-19.51	1.16	1.38	-0.68	1.01	0.909	0.910	0.896	0.918
5	1.07E-03	9.56E-04	1.10E-03	8.52E-04	3.55E-03	3.35E-03	3.60E-03	3.17E-03	2.93E-02	2.72E-02	2.94E-02	2.51E-02	-410.95	-719.68	-292.96	-808.05	1.75	-1.21	-12.00	1.79	0.900	0.889	0.894	0.894
6	1.02E-04	1.24E-04	1.14E-04	1.88E-04	1.10E-03	1.21E-03	1.16E-03	1.49E-03	2.86E-02	9.59E-03	9.06E-03	1.20E-02	-243.09	-290.08	-248.08	-360.10	0.53	0.87	0.64	-1.04	0.913	0.891	0.901	0.842

Vy

POINT	MSE				RMSE				SE				NE				α				R^2			
	COED = 0.5	COED = 1.5	COED = 0.3	COED = 3.0	COED = 0.5	COED = 1.5	COED = 0.3	COED = 3.0	COED = 0.5	COED = 1.5	COED = 0.3	COED = 3.0	COED = 0.5	COED = 1.5	COED = 0.3	COED = 3.0	COED = 0.5	COED = 1.5	COED = 0.3	COED = 3.0	COED = 0.5	COED = 1.5	COED = 0.3	COED = 3.0
1	2.52E-04	2.43E-04	2.60E-04	2.44E-04	1.72E-03	1.69E-03	1.75E-03	1.70E-03	1.35E-02	1.33E-02	1.36E-02	1.34E-02	-70.52	-65.48	-72.99	-67.80	-1.57	9.56	3.34	3.30	0.826	0.868	0.768	0.890
2	7.15E-05	4.72E-05	8.16E-05	3.74E-05	9.17E-04	7.45E-04	9.80E-04	6.63E-04	7.05E-03	5.87E-03	7.60E-03	5.24E-03	-11.77	-10.77	-13.69	-23.63	2.37	1.42	1.31	1.36	0.78030	0.83660	0.74820	0.86670
3	4.34E-05	5.32E-05	4.72E-05	6.50E-05	7.14E-04	7.91E-04	7.45E-04	8.75E-04	1.05E-02	5.71E-03	1.07E-02	6.19E-03	-52.70	-13.78	-59.22	-10.13	-0.74	0.58	1.75	0.57	0.770	0.813	0.730	0.785
4	7.11E-05	8.55E-05	8.39E-05	1.18E-04	9.20E-04	1.01E-03	9.99E-04	1.18E-03	7.06E-03	7.90E-03	7.61E-03	9.17E-03	1121.12	1090.12	1078.30	750.78	0.90	0.61	1.82	1.12	0.8594	0.9025	0.8254	0.9141
5	9.06E-05	1.53E-04	8.93E-05	2.11E-04	1.03E-03	1.34E-03	1.02E-03	1.58E-03	8.31E-03	1.08E-02	8.10E-03	6.97E-03	-3.51	11.11	-7.07	22.90	1.12	0.85	2.24	0.49	0.9185	0.8992	0.9116	0.8922
6	6.23E-05	6.61E-05	6.43E-05	7.14E-05	8.56E-04	8.82E-04	8.70E-04	9.17E-04	6.35E-03	6.81E-03	6.39E-03	6.94E-03	2.64	7.46	1.52	14.20	0.53	0.85	0.43	0.96	0.8921	0.9071	0.8632	0.9038

Note - score:

	4
	3
	2
	1

Total score:

	COED = 0.5	COED = 1.5	COED = 0.3	COED = 3.0
TOTAL	184	191	139	207

APPENDIX-5

ERROR ANALYSIS OF MODEL BEFORE AND AFTER BATHYMETRY REFINMENT

Water level

POINT	MSE		RMSE		SE		NE		α		R^2	
	old	new	old	new	old	new	old	new	old	new	old	new
1	1.43E-05	2.40E-05	4.10E-04	5.31E-04	3.03E-03	4.33E-03	-0.76	-1.88	1.008	1.019	0.988	0.980
2	2.35E-05	2.85E-05	5.26E-04	5.79E-04	3.75E-03	4.33E-03	-2.65	-3.21	1.027	1.032	0.983	0.982
3	1.07E-05	1.48E-05	3.55E-04	4.18E-04	2.37E-03	3.11E-03	-1.07	-1.83	1.011	1.018	0.991	0.987
4	1.45E-05	1.53E-05	4.13E-04	4.24E-04	2.93E-03	3.18E-03	-0.40	-1.17	1.004	1.012	0.989	0.991
5	3.33E-05	3.32E-05	6.26E-04	6.25E-04	4.82E-03	4.75E-03	0.25	-0.32	0.997	1.003	0.968	0.966
6	3.42E-06	7.63E-06	2.00E-04	3.00E-04	1.33E-03	2.37E-03	-0.13	-0.93	1.001	1.009	0.997	0.993

Vx

POINT	MSE		RMSE		SE		NE		α		R^2	
	old	new	old	new	old	new	old	new	old	new	old	new
1	4.01E-04	6.27E-04	2.17E-03	2.72E-03	1.56E-02	1.91E-02	-43.03	-156.03	1.44	2.40	0.876	0.826
2	1.25E-04	1.72E-04	1.21E-03	1.42E-03	9.13E-03	1.04E-02	-20.05	-0.32	1.20	1.32	0.911	0.810
3	1.76E-04	3.68E-04	1.44E-03	2.08E-03	1.04E-02	1.56E-02	-71.84	-18.05	1.72	22.34	0.942	0.863
4	1.59E-04	2.42E-04	1.37E-03	1.69E-03	9.78E-03	1.28E-02	25.95	-37.02	0.74	1.37	0.945	0.886
5	1.19E-03	9.66E-04	3.75E-03	3.37E-03	3.12E-02	2.73E-02	-95.81	-7.78	1.96	1.08	0.954	0.881
6	1.54E-04	1.17E-04	1.35E-03	1.17E-03	9.85E-03	9.37E-03	8.41	0.27	0.92	0.73	0.952	0.898

Vy

POINT	MSE		RMSE		SE		NE		α		R^2	
	old	new	old	new	old	new	old	new	old	new	old	new
1	2.26E-04	2.52E-04	1.63E-03	1.72E-03	1.17E-02	1.34E-02	0.88	-512.16	0.99	6.12	0.839	0.779
2	4.25E-05	5.21E-05	7.07E-04	7.83E-04	5.45E-03	6.14E-03	6.98	-29.27	0.93	1.29	0.851	0.821
3	1.07E-04	4.63E-05	1.12E-03	7.38E-04	8.33E-03	5.42E-03	44.41	26.64	0.56	0.73	0.772	0.811
4	1.60E-04	1.05E-04	1.38E-03	1.12E-03	1.22E-02	8.50E-03	53.83	25.04	0.47	0.75	0.941	0.869
5	2.23E-04	1.72E-04	1.62E-03	1.42E-03	1.22E-02	1.11E-02	65.19	12.87	0.35	0.87	0.963	0.880
6	1.03E-04	7.52E-05	1.10E-03	9.41E-04	6.90E-03	7.36E-03	19.31	-15.71	0.81	1.16	0.920	0.879

Note - score:

	2
	1